Investigation into the effects of infrared, visible and ultraviolet wavelengths of the solar spectrum on human skin cell damage

Catherine Anne Bonn, BA (Hons)

Thesis submitted for the degree of Doctor of Philosophy

Department of Dermatological Sciences

Faculty of Medical Sciences

Translational and Clinical Research Institute

Newcastle University, UK

March 2022

Abstract

Ultraviolet light is known to cause skin damage and photoaging, and chronic exposure can lead to skin cancer. The effects of visible light and infrared light on the skin are less well understood, though some believe they contribute to oxidative stress and photoaging. Understanding the mechanisms of photodamage is important for the development of sunscreens to effectively prevent photodamage and maintain skin health. The objective of this study was to optimise experimental conditions for assaying the irradiation of visible and infrared light on human skin cells in vitro, and determining the effects of these wavelengths on reactive oxygen species (ROS) production and gene expression.

Temperature control during infrared irradiations is critical to understanding the effect of light on chromophores rather than through heating. Without adequate temperature control, tissue culture plates could exceed 60°C, resulting in greater than 90% cell death. Careful consideration of medium conditions is crucial for ensuring results are not due to unexpected interactions of light with medium components. The presence of riboflavin, a component of almost all commercially available cell culture medium, reduced viability in cells irradiated with blue light by 45%.

When adequately controlled, it was found that 2 hours of infrared at solar intensity or a 10-hour equivalent dose at 9 x peak solar intensity did not affect ROS as measured with flow cytometry, and RNA sequencing showed few changes to gene expression with less than 10 differentially expressed genes. A dose of visible light equivalent to one hour of peak solar visible light did not induce a ROS signal measurable after irradiation. However, it was found to affect extracellular matrix genes MMP1 and MMP3 to similar extents to a 2.16 standard erythemal dose of UV and induce ferritin expression where the UV dose did not, indicating a possible effect on photoaging and oxidative stress.

In summary, this thesis demonstrates that infrared light has little effect through absorption of chromophores, but visible light may affect fibroblast extracellular matrix regulation and iron homeostasis.

Declaration

This thesis is submitted for the degree of Doctor of Philosophy. The research for this submission was performed in the Department of Dermatological Sciences, Translational and Clinical Research Institute, Newcastle University, United Kingdom from September 2017 to March 2022, under the academic supervision of Professor Mark A. Birch-Machin. All work is original unless acknowledged via reference. None of the material has been submitted previously for a degree or any other qualification at this university or any other institution.

Abbreviations

ACTB	β-actin
ADP	adenosine diphosphate
ATP	adenosine triphosphate
BER	base excision repair
BRCA1	breast cancer gene 1
cDNA	complementary DNA
COX	cyclooxygenase
COL1A1	collagen type I alpha 1 chain
CO_2	carbon dioxide
CPD	cyclobutane pyrimidine dimers
Ct	cycle threshold
D-loop	dissociation loop region
DCFDA	2',7'-dichlorodihydrofluorescein diacetate
DEG	differentially expressed gene
DMEM	Dulbecco's' modified Eagles medium
DNA	deoxyribonucleic acid
ECM	extracellular matrix
ETC	electron transport chain
$FADH_2$	flavin adenine dinucleotide
FCS	foetal calf serum
Fe^{2+}	iron
FTL	ferritin light chain
FTH1	ferritin heavy chain 1
GAG	glycosaminoglycan
HDFn	neonatal human dermal fibroblast
H_2O_2	hydrogen peroxide
H^+	hydrogen proton
IL	interleukin
IR	infrared
MMP	matrix metalloproteinase
MMP1	matrix metalloproteinase 1

MMP2	matrix metalloproteinase 2
MMP3	matrix metalloproteinase 3
mRNA	messenger RNA
mtDNA	mitochondrial DNA
NAD^+/H^+	nicotinamide adenine dinucleotide
$NADP^+/H^+$	nicotinamide adenine dinucleotide phosphate
nDNA	nuclear DNA
NER	nucleotide excision repair
NF-κβ	nuclear factor kappa-light-chain-enhancer of activated B cells
NO•	nitric oxide
$OH^\bullet$	hydroxyl radical
$ONOO^-$	peroxynitrite
$^1O_2$	singlet oxygen
$O_2^{\bullet-}$	superoxide anion
qPCR	quantitative polymerase chain reaction
RIN	RNA integrity number
RNA	ribonucleic acid
RNS	reactive nitrogen species
ROS	reactive oxygen species
SED	standard erythemal dose
SOD	superoxide dismutase
TMRE	tetramethyl rhodamine ethyl ester
UV	ultraviolet (280 – 400 nm)
UVA	ultraviolet A (315 – 400 nm)
UVB	ultraviolet B (280 – 315 nm)
VIS	visible light
Wnt	wingless-related integration site
8-OHdG	8-oxo-7, 8-dihydroguanine

Acknowledgements

The work in this thesis was supported by the Biotechnology and Biological Sciences Research Council (BBSRC) and CRODA.

I would like to thank CRODA for providing not only funding for this project but support for my academic and personal growth and development. My industrial supervisor, Dr Bhaven Chavan, has provided insight throughout which has undoubtedly benefited the project. I am grateful for his time and efforts towards this.

I would like to thank Professor Mark Birch-Machin for providing me with this PhD opportunity and for the freedom to influence and pursue the direction of research I wanted. To the current and previous members of the research group, Dr Roisin Stout, Dr Lizzie Ruddy, Dr Gewei Zhu, Wil Reynolds, Dr Amy Bowman, Dr Rebecca Hanna, Dr Eyman Rashdan and Dr Matthew Jackson thank you for your support throughout the project, and Dominic Pangilinan for his contribution in doing the lab work forming part of section 3.3.1.

To my family and friends, thank you for supporting me through the highs and lows, and for forgiving my intermittent communications. Dad and Rosin, thanks for proof reading.

Finally, thank you Dr Owen Williams, for putting up with the highs and lows of stress and workload, for supporting the final efforts of writing and for being so understanding.

Table of Contents

Contents

List of Figures

List of Tables

Chapter 1 Introduction

1.1 Skin

1.1.1 Dermis and epidermis

The skin is the largest organ in the human body. It is made up of layers, starting with the outermost stratum corneum, underneath which lies the epidermis, dermis then hypodermis (Figure 1-1). Our skin protects us from external insults such as sunlight, pollution, toxic chemicals, mechanical damage and infectious microbes. However, it can itself be damaged by such insults. DNA strand breaks, oxidative stress and the secretion of pro-inflammatory signals are some of the effects that can be caused by external factors (Birch‐Machin and Bowman, 2016). The resulting damage is not always totally repaired. The accumulation of damage from these insults results in a loss of structure and function, leading to the pronounced wrinkles and pigmentation characteristic of extrinsic skin ageing. This "extrinsic ageing" is different to intrinsic skin ageing which is inevitable and largely a result of genetics (Blume-Peytavi et al., 2016a). Extrinsic skin ageing leads to prematurely aged skin with increased susceptibility to diseases such as cancer (Hudson et al., 2016). As much as 80% of visible ageing in facial skin has been attributed to extrinsic factors, primarily sunlight (Kammeyer and Luiten, 2015).

Beneath the epidermis lies the dermis. These are attached by the dermal-epidermal junction which is important for signalling and cohesion between the two layers (Langton et al., 2016). There are two layers of the dermis. Directly underneath the epidermis lies the papillary dermis, which is more densely populated with cells and blood vessels than the underlying reticular dermis, which is more dense with connective tissue. The dermis also contains hair follicles and sensory neurons. A healthy dermis is comprised of fibroblast cells which produce an extracellular matrix (ECM) made up of collagen, elastic fibres, proteoglycans and glycosaminoglycans (GAGs) (Haydont et al., 2019). Its role is to provide a strong and flexible layer of protection for the underlying structures. Collagen accounts for approximately 70% of the adult dermis dry weight, and the collagens found are primarily collagen type I (85%) followed by type II and type V, and small amounts of other types (Oikarinen, 1994, Waller and Maibach, 2006). The collagen fibres form a large network, which provides structure to

the skin. Alongside this is the elastic network, which allows the skin to return to its original place after being stretched. GAGs are large molecules of polysaccharide chains which bind to water and provide plumpness in the skin. Hyaluronic acid is the most abundant GAG in the dermis (Juhlin, 1997).

Fibroblast cells in the dermis are responsible for the generation and maintenance of the ECM, and also have roles in hair development, wound healing, fibrosis, psoriasis and skin cancer (Sorrell and Caplan, 2004). They interact with endothelial cells, epithelial cells, adipocytes, neurons, inflammatory cells and stem cells through cell-cell communications and through cytokines and grown factor secretion (Sriram et al., 2015). Fibroblasts within the dermis are not heterogeneous, as demonstrated by the fibroblasts of the papillary dermis creating a thinner, looser ECM compared to the denser reticular ECM. In vitro, papillary fibroblasts proliferate at a higher rate than reticular fibroblasts, and in collagen matrices reticular fibroblasts are faster to cause contraction (Sorrell et al., 2004, Sorrell et al., 1996).

With intrinsic ageing, the collagen and elastic networks of the dermal extracellular matrix become more fragmented (Blume-Peytavi et al., 2016b). Hyaluronic acid becomes less abundant, and the thickness of the dermal layer is decreased. This results in wrinkles, loss of elasticity and reduced wound healing capacity. The turnover of ECM components is slow compared to molecules within cells, with an approximate collagen half-life of 15 years, allowing for the accumulation of damage over time (Verzijl et al., 2000). Extrinsic ageing results in enhanced deposition of elastic fibres, leading to skin becoming yellowed, thickened and coarsely wrinkled (Heng et al., 2014). The severity of elastosis is correlated with exposure to sunlight (Kligman, 1969).

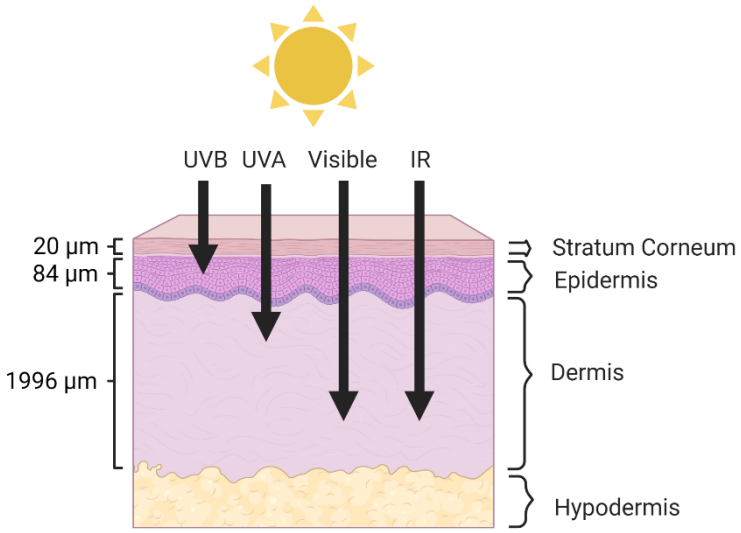

Figure 1-1 Schematic of skin structure.
Created with BioRender.com.

1.1.2 Mitochondria

Mitochondria are organelles of 0.5 – 1 µm that can be found as individual structures within cellular cytoplasm or connected in a mitochondrial network. They have an inner and outer membrane which separates the matrix inside the inner membrane from the intermembrane space. This allows the maintenance of an electrochemical gradient across the inner mitochondrial matrix, which is established by the electron transport chain (ETC) complexes located there and drives the formation of adenosine triphosphate (ATP) by ATP synthase (Figure 1-2). The ETC is a system that allows electrons to be transported from the protonated nicotinamide adenine dinucleotide (NADH) or protonated flavin adenine dinucleotide ($FADH_2$) donors, along the chain of complexes. The energy released by this electron transfer is to be used to pump protons into the matrix, setting up the electrochemical gradient. ATP synthase harnesses this potential energy to form ATP by allowing protons through its pore, which releases the energy required for its conversion from adenosine diphosphate (ADP). The mitochondrial matrix contains NADH and $FADH_2$, the electron donors for the ETC, themselves products of the citric acid cycle that takes place within the matrix.

Though the electron transport chain is efficient, with 98% of the oxygen used leading to ATP production, there is some electron "leak" in the form of ROS rather than ATP from the remaining 1 – 2%, which forms 90% of the ROS produced by the cell under normal

circumstances (Chance et al., 1979). These electrons react with molecular oxygen at complex I or III, leading to the formation of superoxide radicals (O_2^-) (Miwa et al., 2003, Han et al., 2001, Muller et al., 2004, Quinlan et al., 2012, Held, 2012, Murphy, 2009). These radicals are poorly reactive themselves, but can lead to the formation of reactive oxygen species. Superoxide dismutase in the intermembrane space or matrix converts superoxide radicals into hydrogen peroxide (H_2O_2) which can then be converted into water by glutathione peroxidase or catalase, cross the mitochondrial membranes and enter the cytoplasm of the cell. If unbound ions of iron or copper are available however, H_2O_2 will react to generate the hydroxyl radical (OH^-) which is highly reactive with many biological molecules. It will cause damage to lipids, proteins, carbohydrates, amino acids and DNA, but unlike superoxide it cannot be enzymatically neutralised (Reiter et al., 1995). When radicals react, they create new radicals which can themselves be damaging. Such is the case with lipid peroxidation, which can lead to a chain reaction by which the oxidised fatty acid can remove an electron from a neighbouring unsaturated fatty acid, causing this to now be oxidised. Other radicals that can be produced from H_2O_2 include singlet oxygen ($^1O_2$) and reactive nitrogen species (RNS) nitric oxide (NO•) and peroxynitrite ($ONOO^-$).

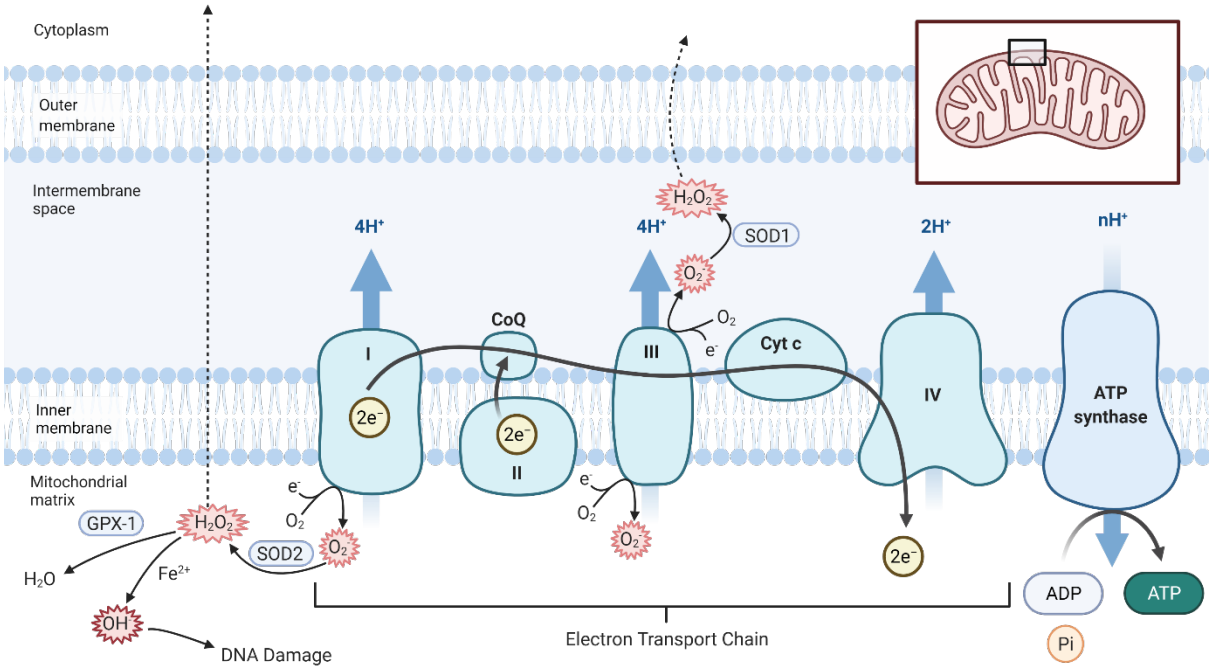

Figure 1-2 Diagram showing origin of ROS from mitochondrial electron transport chain.
Image credits: Improta and Douki 2021,(Improta and Douki, 2021)

When the production of ROS overwhelms the cell's antioxidant capability this results in a redox imbalance which leads to damage to many biological molecules, and the cell is said to be in a state of oxidative stress. The cell may recover, though some damage may remain, or it may lead to apoptosis or necrosis. UV damage is due mainly to ROS initially after irradiation, though reactive nitrogen species such as nitrogen dioxide radicals may contribute to UV damage (Terra et al., 2012, Opländer et al., 2007).

While ROS can be damaging, they also act as essential signalling molecules in cells. Processes such as the inflammatory response, cell differentiation, mitogen-activated protein kinase (MAPK) signalling and pro-apoptotic signalling involved ROS, and elevated ROS activates the nuclear factor erythroid 2-related factor 2 (Nrf2) which regulates the expression of antioxidant genes (Yanes et al., 2010, Finkel, 2011, Fang et al., 2016 , Ray et al., 2012, Imhoff and Hansen, 2009, Formentini et al., 2017). In skin, ROS is necessary for normal epidermal function, without which keratinocyte differentiation abnormalities lead to skin barrier defects, improved by the addition of H_2O_2 (Hamanaka et al., 2013). The positive effects of low concentrations of ROS in cells, while high concentrations lead to damage, is termed

mitohormesis (Yun and Finkel, 2014, Ristow and Schmeisser, 2014). A negative feedback loop in the mitochondrial inner membrane allowing proton leak diminishes the electrochemical gradient and thus ETC activity and ROS production (Brand, 2000, Mailloux and Harper, 2011).

1.1.3 Mitochondrial DNA

While the majority of cellular DNA is stored in the nucleus of the cell, the mitochondria have their own DNA (mtDNA) stored in nucleoids tethered to the inner mitochondrial membrane. Each nucleoid consists of 2 – 8 mtDNA molecules, and each mitochondrion may have 1 – 11 nucleoids. A cell may have one or thousands of copies of mtDNA depending on the tissue (Garrido et al., 2003, Veltri et al., 1990, Shadel and Clayton, 1997). mtDNA codes for 13 proteins, 22 tRNAs and 2 rRNAs, all synthesised within the mitochondria (Figure 1-3). Additional mitochondrial genes are coded in the genomic DNA in the cell nucleus. Given its proximity to the source of mitochondrial ROS, the ETC, mtDNA is particularly at risk of oxidative damage compared to nuclear DNA. Furthermore, it lacks protective histones, and its repair machinery is more limited, leading to a greater burden of mutation. The higher burden of damage and limited repair mechanisms lead mtDNA to have an approximately 10-fold higher rate of mutagenesis (Brown et al., 1979). This can itself lead to ETC components being incorrectly produced, and result in greater ROS production by reducing the efficiency of the ETC. This can further damage both ETC components and mtDNA, which can lead to a cycle of damage. A single mutation of mtDNA does not necessarily have disastrous consequences. The number of mtDNA copies in a cell would mean that undamaged DNA would still be present for the transcription of mitochondrial genes. This allows mitochondria to continue to function with higher levels of mutation than nuclear DNA can (Khrapko et al., 1997).

While some damage can be repaired, high levels of mutation lead to mitochondrial dysfunction. This can be managed through mitophagy, a process by which dysfunctional mitochondria are removed from the cell, allowing only properly functioning mitochondria to remain and thus reducing the mtDNA damage of the cell (Gebhard et al., 2014). Oxidative stress can also lead to apoptosis, so if the mitochondria are that badly damaged then the

affected cells would undergo apoptosis, so on a tissue scale the mtDNA damage burden would be reduced (Bess et al., 2012).

Mutations in mtDNA are more frequent than those in nuclear DNA, and some patterns of mutation are common. The 4977 base pair “common deletion” deletes polypeptides from complexes I, IV and V and 5 mitochondrial tRNAs. This has been shown to increase ROS release and oxidative stress (Birch-machin et al., 1998, Indo et al., 2007). The 3895 deletion is associated with UV damage in skin cells, and has been found to be more frequent in the dermis than epidermis (Powers et al., 2016, Krishnan et al., 2004, Harbottle et al., 2010, Harbottle and Birch-Machin, 2006). It has also been linked to macular degeneration in retinal cells (Gendron et al., 2013). The T414G transversion point mutation can also be used as a biomarker of sun exposure in skin, though it is not thought to affect ROS (Chinnery et al., 2001, Michikawa et al., 1999, Birket and Birch-Machin, 2007, Birket et al., 2009). Other deletions include the 3715 base pair deletion and 6247 base pair deletion (Eshaghian et al., 2006). Though the specific effects are unknown, the deletions overlap with the 3895 and 4977 base pair deletions respectively, so it is possible that they have similar effects on ROS production. Tandem duplications in the D-loop of the mtDNA molecule have also been found, and are thought to be associated with ageing (Krishnan and Birch-Machin, 2006, Wei et al., 1996). Other mutations, which are not location-specific, include 8-oxoG mutations which can lead to mitochondrial dysfunction, senescence and apoptosis (Oka et al., 2008, Chen et al., 1995, Dobson et al., 2000).

One type of mtDNA damage that can lead to mutations is strand breaks. These can be single strand breaks, where only one of the DNA strands is broken, or double strand breaks, where both strands are broken. These can be repaired, though this can result in mutations where the repair was incorrect (Krishnan et al., 2008, Nissanka et al., 2019). Alongside mtDNA mutation assays, it is also possible to assay strand breaks, which can be useful for understanding mtDNA damage and repair (Hunter et al., 2010, Hanna et al., 2019). Strand breaks can be caused by both UVA and UVB, making it a useful assay to understand UV-induced DNA damage (Wischermann et al., 2008, Svobodová et al., 2012).

The free radical theory of ageing, initially proposed by Harman, that the accumulation of oxidative damage is responsible for ageing (Harman, 1956, Harman, 1992). As such, the greater the production of free radicals, the greater the rate of ageing within a cell or tissue. This has been developed further into a mitochondrial free radical theory of ageing, which suggests ROS from mitochondria are the source of this oxidative damage, causing DNA mutations such as the 8-hydroxy-2'-deoxyguanosine (8-OHdG) DNA mutation which accumulates with age causing the ageing phenotype (Fraga et al., 1990). This theory is relevant to ageing in the skin, as UVB and UVA light both lead to mtDNA damage and photoaging in the skin.

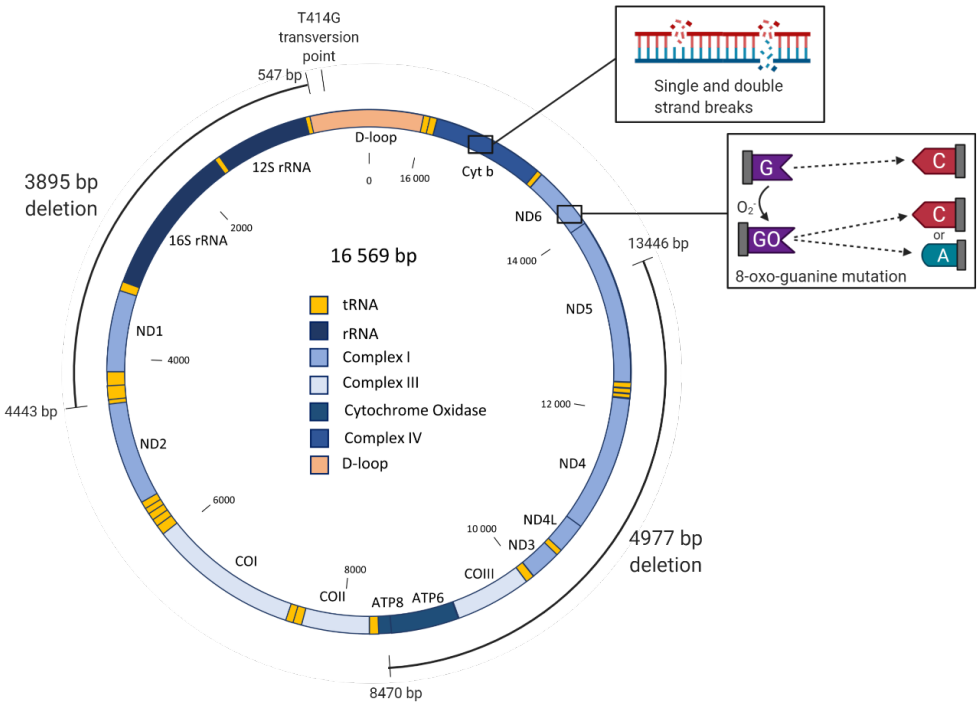

Figure 1-3 Mitochondrial DNA loop showing common mutations.
(Improta and Douki, 2021) Created with BioRender.com

1.2 Solar light

1.2.1 Overview

Solar light consists of UV, visible and infrared wavelengths, with approximately 6% of the light that reaches Earth's surface being UV, 52% visible and 42% infrared (Diffey, 2015). However, calculating the irradiance of light that is actually received by our skin is a more

complex task. The spectrum of solar light that is incident on skin is dependent on many variables. The latitude, time of day and time of year affect the intensity and angle of solar radiation, and then clouds, ozone, humidity, height above sea level, aerosols, pollution or other particulate matter can affect the spectrum of incident light. The angle of incidence affects the distance the light has to travel to get deeper into the skin, thus increasing how much is absorbed by each layer. Furthermore, objects such as buildings and trees, surrounding surfaces which reflect light, clothing and finally sunscreens and makeup change the spectrum of incident light, as does posture the area on the body on which the light is incident, as this will affect the angle of incidence and irradiance of light.

The solar spectrum does not penetrate skin equally either, so when trying to calculate the light that would be received by a certain tissue such as the dermis, this must be considered (Finlayson et al., 2021). Much of the UVB light is absorbed by the stratum corneum, which varies in thickness between individuals and body sites, and can thicken in response to UV light (LockAndersen et al., 1997, Sandby-Moller et al., 2003, Chirikhina et al., 2020). This means the penetration of light into skin can vary within the same individual and same body site at different times of year say. Finlayson et al have created a model calculating the penetration of solar wavelengths into skin, assuming a 20 µm stratum corneum, 64 µm epidermis, 10 µm melanin layer, 10 µm basal layer and 1996 µm dermis above a subcutaneous fat layer for Fitzpatrick type I skin. This model suggests that less than 40% of direct light in the UVB waveband penetrates the stratum corneum, and less than 5% of this travels through the epidermis to the top of the dermis. UVA penetrates further, with up to 85% of light getting to the epidermis and 27% getting to the dermis. However, much of the UV light that enters skin does not enter directly at 90° but rather at an angle, at which penetration will be less.

1.2.2 UV

Ultraviolet (UV) light has been long known to damage skin. It can cause sunburn, tanning, photoaging and cancer (Matsumura and Ananthaswamy, 2004). Short-term effects include immediate pigment darkening, erythema, perivascular infiltration and immune suppression, followed by hyperplasia of the epidermis (Scott et al., 2012, McGregor, 1999). Melanocyte

activity and number increase after UV doses, leading to delayed tanning. The accumulation of damage leads to photoaging, which is associated with deep wrinkles, dyspigmentation, telangiectasia and loss of elasticity.

Compared to the other wavelengths of light from the sun that make it through the atmosphere, visible and infrared, UV light has the highest energy per photon. The spectrum of UV light that arrives on earth can be split by wavelength into two regions, ultraviolet B (UVB, 280 – 315 nm wavelength) and ultraviolet A (UVA, 315 – 400 nm wavelength). Skin damage by UV occurs through the absorption of photons by chromophores. When a chromophore absorbs light, it can either be directly damaged by the structural alteration caused by the photon, or it can act as a photosensitiser to cause damage indirectly, such as by the production of ROS. DNA is a chromophore for UVB particularly, the absorption of which directly causes damage which can lead to mutation. Other chromophores include urocanic acid, found in the stratum corneum which absorbs UV with a peak at 345 nm, amino acids tryptophan and tyrosine in proteins, and melanin (Hanson and Simon, 1998, Young, 1997).

An erythemal action spectrum which weights UV wavelengths by their ability to generate erythema, and is used to define a standard erythemal dose as 10 $mJ.cm^{-2}$ (100 $J.m^{-2}$) of erythemally-weighted UV (McKinlay, 1987 , Webb et al., 2011). The SED itself is used to calculate the UV index which informs people of the risk from UV on a given day and time. Originally, UVA was not accounted for in the action spectrum as it is less able to generate erythema compared to UVB, however UVA has now been included in modern calculations. The calculation of SED doses from a light source is possible when its irradiance spectrum is available, allowing the standardisation of erythemally-weighted doses from different light sources in laboratories and to be able to better compare these to real sunlight exposure.

UVA and UVB are defined by their wavelengths, and their biological effects can be broadly separated. However, they both exist on a spectrum, so there is overlap between their absorbance by chromophores and their biological effects. Both can cause erythema in skin, though UVB is much more powerful in this regard. UVB is primarily absorbed in the stratum corneum and epidermis and causes damage mainly through absorption by DNA, causing

molecular changes to generate photoproducts such as cyclobutene pyrimidine dimers (CPDs) and 6-4 photoproducts which are both highly mutagenic. UVB induces an inflammatory response through cytokines and vasoactive mediators which result in sunburn. Keratinocytes that have received damage which exceeds a threshold undergo apoptosis, while others go into cell cycle arrest to allow for DNA repair. Subsequently, epidermal growth is enhanced, leading to epidermal thickening and increased protection against further UV exposure.

UVA penetrates further into the dermis, where it is primarily absorbed by other chromophores to cause indirect damage through the generation of ROS. ROS can also cause DNA damage, as DNA is reactive with free radicals. This causes mutations such as the 8-OHdG mutation, which is formed from guanine but can pair with adenine instead of cytosine, resulting in a mutation to T/A from G/C (Drobetsky et al., 1995). UV exposure leads to changes in pigmentation of skin, including immediate pigment darkening, persistent pigment darkening, delayed pigmentation and long-lasting pigmentation, which are processes which start and endure at increasing intervals after exposure (Coelho et al., 2009).

1.2.3 Intrinsic and extrinsic ageing in skin

Ageing in skin is driven by two separate processes: intrinsic and extrinsic ageing. Intrinsic ageing is an inevitable process which is largely driven by genetics. In skin, this phenotype presents as a thinning of the skin, fine wrinkling, and loss of elasticity (Blume-Peytavi et al., 2016a). Extrinsic ageing occurs as a result of accumulated damage by external insults. In skin, this includes factors such as sunlight and pollution. The accumulation of damage from these insults results in a loss of structure and function, leading to the coarse wrinkles and pigmentation characteristics of extrinsic skin ageing. This leads to prematurely aged skin with increased susceptibility to diseases such as cancer (Hudson et al., 2016). As much as 80% of visible ageing in facial skin has been attributed to extrinsic factors, primarily sunlight (Kammeyer and Luiten, 2015).

Photoaging refers to the extrinsic ageing caused by sunlight. The generation of ROS in skin by UV light leads to increased expression and activation of transcription factor activator protein 1 (AP-1), which increases the expression of matrix metalloproteinases (MMPs) (Berneburg et al., 2000). Nuclear factor-κB (NF-κB) is also activated, leading to an inflammatory response

including the recruitment of ROS-producing neutrophils, compounding the effects of UV-induced ROS. The action of matrix metalloproteinases in the ECM results in the breakdown of the collagen and elastin in the dermis, which is not then repaired to its original formation. This leads to photoaged skin having shortened collagen fibres and an accumulation of elastin fibre bundles called solar elastosis (Sander et al., 2002), resulting in the coarse wrinkles of the photoaged phenotype.

1.2.4 Infrared

1.2.4.1 Infrared in skin

Infrared from the sun forms 42% of the light that reaches Earth, though the photons have much less energy compared to visible or UV photons. This means that they do not act in the same way as UV, though it has been suggested that the infrared component of sunlight may still have effects on skin. Due to its lower absorbance in skin, infrared penetrates into the dermis at high intensities, easily 90% of the incident intensity although its absorbance and this intensity is wavelength dependent (Finlayson et al., 2021). Compared to UV, the irradiance of infrared in the skin is much higher. Infrared A (IRA, 780-1400 nm) is widely described as being more biologically relevant than infrared B (IRB, 1440-3000 nm) which is the more relevant to the heating of water in skin. At its peak on Earth, infrared (780-3000 nm) does not exceed 48 $mW.cm^{-2}$, and IRA does not exceed 36 $mW.cm^{-2}$ (Diffey and Cadars, 2016).

Human skin temperature varies, depending on factors such as the area of the skin, age, gender, current activity, fitness, subcutaneous fat, time and content of last meal, time in circadian rhythm, external air temperature, humidity and speed, and individual differences. It tends to lie around 32-35°C in “normal” conditions (Freitas, 1999). However, these can vary hugely, which may be relevant when considering the effects on IR as different populations will have different skin temperatures when in the sun. 43°C is generally considered the threshold for thermal damage and heat pain (Zhu and Lu, 2010).

Infrared is the light responsible for the warming of the skin, and the sensation of warmth from the sun comes from the absorbance of infrared by water in the skin and increasing its temperature. The biological effects of infrared light must act through one of three ways;

absorption by chromophores causing direct photochemical effects (the same mechanism as UV effects), by globally increasing skin temperature, or by increasing temperature locally within cells. Alternatively, it may interact with the biological effects of other wavelengths such as UV to modulate its effects. Skin surface temperature is increased by sun exposure, but typically not above 34-36°C (Kurazumi et al., 2014, Petersen et al., 2014, Cho et al., 2008). This has been suggested to be a factor in damage induced by UV, though this is perhaps only relevant at temperatures above 37°C (Bain et al., 1943, Zastrow et al., 2009, Boukamp et al., 1999). The control of temperature in studies of infrared irradiation varies drastically, with some papers having no mention of temperature control at all (Schroeder et al., 2007, Schroeder et al., 2008).

The range of irradiation protocols is very wide. Laser pulse experiments can deliver low doses but over such short times with very high irradiances. One study used delivered a 1.5 $J.cm^{-2}$ dose of infrared, which could be delivered in approximately 40 seconds by the sunlight, but over 5 ns at an irradiance of 3×10^{11} $mW.cm^{-2}$ (Kim et al., 2018). The result was increased expression of collagen I and III, and decreased MMP1, but this is not easily comparable to the irradiation from sunlight. Further complication comes from the use of pulsing lasers, with varying “on” and “off” durations, which deliver lower doses over the same duration as lights with the same irradiance which are constantly on rather than pulsing.

1.2.4.2 Infrared and heat

There are known effects of heat on skin, separate from infrared effects. In 1967 erythema ab igne, a skin condition caused by repeat exposures to high heat such as that from a peat fire, was found to be associated with squamous cell carcinoma and skin ageing phenotype (Cross, 1967). Erythema ab igne, and thus heat, has been associated with elastic fibre hyperplasia and degradation of dermal collagen (Shahrad and Marks, 1977). Heating skin to 43°C in vivo has been found to increase the production of elastin components and elastin degrading MMP-12 in vivo in human skin, suggesting that this could be the cause of the unusual elastin deposition seen by Kligman in 1982, who found infrared to cause damage by itself as well as to amplify that from UV, although skin temperature was seen to rise to 40°C during

irradiations (Chen et al., 2005, Kligman, 1982). Collagen degrading enzymes MMP-1 and 3 have both been induced by heat (Park et al., 2004). Suggested pathways of this induction involve activation of the ERK and JNK pathways by release of IL-6 and autocrine signals at 43°C in human fibroblasts. At 44°C TRPV1 is activated in human keratinocytes, mediating MMP-1 upregulation (Li et al., 2007). This may be through calcium-dependent PKCα signalling (Lee Young et al., 2008). As TRPV1 can be sensitised, it could be possible that this could be activated at lower temperatures in already sunburned skin for example, which is known to be sensitive to heat (Gniadecka et al., 1996). Treatment of hairless mice with chronic heat at 43°C increased wrinkling, induced MMP-13, reduced antioxidant enzyme levels and increased markers of oxidative damage such as protein oxidation and lipid peroxidation (Shin et al., 2012). A direct comparison of water-filtered IRA (wIRA) and heat by Knels et al. showed that increasing temperature to 45°C was necessary to observe apoptotic heat effects on fibroblasts, and that at neither physiological nor high temperatures did wIRA at 30 mW/cm^2 have any effect on apoptosis (Knels et al., 2012). Apoptosis is not, however, the only outcome of damage. One paper by Kim et al compared the effects of IR and heat in vivo in humans (Kim et al., 2006b). The comparison was not completely direct – the irradiation time (67 +/- 3 minutes) was less than the heating time (90 minutes) and differed between individuals depending on the dose it took for their skin to reach a constant temperature (the minimal heating dose). Infrared induced greater vessel density and area covered by vessels at 48 hours post-exposure. Heat alone induced greater vessel size. Stable skin temperature during the irradiation with infrared was 42.1°C from 32°C initially, and heated skin was to 43°C, so it is unknown whether infrared would have the same effect without concurrent heating.

In-vivo experiments have been carried out in humans by the Chung group, who showed increased MMP-1 and decreased procollagen expression with repeated IR doses (Kim et al., 2006a). This study used an IR intensity of 2020 $mW.cm^{-2}$, far higher than sunlight levels, and did not control for heat. They suggested a measure of IR as the minimal heating dose or MHD – the dose required to heat the participant's skin to a stable temperature (Lee Hyoun et al., 2006). This caused skin to reach 40-42°C under the intense IR conditions, which is very high for human skin and would not occur under normal circumstances by solar light.

In addition to temperature, an additional confounding factor in infrared irradiation studies is irradiance. Many studies use irradiances in the order of 333 – 1000 $mW.cm^{-2}$, 8 to 27 times the irradiance from the sun. In 2002 a paper from the Krutmann group showed that fibroblasts irradiated with IR light in vitro increased MMP-1 mRNA and protein expression after irradiation with wIRA (Schieke et al., 2002), concluding that SRK-1/2 activation was necessary in this process. They saw no detectable increase in temperature and no induction of heat shock proteins (HSPs). However, they irradiated the cells with an IRA light intensity of 333 mW/cm^2. As this is so far above physiological exposures, it is impossible to conclude that the effect and mechanism would be the same in sun-exposed skin. Also, heat alone has been shown to induce MMP-1, and some have suggested that heat may still be increased (Park et al., 2004, Shin et al., 2008). Further published work from 2007 in fibroblasts showed that at 105 mW/cm2, an increase of greater than 400% of MMP-1 mRNA could be induced by wIRA (Schroeder et al., 2007). This was through ETC ROS production, a mechanism different to both UVA and UVB damage. This is still however at a higher light intensity than would be received outside, as pointed out in a letter by the Piazena group (Piazena and Kelleher, 2008). Krutmann's rebuttal to Piazena stated that as they used a monolayer and about 90% of the infrared was transmitted through the flask and thus unabsorbed by the cells, the remaining 10.5 $mW.cm^{-2}$ that was absorbed was similar to that absorbed in vivo (Schroeder and Krutmann, 2008).

Doses of 360 $mW.cm^{-2}$ have been in continuous use by Krutmann's group (Calles et al., 2010, Buechner et al., 2008, Grether‐Beck et al., 2015), demonstrating increased MMP-1 expression and the ability to protect skin from this IR intensity in-vivo with antioxidants. One study looking at keratinocytes with a HaCaT suspension showed an increase of 10% in ROS after irradiation and a decrease in the endogenous antioxidant glutathione. The infrared intensity was 24 $mW.cm^{-2}$, and cells were irradiated for half an hour, but in this case, infrared was used in conjunction with visible light, which has itself been implicated in ROS generation (Liebel et al., 2012).

An in-vivo study used natural sunlight and a UV filter to allow exposure to only IR and visible from the sun together (Cho et al., 2008). MMP-1 was increased by 15% compared to the

cloth-covered skin control, whereas complete sunlight increased it by over 500%. Compared to normal, pre-irradiation skin, the cloth control also had double the MMP-1 mRNA. Temperature was not completely consistent however as the skin under unfiltered solar light reached 36.4 ± 1.6°C. Type-1 procollagen was decreased by solar light – by 86% in unfiltered light, 44% in UV filtered light and unchanged under the cloth. This suggests that visible, IR or visible + IR from the sun together may contribute to a change in the collagen matrix, be this by absorption by chromophores and/or heating effects.

Tumourigenesis in mice was found to be unaffected by a repeated dose of wIRA equivalent to 1-2 hours in the sun (though light intensity and exposure duration were not stated) (Jantschitsch et al., 2011). However, the aggressiveness was seen to be increased in the wIRA exposed mice, increasing proliferation markers and the in vitro proliferation of tumour cells from non-epithelial (but not epithelial) tumours.

Different skin types can be differently affected by UV, but this has also been seen in longer wavelengths. IR scattering was found to be affected by Fitzpatrick skin type below 900nm through the effects of melanin but was unaffected above 900nm where water effects dominate (Piazena et al., 2017). When people with Fitzpatrick skin type V and IV were compared to type II skin, on which most work regarding effects of light in skin has previously been carried out, it was found that while UV caused comparatively less radical production, infrared at close to physiological irradiance (61 $mW.cm^{-2}$) caused greater radical production over 6 minutes as measured in vivo with electron paramagnetic resonance spectroscopy (Albrecht et al., 2019).

1.2.4.3 Arguments against effects of infrared

There is some experimental evidence against the hypothesis of a chromophore absorption mechanism rather than a heating effect of infrared light on skin. Piazena et al. conducted IR experiments using a bovine udder system model and an irradiation intensity of 190 mW/cm2, over 5 times higher than from sunlight (Piazena et al., 2014). They found that at 37°C there was no effect on cell viability, inflammation or ROS generation. When heated to 45°C they found a large increase in free radicals, but again no change in viability or inflammation. This is surprising, as this exceeds the 43°C reported lower limit of heat pain

felt in humans, which supposedly increases heat shock protein expression and decreases viability. It may be the case that the bovine ex vivo model is not truly comparable to human skin in vivo, however, the lack of any response to infrared at 37°C indicates that perhaps there is little biological impact other than that through heating.

Other studies have also found wIRA to have no effect on skin cells. Jung et al. found no effect of 245 $mW.cm^{-2}$ on fibroblasts when temperature was controlled (Jung et al., 2010). They suggest that only heat causes any effect on the cell. Karu et al. state the often suggested site of IR absorption, the mitochondrial ETC, only accounts for 0.6% of the IR absorption at 750-780 nm, the rest being largely absorbed by cellular water (Karu et al., 2005). It could be possible that not much IR needs to be absorbed by mitochondrial chromophores to affect the ETC. Experiments carried out at physiologically relevant 30 $mW.cm^{-2}$ infrared intensity on mouse fibroblasts for 1 hour found no effect at 37°C. In fact, 40°C showed little effect; only at 42°C was any decrease in viability found, and only at 45°C was a decrease in mitochondrial membrane potential detected (Knels et al., 2012).

1.2.4.4 Infrared protective sun effects

There have been suggestions that infrared can stimulate the skin to protect itself from subsequent UV light. When fibroblasts in vitro were irradiated with a physiological intensity and dose of infrared (45 $mW.cm^{-2}$ for 30 minutes), there was a protection from a reduction in viability from subsequent UV irradiation (Menezes et al., 1998). Further work from the group suggested the mechanism of this was through the p53 signalling pathway (Frank et al., 2006). Ferritin has been shown to increase in response to infrared irradiation, suggesting protection against oxidative stress by UV (Applegate et al., 2000).

It was found that heating mouse skin to 40°C reduced UV-induced apoptosis (Kane and Maytin, 1995). It could be the case that the heat-induced by infrared has the potential to be protective against further damage, or that the reduction in apoptosis would be a negative thing as more damaged cells would continue to live in the tissue and negatively affect the other cells and overall tissue performance.

1.2.4.5 Infrared as therapy

There is another camp of thought that believes that infrared light is not harmful, and instead believe that the opposite is true. Some further suggest that both can be true; that IR is beneficial at low doses but not beneficial, possibly even detrimental, at high doses in a biphasic dose-response (Karu et al., 2005). This would suggest that both mitohormesis and oxidative stress may be affected, and this may explain some of the differences in results seen between studies of IR in skin.

Photobiomodulation is the use of low intensity visible or infrared light, either constant or pulsed, used for the treatment of various conditions (Barolet et al., 2016). The purported mechanism of action is through absorption of an infrared or red photon by cytochrome c oxidase results in the release of nitric oxide, increased enzyme activity, ATP production and ROS release.

IR, particularly wIRA, has been found useful clinically in wound healing. Wounds are often hypothermic due to their reduced blood supply compared to normal skin, though this itself then constricts vessels to reduce blood supply further, failing to improve the situation. Infrared light can be targeted to areas such as wounds without overheating the rest of the body, unlike merely increasing ambient temperature. Furthermore, its ability to penetrate tissue can increase temperatures more deeply and aseptically than other methods of warming wounds, such as bathing in warm water, which are likely to constitute sources of infection. The increased temperature in the wound increases the oxygen partial pressure and thus tissue perfusion, improving the rate of healing (Hoffmann, 2007). On top of this, there has been demonstrated alleviation of pain, reduced inflammation and increased infection defences with wIRA irradiation. This has shown to be beneficial in both acute and chronic wounds (Hoffmann, 2009). Surprisingly IR has been shown to improve post-operative outcomes with a single pre-operative dose (Kunzli et al., 2013). This suggests that the effects are due to more than immediate temperature effects alone, potentially through influencing angiogenesis or antioxidant balance.

Cosmetic effects of infrared light have been tested. One use of infrared as a treatment to tighten skin in the face and neck area has been proposed (Chua et al., 2007). This involves

slightly elevated irradiances (23-36 mW.cm^{-2} in the study compared to 7-16 mW.cm^{-2} found in sunlight) for the wavelength band they used (1100-1800 nm) but irradiated for only 20 minutes 3 times over 2 months. Skin was cooled but temperature was not measured so may have still been elevated on and under the surface. This was found to reduce skin sagging 3 and 6 months after treatments. Collagen synthesis was hypothesised to be the causative factor, but no biological markers were tested, the only data was from observation of photographs.

One study using a very low IR irradiance of 0.48 mW.cm^{-2} found that 3T3 fibroblasts maintained at 37°C +/- 0.1°C would extend pseudopodia towards an infrared light source over 1-2 hours (Albrecht-Buehler, 1991). This indicated that the wavelengths could have some kind of an effect on cells, even if not related to damage. Potentially this relates to the migratory effect that is thought to occur in therapeutic wound healing with IR.

1.2.4.6 Infrared chromophores in skin

There is evidence that suggests that infrared can be absorbed by chromophores in the skin (Karu, 1999). Cytochrome C oxidase – complex IV of the ETC – in particular has been indicated as an infrared chromophore. One paper found that irradiation of cells with 830 nm light (within the wIRA range) promoted the reduction of oxidised cytochrome C oxidase (Karu et al., 2005). They suggested that this wavelength increased the electron availability within the enzyme, increasing this electron transfer stage. They found an increase in DNA synthesis and cell adhesion to a matrix. How this would relate to cell behaviour in vivo is unclear but that there was a detectable change suggests that this mitochondrial chromophore has the potential to be important in wIRA effects. In addition, as other wavelengths including 620 nm, 680 nm and 760 nm are also absorbed by copper of various redox states in cytochrome C oxidase, the relative proportions of these wavelengths in the incident light to the examined cell layer could be important (Karu and Kolyakov, 2005).

It could however be the case that the absorbance of infrared by skin chromophores does not lead directly to a chemical change with a biological effect, but may instead be dissipated as heat, causing local temperature changes (Karu, 1999). This could change the speed of reactions, such as electron transfer, or conformation of the protein to which the

chromophore is attached, potentially changing its biochemical activity. Should this affect the ETC, it could impact ROS production. This could be beneficial ROS in the case of mitohormesis or damaging in the case of oxidative stress. It could be that IR has the capacity to induce either depending on the conditions (Karu Tiina, 2010). While the biological pathways of these are not fully known, there has been some suggestion that mitochondrial retrograde signalling may be one pathway involved (Schroeder et al., 2007).

While it has been known that information from the nucleus is signalled to the mitochondria, the idea that the reverse also happens is relatively new. It has now been shown to happen in mammalian myocytes and cancers, where information about the functional state of the mitochondria is delivered to the nucleus (Karu Tiina, 2008). This can be through mitochondrial membrane potential, [Ca2+] and ROS. The Krutmann group suggest that IR, but not UV, stimulates MMP-1 induction through this process in skin cells (Schroeder et al., 2007). Mitochondrially targeted antioxidants and ETC blockers reduced wIRA induced MMP-1 upregulation but did not change upregulation by UVA or UVB. This could be due to UVR induction of MMP-1 being mainly through DNA damage (Dong Kelly et al., 2008). This was carried out with a wIRA intensity of 105 mW/cm2, so whether this would occur at a lower, solar light intensity is unknown.

1.2.5 Visible light

1.2.5.1 Visible light and skin

Visible light is the part of the electromagnetic spectrum that can be seen by human eyes, from 400 to 780 nm. In the skin, it can have effects on people with diseases such as solar urticaria, where the skin reddens, and the patient experiences a burning sensation. This can happen in patients in response to UV alone, UV and visible light or visible light alone (Uetsu et al., 2000, Montaudié et al., 2014). This can occur without disease-causing high levels of photosensitising molecules such as porphyrins in the skin, so presumably, the light is being absorbed by chromophores found at normal levels in skin.

The division between visible light and UV is somewhat arbitrary, and the response of skin to light is a function of the wavelength spectrum, so it would be expected that the biological effects of say 401 nm light would not be drastically different to 399 nm light. Because of this

there has been a focus on the blue light end of the visible spectrum which has been shown to be able to cause radical generation in skin cells (Mann et al., 2020, Opländer et al., 2011, Nakashima et al., 2017) but also retinal pigment epithelial cells (Godley et al., 2005, King et al., 2004). When a free radical action spectrum in skin was created it demonstrated the ability of the entire visible light spectrum to generate ROS in skin, and in fact induce up to 50% of radicals in ex vivo skin (Zastrow et al., 2009), with blue light near the UV wavelengths having the greatest potential to generate ROS (Mann et al., 2020). It has been demonstrated to induce oxidative stress which causes DNA damage in CHO cells (Kielbassa et al., 1997). Others have shown blue light to reduce proliferation (Liebmann et al., 2010). When a 100 $J.cm^{-2}$ dose of blue light (irradiance and duration not specified) was delivered to human volunteer skin in vivo for 5 consecutive days it was shown to increase melanogenesis though not DNA damage or apoptosis, which could have been related to ROS generation and signalling (Kleinpenning et al., 2010). Light up to 436 nm was shown to be able to induce melanomas in melanoma-sensitive Xiphophorus (Setlow et al., 1993). It is thought that it can also affect skin in vivo by interfering with the circadian rhythm of the whole organism thus inducing stress in skin (Mahmoud et al., 2008). There has been some suggestion that visible light from screens could negatively impact the skin through pigmentation, though the irradiance from these devices is typically 100 to 1000 times less than that from the sun and has not shown any effects over 5-day exposures in vivo (Duteil et al., 2020).

Other wavelengths have been shown to be biologically active. Green light has also been shown to have a beneficial impact during wound healing, better than red or blue light (Fushimi et al., 2012). Red light, like infrared light, has been implicated in photobiomodulation. Human fibroblasts irradiated with 628nm red light at 11.46 $mW.cm^{-2}$ for 3 minutes with a dose of 2 $J.cm^{-2}$, with temperature control, once a day for three days was shown to cause an increase in cell numbers of 28% (Song et al., 2003). 111 genes were upregulated, particularly in pathways enhancing cell proliferation and inhibiting apoptosis. These effects were not seen above a dose of 4 $J.cm^{-2}$ at the same irradiation level, with cell numbers returning to that of the control. Dose was only tested to 8.68 $J.cm^{-2}$. 632.8 nm, 660 nm, and 670 nm light also modulated cell growth.

Visible and infrared light together were shown to increase MMP1 and decrease collagen production in human skin irradiated by sunlight through a filter which absorbed UV light, though this may have been due to the blue component or heat as the skin reached 36.3°C (Cho et al., 2008). Visible light irradiation was found to induce inflammation markers in vivo (Kohli et al., 2020). Blue light and infrared together have been shown to improve post-surgical wound healing but also improve ageing phenotypes through photorejuvenation (Lask et al., 2005). The conflicting results suggest that the effects of light may depend on irradiation parameters and protocols, where irradiation may show benefit or harm.

1.2.5.2 Visible light chromophores in skin

Chromophores suggested to be responsible for responses of skin to visible light include riboflavin, opsins and cytochrome c oxidase (Pourang et al.). Riboflavin absorbs visible light and can generate ROS as a result (Grzelak et al., 2001). Given the role of flavins in the cells in redox homeostasis, the production of ROS as a result of visible light irradiation could cause oxidative stress responses within cells. Opsin receptors have been found to be expressed in epidermal keratinocytes and dermal fibroblasts, and the silencing of opsin 3, which absorbs both blue and UV light, in keratinocytes was shown to decrease the effect of blue light on differentiation (Castellano-Pellicena et al., 2019). Red light is thought to be absorbed by cytochrome C oxidase, affecting its redox state and thus potentially influencing ROS and ATP production (Karu, 1999, Karu Tiina, 2010).

1.3 Aims

The effect of infrared and visible light from the sun are not fully understood, and the results in the current literature are mixed. This thesis aims to determine the best methodology for irradiation of visible and infrared light for skin cells in vitro and for measuring ROS as a result. The effects of solar irradiances and doses of visible and infrared lights on ROS and gene expression are then compared to those of UV to examine how these light components may affect skin exposed to solar light. It was hypothesised that if infrared did affect cells, it would be evident from the ROS assays and RNA sequencing, and that high and low irradiances may have different effects. It was also hypothesised that visible light, particularly blue light, may have an impact on cells through ROS generation.

Chapter 2 General materials and methods

2.1 General cell culture

2.1.1 Maintenance of HDFn cells

For all cell experiments, neonatal human dermal fibroblast cells (HDFn cells, Invitrogen, UK) were used. Cells were maintained in high glucose Dulbecco's modified Eagles medium (DMEM) containing L-glutamine, phenol red, sodium pyruvate and sodium bicarbonate (Sigma Aldrich, UK). DMEM was supplemented with 10% foetal bovine serum (FBS) and 1% penicillin and streptomycin (Sigma Aldrich, UK), and this is referred to in this thesis as "complete" DMEM, whether phenol-containing or phenol-free. Cells were maintained in a 37 °C, 5% CO_2 humidified incubator and discarded after passage 30. Cells were split 2 to 3 times per week at 70-90% confluency, detached using trypsin-EDTA solution (Sigma Aldrich, UK) and Cell numbers were counted with a haemocytometer. Cells were seeded into 35 mm dishes (TPP, Switzerland) or clear, tissue culture-treated 96-well plates (Corning, US) unless otherwise specified. DPBS used to wash cells was calcium and magnesium-free.

Mycoplasma testing was carried out with either the MycoAlert Mycoplasma Detection Kit (Lonza, Switzerland) or MycoStrip Mycoplasma Detection Kit (InvivoGen, France).

2.1.2 Cell seeding

Unless otherwise specified, the protocol for seeding cells was as follows. In 35 mm TPP cell culture dishes, HDFn cells were seeded at 140 000 cells per dish in 2 ml complete, phenol-containing DMEM. Cells in 96-well plates were seeded at 5000 cells per well. Cells were allowed to adhere overnight in a 37 °C, 5% CO_2 humidified incubator before treatment the following day (either irradiation or washout).

Unless otherwise specified, 35 mm dishes were used for all RNA extractions, DNA extractions, cell counting and flow cytometry. Clear 96-well plates were used for MTS, alamar blue and crystal violet, and white-walled, clear-bottomed 96-well plates were used for ROS Glo and DCFDA in plate assay.

2.2 Irradiation

2.2.1 Solar simulation

A Newport solar simulator (Newport Oriel model 91292, 1000 W, MKS Instruments, Inc., USA) was used to irradiate cells with UV, visible and infrared light in various combinations (except for infrared light alone, which was performed with a Hydrosun lamp, see Section Infrared2.2.3.4). The output of the solar simulator as measured with the FLAME spectroradiometer (see section 2.2.2) can be seen in Figure 2-1 as compared to the solar output as calculated by Diffey (Diffey, 2015) for the global irradiance expected from the sun at solar noon in midsummer in the Mediterranean at 45° latitude.

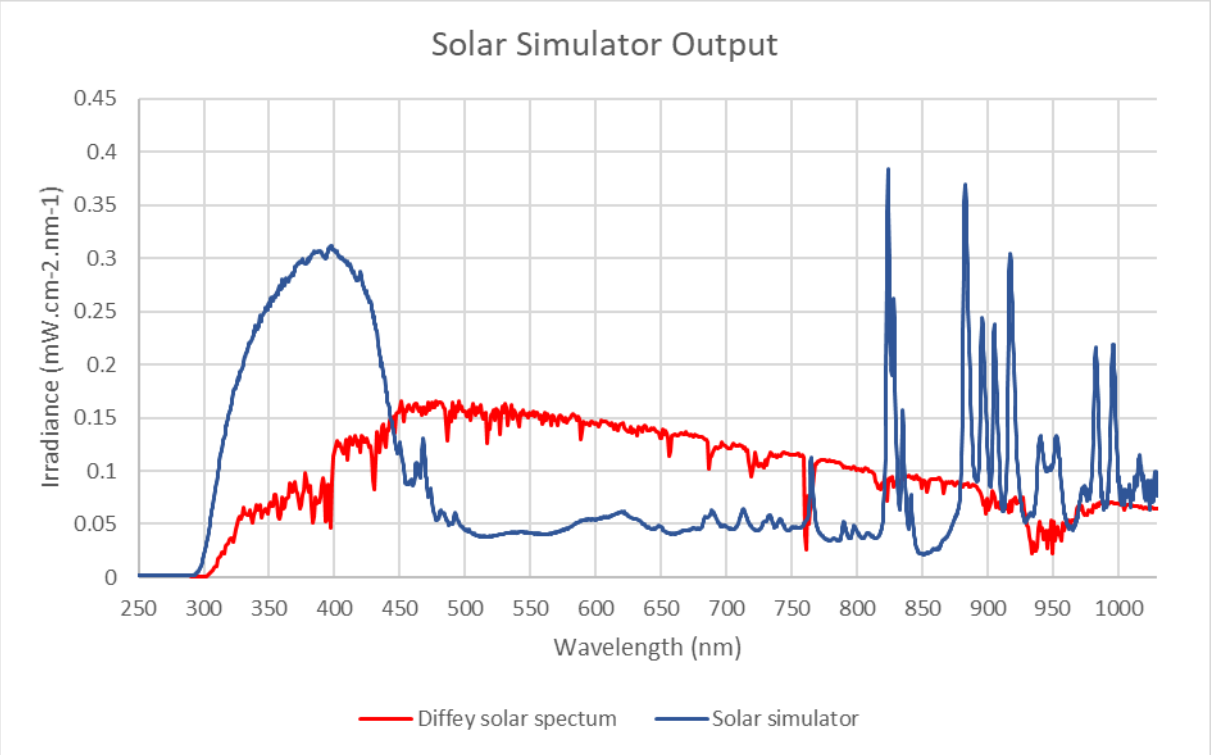

Figure 2-1 Spectrum of irradiation from solar simulator and from sun

2.2.2 Solar simulator calibration

Irradiance from the solar simulator was measured using a FLAME-S-XR1-ES spectroradiometer with CC-3-DA direct-attach cosine corrector with spectralon diffuser (OceanOptics, Netherlands). Calibration to absolute irradiance was carried out by OceanOptics. Measured irradiance from the FLAME spectroradiometer was compared to measurements taken with the Bentham DMc150 double monochromator calibrated to

absolute irradiance (Bentham Instruments, UK). The Bentham instrument has greater sensitivity and a lower limit of detection at low levels of light compared to the (Figure 2-2), allowing better estimation of UV levels below 300 nm. The FLAME spectroradiometer was found to be inaccurate below 290 nm as at wavelengths shorter than this the light levels were below the limit of detection. From the readings made with the Bentham monochromator, it was established that the contribution to the erythemal irradiance of wavelengths below 290 nm was 0.07% of the total erythemal irradiance from the solar simulator. Given this, calibrations made with the FLAME spectroradiometer were made using only data measured above 290 nm.

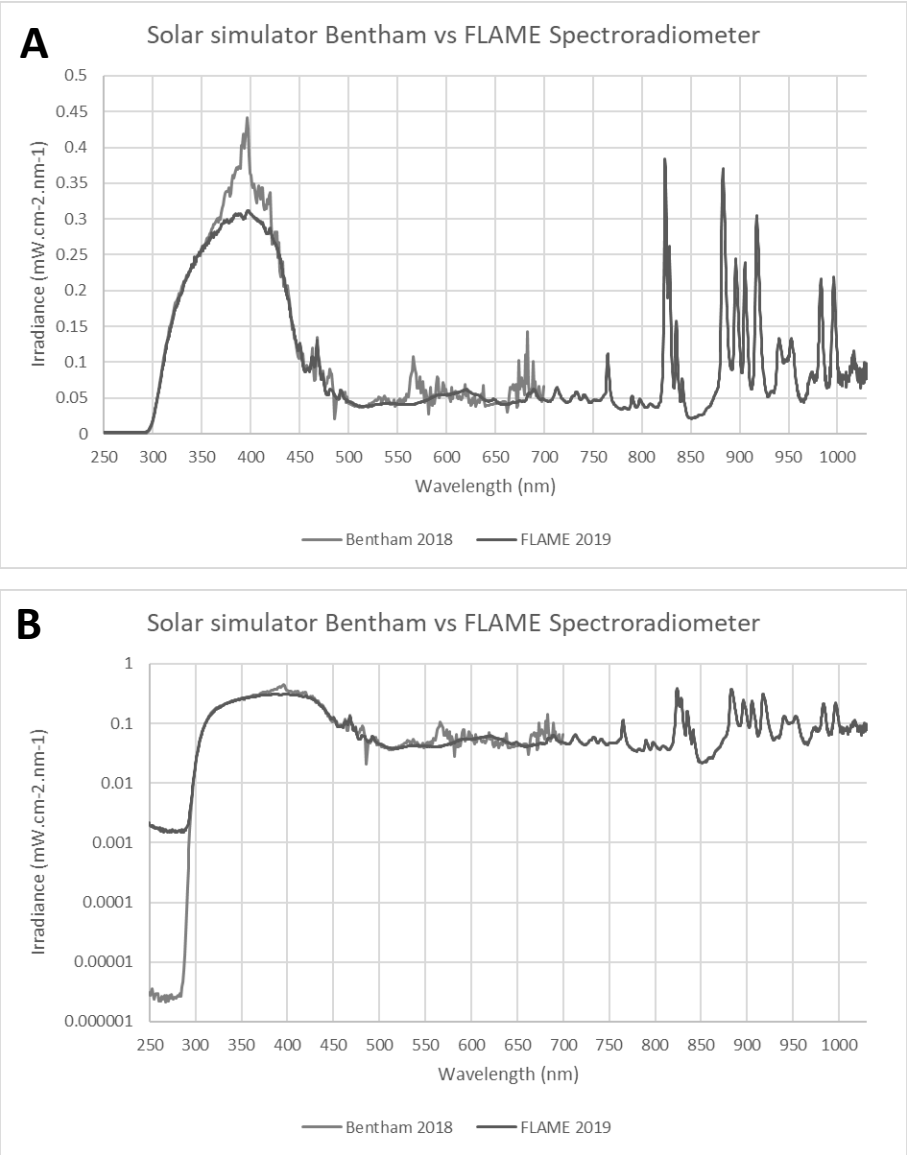

Figure 2-2 Difference in limit of detection in Bentham and FLAME instruments.
FLAME spectroradiometer and Bentham monochromator measurements of solar simulator output on A: linear y-axis and B: logarithmic y-axis. Betham has better sensitivity, FLAME has extended range.

2.2.2.1 SED calibration

1 standard erythemal dose (SED) is equivalent to 10 $mJ.cm^{-2}$ of erythemally-weighted effective UV light. This is calculated using the erythemal action spectrum calculation (Webb et al., 2011). To calibrate the output from the Newport solar simulator, the solar simulator was allowed to warm up for 10 minutes to allow the output to stabilise. The spectrum was measured with the FLAME spectroradiometer at the same distance from the lamp that cells are placed at during irradiations, and the erythemal weighting was applied to the UV

wavelengths up to 400 nm. The time to deliver 1 SED of UV was calculated, and from this the time to deliver 2.16 SED (or other dose, depending on the experiment) using Equation 2, derived from Equation 1 which details the calculation of irradiation duration from desired dose to deliver and known irradiance. To account for daily variations in the output of the lamp, at the same time as the spectral measurement was taken, a measurement was made with a radiometer (model IL1400A, serial 8524 with UVA sensor, serial 867, International Light Technologies, USA). The daily reading on the radiometer after allowing the output from the solar simulator to stabilise was compared to that on the day the calibration was carried out, and the duration of exposure was calculated. Sham irradiated control cells were treated with the same procedures as irradiated cells but covered in foil for the duration of the irradiation. To deliver 1 SED of complete solar simulated light with the solar simulator with no filters, 10 mJ.cm^{-2} of erythemally weighted UV was delivered, or 1172 mJ.cm^{-2} of unweighted UV. The irradiances and relative contributions of UVB and UVA can be seen in **Error! Reference source not found.**.

$$Irradiation\ time\ (s) = \frac{Dose\ (mJ.cm^{-2})}{Irradiance\ (mW.cm^{-2})}$$

Equation 1 *Irradiation duration calculation using mJ.cm^{-2} and mW.cm^{-2}*

$$Irradiation\ time\ (s) = \frac{Dose\ (SEDs)}{Irradiance\ (SEDs/s)}$$

Equation 2 *Irradiation duration calculation using SEDS and SEDs/s*

2.2.2.1.1 UV only condition

For irradiation with UV only, an IR/VIS blocking filter was used (Figure 2-3). This filter blocks the infrared and visible light wavelengths, but also a portion of the UVA. Like with the complete solar light condition, the SED calibration of the UV only condition was calculated using the erythemally weighted wavelengths between 290 and 400nm. As the IR/VIS filter also blocks some wavelengths of UV, irradiations with this filter in would typically take 42% longer, though this was always calculated from the readings taken with the ILT-1400 radiometer with the appropriate filters in place.

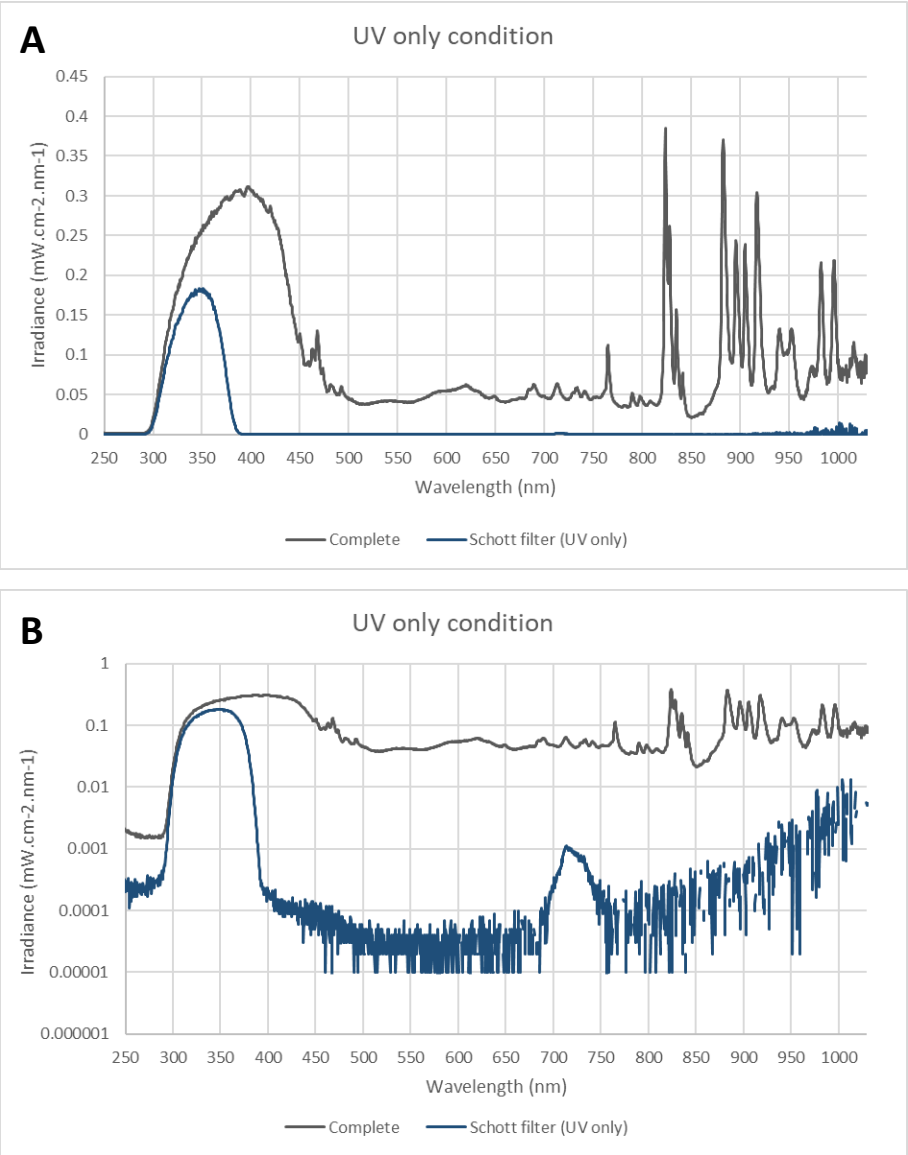

Figure 2-3 Spectrum from solar simulator with Schott UG11 IR/VIS filter.
A shows irradiance graph on a linear scale, B shows logarithmic scale.

The calculation of SEDs delivered per second was done using the spectra recorded by David Rawlings with the Bentham Monochromator because of its greater sensitivity, particularly in the UVB range. This was then used in the irradiation time calculation using Equation 2 for the delivery of UV to cell cultures. It can be seen in **Error! Reference source not found.** that while there is much greater irradiance from the UVA component of light (unweighted) in both complete (no filter) and UV-only (IR/VIS filter) conditions, but UVB accounts for the vast majority of erythemally-weighted light. This is because UVB has a much greater power to

cause erythema, but it would be expected that other forms of UVA damage not related to erythema would be greater in the complete condition rather than the UV-only condition.

Table 2-1 Irradiance from solar simulator with no filter and with IR/VIS filter
UVB: 280 – 315 nm, UVA: 315 – 400 nm. Calculated from spectra recorded by David Rawlings with Bentham monochromator, 2018. 1 SED with no filter would take 47 seconds to irradiate, with a filter would take 67 seconds. 2.16 SEDs would take 101 and 144 seconds respectively. Irradiance is the same for all doses, so this was only filled in once.

			Dose (mJ.cm-2)		Irradiance (mW.cm-2)	
			No filter	IR/VIS filter	No filter	IR/VIS filter
1 SED	weighted	UV (UVB + UVA)	10.0	10.0	0.213	0.150
		UVB	8.6	9.3	0.184	0.129
		UVA	1.4	0.7	0.029	0.020
	unweighted	UV (UVB + UVA)	1172.2	703.2	25.0	10.5
		UVB	52.9	92.4	1.1	0.8
		UVA	1119.3	610.8	23.8	9.7
2.16 SED	weighted UV	UV (UVB + UVA)	21.6	21.6		
		UVB	18.6	20.0		
		UVA	3.0	1.6		
	unweighted UV	UV (UVB + UVA)	2532.0	1518.9		
		UVB	114.2	199.6		
		UVA	2417.8	1319.3		

2.2.2.1.2 Irradiation through a plate lid

For the visible light and infrared irradiations, the irradiation was carried out with the lid of the culture dish or plate in place. For UV irradiation the lid was removed for the duration of the irradiation. The absorbance of light by the plastic of the lid in the visible and infrared wavelengths was minimal as measured through the lid of a 35 mm TPP tissue culture dish (Figure 2-4). When the calibration of the visible light was carried out the measurements were taken with a lid in place above the sensor of the FLAME spectroradiometer, so any effects on the spectrum were accounted for.

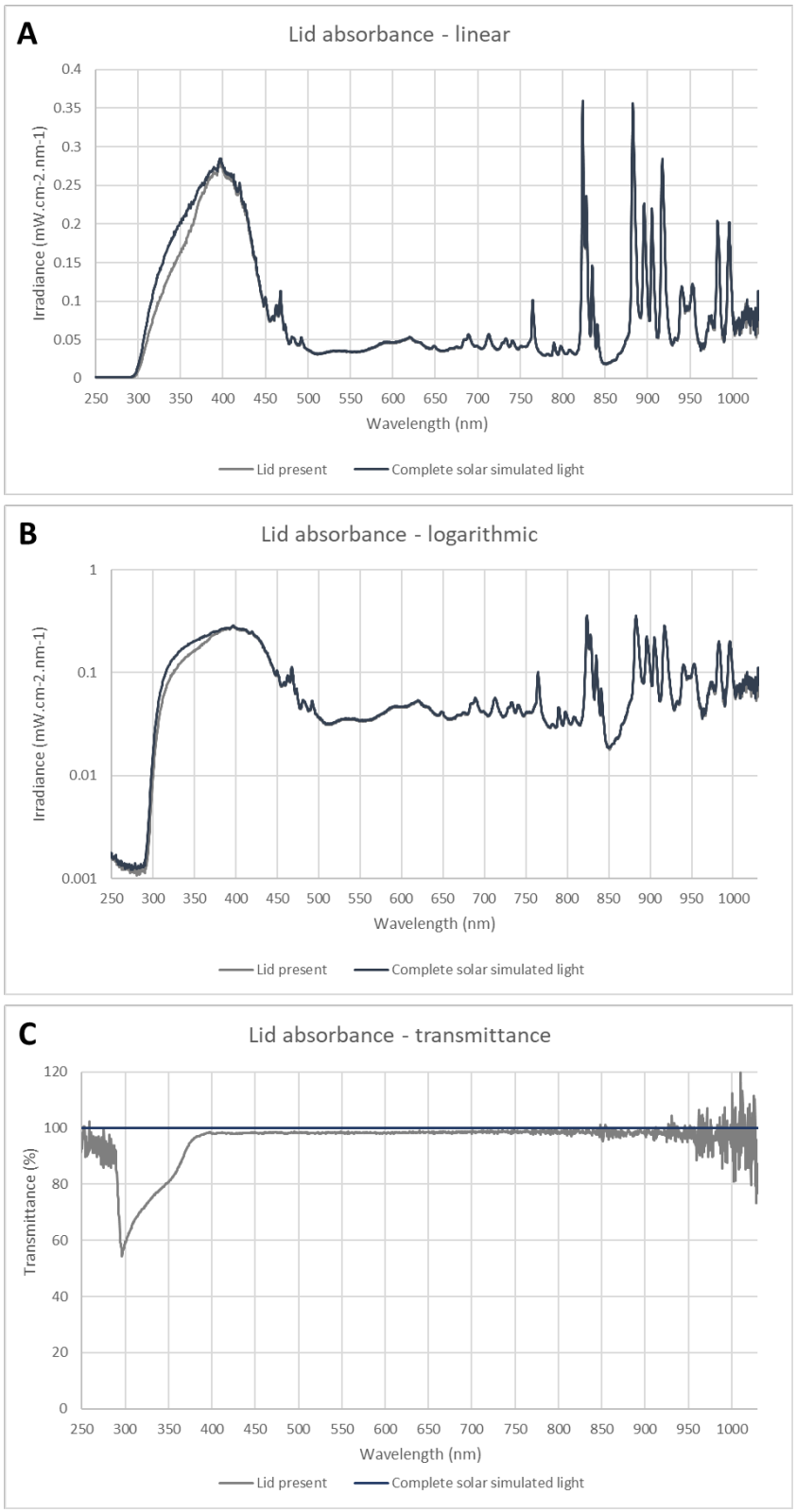

Figure 2-4 Spectrum from solar simulator with plastic of lid over FLAME sensor.
A shows irradiance graph on a linear scale, B shows logarithmic scale and C shows transmittance as % of spectrum without lid present.

2.2.2.2 Visible light calibration

2.2.2.2.1 Elimination of UV

Visible light measurements were taken using the FLAME spectroradiometer. In order to isolate the visible light output from the solar simulator, filters were placed inside the housing in a holder for 50 mm x 50 mm filters. The filter holder contained 3 filters; an 810 nm shortpass (ZIS0810, Asahi, Japan) and 2 UV blocking filters (UVK-5051, UQG Optics, UK). UV contamination through one UV blocking filter was measured with the Bentham monochromator to have an effective irradiance of 2.1×10^{-5} $mW.cm^{-2}$ (Figure 2-5). This means in 4 hours (the maximum irradiation time with visible light) there would be a dose of 3.1×10^{-4} $J.cm^{-2}$ delivered, or $2.1 \times 10^{4-}$ SEDs. It would take 129 hours to irradiate 1 SED at this irradiance. Given the filter holder contained 2 of these filters, it was assumed that the contribution of UV in the visible light experiments was negligible. Putting the filters in the filter holder within the housing of the solar simulator itself meant that the entire beam had to pass through it before exiting the solar simulator. This minimised any stray UV light that would otherwise be reflected off of other surfaces during the irradiation if the filters were placed on top of the irradiation dish/plate.

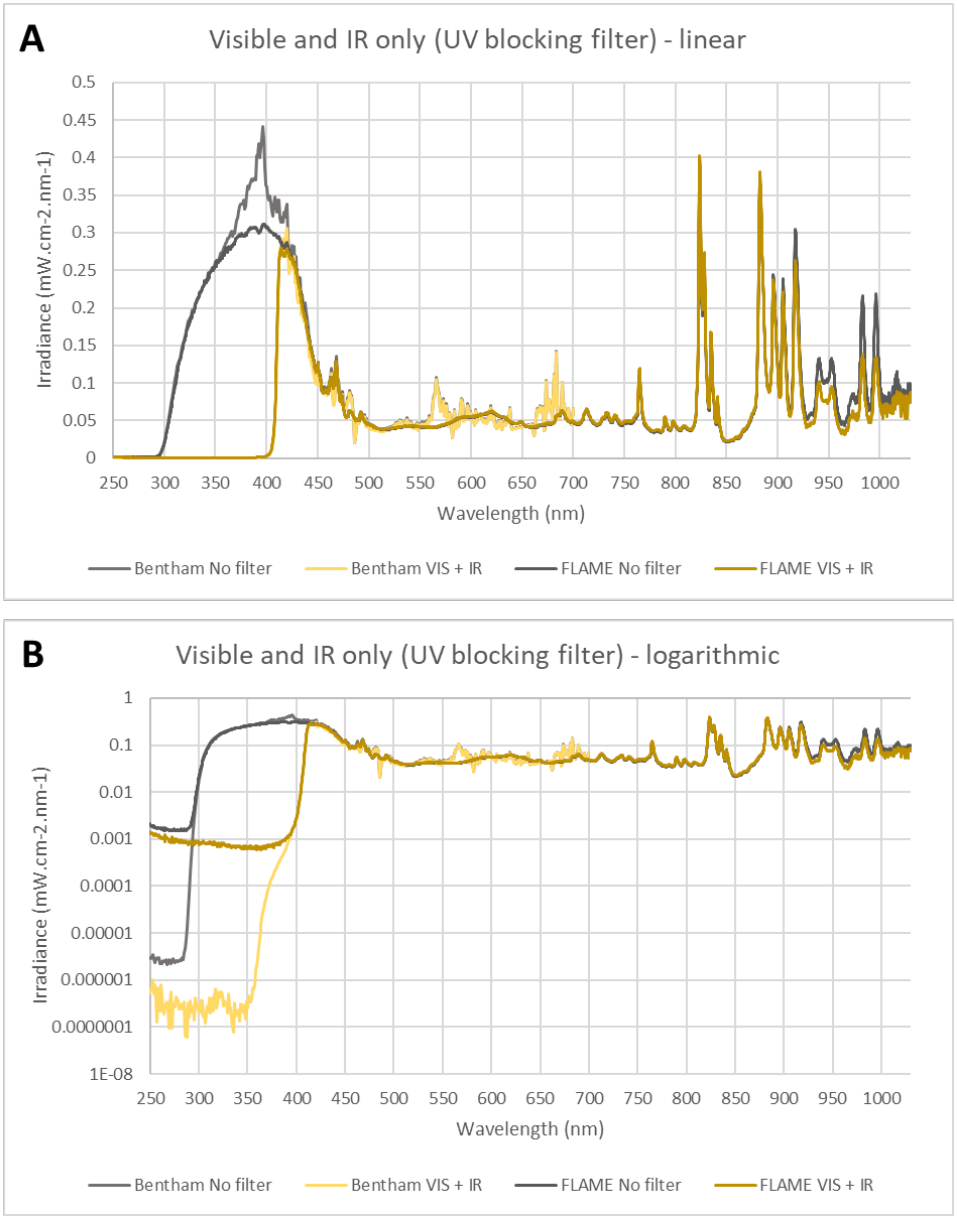

Figure 2-5 Blocking of UV light by UV blocking filter.
A shows output of solar simulator with and without the UQG UV blocking filter in place, with FLAME spectroradiometer and Bentham monochromator. B shows the same data on logarithmic axes to highlight differences in lower limit of detection.

2.2.2.2.2 Calibration and calculations

The output of the lamp with these filters between 50% cut-on and cut-off values (as compared to the lamp without any filters) was 412-810 nm. The irradiance between these wavelengths was 19.8 $mW.cm^{-2}$. Visible light exposures were calculated using the Diffey irradiance calculation spreadsheet, with inputs to represent global Mediterranean, noon, midsummer sunlight (45° latitude, 21st of June, solar noon) (Diffey, 2015). The irradiance

between 412-810 nm from the sun using this calculation was 53.5 mW.cm^{-2}. The duration of irradiation from the solar simulator to deliver the dose skin would receive during one hour of exposure to the sun was found using Equation 3. Like with the daily calculation of SEDs, the ILT-1400 radiometer was used to calculate the duration of exposure relative to the day the calibration was carried out. Though the ILT-1400 radiometer is designed for sensing UVA, it could detect low wavelength blue light which was used to represent the whole visible spectrum. While the UV blocking and 810 shortpass filters were in a filter holder within the housing of the solar simulator, other filters using during irradiations were placed directly on top of the culture dish or plate the cells were in. Table 2-2 shows the irradiation duration calculations for the different wavebands separated using filters. Details of the filters used are in Table 2-3. The output of light in each of the visible conditions can be seen in Figure 2-6.

$$Duration\ of\ irradiation\ (seconds) = \frac{Irradiance\ from\ solar\ simulator\ (mW.cm^{\ 2})}{Dose\ from\ sun\ in\ 1\ hour\ (mJ.cm^{\ 2})}$$

Equation 3 Calculation of visible light irradiation duration.

Table 2-2 Irradiance of light through filters and calculation of irradiation duration.

	Blue	Green	Red	Far red	Complete Visible
Additional filters Used:	510 nm shortpass, IR blocking	515 nm longpass, 610 nm shortpass	610 nm longpass, 710 nm shortpass	715 nm longpass	none
50% transmission cut on (nm) (inclusive)	412.764	519.537	613.581	722.251	411.88
50% transmission cut-off (nm) (inclusive)	506.196	607.311	710.556	809.32	810.098
Irradiance through filter (mW.cm^{-2})	8.7	3.5	4.4	3.0	19.8
Irradiance from sun (mW.cm^{-2})	13.8	13.2	12.8	9.1	53.3
Dose in 1 hr sunlight (J/cm^{-2})	49.7	47.5	46.2	32.9	191.9
Hours to 1 hour Sun equivalent dose:	01:35:13	03:46:43	02:54:21	03:05:40	02:41:31

Table 2-3 Details of filters used

Name	Description	Manufacturer	Product number
UV filter	Blocks light below 410 nm	UQG Optics, UK	UVK-5051
515 longpass	Blocks light below 515 nm	Newport	20CGA-515
610 longpass	Blocks light below 610 nm	Newport	20CGA-610
715 longpass	Blocks light below 715 nm	Newport	20CGA-715
780 longpass	Blocks light below 780 nm	Newport	20CGA-780
IR/VIS filter	Blocks light above 410 nm	Schott	UG-11
510 shortpass	Blocks light above 510 nm	Asahi, Japan	ZVS0510
610 shortpass	Blocks light above 610 nm	Asahi, Japan	ZVS0510
710 shortpass	Blocks light above 710 nm	Asahi, Japan	ZVS0510
810 shortpass	Blocks light above 810 nm	Asahi, Japan	ZIS0810
IR filter	Blocks light below 410 nm and above 620 nm	UQG Optics, UK	IRC-09
ND filter	0.5 opitcal density neutral density. Blocks 60% of photons equally at all wavelengths	Newport	FSQ-ND05
Window glass	Glass from an actual window – filters out all UVB and 51% of UVA		
Plastic filter	Blocks all UVB and 89% of UVA		

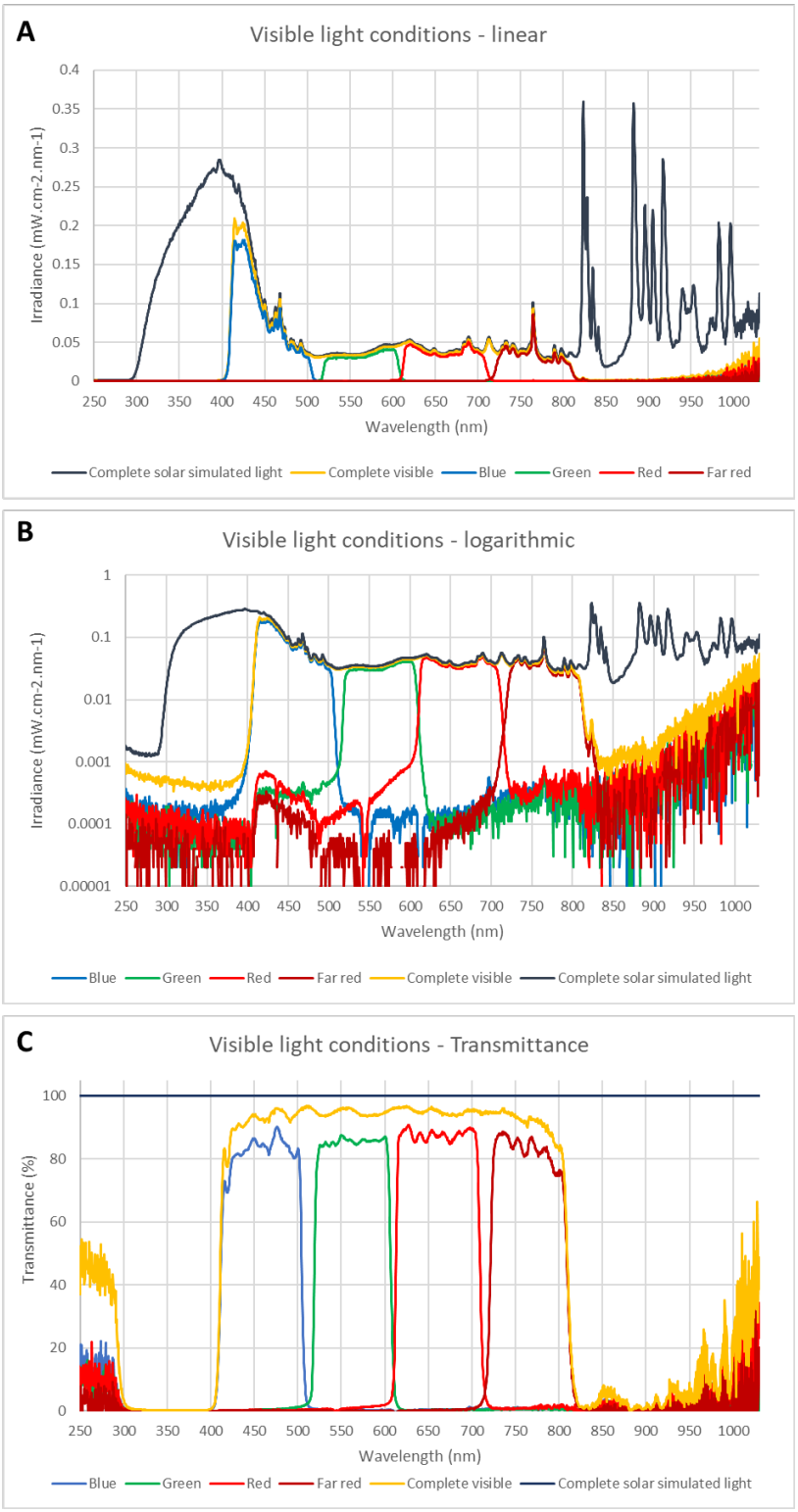

Figure 2-6 Irradiance of visible light conditions.
A shows the irradiance spectra of each of the 5 visible light conditions and that of the solar simulator with no filters. B shows the same thing on a logarithmic scale. C shows the transmission through each filter condition as a percentage of that from the solar simulator without filters.

2.2.2.2.3 Addition of IR filter in blue light condition

The 510 nm shortpass filter is effective at blocking light above 510 nm but only up to 700 nm. Due to the light from the solar simulator with the UV blocking and 810 shortpass filters in ranging from 410 nm to 810 nm, the wavelengths between 710 nm and 810 nm let through by the 510 nm shortpass filter would not allow separation of effects from blue and far red light. To mitigate this, an IR blocking filter with the ability to block light above 700nm was included in blue light irradiations. The spectrum of the blue light condition with and without the IR filter can be seen in Figure 2-7.

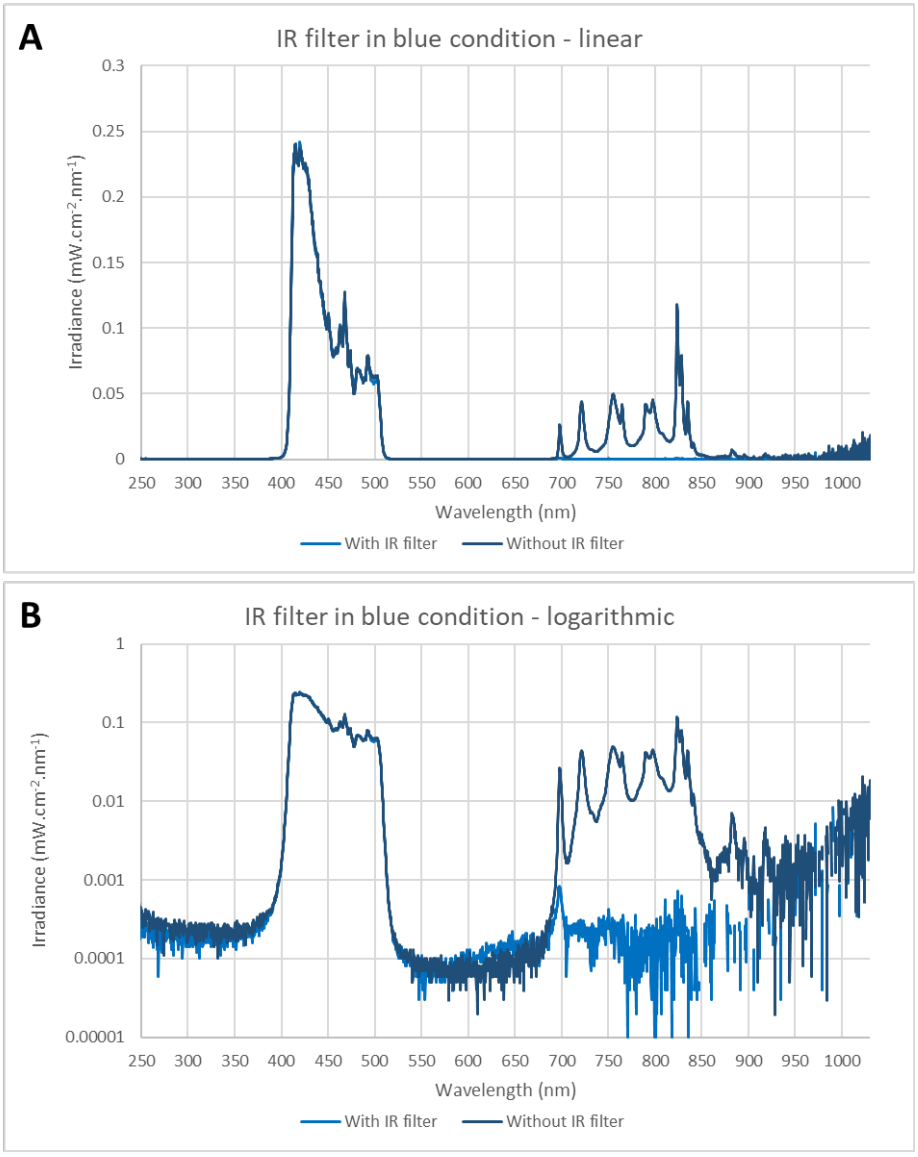

Figure 2-7 Blue light condition with and without additional IR filter.
Graph A shows the data on a linear scale, B shows data on a logarithmic scale.

2.2.2.2.4 Reflection of light from under the solar simulator beam

With the irradiation of visible light from the solar simulator light reflected back onto the cells from the surface underneath them needs to be considered on top of that coming from the lamp above. While wavelengths below 410 and above 810 were blocked by the filter within the housing of the solar simulator, the additional filters were placed on top of the plate or dish itself, so stray wavelengths from the other wavebands would be scattered and reflected from the surface underneath the plate/dish, which was held by a stand about 4 cm above the bench surface. In order to find the least reflective material, the FLAME spectroradiometer was held in place 5 cm above the bench surface while the solar simulator was on and shutter open, and measurements of the light reflected back were taken (Figure 2-8). The FLAME itself is opaque and thus blocked some of the incident light, but each material was compared to a control of white paper to account for this. It was found that black plastic reflected the least visible light (between 410-810nm, a maximum of 4.4% of that reflected by white paper at 410 nm) and was used in the experiments going forward. This was a rough way of minimising reflected light, which did not take into account distance from the light source or reflected material, or scatter. This measure minimised any scattered wavelengths but did not completely eliminate them.

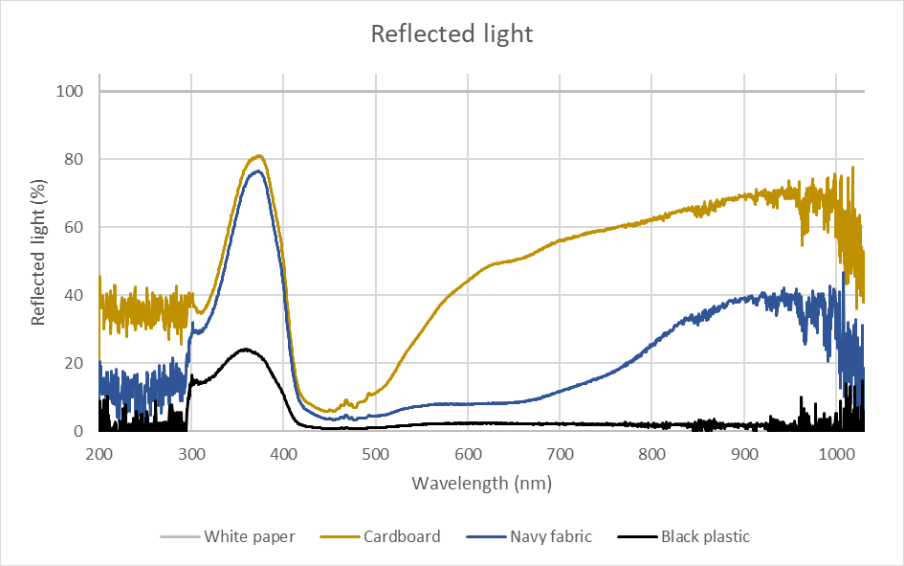

Figure 2-8 Solar simulated light reflected by materials as compared to that reflected by white paper.

2.2.3 Irradiation protocol

2.2.3.1 Complete solar simulated light

Irradiation of complete solar simulated light was carried out using the solar simulator without additional filters in the housing of the lamp. After switching on, the solar simulator was allowed to warm up for 10 minutes, following which a measurement was taken with the ILT-1400 radiometer at the same distance from the lamp as the cells would be irradiated at. This was used to calculate the irradiance of the solar simulator in SEDs per second ($SEDs.s^{-1}$) using Equation 4. Irradiation time required to deliver the desired dose of SEDs was calculated using Equation 2. The calibration was carried out yearly. The UV-only and complete solar simulated light conditions produced different irradiances in $SEDs.s^{-1}$ and different measurements on the ILT-1400 radiometer, so the calculations of irradiance and exposure time were carried out separately.

$$I = M \times \frac{I_C}{M_C}$$

Equation 4 *Calculation of irradiance (I, $SEDs.s^{-1}$) at a given time using measurement from ILT-1400 (M, mA), and previously measured irradiance at time of calibration (I_C, $SEDs.s^{-1}$ and ILT-1400 measurement (M_C, mW) taken at time of calibration.*

Unless otherwise specified, the protocol for irradiation was as follows. Prior to irradiation the day after seeding, cells were washed 2 x with 1 ml DPBS and placed in 2 ml PBS for irradiation. For irradiation, the plates or dishes were suspended by a stand 4 cm above the bench surface which was covered in black plastic to reduce reflection and scatter. The stand allowed light to pass through the bottom of the plate by only resting it on the edges of the plate, and the dish by holding it by the gripping ring. After irradiation, cells were returned to complete, phenol-containing DMEM with 10% FCS.

2.2.3.2 UV

As with complete solar simulated light, Irradiation of solar simulated UV was carried out using the solar simulator without additional filters in the housing of the lamp. However, in the case of UV irradiation, a Schott UG11 filter was placed above the cells, blocking IR and visible light and some UV primarily in the UVA region (320 – 400 nm). Like with irradiation with complete solar simulated light, after an initial warm up a reading was taken with the

ILT-1400 radiometer and used to calculate irradiation duration for the desired dose based on a calibration carried out yearly. Cells were treated in the same way for irradiation as with complete solar simulated light.

2.2.3.3 Visible light

A filter holder containing 2 x UQG UV blocking filters and an 810 nm shortpass filter was placed into the housing of the solar simulator prior to being switched on. After allowing the lamp to warm up, a reading was taken with the ILT-1400 radiometer and used to calculate irradiation duration as per the calibration carried out with the FLAME. Cells were seeded in 2 ml MEMO + SOS and irradiated the next day in the same medium. Once removed from the incubator, dishes were wrapped around the lid-dish junction with parafilm to minimise gas exchange. Dished were placed under the lamp at the same time, though all were wrapped in foil until the start of their exposure time, calculated so all exposures would finish at the same time. Green light irradiated cells were exposed first, as this irradiation took the longest, with the appropriate filters placed on top of the dish to fully cover the lid. At the start of the exposure period for the other dishes, the foil was removed, and they were replaced under the lamp with the appropriate filters in place. At the end of the irradiation, the medium was replaced with fresh MEMO + SOS and cells were returned to the incubator.

For irradiations in 96-well plates, the plate was wrapped around the side with parafilm, and separate conditions were in separate plates so the whole plate could be wrapped in foil before the start of irradiation to eliminate any stray light.

2.2.3.4 Infrared

Infrared irradiations were carried out with the Hydrosun 750 infrared lamp (Hydrosun, Germany). The output of this is in the infrared A region (780 to 1400 nm) and the lamp contains a water filter, which absorbs certain wavelengths better than others and more closely matches the spectrum coming from the sun through Earth's atmosphere which contains water vapour. Temperature was controlled by having the plate or dish resting on a stand in a water bath, allowing the bottom to make contact with the water but the top to be kept dry. A stirrer circulated the water to ensure no local heating. The water bath

temperature was set to 26°C, though during irradiation the water temperature would increase to ~ 31°C. Irradiations were carried out with the lid on.

Irradiance was varied by changing the distance from the lamp and using a filter. High intensity infrared was measured with the supplied radiometer to be 360 $mW.cm^{-2}$ at a distance of 13 cm from the lamp. A 10-hour equivalent dose of 1440 $J.cm^{-2}$ was delivered over 66 minutes and 40 seconds, and lesser doses were delivered by reducing irradiation time accordingly. Low or "solar" intensity infrared was delivered at a distance of 35 cm from the lamp, at which the intensity was 100 $mW.cm^{-2}$, so an additional neutral density filter (FSQ-ND05, Newport, UK) was used to reduce this to 40 $mW.cm^{-2}$. The dose of 288 $J.cm^{-2}$ was delivered over 2 hours.

After seeding in the same way as for complete solar simulated light, cells were irradiated the day after seeding in the same complete, phenol-free medium they were seeded in. After irradiation, this was replaced with fresh medium and the cells returned to the incubator.

2.2.3.5 Controls

Unirradiated controls were wrapped in foil for the duration of irradiation, but the plate/dish remained under the lamp so was exposed to same environmental conditions otherwise. In 96-well plates, when controls were present on the same plate as the irradiated conditions, only opaque-walled, plates were used. Control wells were covered in a layer of black plastic (to absorb any small amounts of stray light that made it past the foil) that was then covered in foil to reflect any incoming light. A minimum of two empty wells distance was left between unirradiated and irradiated cells to minimise stray light.

Where incubator controls were included, cells experienced the same washes and medium changes as the irradiated cells and irradiation controls, but instead of being out of the incubator for the duration of irradiation were returned to the humidified incubator at 37°, 5% CO_2. This was to test any effects on cells of being outside the incubator in an environment with different humidity, temperature and gas compositions for the irradiation duration.

2.3 MTS viability assay

The MTS assay was used to measure viability/metabolism in cells. MTS tetrazolium is reduced to a brown formazan product which absorbs visible light. To determine viability, 20 ul of MTS (Promega, UK) was added to 100 ul of phenol-red free DMEM in the wells of the clear 96-well plate. After incubation for 4 hours in a humidified 37°C, 5% CO_2 incubator, the plate was shaken briefly, and absorbance read at 490 nm on a SpectraMax 250. Absorbance from control wells with DMEM and MTS but no cells were used to subtract background absorbance from that of the test wells.

2.4 Alamar blue viability assay

Alamar blue (ThermoFisher Scientific, USA) was also used as an alternative measure of viability/metabolism in cells whereby resazurin is reduced to fluorescent resorufin. A 1 in 10 dilution of alamar blue assay was made up in complete phenol-free DMEM. 20 ul of this was added to the 100 ul of complete phenol-free DMEM in the clear 96-well plate and incubated in a humidified 37°C, 5% CO_2 incubator for 2 hours. After incubation, the fluorescence was read with a TECAN plate reader (Tecan, Switzerland) with excitation at 560 nm and fluorescence at 590 nm. Fluorescence from control wells with DMEM and alamar blue but no cells were used to subtract background absorbance from that of the test wells.

2.5 Crystal violet stain viability assay

Crystal violet staining was used as a measure of biomass of cells in clear 96-well plates, that would be unaffected by metabolism. Crystal violet solution was made up to 0.5% weight per volume in 20% ethanol, 80% purified water. Cells were washed twice with 200 ul of DPBS before incubating at room temperature with 50 ul of crystal violet solution for 20 minutes on a shaking rocker. After this, cells were washed six times with tap water, and plates were left to dry upside down, overnight at room temperature. The next day, 200 ul of 1% SDS weight per volume in water was added and incubated at room temperature on a shaking rocker for 30 minutes. Absorbance was read at 570 nm on the SpectraMax plate reader. Absorbance from control wells with crystal violet but no cells were used to subtract background absorbance from that of the test wells.

2.6 Cell counting

To count, a 35 mm dish was washed twice with DPBS and 200 ul of trypsin/EDTA was added. After 3-5 minutes in the incubator, 200 ul of complete, phenol-free, 10% FCS DMEM was added, and the cells were pipetted to mix. 3 counts from each dish were taken using a hemocytometer.

2.7 DCFDA plate assay

DCFDA was used to measure ROS in cells after irradiation. Cells were seeded in white 96-well plates at 5000 cells/well and left to adhere overnight in a humidified incubator at 37° and 5% CO_2. After irradiation, cells were washed gently with 200 ul of DPBS, then 100 ul of 15 uM H_2DCFDA (Bio-Techne, US) was added to wells and incubated for 30 minutes in a humidified 37°C, 5% CO_2 incubator. After incubation, DCFDA was removed by pipetting and 200 ul of DPBS was added gently as a wash. This was gently removed by pipette and replaced with 100 ul DPBS. Fluorescence was measured on the TECAN plate reader with 488 nm excitation and 535 nm emission. Unless otherwise indicated, ROS was measured immediately after irradiation.

2.8 Flow cytometry

HDFn cells were seeded at 140 000 cells per well in 35 mm TPP dishes in phenol-containing DMEM with 10% FCS, and incubated overnight in a humidified incubator at 37° and 5% CO_2. Following irradiation, cells were trypsinised, scraped and collected in a round-bottomed polystyrene 96-well plate. Staining steps were all carried out in the 96-well plate, and test conditions were run through the flow cytometer sampling directly from the 96-well plate. Control cells (unstained, single-stained and dead) were transferred to FACS tubes after staining to run through the flow cytometer, for finer control over the running of these samples. TMRE negative control cells were prepared while the test cells were being irradiated by adding 2 ul of 10 mM FCCP (Abcam, UK) to the 2 ml medium on cells to a final concentration of 10 uM 30 minutes before trypsinisation. MitoSOX positive control cells were prepared by adding 2 ul of 1 mM antimycin A to the 2 ml of medium on cells to a final concentration of 1 uM (Sigma-Aldrich, Germany). Cells were washed in 4 ml DPBS

supplemented in 1% FCS. Positive control dead cells were placed on a heat block for 45 minutes at 56°C before staining alongside the live cells.

200 ul of 5 uM MitoSOX diluted in FCS-free, phenol-free medium was added to the wells and mixed by pipetting before incubating for 30 minutes in a humidified incubator at 37°C, 5% CO_2. Antimycin A was added to MitoSOX positive control cells during staining to a concentration of 1 uM. DCFDA was added to wells and mixed with cells by pipetting, then incubated in 200 ul of 0.15 uM DCFDA in FCS-free, phenol-free medium for 30 minutes in a humidified incubator at 37°C, 5% CO_2. To TMRE stained cells, 8 ul of 0.1 uM was added to cells in 192 ul of FCS-free, phenol-free medium to a final concentration of 4 nM and incubated for 10 minutes in a humidified incubator at 37°C, 5% CO_2. FCCP was added to TMRE positive control cells during staining to a concentration of 10 uM.

After staining, cells were washed in 200 ul of DPBS with 1% FCS and kept on ice in 50 ul DPBS with 1% FCS. 1 ul of 2.5 ug/ml propidium iodide (PI, Abcam, UK) was added to DCFDA- and TMRE-stained cells to a final concentration of 50 ng/ul. 1 ul of 5 uM DAPI (Sigma-Aldrich, UK) was added to MitoSOX-stained cells to a final concentration of 0.1 uM. Alongside the double-stained MitoSOX + DAPI, TMRE + PI and DCFDA + PI cells were single stains for all, with PI and DAPI positive control dead cells and control live cells, MitoSOX single-stained positive control Antimycin A and control live cells, TMRE single-stained negative controls with FCCP and control cells without FCCP. The positive control used for DCFDA was cells irradiated with 2.16 SED complete solar simulated light.

The positive controls for each dye were used to set the voltage on the BD Symphony flow cytometer (BD Biosciences, USA). The following configuration was used; 561 nm laser with 586/15 nm bandpass filter was used for TMRE signal (λex = 560 nm, λem = 574 nm), a 488 nm laser with 610/20 nm bandpass filter was used for MitoSOX signal (λex = 510 nm, λem = 580 nm), a 488 nm laser with 530/30 nm bandpass filter was used for DCFDA (λex = 458 nm, λem = 535 nm), a 561 nm laser with 610/20 filter was used for PI (λex = 493 nm, λem = 636 nm), and a 405 laser with 450/50 nm bandpass filter was used for DAPI (λex = 340 nm, λem = 488 nm). Compensation did not need to be calculated for the combinations of dyes used

(MitoSOX + DAPI; DCFDA + PI) as spectra did not overlap. Analyses were carried out with the FCS Express software.

Gating out of debris was carried out using side scatter area versus forward scatter area, the single cells were gated using forward scatter height and side scatter width versus forward scatter area (Figure 2-9). Gating dead cells was carried out based on signal in PI or DAPI channel.

Flow cytometry data were analysed using the median fluorescence measurements from each dye. Statistics were carried out on log transformed data.

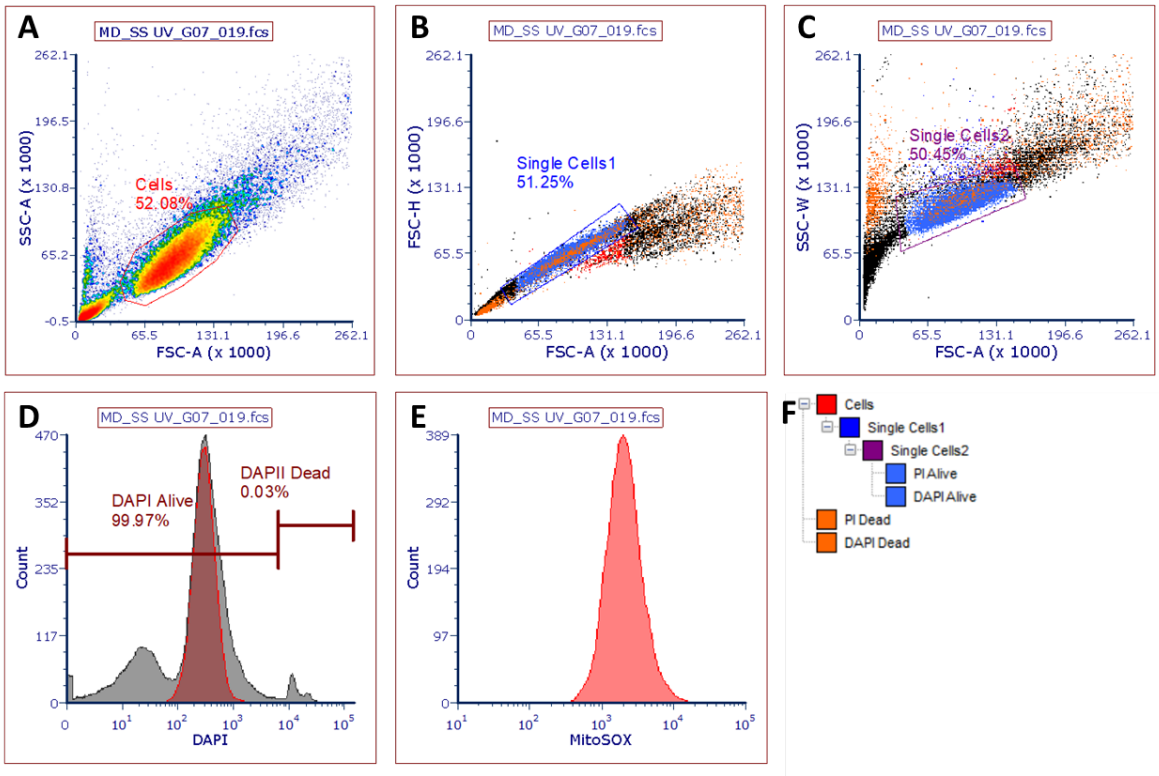

Figure 2-9 Gating of flow cytometry data.
A shows all events captured and gate for cells. B shows gate for single cells. C shows additional gate for single cells. D shows DAPI fluorescence for all events (grey) and single cells (red), with gates for live and dead DAPI stained cells. E shows MitoSOX fluorescence of events in live cell gates. F details mother/daughter relationships of gates.

2.9 RNA extraction and reverse transcription

HDFn cells seeded at 1.4 x 10^5 were allowed to adhere overnight at 37°C, 5% CO2 in humidified incubators. Following irradiation the next day, cells were returned to the

incubator for 24 hours before trypsinising, scraping and pelleting. Total RNA was isolated with the RNeasy mini kit (Qiagen, UK) as per the manufacturer's instructions. Concentrations were measured using a NanoDrop ND-100 (Nanodrop Technologies LLC, ThermoFisher Scientific, USA). The 260/280 nm ratio was used to assess RNA purity. Reverse transcription was carried out using the High Capacity cDNA Reverse Transcription Kit (ThermoFisher Scientific, USA) as per the manufacturer's instructions with RNase inhibitor (ThermoFisher Scientific, USA). cDNA was stored at -20°C.

2.10 Relative quantitation of gene expression with TaqMan qPCR

qPCR was carried out using a standard settings on the Applied Biosystems StepOnePlus ABI cycler (ThermoFisher Scientific, USA) and Applied Biosystems QuantStudio3 (ThermoFisher Scientific, USA). Primers used are detailed in **Error! Reference source not found.**, all from ThermoFisher Scientific, USA. Each reaction was comprised of 10 ul 2 x TaqMan Master Mix (4369016, ThermoFisher Scientific, USA) 4 ul of 5 ng/ul DNA in RNase-free water, 5 ul of RNase-free water and 1 ul of 20 x TaqMan primers. GAPDH was used as a housekeeper in all cases unless otherwise specified.

Technical repeats were carried out in triplicate, and a mean of the Ct values was calculated. Fold changes were calculated using the ΔΔCt method, whereby ΔCt represents the difference in expression between the gene of interest and the housekeeping gene within the same cDNA sample. ΔΔCt was then calculated as the difference in ΔCt between irradiated cell cDNA and control cell cDNA. Fold change was calculated as $2^{-\Delta\Delta Ct}$. The cut-off for Ct values was 35 cycles. Statistical analysis of gene expression data was carried out on the ΔΔCt data and transformed into linear data for graphical presentation with geometric mean and geometric standard deviation.

Table 2-4 TaqMan primers used in qPCR assays

Target	Dye	Code
MMP1	FAM	Hs00899658_m1
MMP2	FAM	Hs01548727_m1
MMP3	FAM	Hs00968305_m1
COL1A1	FAM	Hs00164004_m1
MMP9	FAM	Hs00957562_m1
GAPDH	VIC	Hs02758991_g1
ACTB	VIC	Hs99999903_m1

2.11 Statistical analyses

For all qPCR and ROS generation assays, within each biological repeat, a fold change value was calculated for each technical repeat compared to control. These fold change values were log transformed to account for skew, and the transformed data was used to calculate the mean fold change for each biological repeat. A 2-tailed, one-sample t-test was carried out using the means from the biological repeats, compared to 0, on the now normalised data. Data were considered to be significantly different if the calculated p-value was ≤ 0.05. Data were presented on linear graphs with geometric mean and geometric SD to account for skew.

For viability assays (MTS, alamar blue, crystal violet and counting), a background reading from wells containing medium and the assay only (no cells) was taken, the mean of which was subtracted from the readings from the wells containing cells. The mean fold change of the technical repeats within each biological repeat was calculated compared to the control as a fold change. A 2-tailed, one-sample t-test was carried out using the means from the biological repeats, compared to 0, on the now normalised data. Data were considered to be significantly different if the calculated p-value was ≤ 0.05. Data were presented on linear graphs with mean and SD.

The RNA sequencing experiment used three biological repeats with one technical repeat for each. The fold change between the test and control for each gene was calculated from the raw count values. P-values were calculated using 2-way t-tests and adjusted p values were calculated using the Benjamini-Hochberg method.

Chapter 3 Light measurement, temperature control and medium conditions in irradiation experiments

3.1 Introduction

3.1.1 Medium components

Cell medium is designed to best support the maintenance and growth of cells in culture and contains a mixture of many components. While most of these components do not interact with light, some of them absorb light or interact with those that do, adding a layer of complexity when it comes to examining the effects of light on cultured cells. The components known to be involved in photosensitising reactions are riboflavin, HEPES, tryptophan, tyrosine, FCS and phenol red.

Riboflavin, also known as vitamin B_2, cannot be synthesised by mammals, so it must be obtained through the diet. It forms flavocoenzymes flavin adenine dinucleotide (FAD) and flavin mononucleotide (FMN), which are necessary for the function of many flavoproteins including dehydrogenases, monooxygenases, oxidases and reductases. These have roles in the mitochondrial ETC (electron transport chain), redox homeostasis and biosynthesis of other cofactors and hormones (Balasubramaniam and Yaplito-Lee, 2020).

In the mitochondrial ETC, riboflavin is involved in the form of $FMNH_2$ as a cofactor for NADH ubiquinone oxidoreductase (complex I) and $FADH_2$ as a cofactor for succinate-ubiquinone oxidoreductase (complex II). Deficiency of riboflavin in mitochondria results in disruption of the ETC and production of ROS leading to oxidative stress (Ashoori and Saedisomeolia, 2014). In skin, animals deficient in riboflavin have impaired wound healing and impaired skin collagen development (Lakshmi et al., 1989, Lakshmi et al., 1990). Mutations of genes of proteins involved in riboflavin transportation and metabolism are known to lead to several diseases and mitochondrial dysfunctions (Balasubramaniam and Yaplito-Lee, 2020).

Riboflavin acts as a photosensitiser and absorbs light in the UV and visible regions of the solar spectrum up to ~520 nm, with absorption peaks at 371 nm (UVA) and 442 nm (visible blue light). It is the primary photosensitising component of cell culture medium. HEPES acts as a buffer in medium when cells are exposed to low CO_2 concentrations such as that found

in normal room air rather than 5% CO_2 incubators. However, it can react with photosensitisers to produce H_2O_2 when exposed to light. HEPES, riboflavin and tryptophan can work synergistically when irradiated with light to produce reactive oxygen species (ROS) such as singlet oxygen ($^1O_2$), hydroxyl radical (OH^-), hydrogen peroxide (H_2O_2) and superoxide ($O_2^{\bullet-}$) in cell culture medium (Silva et al., 1994, Wang, 1976, Grzelak et al., 2001, Mahns et al., 2003, J. S. Zigler et al., 1985). On absorbing a photon, an electron of riboflavin is promoted to a higher energy level into singlet state. Inter-system crossing allows this electron to change spin direction to put the riboflavin molecule in triplet state, which is reactive in two ways. It can react with molecular oxygen to form singlet oxygen, which itself is highly reactive (type II photosensitisation), or it can oxidise another molecule, which here can be tryptophan or HEPES, reducing the riboflavin into an anion which can react with molecular oxygen to form superoxide (type I photosensitisation). The oxidised HEPES cation after deprotonation reacts with molecular oxygen to further produce superoxide, adding to the superoxide already generated by the riboflavin anion. After these reactions, the riboflavin is returned to its original state, from which it can react again on absorption of another photon. A pitfall that experiments with visible light irradiation of cells falls into is the use of medium containing riboflavin photosensitising cells when exposed to wavelengths below 540 nm (Hopkins et al., 2016).

Even without HEPES present in medium, riboflavin is phototoxic, presumably due to the ability of tryptophan to act similarly to HEPES. Cells incubated with medium that has been exposed to normal fluorescent room lighting for 2 days had reduced cloning efficiency by over 50% compared to cells incubated with medium that was kept in the dark (Wang, 1976). On removal of riboflavin and tryptophan, this effect was mitigated.

Phenol red is commonly used in cell culture as an indicator of infection. With increasing pH, medium containing phenol red becomes a darker red colour, and with decreasing pH it becomes more yellow. Bacterial infections in cell cultures are typically acidifying, so it acts as a quick indication of culture health. Its ability to absorb visible light, giving it its red colour, is conferred through its phenolic chemical structure, though its absorption spectrum also extends into UV, absorbing both UVA and UVB. Its absorption spectrum is of course pH

sensitive, and at pH 7.4 there are two absorption peaks, one at 415 nm and one at 560 nm. It appears to be able to enter cells from the culture medium, and when there it interacts with riboflavin inside the cell, affecting the radical formation processes (Maguire et al., 2011)

Foetal calf serum (FCS) contains many components which support the growth of cells in culture including growth factors, hormones, lipids, sugars, and vitamins to name just a few. FCS can greatly influence cell behaviour and morphology, and HDFn cells typically grow best in medium containing 10% FCS. FCS has a translucent brown colour and contains coloured components such as bilirubin which has been shown to be photosensitising (Bruzell Roll and Christensen, 2005, Böhm et al., 1995). The absorption of light by FCS components could lead to the production of radicals, though this seems to be countered by its catalase component (Wang and Nixon, 1978), the process of which itself could also interfere with measurements of oxidative stress as a result of irradiation. In any case, its presence in medium would absorb light that would otherwise be reaching the irradiating cells, interfering with the spectrum of wavelengths they receive.

To avoid these issues, one option is to remove the serum from the cells being irradiated, although this comes with its own caveats. The term “serum starvation” refers to a state in which cells are grown in reduced or no serum for a period of time. Cell responses can vary depending on the duration, the presence or absence of low levels of serum, the presence of other proteins or growth hormones and the cell type (Pirkmajer and Chibalin, 2011). However, over a period of 24 hours, it generally leads to a reduction in activation of the mTOR pathway and changes in AMPK and Akt phosphorylation. Changes can be seen after as little as one hour of serum starvation and are not constant over the 24-hour period. 48-hour serum starvation and return to serum-containing medium has shown in HeLa cells to initiate changes which increase mitochondrial gene transcription, membrane potential and ATP production in the 24 hours after return to serum (Xiong et al., 2012).

While riboflavin is known to be photosensitive in the UV and visible regions of the visible spectrum, especially alongside tryptophan and HEPES, it is unknown whether irradiation with infrared light of cells in medium containing these components is affected by this, given that the absorption spectra of these compounds does not extend to infrared wavelengths.

To determine this, viability of cells in medium containing riboflavin, tryptophan and HEPES were exposed to high and solar-intensity infrared light was examined. To determine the best medium conditions for visible light irradiation, cells were irradiated with visible light in conditions containing HEPES and riboflavin, containing only riboflavin and finally containing neither HEPES nor riboflavin. This MEMO medium (Cell Guidance Systems, UK, used with supplement A and insulin as recommended per manufacturer protocol) is identical in ingredients to the standard DMEM used to culture HDFn cells (11995065, Gibco, USA) except that it contains no riboflavin or phenol red.

While the effects of UV are large enough that they can be easily measured after a single, acute dose, the effects of visible and infrared are expected to be much smaller if they are kept within a physiologically relevant range. Human skin is exposed to light daily, so it is possible that chronic exposure is having a larger effect than is easily measured after a single exposure. Though it is possible to increase the dose of light delivered to be much greater than one could feasibly receive from the sun in a day, another approach would be to expose cells to a dose of light delivered across multiple days. This chapter details the limitations of multiple-day exposures to visible light, where the prolonged deprivation of light-sensitive components of culture medium affects cell behaviour.

3.1.2 Assays used

The MTS assay is a viability assay that relies on the metabolism of tetrazolium salts into a light-absorbing formazan product which can be detected by absorbance. The use of MTS as a viability assay is not without issue. It is affected by the rate of metabolism in the cells, as a reduced rate of metabolism will lead to a reduction in the rate at which the formazan product is formed. The same number of cells will therefore have a lower MTS signal if metabolism rate has been affected by a condition. When the MTS assay is used immediately after exposure to a condition, the result can be due either to an effect on metabolism or on cell death, as cells which have died during an irradiation would be expected to detach from the plate and be washed off when the medium was replaced and MTS assay added. When measured 24 hours after exposure to a condition, differences in MTS signal can reflect either differences in metabolism, cell death or change in rate of proliferation. However further

complications can be seen when MTS is used in medium containing serum such as FCS. Huang et al demonstrated that components of FCS such as albumin and fatty acids affect the signal from the formazan product, interfering with the measurement of cell number (Huang et al., 2004). BSA was thought to bind to the formazan product, reducing absorbance at 490 nm, and fatty acids were thought to compete with this albumin binding creating more unbound formazan and increased absorbance. Glucose concentration also affects signal. Reducing agents such as ascorbic acid (vitamin C) also react with MTS to produce formazan.

While MTS measures viability through the metabolism of MTS tetrazolium into coloured formazan product, the crystal violet stain stains cell biomass which is adhered to the well. In this way it better reflects the number of cells present, rather than metabolism, although with somewhat less sensitivity in 96-well format compared to MTS due to low staining signal. By using both measures, viability can be more reliably estimated than with either alone.

Alamar blue cell viability reagent is another measure of cell viability that relies on metabolism by cells, where resazurin dye is reduced to fluorescent resofurin. Like MTS it is metabolised by reductases and dehydrogenases by the cell. It can be more sensitive than MTS, so was included as an additional assay for comparison.

3.2 Materials and methods

3.2.1 Temperature control

3.2.1.1 Hydrosun IR lamp

The Hydrosun lamp was used as per Chapter 2, except where temperature was differently or not controlled. Where there was no temperature control in place, instead of a water bath with a stirrer, the plate or dish was placed on a stack of pipette tip boxes to raise the plate or dish to the height required to reach the desired irradiance.

3.2.1.2 Temperature measurement

Temperature recordings were carried out using a FLIR A305SC (TI Thermal Imaging, USA) and analyses were carried out using ResearchIR software. Before irradiation, a still image was taken of the dish or plate. After irradiation, a recording was set up with focus in the correct plane to immediately record temperature as soon as the plate/dish had been removed from

the water bath onto the bench with the lid removed. Recordings of temperature during irradiation were of the plate lids or surfaces under the beam of the lamp. Temperatures of 100 ul of water wells in 96-well plates were collected using an average temperature of a 9-pixel square in the centre of the well. Temperatures of 2 ml of water in dishes were collected using an ellipse to take an average across the whole of the bottom of the dish.

3.2.2 Medium conditions with light irradiation

3.2.2.1 pH of medium during irradiation

pH was measured using a pH probe calibrated each day before measurements were taken. The medium used was phenol-containing DMEM and 10% FCS, 1% penicillin/streptomycin with no HEPES. pH in DMEM was altered by incubating at 5% CO_2 in a 37° humidified incubator in a 50 ml falcon tube with the cap loose, or by leaving outside the incubator in a 100 mm dish with lid on. Fresh DMEM was used each day the experiment was carried out to ensure no bacterial or other contamination. 100 ul of DMEM was added to a well of a 96-well plate. Absorbance at 560 nm was measured on a SpectraMax 340 PC 384 microplate reader. Technical repeats were carried out in triplicate. Absorbance was plotted against pH and a line of best fit was calculated with simple linear regression.

To test the effects on pH of 4 hours out of an incubator, clear, 96-well plates were filled with 100 ul of medium per well, and 35 mm dishes were filled with 2 ml medium. The absorbance of the medium put into the plates and dishes was measured in the 96-well plate on the SpectraMax 340 PC 384 microplate reader immediately after putting it into the plate. Plates and dishes with film on were wrapped securely with parafilm around the join of the lid and plate/dish. 4 hours after incubation on the bench at room temperature, the plates were measured directly on the plate reader and 100 ul of medium from the dishes was read in a fresh 96-well plate. pH was calculated using the equation of the line of best fit from the standard curve.

3.2.2.2 Presence and absence of FCS for irradiation duration

An experiment was carried out to determine the effects of the absence of FCS during the 4-hour irradiation that would be necessary for irradiation with an hour equivalent of solar visible green light. HDFn cells were seeded at 5000 cells/well in a clear, 96-well plate in

complete, phenol-containing DMEM (10% FCS, 1% penicillin/streptomycin) and left to adhere overnight in a humidified incubator at 37°C, 5% CO_2. The following day, the seeding medium was washed off with DPBS and replaced with either phenol-free medium, either complete or FCS-free. The plate was then left in the dark for the 4-hour duration, after which the medium was removed and replaced with phenol-free, complete medium. The MTS protocol as per Chapter 2 was used, and the cells were assayed immediately after the 4-hour period or returned to the incubator and assayed 24 hours after the end of the 4-hour period.

3.2.2.3 HEPES and riboflavin during infrared and visible light irradiation

3.2.2.3.1 HEPES and riboflavin presence

HDFn cells were seeded as per protocol in Chapter 2. The next day the seeding medium was washed off with DPBS and replaced with phenol-free, FCS-free, 0.4 mg/l riboflavin, 25 mM HEPES DMEM (21063029, Gibco, USA) and irradiated with either low or high intensity infrared light as per protocol in Chapter 2, (maximum duration 2 hours). After irradiation, the medium was replaced with complete, phenol-free, 0.4 mg/l riboflavin, 25mM HEPES DMEM and either assayed immediately or returned to the incubator and assayed 24 hours after the end of irradiation. Either the MTS or crystal violet stain assay was used as per protocol in Chapter 2.

The effects of HEPES and riboflavin presence in visible light irradiations were tested in the same way, but the cells were exposed to either blue (410-510 nm) or red (610-710 nm) wavebands of light as detailed in the protocol in Chapter 2. The MTS assay was used as a measure of viability.

To determine the effects of riboflavin without the presence of HEPES on HDFn cells was tested in a similar way, but the irradiation medium was instead phenol-free DMEM without HEPES (31053028, Gibco, USA, plus 4 mM L-glutamine and 1 mM sodium pyruvate). After irradiation, the cells were returned refreshed with this same medium for assay.

Finally, cells were tested under visible light conditions with medium containing neither HEPES nor riboflavin. The MEMO medium used to test this was, like above, used to replace the previous medium for the duration of irradiation only, then returned to HEPES-fee and

phenol red-free medium immediately after irradiation. Differences in viability of cells incubated in MEMO and those incubated in normal, complete, phenol-containing, 10% FCS DMEM for the 4 hours duration were tested with MTS.

3.2.2.3.2 MMP and collagen expression of cells cultured in MEMO

To determine if the expression of target genes MMP1, MMP2, MMP3 and procollagen 1α (COL1A1) were changed as a result of the riboflavin and serum starvation, HDFn cells were seeded as per protocol in Chapter 2 in MEMO. The next day they were returned to DMEM with 10% FCS, and RNA was extracted 24 hours later as per protocol in Chapter 2. These were compared to cells that were instead seeded in phenol-free, HEPES-free DMEM with 10% FCS, the medium of which was refreshed the day after seeding, with RNA extraction at the same time as the cells seeded in MEMO.

3.2.2.4 Multiple day exposures

3.2.2.4.1 Cell counting to determine proliferation in MEMO over 4 days

To determine the effects on proliferation of keeping cells for multiple days in medium without riboflavin and FCS, a cell count was carried out. HDFn cells were seeded in 35 mm dishes as per protocol in Chapter 2 at 5 x 10^4 cells/dish in the complete, phenol-free DMEM + 10% FCS condition, or 7 x 10^4 cells/dish for cells seeded in MEMO. Medium was not changed in any of the conditions until day 3, the last day of irradiation for the irradiated condition, at which point all conditions had their medium replaced with fresh, complete, DMEM + 10% FCS.

Irradiated cells were dosed with a 1-hour equivalent dose of complete visible light (410-810 nm, 191.9 J.cm^{-2}) irradiated before counting. Only irradiated cells were removed from the incubator, unirradiated cells were left in the incubator for the duration of the irradiation. A measurement was not taken for irradiated cells after the first irradiation (day 1) since this was not expected to have affected cell number at this point. A different well was seeded for each day the condition was to be counted. Cells were counted as per protocol in Chapter 2. 24 hours was left between each count.

3.2.2.4.2 Optimising medium conditions for multiple day irradiations

This protocol does not include irradiation, though was designed to optimise medium conditions for when cells would be irradiated over three consecutive days. For this, cells were seeded as per protocol in Chapter 2 but in MEMO with no FCS and remained in this for three days. On the third day (after the cells would have had their final dose of light if in the irradiation protocol) the cells were returned to complete, phenol-free DMEM + 10% FCS. The effects of this, versus the effects of leaving the cells in the same MEMO, refreshed MEMO or phenol-free DMEM with no FCS was assessed through cell counting, crystal violet staining and MTS assay on day 4, 24 hours after the medium had been changed. Cell count, MTS and crystal violet assays were performed as per protocol in Chapter 2.

3.2.2.4.3 Gene expression in cells incubated in MEMO for 3 days

HDFn cells were seeded as per protocol in Chapter 2 in MEMO. Cells were left in this medium for 3 days, and on the third day medium was changed back into complete, phenol-free DMEM + 10% FCS. 24 hours after the medium change, RNA was extracted as per protocol in Chapter 2.

3.2.2.4.4 Complete solar simulated light, UV-only light, and infrared in MEMO

HDFn cells were seeded as above in section 3.2.2.4.3. The only difference was that starting the day after seeding in MEMO, cells were irradiated with 2.16 SEDs of complete solar simulated light, solar simulated UV only, low intensity infrared light or high intensity infrared light as per protocol in Chapter 2 but without washing before or after irradiation. After irradiation, the cells were returned to the incubator, until the following day when the irradiation was repeated. After the third and final irradiation, the medium was replaced with complete, phenol-free DMEM + 10% FCS and the cells returned to the incubator. The cells were kept in the same MEMO for the three days of irradiation. 24 hours after the final irradiation and subsequent return to complete, phenol-free DMEM + 10% FCS, RNA was extracted as per protocol in Chapter 2.

3.2.2.5 Optimising washout periods prior to irradiation

Given the potential of riboflavin and FCS components to photosensitise cells, different washout periods for riboflavin were tested using a protocol detailed in Figure 3-1. The two

conditions under test were both seeded in complete, phenol-free DMEM with 10% FCS, as this is what they had been grown in as they typically seed more successfully in this than in a different medium. After seeding as per protocol in Chapter 2, the medium was replaced with MEMO with either 1% FCS or 0% FCS. The reasoning is that the cells may be less "shocked" by having the 1% FCS present during the 24 hours leading up to the irradiation than being serum-starved. 22 hours later, the medium in the MEMO + 1% FCS condition was replaced with MEMO and another 2-hour washout period was allowed. Immediately before irradiation, the medium on both conditions was replaced with fresh MEMO to remove any remaining riboflavin or FCS. The cells were irradiated with 1-hour equivalent of visible light, then the medium was replaced with complete, phenol-free DMEM + 10% FCS (phenol-free) for assaying immediately or returning to the incubator to assay 24 hours after irradiation. A third condition acted as a positive control, whereby cells were irradiated in complete, phenol-free DMEM (with normal riboflavin content) containing 10% FCS, which was left in place after irradiation, which was expected to greatly stress the cells due to the ROS presence in the medium. The details of these washout periods can be seen in Table 3-1.

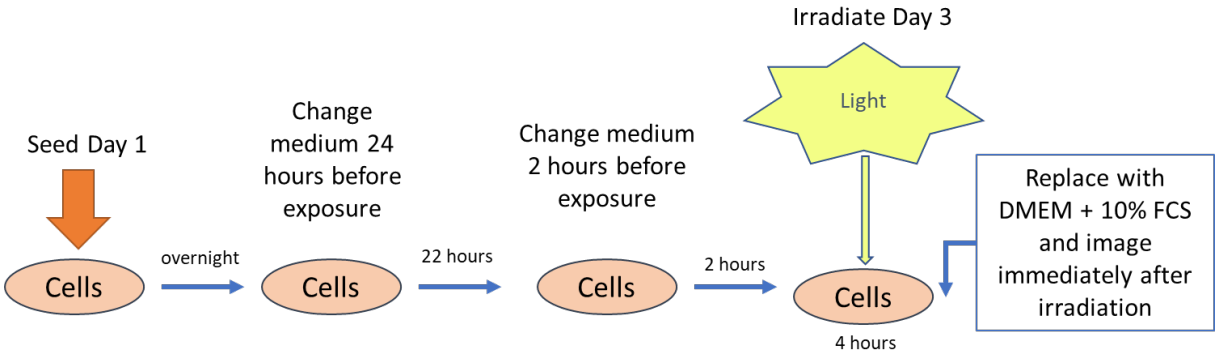

Figure 3-1 Diagram showing incubation periods used for optimising conditions

Table 3-1 Washout periods for visible light irradiation condition optimisation
"same" indicates the medium was not washed off or replaced.

	Seeded	24 hours before irradiation	2 hours before irradiation	before irradiation	After irradiation (no wash)
1	DMEM + 10% FCS (phenol-free)	MEMO + 1% FCS	MEMO	MEMO	DMEM + 10% FCS (phenol-free)
2	DMEM + 10% FCS (phenol-free)	MEMO	same	MEMO	DMEM + 10% FCS (phenol-free)
3	DMEM + 10% FCS (phenol-free)	DMEM + 10% FCS (phenol-free)	same	same	same

Images were taken of HDFn cells treated as above. Live cell brightfield imaging was carried out using the Nikon TiE with Nikon DS-Fi1 colour camera (Nikon, Japan). Cells were imaged immediately after changing the medium post-irradiation. They were removed from the incubator for the duration of taking the images and returned immediately after, until 24 hours later when the same dished were imaged for a second time. Four images per dish were taken on each occasion.

Viability assays were carried out with MTS at 0 and 24 hours post-irradiation, alamar blue at 0 and 24 hours post-irradiation, and crystal violet stain 24 hours after irradiation as per protocols in Chapter 2.

3.2.2.6 Effect of medium on response to UV light

HDFn cells were seeded at as per protocol in Chapter 2 in DMEM (with phenol red or phenol-free) containing 10% FCS or MEMO with no FCS. The following day, cells were washed 2 x with DPBS, and put into DPBS for irradiation, except for the MEMO condition in which the cells remained in MEMO for the irradiation. The cells were irradiated with 2.16 SEDs of complete solar simulated light as per irradiation protocol in Chapter 2. The DPBS or MEMO was replaced with phenol-free DMEM with 10% FCS and cells were assayed either immediately or 24 hours later with MTS as per protocol in Chapter 2.

3.3 Results

3.3.1 Controlling temperature in light experiments

3.3.1.1 High intensity infrared irradiation without temperature control

When temperature was not directly controlled, and tissue culture plates and dishes were placed 13 cm from the Hydrosun lamp on stacked tip boxes, irradiation with 360 mW.cm^{-2}

for 66 minutes 40 seconds for a dose of 1440 J.cm^{-2} caused temperature to increase (Figure 3-2). Before irradiation, temperature in plates and dishes was approximately 18°. In 96-well plates, the temperature of 100 ul of water reached 53°C in foil-covered unirradiated control wells and was significantly higher at 66°C in irradiated wells (p = 0.0024). In 35 mm dishes, temperature of the 2 ml water reacted 44°C and 50°C in unirradiated and irradiated dishes respectively, though this difference was not significant (p = 0.0583). Data collected by Dominic Pangilinan.

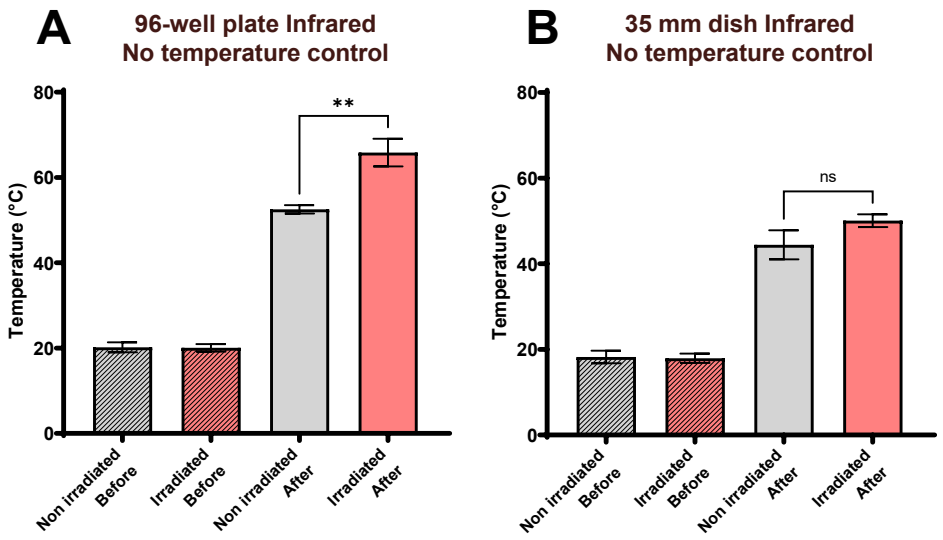

Figure 3-2 Change in temperature in plates and dishes irradiated with infrared light without temperature control

*96-well plates (A) and 35 mm dishes (B) containing water irradiated with 1440 J.cm^{-2} infrared light at 360 mW.cm^{-2} over 66.7 minutes without temperature control as measured with FLIR thermal camera. Controls were under lamp but covered with foil, receiving 0 J.cm^{-2}. A student's t-test was used to compare unirradiated and irradiated conditions after irradiation in both 96-well plates and 35 mm dishes. ** = p < 0.01. Data collected by Dominic Pangilinan. Data represent means ± SD, N = 3*

3.3.1.2 Infrared irradiation temperature control

3.3.1.2.1 Temperature control of low and high intensity infrared irradiation

When temperature was controlled using a stirred water bath set to 26°C at the start of irradiation, temperature did not exceed 34°C in and repeat in either clear plates or dishes with irradiation of 2 hours of low intensity infrared or 10 hours equivalent of high intensity infrared (Figure 3-3). The temperature of irradiated plates/dishes increased to the same degree as foil-covered, unirradiated dishes, from room temperature of ~20°C to ~33°C. The

difference between irradiated and unirradiated after irradiation was not significant for high or low intensity infrared in dishes or plates (2-tailed, unpaired students t-test, P > 0.05). Data collected by Dominic Pangilinan.

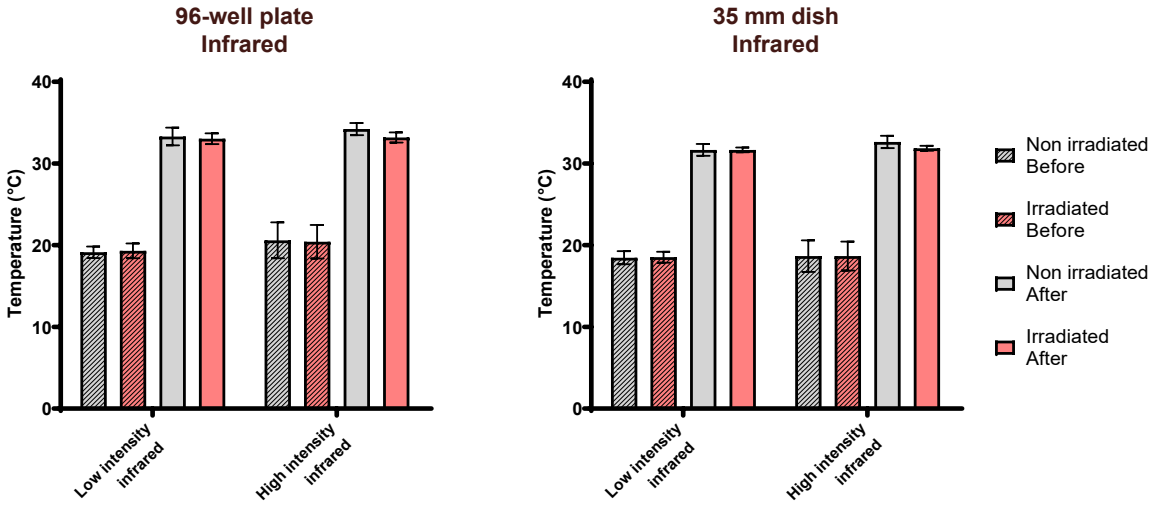

Figure 3-3 Change in temperature in plates and dishes irradiated with infrared light in a stirred water bath

Plates (left) and dishes (right) irradiated with 1440 J.cm^{-2} infrared light at 360 mW.cm^{-2} over 66.7 minutes in a stirred water bath as measured with FLIR thermal camera. Controls were under lamp but covered with foil, receiving 0 J.cm^{-2}. A student's t-test was used to compare unirradiated and irradiated conditions after irradiation in both 96-well plates and 35 mm dishes at both intensities. No significant differences were found. Data collected by Dominic Pangilinan. Data represent means ± SD, N = 3

3.3.1.2.2 Effect of plate colour on temperature

When clear, black and white-walled, clear bottomed, 96-well tissue culture plates containing 100 ul of water were irradiated with high intensity infrared light for up to 66 minutes 40 seconds at 360 mW.cm^{-2} to deliver a dose of 1440 mJ.cm^{-2}, the temperature in irradiated black wells was found to increase to above 43°C (Figure 3-4). Irradiation of white and clear plates did not result in such an increase, with irradiated wells remaining below 35°C.

A

Clear plate

	Unirradiated				2.5hr		5hr		7.5hr		10hr	
	1	2	3	4	5	6	7	8	9	10	11	12
A	31.7	31.8	32	32.7	33.2	33.2	33.4	33.4	33.3	33.1	32.8	32.5
B	31.8	32	32.3	33.4	34.2	34.4	34.5	34.4	34.4	34.1	33.8	32.7
C	31.9	32.2	32.5	33.6	34.5	34.7	34.9	34.6	34.7	34.5	34	33.1
D	32.1	32.4	32.6	33.7	34.8	34.7	34.7	34.6	34.6	34.4	34.1	33.3
E	32.2	32.5	32.7	33.7	34.7	34.6	34.5	34.5	34.5	34.4	34.3	33.6
F	32.1	32.3	32.6	33.7	34.6	34.5	34.4	34.4	34.4	34.3	34.2	33.5
G	31.9	32.1	32.3	33.5	34.4	34.2	34.1	34.2	34.3	34.2	33.9	33.5
H	31.7	32	32.1	32.9	33.7	33.5	33.4	33.3	33.4	33.4	33.1	33.3

B

Black plate

	1	2	3	4	5	6	7	8	9	10	11	12
A	32.3	32.4	32.7	34.1	37.1	38.5	39.8	41.1	41.2	41.4	41.6	41.9
B	32.2	32.4	32.8	34.5	38.1	39.5	41	41.6	42.5	42.7	42.4	43.1
C	32.3	32.5	33	35	38.8	40.6	42	42.3	42.9	43.2	42.5	43.1
D	32.2	32.5	33.1	35.3	39.5	40.9	42.2	42.5	42.7	42.5	42.6	42.7
E	32.3	32.6	33.1	35.5	40	41.4	42.5	42.3	42.5	42.3	42.5	43.2
F	32.2	32.6	33.1	35.8	41.5	43.8	42.8	42.2	42.3	42	41.7	42.7
G	32.1	32.5	33.1	35.9	41.3	42.4	43.2	42.2	43	42.2	42.8	42.3
H	32.1	32.4	33	35.9	39.3	40.7	41.8	42.1	42.3	42	42.3	41.8

C

White plate

	1	2	3	4	5	6	7	8	9	10	11	12
A	30.6	31	31.2	31.7	32.4	32.5	32.5	32.7	32.6	32.5	32	29.9
B	31	31.1	31.5	32	33	33.2	33.4	33.2	33.6	33.3	32.9	32.3
C	31	31.2	31.5	32.2	33.4	33.8	34	33.8	33.8	33.5	33.1	32.4
D	31.1	31.3	31.6	32.2	33.5	34	34.1	34.3	33.8	33.5	33.3	32.5
E	31.1	31.3	31.5	32.3	33.2	33.6	33.9	33.8	33.5	33.4	33.2	32.7
F	30.9	30.9	31.4	32.3	33.2	33.5	33.9	33.8	33.5	33.3	33.4	32.8
G	30.7	31.1	31.2	32.1	33.2	33.3	33.8	33.6	33.5	33.5	33.3	33
H	30.3	30.7	31.1	31.9	32.9	33.1	33.2	33.5	33.4	33.4	33.3	33

Figure 3-4 Temperature in different colours of 96-well plate after high intensity infrared irradiation in a stirred water bath

Temperature of water in clear (A), black (B) or white (C) 96-well plate after 0, 2.5, 5, 7.5 or 10 hours equivalent of high intensity infrared irradiation (360, 720, 1080 and 1440 mJ.cm^{-2} delivered over 16.7, 33.4, 50.1 and 66.7 minutes respectively with 360 mW.cm^{-2} infrared light) in a stirred water bath as measured with FLIR thermal camera. Controls (columns 1- to 3) were foil-covered for the duration of irradiation, receiving 0 J.cm^{-2} of light. N = 1

During the course of the 66 minute, 40 second irradiation with high intensity infrared light, the temperature of the lid of the plate was measured (Figure 3-5). Temperature of the plate lid of the black plate reached 65°C, while the temperatures of the lids of the white and clear plates did not exceed 36°C.

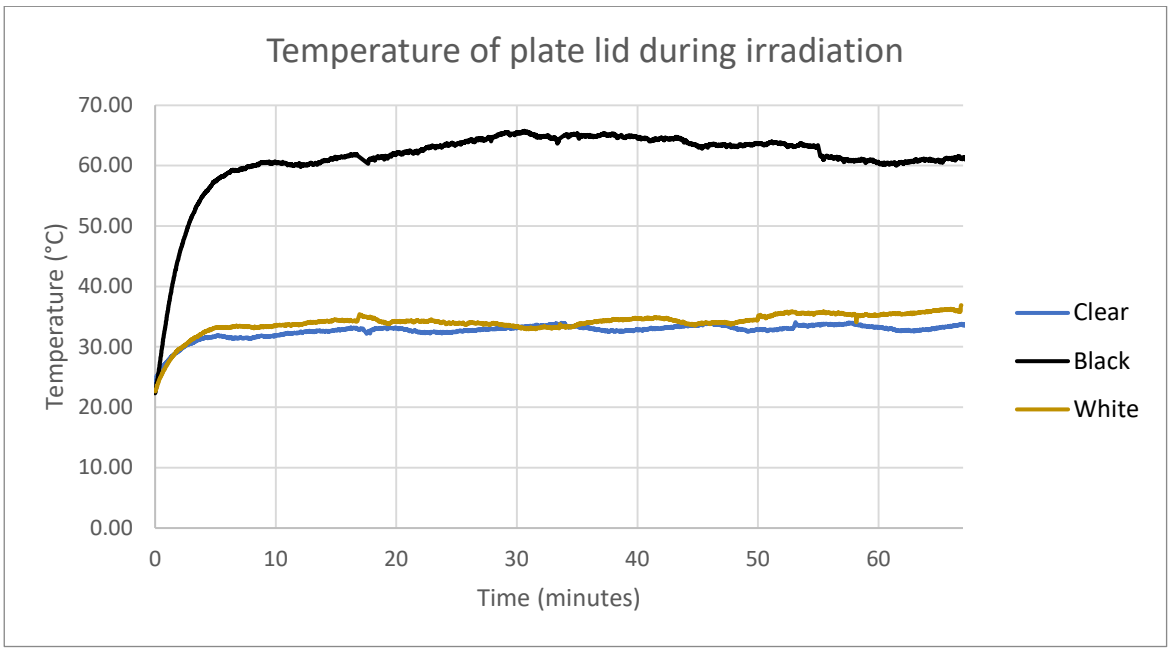

Figure 3-5 Temperature of exposed plate lid during irradiation of high intensity infrared *1440 mJ.cm^{-2} dose of infrared light at 360 mW.cm^{-2} delivered over 66 minutes 40 seconds to a plate (made of clear, black or white plastic) in a stirred water bath. Temperature of clear plate lid during irradiation measured with FLIR thermal camera. N = 1*

3.3.1.3 Solar simulator irradiation temperature control

3.3.1.3.1 Complete solar light and solar UV irradiation

When irradiated with 2.16 SEDs of complete solar simulate light or UV only while raised 4 cm above the bench on a stand, there was no large change in temperature over the course of irradiation (Figure 3-6). The difference between irradiated and unirradiated after irradiation was not significant for complete solar simulated light or UV only (2-tailed, unpaired students t-test, $P > 0.05$). Data collected by Dominic Pangilinan.

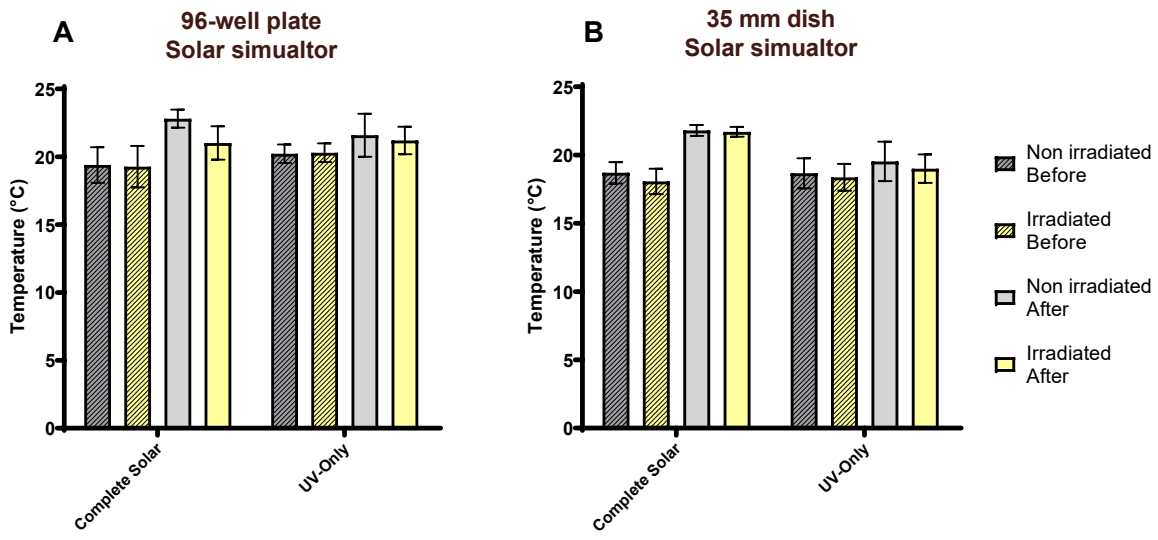

Figure 3-6 Change in temperature in plates and dishes irradiated with complete solar simulated light or UV only

Clear plastic 96-well plates (A) and 35 mm dishes (B) irradiated with 2.16 SEDs of complete solar simulated light or UV only over ~2 or ~3 minutes respectively on a stand as measured with FLIR thermal camera. Unirradiated controls were foil-covered and received no light. Data collected by Dominic Pangilinan. Data represent means ± SD, N = 3

3.3.1.3.2 Visible light irradiation

While black plastic reflects the least light, this means it absorbs more and thus increases in temperature during irradiation. This was measured with the FLIR Thermal Camera recording the temperature of the plastic under the solar simulator beam and the plate lid of a plate on the stand 4 cm above the bench top for 4 hours to represent the duration of a visible light irradiation (Figure 3-7). The temperature of the black plastic reached 43°C, but the temperature of the plate lid did not exceed 26°C.

There was a cycle of increasing then decreasing temperature between ~38°C and 43°C for the black plastic surface and ~23°C and 26° for the plate lid with a period of approximately 12 minutes. This is likely to be due to the air conditioning cycling on and off to maintain room air temperature of 19°C, resulting in increased air movement and decreased air temperature when it was on, reducing the temperature of the irradiated surfaces, which would then increase while the air conditioner was off.

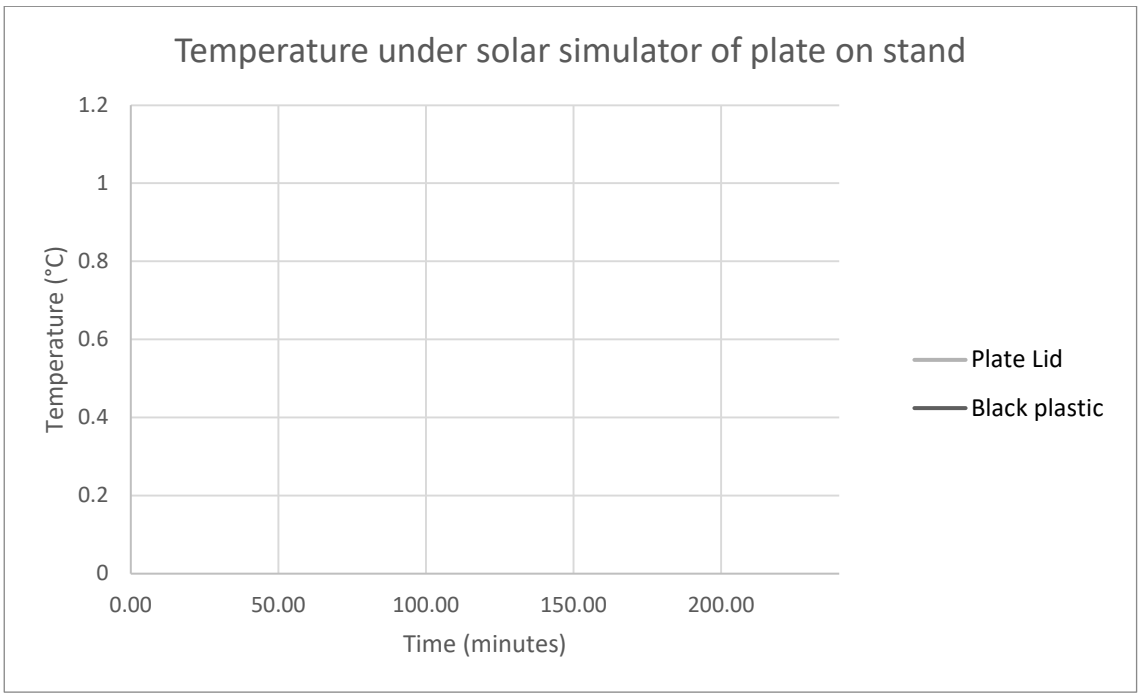

Figure 3-7 Temperature of black plastic surface and plate lid under solar simulator
4-hour duration, 19.8 mW.cm^{-2}, 285 J.cm^{-2} dose, temperature measured with FLIR thermal camera.

When temperature in 35 mm dishes exposed to blue, green, red, far red and complete visible wavebands of visible light, the temperature significantly increased in all conditions after irradiation compared to before, from ~17.5°C to ~24°C ($p < 0.002$ for all comparisons). There was no significant difference in temperature after irradiation in any of the irradiated conditions compared to the control which remained in foil for the duration of irradiation ($p > 0.1445$ in all comparisons). Data collected by Dominic Pangilinan.

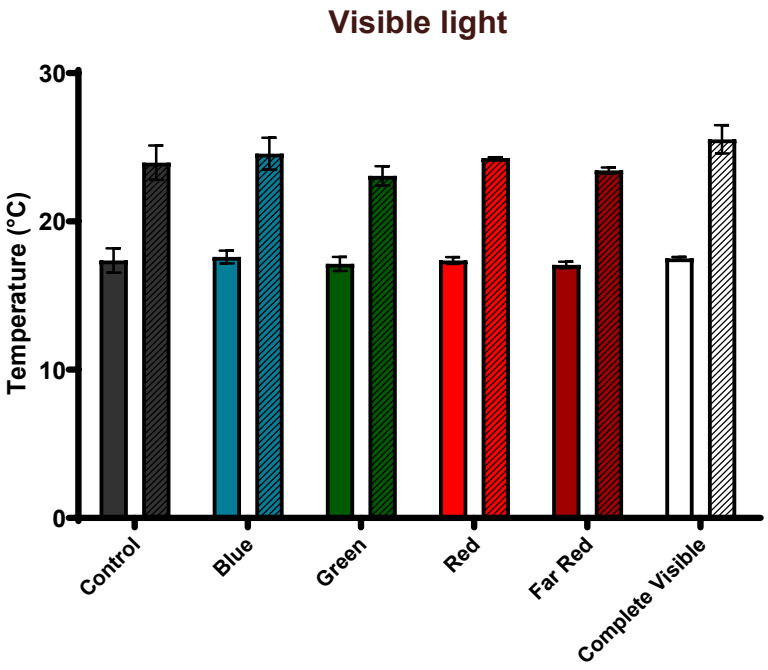

Figure 3-8 Change in temperature in dishes irradiated with visible light wavebands
Temperature change in 2 ml of water in 35 mm dishes. Carried out on a stand, measured with FLIR thermal camera. Control sample was under the lamp but foil-covered for the duration of irradiation, receiving 0 J.cm^{-2}of light. Plain bars represent temperature before irradiation, dashed bars represent temperature after irradiation.

Blue condition exposed to 410-510 nm light at 8.7 mW.cm^{-2} for 1 hour 35 minutes with dose of 49.7 J.cm^{-2}. Green condition exposed to 515-610 nm light at 3.5 mW.cm^{-2} for 3 hours 47 minutes with dose of 47.5 J.cm^{-2}. Red condition exposed to 610-710 nm light at 4.4 mW.cm^{-2} for 2 hours and 54 minutes with dose of 46.2 J.cm^{-2}. Far red condition exposed to 715-810 nm light at 3 mW.cm^{-2} for 3 hours and 5 minutes with dose of 32.9 J.cm^{-2}. Complete visible condition exposed to 410-810 nm light at 19.8 mW.cm^{-2} for 2 hours and 41 minutes with dose of 191.9 J.cm^{-2}.

Data collected by Dominic Pangilinan. Data represent means ± SD, N = 3

3.3.1.4 Viability with and without temperature control during infrared irradiations

3.3.1.4.1 Without temperature control

Cells irradiated with medium intensity infrared light (irradiance 100 mW.cm^{-2}, duration 1 hour, dose 360 J.cm^{-2}) or high intensity infrared light (irradiance 360 mW.cm^{-2}, duration 16 minutes 40 seconds, dose 360 J.cm^{-2}) in 96-well plates were assayed with MTS to determine viability after irradiation (Figure 3-9). Unirradiated controls had high variance and were not significantly different to incubator controls. Both immediately and 24 hours after irradiation,

at both medium and high intensity infrared there were significant decreases in viability as measured with MTS absorbance.

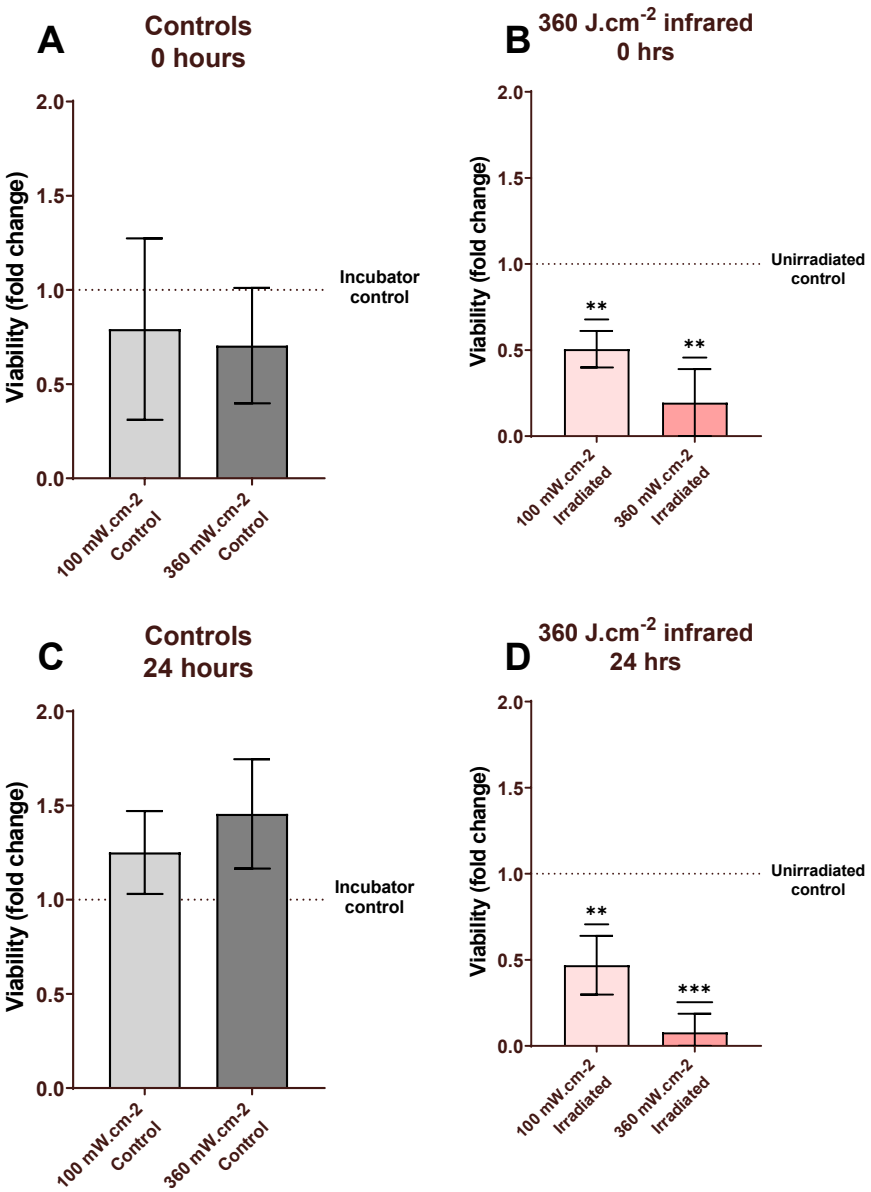

Figure 3-9 Effect of infrared on HFDn cell MTS viability without temperature control
Effect of 360 J.cm^{-2} of infrared at either 100 mW.cm^{-2} or 360 mW.cm^{-2} on viability at 0 and 24 hours after irradiation. Incubator controls experienced the same wash steps but remained in the incubator during irradiation. Unirradiated controls were under the lamp during irradiation but covered in foil to receive 0 J.cm^{-2} of light. Panels A and C show unirradiated controls compared to incubator controls 0 and 24 hours after irradiation respectively. Panels B and D show irradiated cell viability compared to unirradiated controls at 0 and 24 hours after irradiation respectively. (**): p ≤ 0.01, (***): p ≤ 0.001, one-sample t-test compared to unirradiated control; data represent means ± SD, N = 4, n = 3

3.3.1.4.2 With temperature control

3.3.1.4.2.1 Low intensity IR

With temperature control, consisting of suspending the plates in a stirred water bath that does not exceed 32°C over the course of irradiation, there were no significant effects of low intensity infrared (irradiance 40 $mW.cm^{-2}$, duration 2 hours, dose 288 $mW.cm^{-2}$) on viability as measured by MTS. HDFn cells were irradiated in FCS-free, phenol-free DMEM containing 25 mM HEPES and the standard 0.4 mg/l riboflavin. The incubator control condition was treated in the same way as the irradiated cells regarding washing and media, but instead of being outside of the incubator during the 2-hour irradiation, it was returned to the humidified, 37°C, 5% CO_2 incubator. This was to measure any effects the lower temperature (26-32°C) and CO_2 (0.04%) atmosphere the cells were subjected to during irradiation.

Unirradiated controls were not significantly different from incubator controls at 0 or 24 hours post-irradiation, and irradiated cells were not significantly different to unirradiated controls 0 or 24 hours after irradiation.

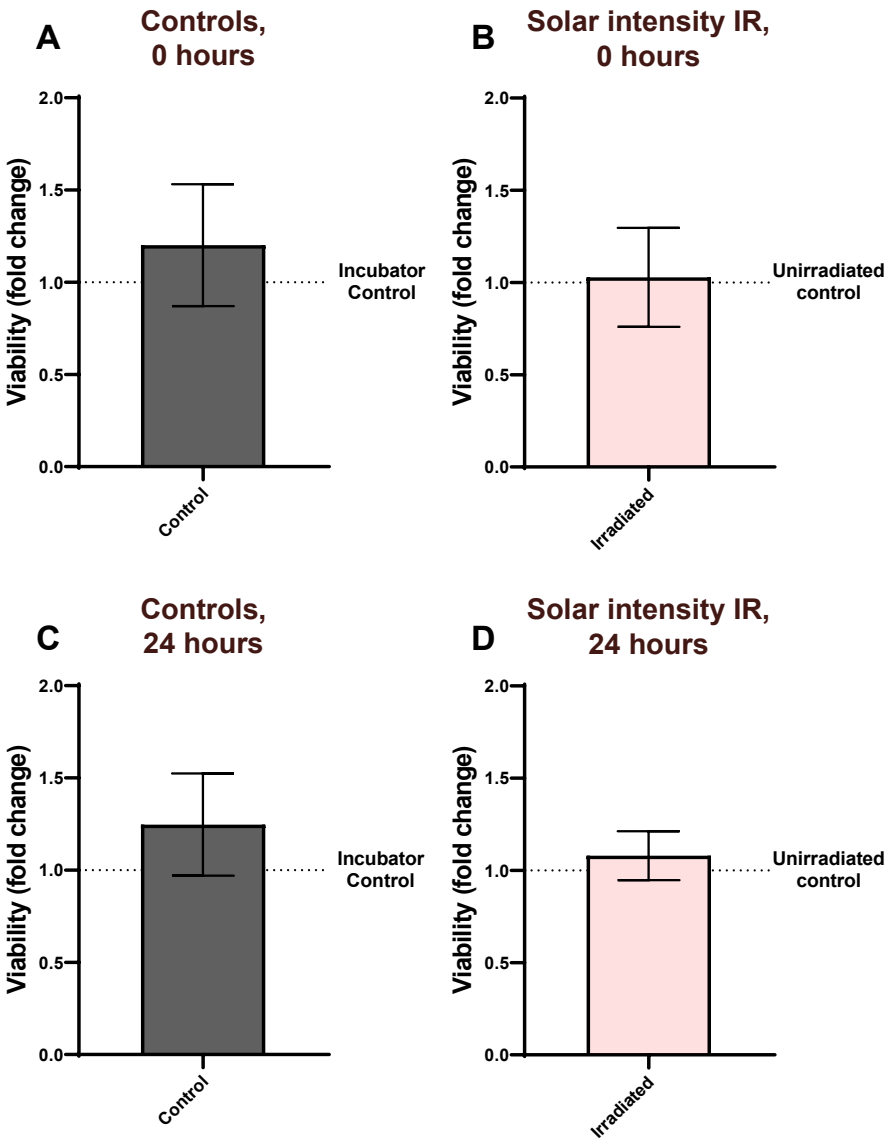

Figure 3-10 Effect of low intensity infrared on HDFn cell MTS viability with a stirred water bath
Effect of 288 J.cm^{-2} of infrared at 40 mW.cm^{-2} for 2 hours on viability compared to unirradiated, 0 J.cm^{-2}, foil-covered controls, 0 and 24 hours after irradiation (panels B and D respectively). Panels A and C show unirradiated controls compared to incubator controls, which experienced the same wash steps but remained in the incubator during irradiation, 0 and 24 hours after irradiation respectively. A stirred water bath was used for temperature control. No significant differences with one-sample t-test; data represent means ± SD, N = 3, n = 3

3.3.1.4.2.2 High intensity IR

As for low intensity infrared, with temperature control there were no significant effects of high intensity infrared (irradiance 360 mW.cm^{-2}, duration 13 minutes 20 seconds to 66 minutes 40 seconds, dose 288 to 1440 mW.cm^{-2}) on viability as measured by MTS (Figure

3-11). Unirradiated controls were not significantly different from incubator controls at 24 hours post-irradiation, though at 0 hours there was a significant increase (29%, p = 0.0438). Irradiated HDFn cells were not significantly different to unirradiated controls 0 or 24 hours after irradiation at any of the doses up to and including 10 hours equivalent of high intensity infrared.

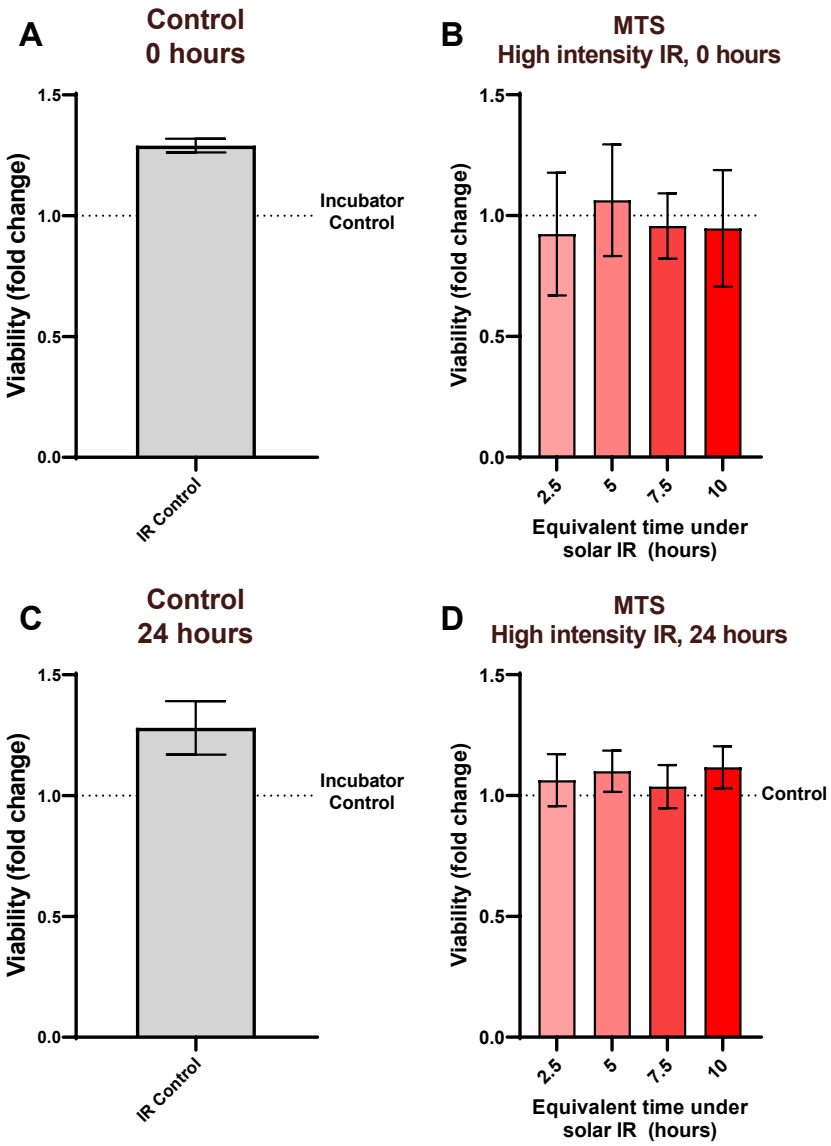

Figure 3-11 Effect of high intensity infrared on MTS viability with a stirred water bath
Effect of up to 1440 J.cm^{-2} of infrared on MTS viability compared to unirradiated, 0 J.cm^{-2}, foil-covered controls 0 and 24 hours after irradiation (panels B and D respectively). Panels A and C show unirradiated controls compared to incubator controls, which experienced the same wash steps but remained in the incubator during irradiation, 0 and 24 hours after irradiation respectively. A stirred

water bath was used for temperature control. No significant differences with one-sample t-test; data represent means ± SD, N = 2, n = 3.

3.3.2 Medium conditions with light irradiation

3.3.2.1 pH changes over the course of an irradiation

A standard curve of absorbance at different pH levels was used to calculate the pH of medium in plates and dishes by measuring the absorbance of the medium at 560 nm (Figure 3-12).

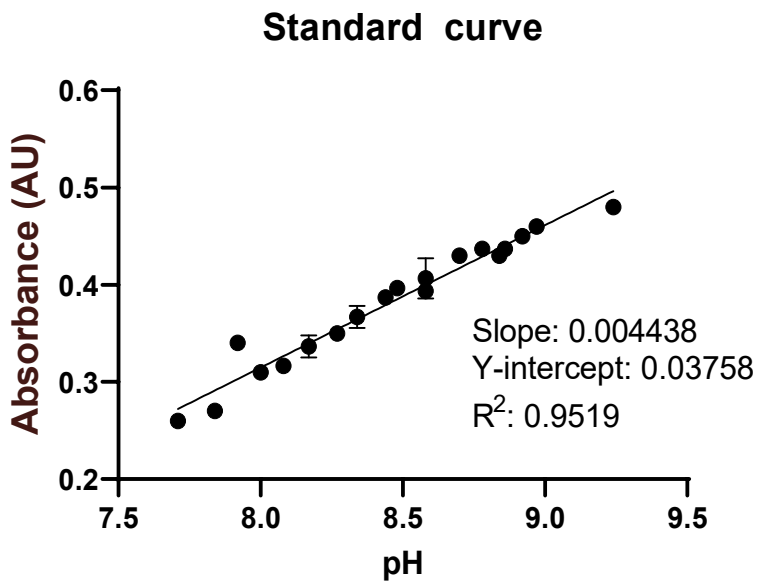

Figure 3-12 Standard curve of absorbance at 560 nm of DMEM containing phenol red at different pHs.
Data represent mean ± SD. N = 1, n = 3

4 hours after being taken from the incubator and being left with the lid resting normally on top, the pH in dishes and plates had both increased from pH 7.5 to pH 9 (Figure 3-13). When parafilm was placed around the lid of the dish or plate, this limited the increase in pH 8 or 8.3 respectively.

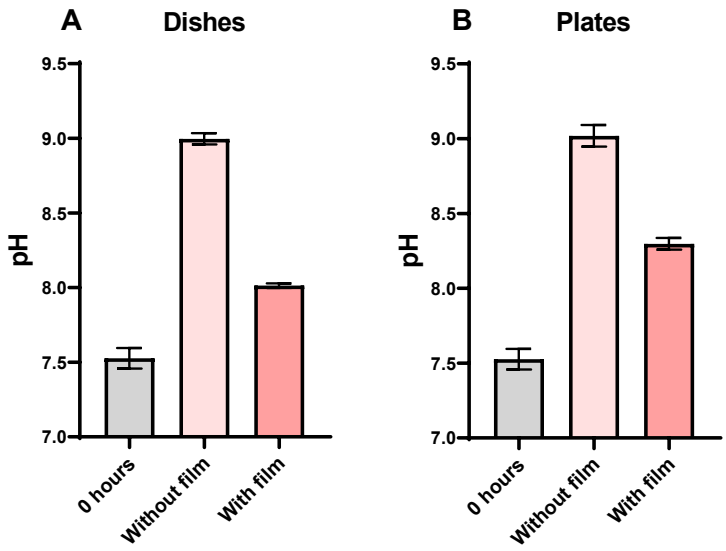

Figure 3-13 pH in plates and dishes after 4 hours outside a 5% CO_2 incubator.
pH measured in 35 mm dishes (panel A) and 96-well plates (panel B) N = 1, n ≥ 3.

3.3.2.2 Presence of FCS does not protect cell viability when out of incubator

During visible light irradiations, cells would be out of the incubator and under the lamp for 4 hours, during which temperature and pH would not be maintained. Effects of this on viability/metabolism were assayed using the MTS viability assay (Figure 3-14). Immediately after irradiation, there was a significant difference in metabolism/viability between the cells kept in the incubator in medium containing FCS versus cells kept outside the incubator ("Bench" condition) in medium without FCS (51% decrease, $p = 0.0287$), but no significant difference between cells that were outside the incubator with versus without FCS (one-sample t-test, $p > 0.05$). 24 hours after irradiation, there was a significant decrease in viability between the cells kept in the incubator with FCS and those kept outside without FCS (25% decrease, $p = 0.0121$), but again no significant difference between cells that were outside the incubator with versus without FCS (one-sample t-test of data from cells without FCS normalised to those with FCS, $p > 0.05$).

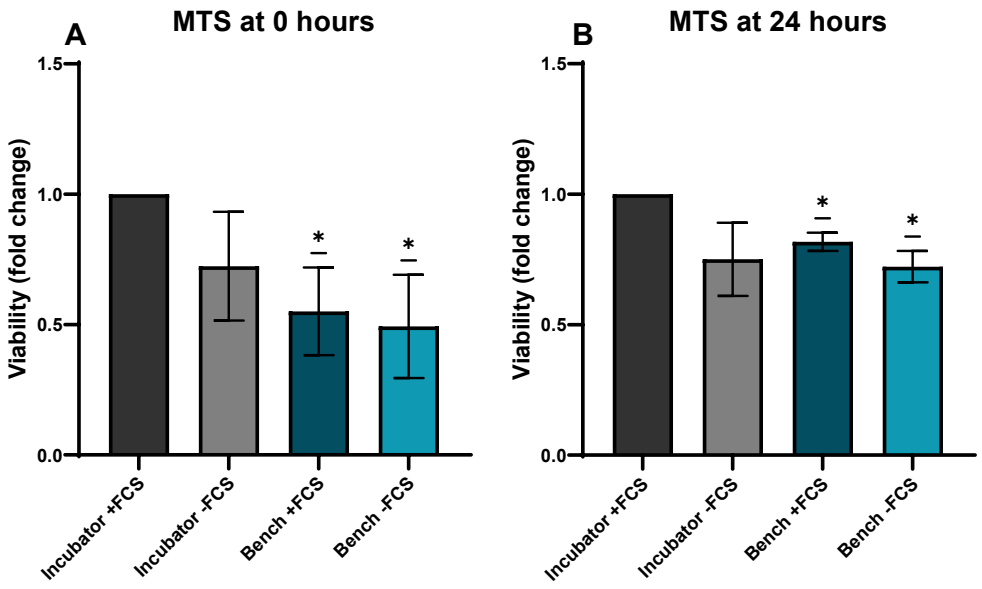

Figure 3-14 Effect of time outside incubator of HDFn cells in medium with and without FCS on viability assessed with colourimetric MTS assay.
A: cell viability immediately after 4 hours out of incubator. B: viability 24 hours after 4 hours in incubator. In all cases, cells were in grown in complete, phenol-containing DMEM with 10% FCS before the 4-hour incubation in the medium indicated on the graph and returned to complete DMEM with 10% FCS after incubation. (*): $p \leq 0.05$, one-sample t-test; data represent means ± SD, N = 3, n = 3

3.3.2.3 HEPES and riboflavin presence do not affect viability after infrared irradiation

3.3.2.3.1 High intensity infrared

Fibroblasts were assayed using the MTS and crystal violet stain viability assay after irradiation in FCS-free, phenol-free DMEM containing 25 mM HEPES and 0.4 mg/l riboflavin (Figure 3-15). HDFn cells irradiated with high intensity infrared (360 $mW.cm^{-2}$) were unaffected by up to a dose equivalent to 10 hours of peak noon sunlight infrared intensity (1440 $mJ.cm^{-2}$). Irradiation was temperature-controlled with a stirred water bath. Viability/metabolism was unaffected immediately or 24 hours after the end of the irradiation.

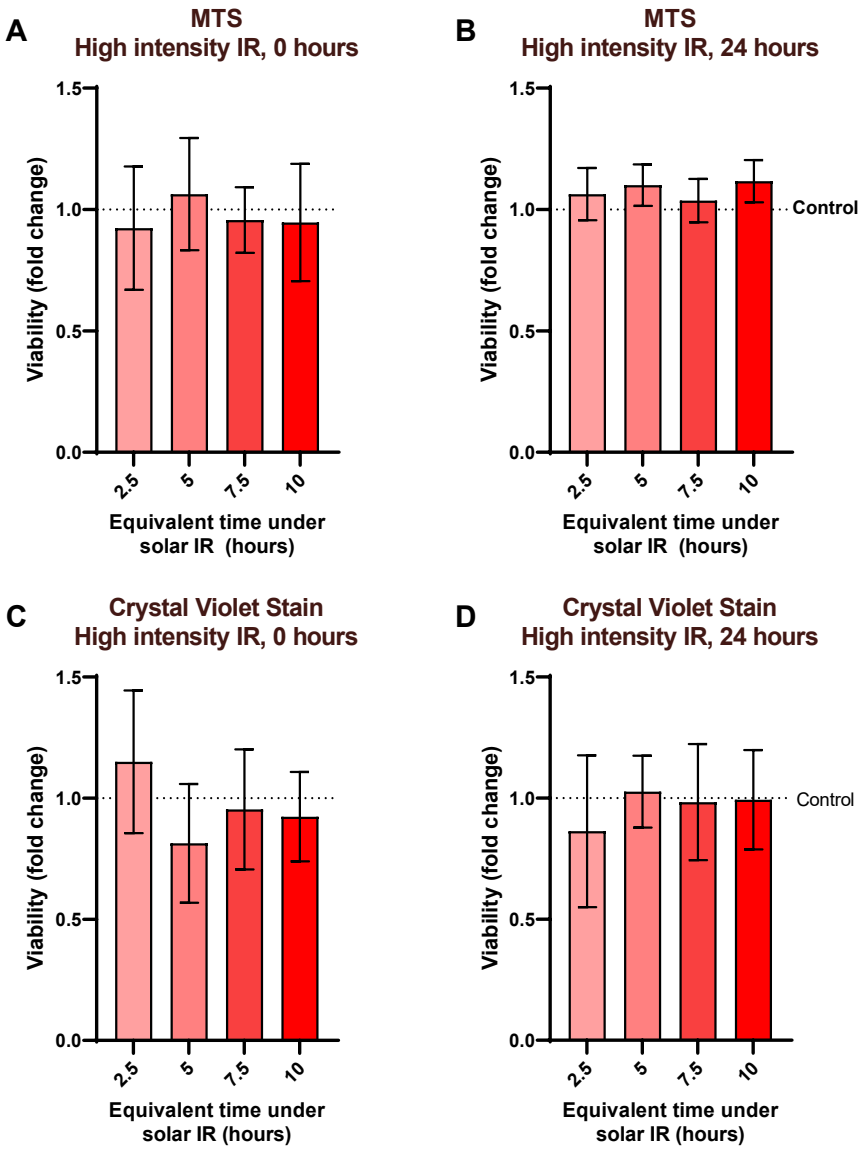

Figure 3-15 Effect of high intensity infrared on HDFn cells on MTS and crystal violet stain viaibilty *360 mW.cm^{-2} of infrared at equivalent doses of sunlight of 2.5 hours (360 J.cm^{-2}), 5 hours (720 J.cm^{-2}), 7.5 hours (1080 J.cm^{-2}) and 10 hours (1440 J.cm^{-2}) delivered over 16.7, 33.3, 50 or 66.7 minutes respectively. Temperature was controlled with a stirred water bath. Unirradiated controls were in foil under lamp for duration of irradiation receiving 0 J.cm^{-2}. Panels A and B show MTS viability as compared to unirradiated control at 0 and 24 hours after irradiation respectively. Panels C and D show crystal violet stain measured viability 0 and 24 hours after irradiation respectively. Panels A and B the same as panels B and D in Figure 3-11. No significant differences as tested by a one-sample t-test; data represent means ± SD, N = 3, n = 3*

3.3.2.4 HEPES induces cell death in the presence of visible light

Effects of visible light on cell viability/metabolism with FCS-free, phenol-free DMEM containing HEPES buffer as assessed using the MTS viability assay (Figure 3-16). HDFn cells

were exposed to blue light (410-510 nm) and red light (610-710 nm) for an equivalent of 1 hour of visible light from the sun at peak intensity. Irradiation was temperature-controlled using a stand. Immediately after irradiation, cell viability was reduced by 100% in the blue light irradiated cells and 52% in the red light irradiated cells. After 24 hours, viability in the blue light irradiated cells was reduced by 76% and in the red light irradiated cells by 50%.

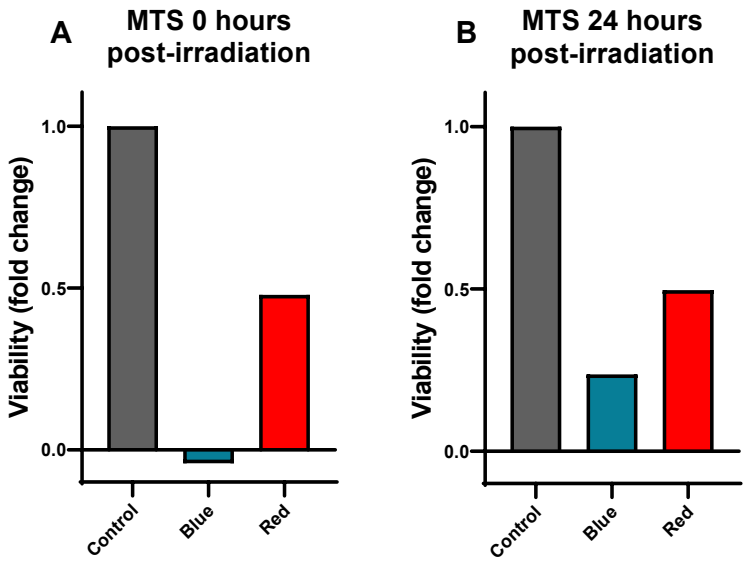

Figure 3-16 Effect on viability of HDFn cells of 1-hour equivalent visible light dose from the sun in medium containing HEPES

Blue condition exposed to 410-510 nm light at 8.7 mW.cm^{-2} for 1 hour 35 minutes with dose of 49.7 J.cm^{-2}. Red condition exposed to 610-710 nm light at 4.4 mW.cm^{-2} for 2 hours and 54 minutes with dose of 46.2 J.cm^{-2}. Unirradiated controls were wrapped in foil under the lamp for duration of irradiation to receive 0 J.cm^{-2} of light . Panel A: MTS measured immediately after irradiation, B: 24 hours after irradiation. Results not tested for significance as only one biological repeat N = 1, n = 3

3.3.2.5 Presence of riboflavin and FCS in visible light and UV irradiations

3.3.2.5.1 Riboflavin presence induces death in HDFn cells during visible light irradiation

Cell viability/metabolism was measured using the MTS viability assay after cells had been exposed to visible light in medium containing riboflavin but no HEPES, in the following wavebands: blue (41-510 nm), green (515-610 nm), red (610-710 nm) and far red (715-810 nm) (Figure 3-17). An incubator control was kept in the incubator while the visible control was kept under the lamp but wrapped in foil to block the light. Irradiation was temperature-controlled using a stand. Viability in these was not significantly different immediately or 24 hours after exposure. Compared to the visible control, the visible wavebands were not

significantly different at 0 or 24 hours post-irradiation, except for the blue waveband, which had viability reduced by 58% (p = 0.0146) and 45% (p = 0.0147) respectively.

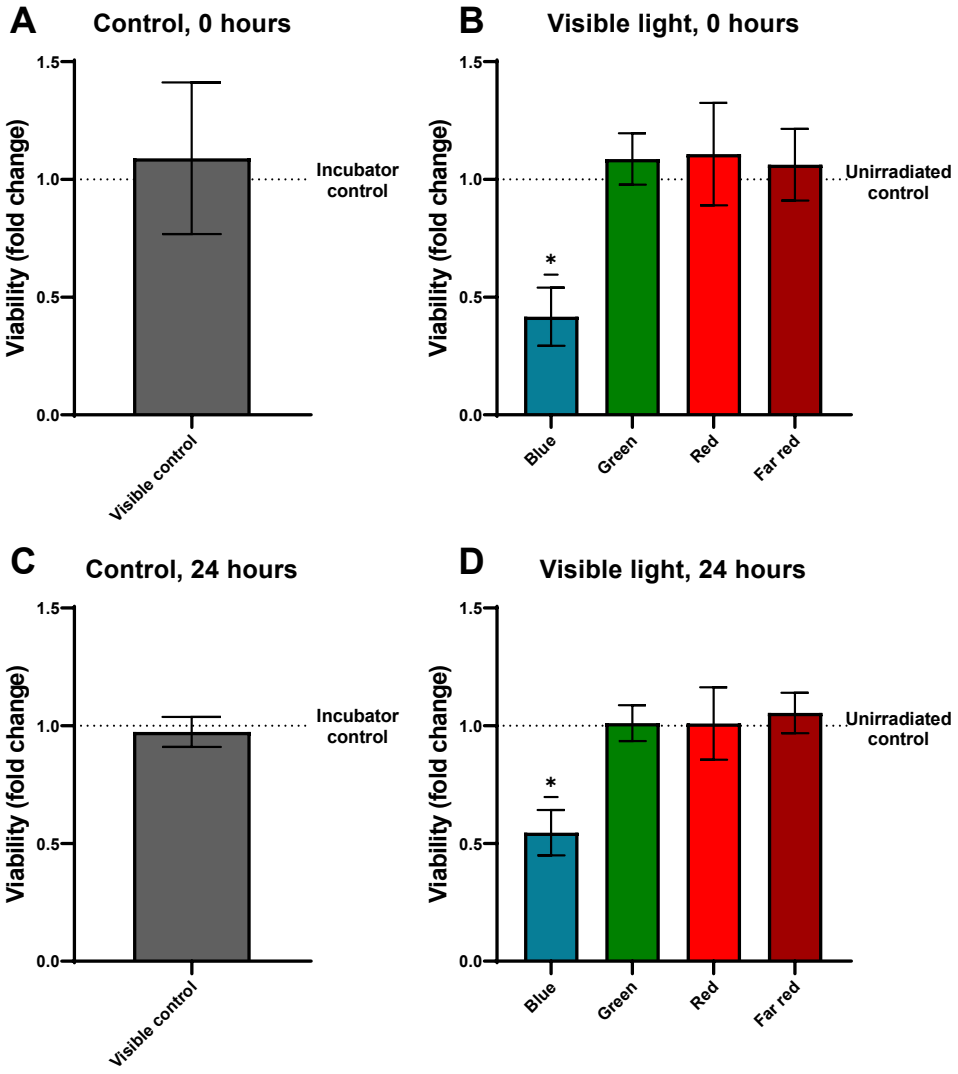

Figure 3-17 Effect on viability visible light in FCS-free, phenol-free DMEM without HEPES but with riboflavin

Cell viability/metabolism measured with MTS. Blue condition exposed to 410-510 nm light at 8.7 mW.cm^{-2} for 1 hour 35 minutes with dose of 49.7 J.cm^{-2}. Green condition exposed to 515-610 nm light at 3.5 mW.cm^{-2} for 3 hours 47 minutes with dose of 47.5 J.cm^{-2}. Red condition exposed to 610-710 nm light at 4.4 mW.cm^{-2} for 2 hours and 54 minutes with dose of 46.2 J.cm^{-2}. Far red condition exposed to 715-810 nm light at 3 mW.cm^{-2} for 3 hours and 5 minutes with dose of 32.9 J.cm^{-2}. Incubator controls experienced the same wash steps but remained in the incubator during irradiation. Unirradiated controls were under the lamp during irradiation but wrapped in foil to receive 0 J.cm^{-2} of light. HDFn cells were seeded in complete phenol-containing DMEM with 10% FCS. Immediately before irradiation, medium was washed off and replaced with phenol-free DMEM with no HEPES and no FCS. After irradiation, cells were returned to complete DMEM with 10% FCS. Temperature was controlled

using a stand. Panel A: unirradiated control versus incubator control immediately after irradiation. B: irradiated cells versus unirradiated control immediately after irradiation. C: unirradiated control versus incubator control 24 hours after irradiation. D: irradiated versus unirradiated control 24 hours after irradiation. (*): $p < 0.05$, two-tailed one-sample t-test; data represent means ± SD, N = 3, n = 3

3.3.2.5.2 Removal of riboflavin by using MEMO reduces damage from photosensitisation with visible light

When irradiated in MEMO medium, which has the same formulation as DMEM but without riboflavin (or HEPES), cell viability as measured with MTS was not significantly changed by a one-hour equivalent dose any of the visible light conditions immediately or 24 hours after irradiation (as tested with one-sample t-test) (Figure 3-18). Irradiation was temperature-controlled using a stand. There was additionally no significant difference between the visible irradiation control and the incubator control. However, there was a non-significant decrease of 28% in MTS signal in HDFn cells irradiated with a dose of “complete” visible light with wavelengths from 410-810 nm, both immediately and 24 hours after irradiation.

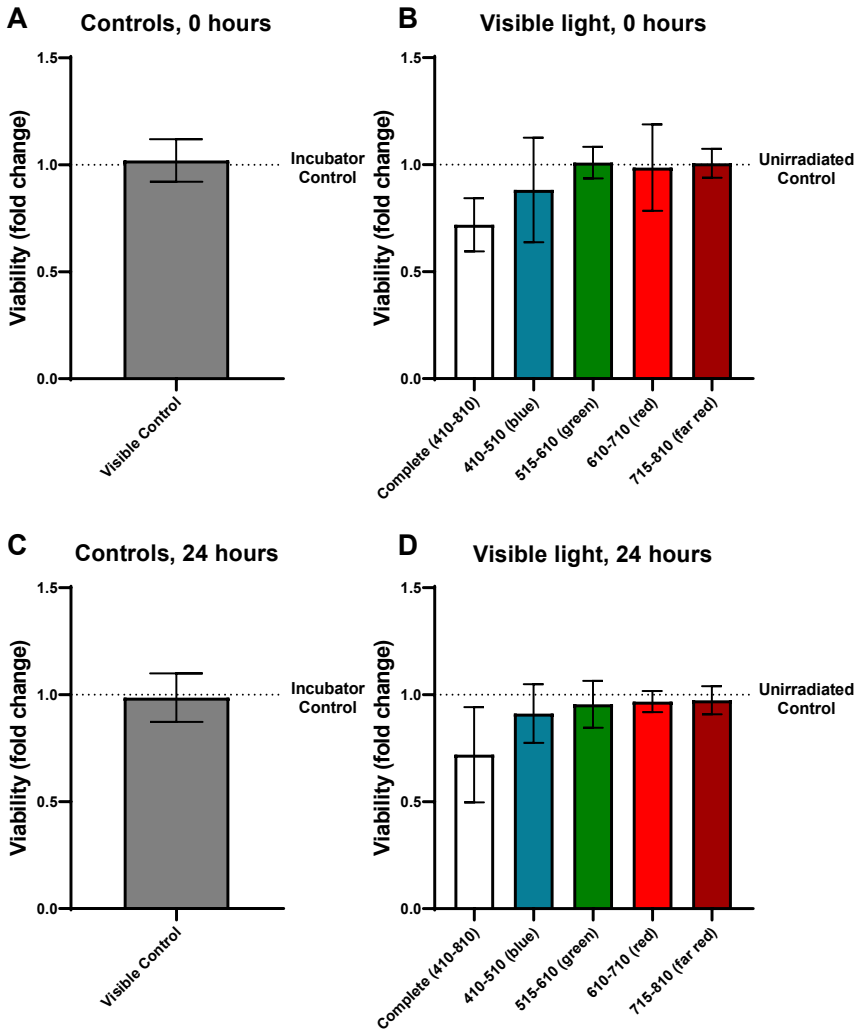

Figure 3-18 Effect on viability visible light in phenol-free DMEM without HEPES, riboflavin or FCS (MEMO)

Effect of equivalent dose of 1 hour of peak solar light on viability as measured with MTS. Blue condition exposed to 410-510 nm light at 8.7 mW.cm^{-2} for 1 hour 35 minutes with dose of 49.7 J.cm^{-2}. Green condition exposed to 515-610 nm light at 3.5 mW.cm^{-2} for 3 hours 47 minutes with dose of 47.5 J.cm^{-2}. Red condition exposed to 610-710 nm light at 4.4 mW.cm^{-2} for 2 hours and 54 minutes with dose of 46.2 J.cm^{-2}. Far red condition exposed to 715-810 nm light at 3 mW.cm^{-2} for 3 hours and 5 minutes with dose of 32.9 J.cm^{-2}. Complete visible condition exposed to 410-810 nm light at 19.8 mW.cm^{-2} for 2 hours and 41 minutes with dose of 191.9 J.cm^{-2}. Incubator controls experienced the same wash steps but remained in the incubator during irradiation. Unirradiated controls were under the lamp during irradiation but wrapped in foil to receive 0 J.cm^{-2} of light. HDFn cells were seeded in complete phenol-containing DMEM with 10% FCS. Immediately before irradiation, medium was washed off and replaced with MEMO with no FCS. After irradiation, cells were returned to complete DMEM with 10% FCS. Temperature was controlled using a stand. Panel A: unirradiated control versus incubator control immediately after irradiation. B: irradiated cells versus unirradiated control immediately after irradiation. C: unirradiated control versus incubator control 24 hours after irradiation. D: irradiated cells versus unirradiated control 24 hours after irradiation. No significant differences with one-sample t-test; data represents means ± 95% CI, N = 3, n = 3

3.3.2.5.3 Removal of riboflavin and FCS with MEMO does not change viability

Cell viability after in MEMO (DMEM containing no phenol red or riboflavin) with no FCS is not significantly changed compared to HDFn cells cultured in complete, phenol-free DMEM with 10% FCS for the 4-hour duration in the dark (unirradiated) (Figure 3-19). This experiment did not involve irradiation; the 96-well plates were left at room temperature outside the incubator in the dark for the 4-hour duration.

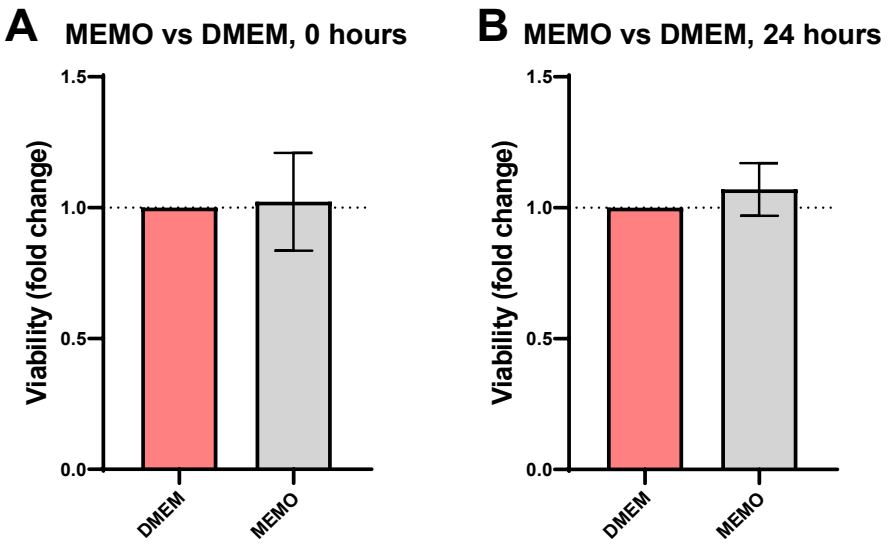

Figure 3-19 Effect of 4 hours of culturing in MEMO versus complete, phenol-free DMEM
HDFn cells were seeded in complete, phenol-containing DMEM with 10% FCS. The next day, medium was replaced with either MEMO or complete, phenol-free DMEM with 10% FCS. After 4 hours, the medium was removed and in both conditions replaced with complete, phenol-free DMEM with 10% FCS. Viability measured with MTS immediately (A) and 24 hours (B) after returning to complete, phenol-free DMEM (B). Data were normlised to DMEM condition. No significant differences with one-sample t-test; data represents means ± SD, N = 3, n = 3

3.3.2.5.4 Effect of medium on gene expression

3.3.2.5.4.1 Gene expression is changed in unirradiated HDFn cells in different media

To determine how cells would behave differently when in MEMO medium (DMEM without riboflavin, phenol red and FCS), the expression of matrix metalloproteinases 1, 2 and 3 (MMP1, MMP2 and MMP3) and procollagen α1 (COL1A1) was compared between cells cultured in MEMO for 24 hours, then returned to complete, 10% FCS, phenol red-free DMEM for 24 hours before extraction versus those cultured in complete, 10% FCS DMEM, with or without phenol red, prior to irradiation (Figure 3-20).

Compared to phenol-containing DMEM, cells in phenol-free DMEM did not have significantly different expression, though MMP1 was higher (2.15-fold increase, p = 0.09, unpaired 2 tailed t-test) and MMP3 was slightly higher (1.45-fold higher, p = 0.11, unpaired 2 tailed t-test).

Cells in MEMO compared to those in phenol-containing DMEM had significantly higher MMP2 expression (2.4-fold higher, p = 0.002, unpaired 2 tailed t-test) and procollagen expression (3.3-fold, p = 0.004, unpaired 2 tailed t-test). MMP1 and MMP3 were lower in MEMO but not significantly (28% reduction, p = 0.3 and 57% reduction, p = 0.1 respectively, unpaired 2 tailed t-test).

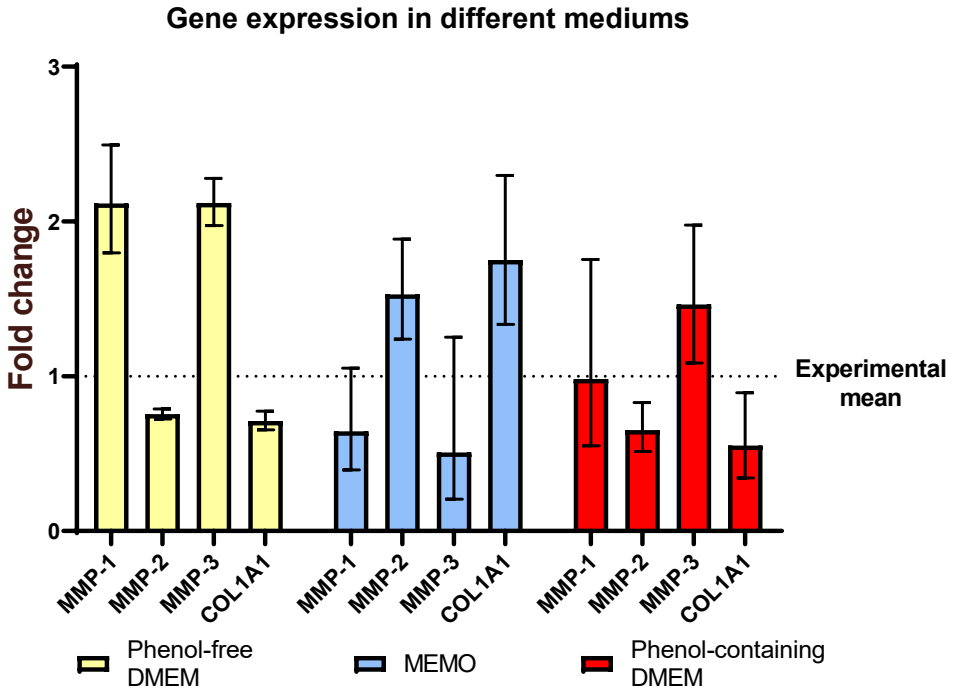

Figure 3-20 Effect of 24 hours of culturing in MEMO versus complete, phenol-free DMEM. *HDFn cells were seeded in either MEMO, phenol-free complete DMEM with 10% FCS or phenol-containing complete DMEM with 10% FCS. 24 hours after seeding, the medium on all conditions was replaced with complete, phenol-free DMEM with 10% FCS. RNA extracted 24 hours after later. Expression assayed with TaqMan qPCR. Data were normalised to experimental mean – a mean of all biological repeats across all conditions. Stats were carried out on log2 transformed data. Data represent geometric means ± geometric SD, N = 3, n = 3*

3.3.2.5.4.2 MEMO responds to solar light in a dose-dependent manner

HDFn cells cultured and irradiated in MEMO (DMEM without riboflavin, phenol red or FCS) were irradiated with one of 3 doses to create a dose-response graph of gene expression of MMP-1, MMP-2, MMP-3 and COL1A1 (Figure 3-21). The best-fit slope of each line tested with a least squares fit was compared to a null hypothesis of the slope = 0, constrained to y-intercept = 1 on log transformed data. The slope of each line was significantly different to 0 for all genes (MMP-2 $p = 0.0171$, all others $p < 0.0001$), indicating the dose-dependency of the change in gene expression in these genes exposed to up to 2.16 SEDs of solar simulated light.

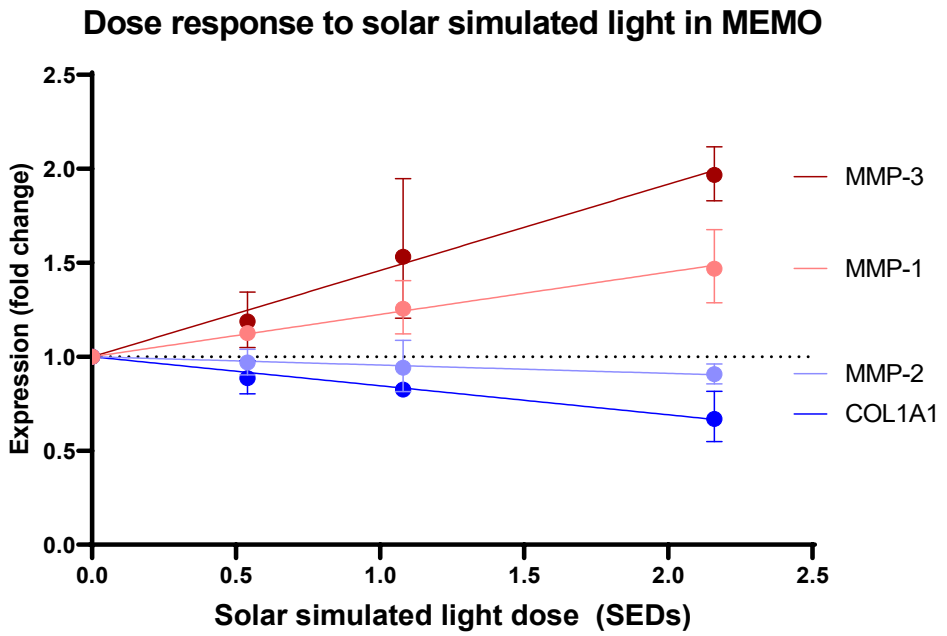

Figure 3-21 Dermal fibroblast gene expression profile after a dose of solar simulated radiation. *Monolayer HDFn cells were seeded in MEMO. The next day, they were irradiated 0.54, 1.08 or 2.16 SEDs of complete solar light in MEMO over ~0.5, 1 or 2 minutes respectively. Subsequently, the medium was replaced with complete, phenol-free DMEM with 10% FCS. RNA was extracted 24 hours after the end of irradiation. Temperature was controlled using a stand. Unirradiated controls were under the lamp during irradiation but wrapped in foil to receive 0 J.cm^{-2} of light. Gene expression was assessed with TaqMan PCR primers. Data were normalised to unirradiated control. Least squares regression slope of each line tested with an extra sum-of-squares F test was compared to a null hypothesis of the slope = 0, constrained to y-intercept = 100, on log2 transformed data. The slope of each line was significantly different to 0 for all genes. Data represent geometric means ± geometric SD, N = 3, n = 3*

3.3.2.5.5 Complete solar light has different effects on viability and gene expression

3.3.2.5.5.1 Phenol-containing DMEM

When HDFn cells were seeded in complete, phenol-containing DMEM with 10% FCS, then washed and irradiated in DPBS the following day with 2.16 SEDs of complete solar simulated light, there was a significant decrease in viability as measured with MTS both immediately (21% decrease, p = 0.01) and 24 hours (24% decrease, p = 0.02) after irradiation as compared to the irradiation control (Figure 3-22).

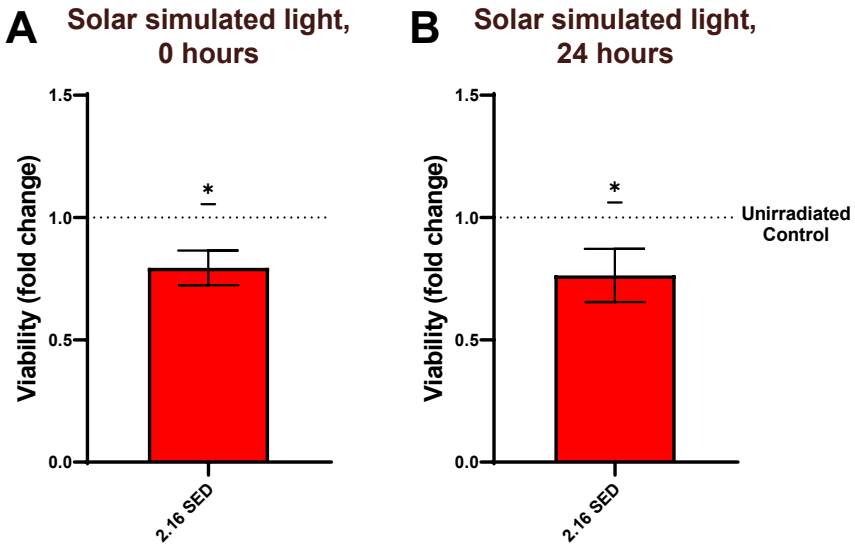

Figure 3-22 Viability as measured with MTS in HDFn cells seeded in complete, phenol-containing DMEM after irradiation with 2.16 SEDs of complete solar simulated light
Cells were seeded in complete, phenol-containing DMEM with 10% FCS. Irradiation was carried out in PBS, after which the medium was replaced with complete, phenol-free DMEM with 10% FCS. Panel A: viability immediately after irradiation. B: viability 24 hours irradiation. Unirradiated controls were under the lamp during irradiation but wrapped in foil to receive 0 J.cm^{-2} of light. Data were normalised to unirradiated control. (*): p ≤ 0.05, one-sample t-test; data represent means ± SD, N = 4, n = 3

3.3.2.5.5.2 Phenol-free DMEM

When seeded in complete, phenol-free DMEM with 10% FCS and irradiated the next day with 2.16 SEDs of complete solar simulated light, there was a significant decrease in viability of HDFn cells immediately after irradiation (19% decrease, p = 0.02) but no such difference 24 hours after irradiation (Figure 3-23). Compared to incubator controls, irradiation controls had no significant difference in viability.

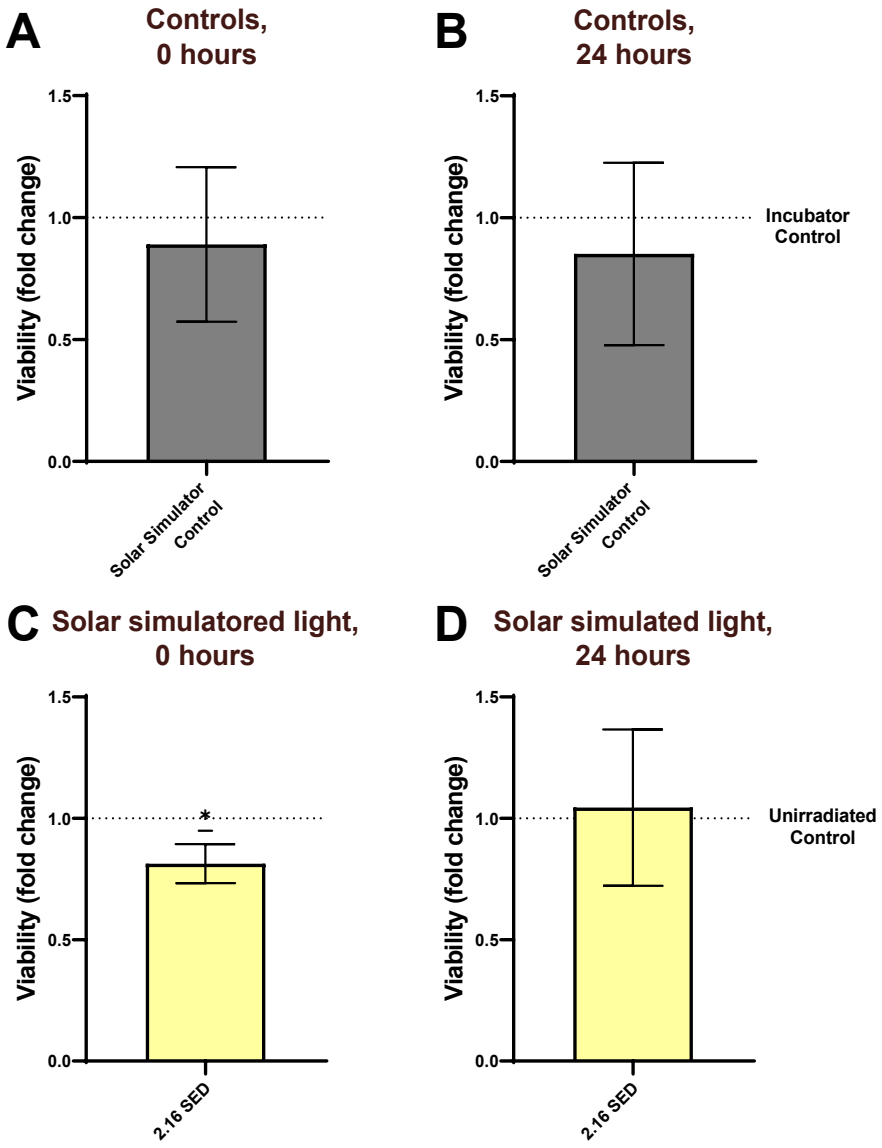

Figure 3-23 Viability as measured with MTS in HDFn cells seeded in phenol-free DMEM.
Cells were seeded in complete, phenol-free DMEM with 10% FCS. The following day, medium was replaced with PBS for irradiation with 2.16 SEDs of complete, solar simulated light over ~ 2 minutes. Incubator controls experienced the same wash steps but remained in the incubator during irradiation. Unirradiated controls were under the lamp during irradiation but wrapped in foil to receive 0 J.cm^{-2} of light. Data from irradiated cells were normalised to unirradiated controls. Unirradiated control data were normalised to incubator controls for comparison. Temperature was controlled using a stand. Panels A and B represent unirradiated controls compared to incubator controls 0 and 24 hours after irradiation respectively. Panels C and D represent irradiated cells versus unirradiated controls 0 and 24 hours after irradiation respectively. (*): $p \leq 0.05$, one-sample t-test; data represent means ± SD, N = 3, n = 3

3.3.2.5.5.3 Complete solar light has different effects on gene expression depending on the culture medium prior to irradiation

Fibroblasts were cultured in complete, phenol-free DMEM before immediate irradiation in DPBS with 2.16 SEDs of complete solar light and returned to complete, phenol-free DMEM for 24 hours before RNA extraction (Figure 3-24). Expression of MMPs was unchanged in response to 2.16 SEDs of complete solar light after culture in complete, phenol-free DMEM with 10% FCS when compared to unirradiated control cells treated to the same medium conditions. In cells cultured in complete, phenol-containing DMEM with 10% FCS, MMP-3 expression was changed (61% increase, $p = 0.0154$, two-tailed one-sample t-test). In cells cultured in MEMO (and irradiated in MEMO rather than DPBS), MMP-1 and MMP-3 were significantly increased by 47% ($p = 0.0371$, two-tailed one-sample t-test) and 97% ($p = 0.0038$, two-tailed one-sample t-test) respectively. When comparing between the differences in gene expression between the conditions using a one-way ANOVA for each gene, MMP-3 was expressed differently, with expression 33% higher in phenol-containing DMEM than phenol-free DMEM ($p = 0.255$), and 63% higher in MEMO than phenol-free DMEM ($p = 0.0018$).

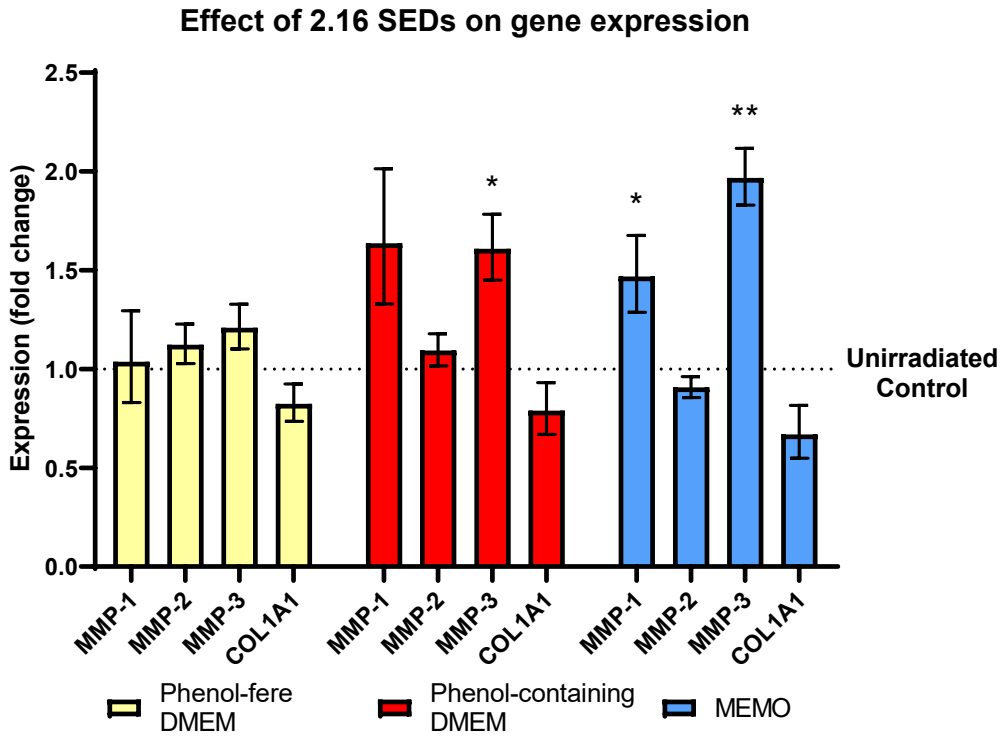

Figure 3-24 HDFn cell gene expression profile after a 2.16 SED dose of solar simulated radiation. *Monolayer HDFn cells were seeded in complete, phenol-free DMEM with 10% FCS, complete, phenol-containing DMEM with 10% FCS or MEMO. The next day, they were irradiated with 2.16 SEDs of complete solar light in DPBS (MEMO for MEMO condition). Following irradiation cells were returned to complete, phenol-free DMEM for 24 hours before RNA extraction. Unirradiated controls were under the lamp during irradiation but wrapped in foil to receive 0 J.cm^{-2} of light. Temperature was controlled using a stand. Gene expression was assessed with TaqMan PCR primers. Data from irradiated cells were normalised to unirradiated controls. (*): $p < 0.05$, (**): $p < 0.01$, one-sample t-test of each gene on log2 transformed data. Data represent geometric means ± geometric SD, N = 3, n = 3*

3.3.2.6 Multiple day exposures

3.3.2.6.1 Proliferation in MEMO over multiple day irradiations

HDFn cells seeded in complete, phenol-free DMEM + 10% FCS or MEMO with no FCS were counted on subsequent days to examine proliferation (Figure 3-25). A further condition of irradiated cells in MEMO was counted. 50,000 cells per 35 mm dish were seeded in the complete DMEM condition, while 70,000 cells per well were seeded in the MEMO conditions, to account for differences in proliferation rate, to allow cells to be dense enough to proliferate but have enough space to not be 100% confluent on day 4. The number of cells in each dish on day 1 was less than the number seeded as not all cells will have adhered and

dead cells were not counted as they would have been washed off. Compared to day 1, the number of cells in the complete, phenol-free DMEM + 10% FCS condition on day 4 had increased 7.2-fold in 36 hours, indicating a doubling time of 25 hours. For cells seeded in MEMO, the cell number increased 2.07-fold over 3 days, indicating a doubling time of 69 hours. Cells irradiated with complete visible light in MEMO increased by 1.16 fold over 3 days, with an effective doubling time of 14 days. For cells in both complete, phenol-free DMEM + 10% FCS and in MEMO the fold change per day decreased over the 4 days, as seed from the data in **Error! Reference source not found.**.

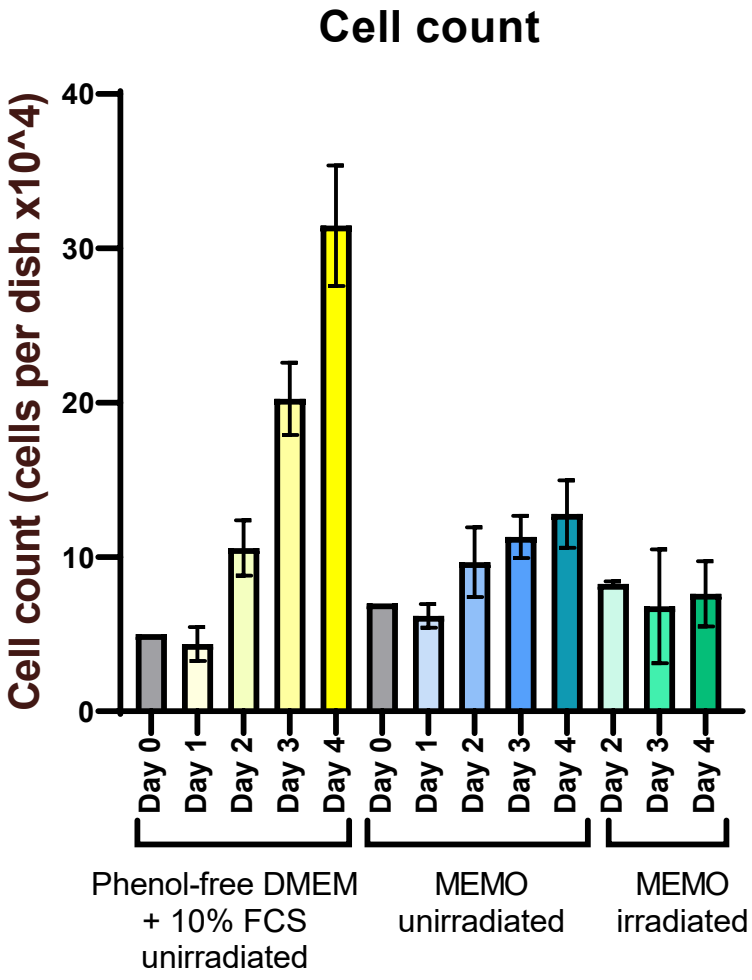

Figure 3-25 Cell count in different mediums each day after seeding in complete, phenol-free DMEM or MEMO with or without irradiation

50,000 cells/35 mm dish (DMEM) or 70,000 cells/35 mm dish (MEMO) were seeded. Count was carried out prior to irradiation on each day, at 24-hour intervals. Irradiated cells were irradiated in the same medium they were seeded in. Irradiated cells were treated with complete visible 410-810 nm light at 19.8 mW.cm^{-2} for 2 hours and 41 minutes with dose of 191.9 J.cm^{-2}. Temperature was

controlled using a stand. Unirradiated cells remained in the incubator for the duration of irradiation. Data represent means ± SD, N = 2, n = 3

Table 3-2 Daily fold change and doubling time calculated from cell count data presented in Figure 3-25.

	Cell count (cells per dish x 10^4)				Fold change			Doubling time (hours)		
Medium	day 1	day 2	day 3	day 4	day 1 - day 2	day 2 - day 3	day 3 - day 4	day 1 - day 2	day 2 - day 3	day 3 - day 4
DMEM	4.4	10.6	20.3	31.5	2.4	1.9	1.6	18.8	25.6	37.7
MEMO	6.2	9.7	11.3	12.8	1.6	1.2	1.1	37.3	106.0	134.9
MEMO irradiated	6.2	8.3	6.8	7.2	1.3	0.8	1.1	57.7	-86.5	326.5

3.3.2.6.2 Changing medium on day 3 affects MTS signal

To determine the best medium conditions for irradiation over three days, HDFn cells were kept in different medium conditions but not irradiated (Figure 3-26). After 3 days of being in MEMO with no FCS, medium was either not replaced ("Same MEMO") or replaced with fresh MEMO with no FCS, phenol-free DMEM with no FCS or complete, phenol-free DMEM with 10% FCS. Cells were counted with a hemocytometer, assayed with MTS viability/metabolism assay or crystal violet stain (CVS). Results from each assay were normalised to those seen from cells in unchanged medium and presented as fold change from this. There was no difference between any of the conditions in cell count or crystal violet stain, however, cells returned to DMEM with or without 10% FCS both had significantly increased in MTS signal by at least 2-fold.

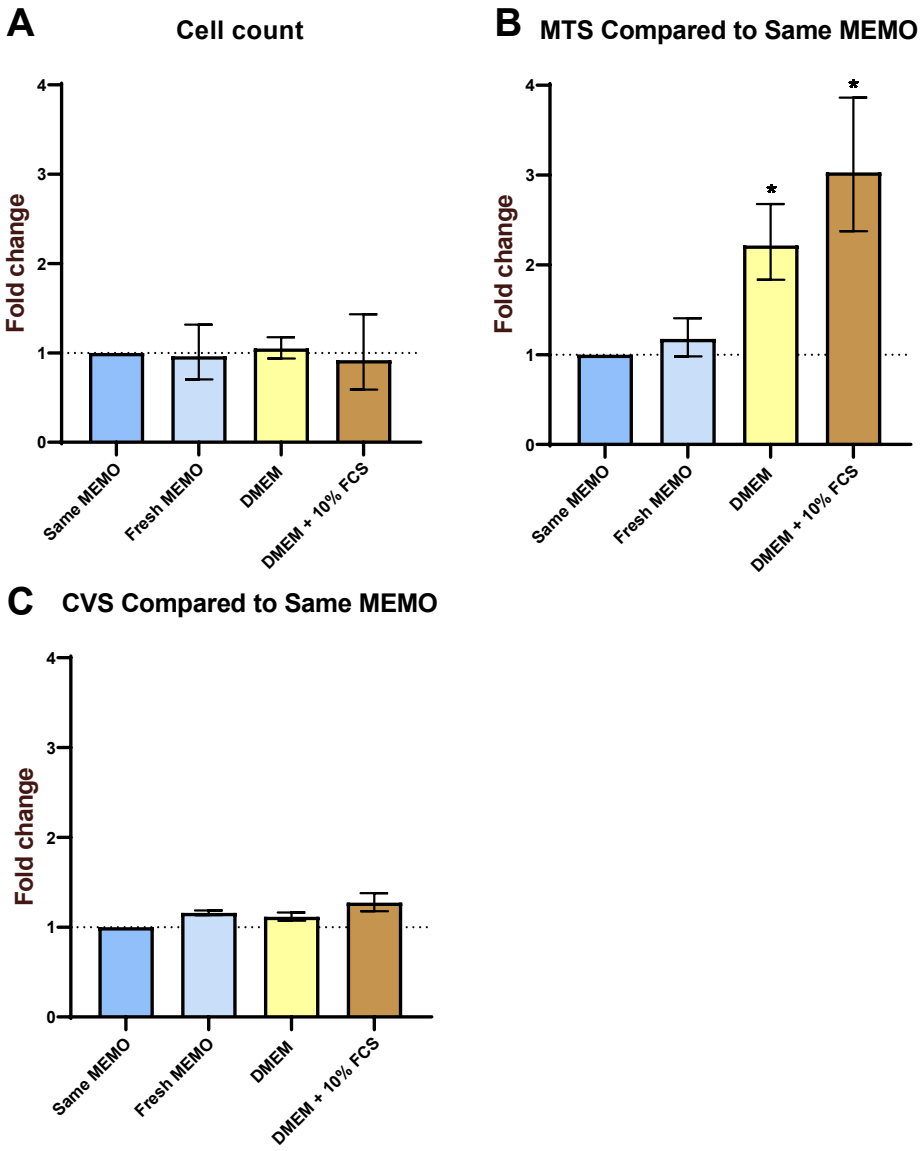

Figure 3-26 HDFn cells seeded in MEMO with medium change 3 days later to medium indicated. Assays were carried out on day 4, 24 hours after medium change.
Cells were seeded in MEMO and remained in this for three days, after which the medium was left the same, or replaced with fresh MEMO, phenol-free DMEM with no FCS or complete phenol-free DMEM with 10% FCS. Viability was measured 24 hours after the medium was changed. Data were normalised to the viability measured in the cells in which the medium was unchanged. A: cell count; B: MTS signal; C: crystal violet stain (CVS). (*): $p < 0.05$, one-sample t-test on log2 transformed data; data represent geometric means ± geometric SD, N = 3 for cell count and MTS, N = 2 for crystal violet stain data.

3.3.2.6.3 Greater differences in gene expression in cells incubated in MEMO for 3 days

As above, HDFn cells were kept in MEMO or complete, phenol-free DMEM + 10% FCS for three days before replacement with complete, phenol-free DMEM + 10% FCS. RNA was

extracted 24 hours later (Figure 3-27). The pattern of difference between the complete, phenol-free DMEM + 10% FCS and MEMO conditions was opposite to that when the cells were cultured in MEMO for 1 day (data here reproduced from Figure 3-20), where MMP-2 and procollagen were seen to decrease and MMP3 was seen to increase. Compared to complete, phenol-free DMEM + 10% FCS, cells after 3 days in MEMO had significantly reduced MMP2 ($p = 0.03$) but the differences in other mRNAs were not significant. When comparing between the 1- and 3-day conditions, the 3-day condition had significantly lower MMP2 ($p = 0.0016$), COL1A1 ($p = 0.03$) and higher MMP3 ($p = 0.03$). The variance was much higher in the cells exposed to MEMO for three days.

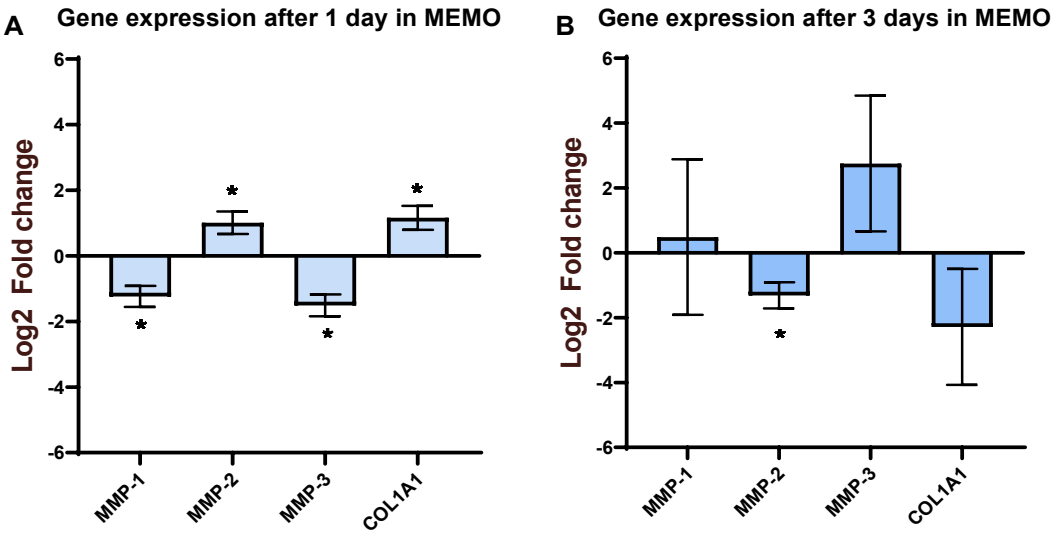

Figure 3-27 Effect of 1 or 3 days of culturing in MEMO versus complete, 10% FCS, phenol-free DMEM

Test cells were seeded in MEMO, while control cells were seeded in complete phenol-free DMEM with 10% FCS. After 1 (Panel A) or 3 days (Panel B), medium in test and control dishes was replaced with fresh, complete, phenol-free DMEM with 10% FCS. RNA was extracted 24 hours after returning conditions to DMEM + 10% FCS. Expression was assayed with TaqMan qPCR. Data were normalised to expression from cells seeded in complete, phenol-free DMEM with 10% FCS. (*): $p < 0.05$, one-sample t-test on log2 transformed data; data represent means ± SD, N = 3, n = 3

3.3.2.6.4 Gene expression in HDFn cells irradiated daily with solar simulated light for 3 days

When HDFn cells in MEMO were irradiated daily for 3 days with 2.16 SEDs of complete solar simulated light or solar simulated UV only, there was a significant increase in MMP3 and decrease in COL1A1 compared to unirradiated control cells in both conditions (Figure 3-28).

The UV only condition also had a significant increase in MMP1 expression, though between the two conditions, none of the genes were significantly differently expressed ($p > 0.05$ for each mRNA as tested with a 2-tailed unpaired students t-test).

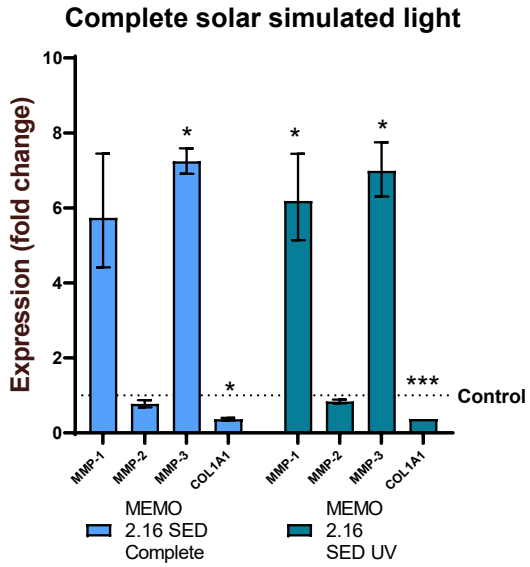

Figure 3-28 Gene expression in HDFn cells in MEMO irradiated with a dose of 2.16 SEDs of complete solar simulated light or solar simulated UV every day for 3 days.
Cells were seeded in MEMO. For the following three days, cells were irradiated daily with 2.16 SEDs of complete solar simulated light or UV only over ~3 or ~2 minutes respectively, to give a total dose of 6.48 SEDs over all three days. After the final irradiation, MEMO was replaced with complete, phenol-free DMEM with 10% FCS. RNA was extracted 24 hours later. Temperature was controlled using a stand. Expression assayed with TaqMan qPCR. (*): $p < 0.05$, (***): $p < 0.001$, one-sample t-test on log2 transformed data; data represent geometric means ± geometric SD, N = 2, n = 3

3.3.2.7 Optimising method for riboflavin and FCS washout before visible irradiation

3.3.2.7.1 Imaging

Brightfield images of HDFn cells after exposure to visible light with different washout conditions in the 24 hours before irradiation were taken to assess morphological indicators of cell death. Immediately after irradiation cells appear to be similar to the unirradiated and incubator controls. 24 hours after irradiation, cells in MEMO + 1% FCS and in MEMO appear similar to the unirradiated and incubator controls, and cells in the complete, phenol-free DMEM + 10% FCS condition appear to be fewer and more shrivelled, indicating cell death due to the presence of riboflavin and FCS components during irradiation (Figure 3-29 and Figure 3-30).

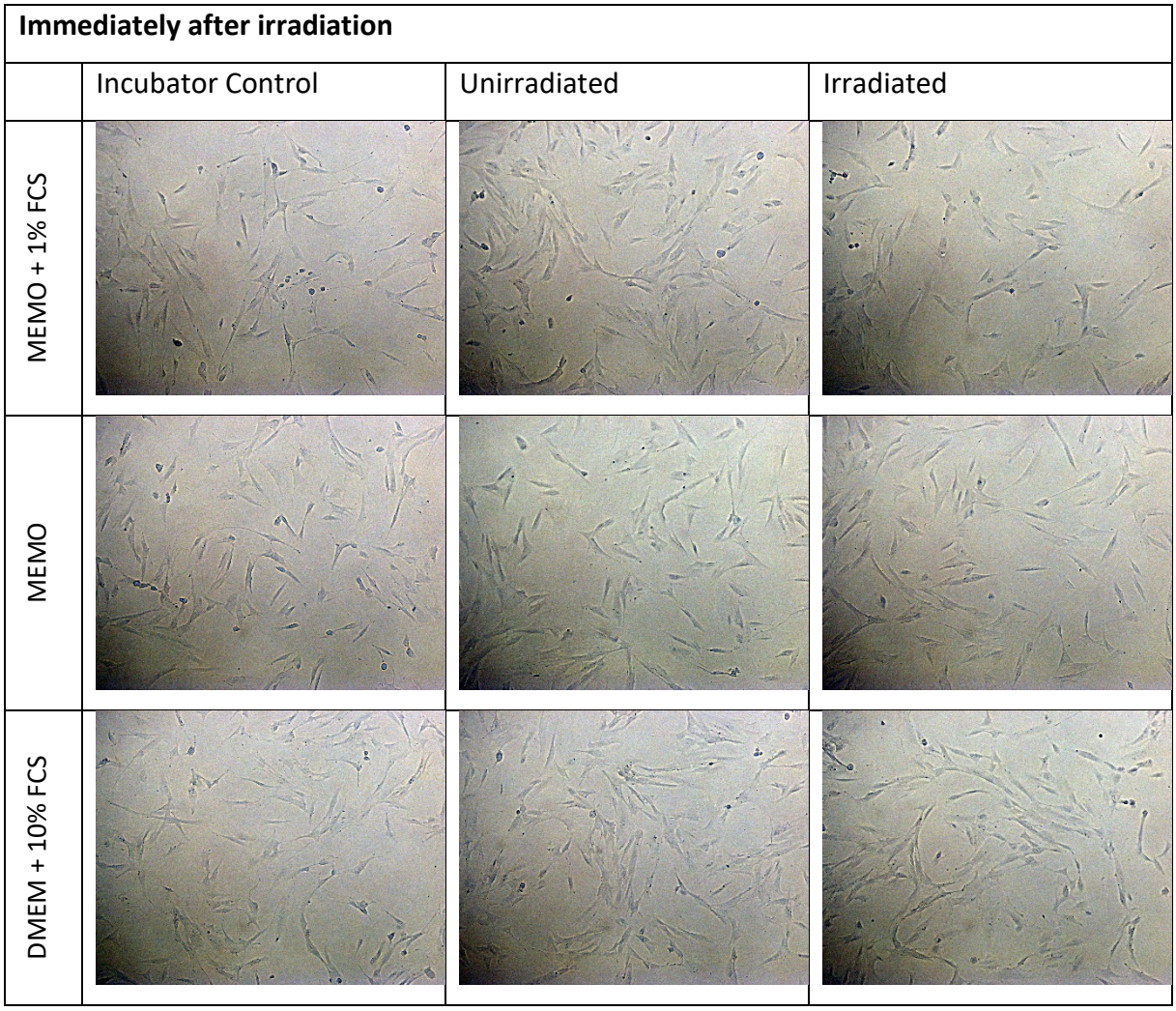

Figure 3-29 Brightfield microscopy of live HDFn cells after visible light irradiation

Cells were seeded in complete, phenol-free DMEM with 10% FCS. The following day the medium was replaced with either MEMO with 1% FCS, MEMO with no FCS, or remained unchanged, in the DMEM with 10% FCS. The following day, 2 hours before irradiation, the 1% FCS MEMO condition was replaced with MEMO with no FCS. Immediately before irradiation, both MEMO conditions had their medium replaced with fresh MEMO with no FCS. Cells were irradiated with complete visible light of 410-810 nm at 19.8 mW.cm^{-2} for 2 hours and 41 minutes with dose of 191.9 J.cm^{-2}. Images were taken immediately after irradiation. 4 images were taken of each slide, one of which is displayed here as an example.

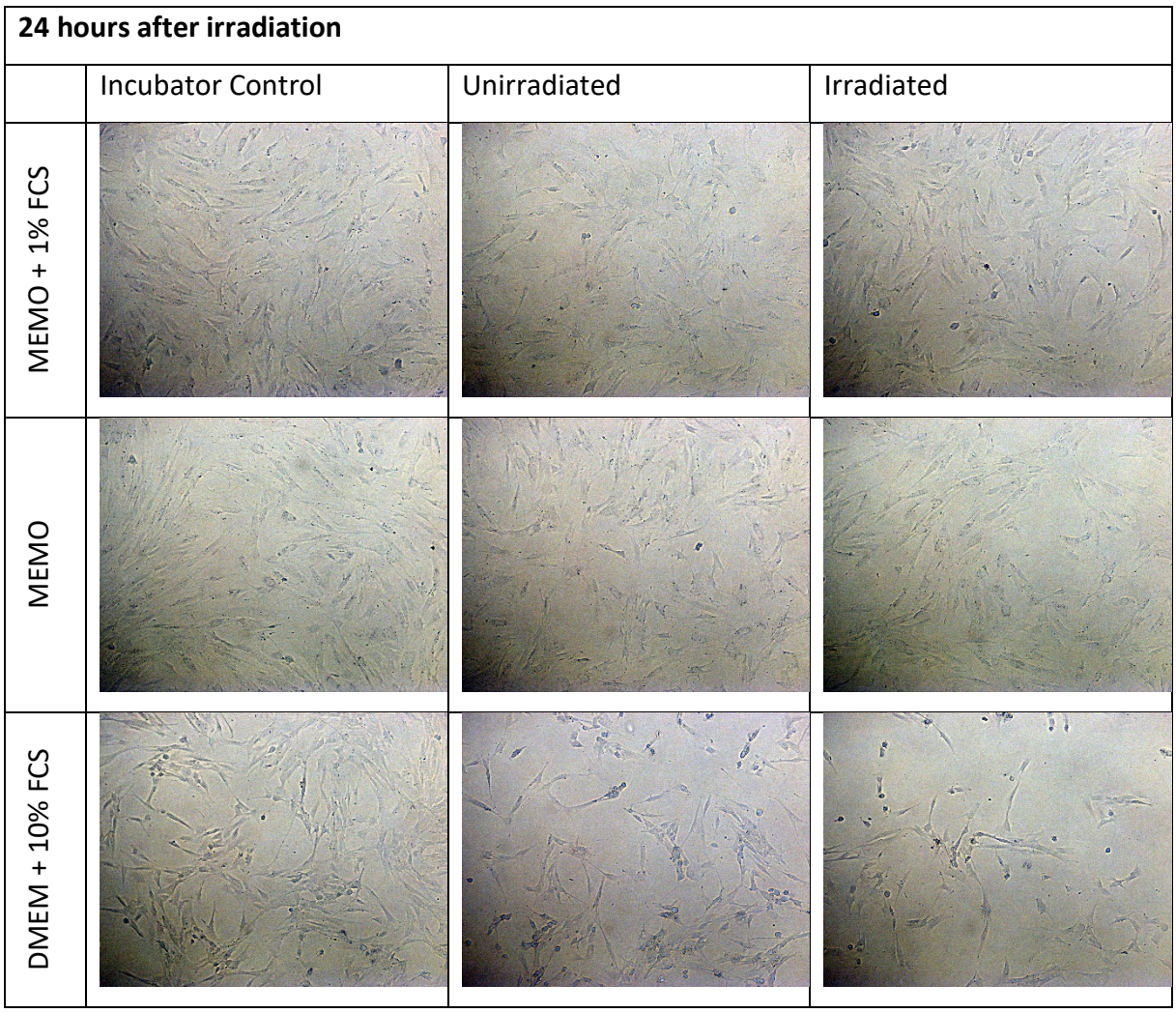

Figure 3-30 Brightfield microscopy of live HDFn cells after visible light irradiation
Cells were seeded in complete, phenol-free DMEM with 10% FCS. The following day the medium was replaced with either MEMO with 1% FCS, MEMO with no FCS, or remained unchanged, in the DMEM with 10% FCS. The following day, 2 hours before irradiation, the 1% FCS MEMO condition was replaced with MEMO with no FCS. Immediately before irradiation, both MEMO conditions had their medium replaced with fresh MEMO with no FCS. Cells were irradiated with complete visible light of 410-810 nm at 19.8 mW.cm^{-2} for 2 hours and 41 minutes with dose of 191.9 J.cm^{-2}. Images were taken 24 hours after irradiation. 4 images were taken of each slide, one of which is displayed here as an example.

3.3.2.7.2 Viability assays

To find the optimal method for the 24-hour washout of riboflavin and FCS components before the final 2-hour washout in MEMO with no FCS before irradiation, the MTS viability assay, alamar blue viability assay and crystal violet assay were used. HDFn cells were incubated with either MEMO + 1% FCS, MEMO with no FCS or complete, phenol-free DMEM with 10% FCS. Fibroblasts were irradiated with a one-hour equivalent dose of visible light. As

there was no specific control since all the conditions were to be compared to find the best, the data were normalised to an experimental mean of all the data from that assay at that timepoint.

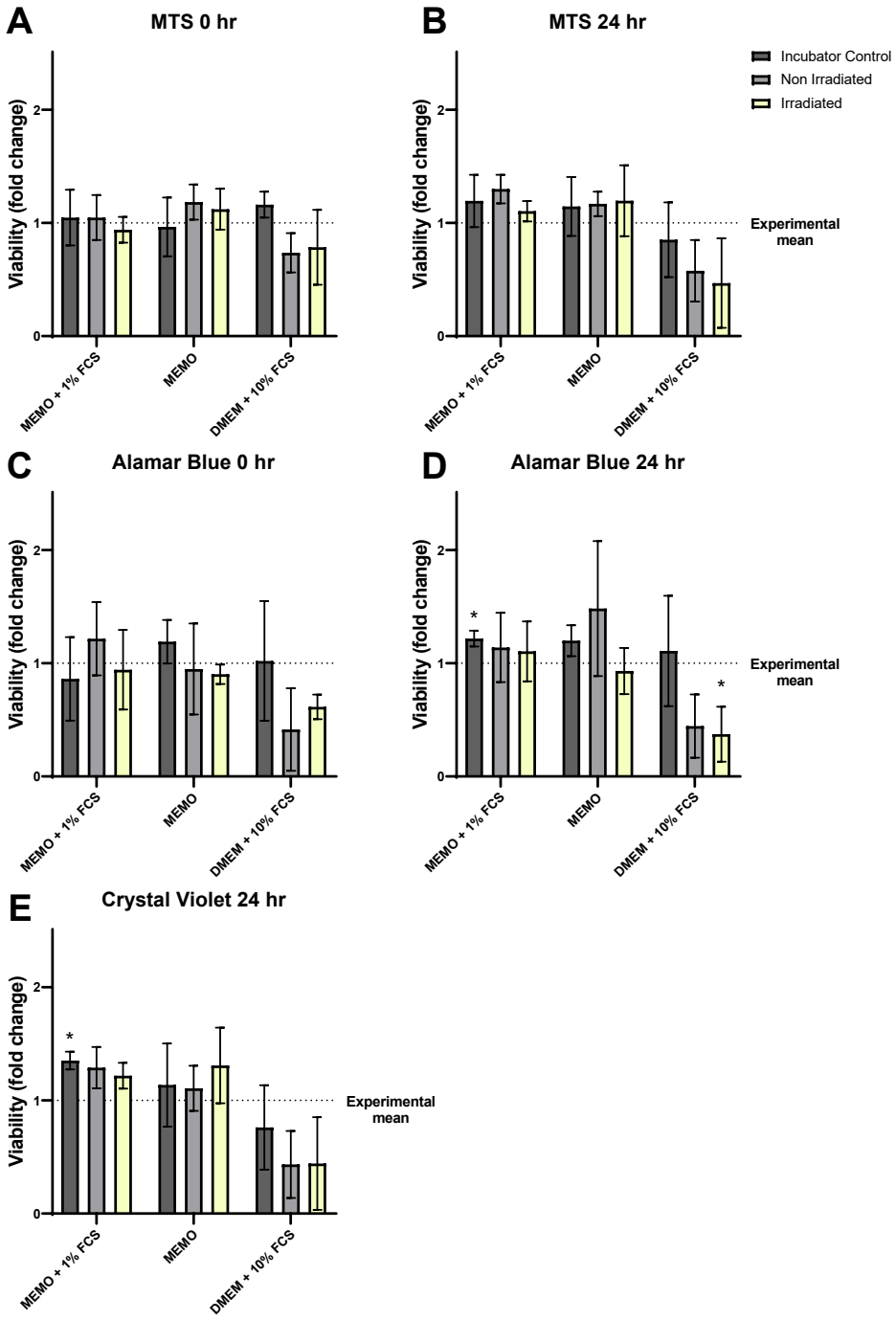

Figure 3-31 Viability testing for the optimal medium conditions for the washout of riboflavin and FCS in 24 hours before irradiation with the equivalent of 1 hour of solar visible light.
Viability was assessed with colourimetric MTS assay 0 and 24 hours after irradiation (Panel A and B respectively), fluorometric alamar blue assay at 0 and 24 hours after irradiation (Panel C and D respectively) and colourimetric crystal violet assay 24 hours after irradiation (Panel E). Cells were seeded in complete, phenol-free DMEM with 10% FCS. The following day the medium was replaced with either MEMO with 1% FCS, MEMO with no FCS, or remained unchanged, in the DMEM with 10%

FCS. The following day, 2 hours before irradiation, the 1% FCS MEMO condition was replaced with MEMO with no FCS. Immediately before irradiation, both MEMO conditions had their medium replaced with fresh MEMO with no FCS. Cells were irradiated with complete visible light of 410-810 nm at 19.8 mW.cm^{-2} for 2 hours and 41 minutes with dose of 191.9 J.cm^{-2}. Viability was compared to experimental mean across all medium and irradiation conditions of each assay and timepoint. (*): p ≤ 0.05, one-sample t-test; data represent means ± SD, N = 3, n = 3

3.4 Discussion

3.4.1 Temperature control

The data in this thesis show that if temperature is not controlled, it can reach biologically damaging heights of 66°C. The temperature reached by cells in infrared irradiations is dependent on many factors, such as the irradiance, duration of exposure, ambient temperature, airflow, and the surface on which the plate or dish is resting. Where no form of temperature control has been reported in a paper, it is possible that the cells have been reaching temperatures much higher than skin cells would normally experience under sunlight. Humans are generally good at regulating their temperature, and it would be unlikely that anyone would allow their skin to reach 66°C, given that heat-induced pain occurs at 43°C (Hagander et al., 2000). This is normally enough to encourage someone to remove themselves from exposure to the source of this heat.

It has been shown that increases in MMP1 and MMP3 but not MMP2 in fibroblasts can be due to heating above 43°C (Park et al., 2004) and the same pattern can be seen from HaCaT keratinocytes from MMP1 and MMP2 (Shin et al., 2008). When human skin is irradiated for 30 minutes in vivo with infrared light over 4.5 times as bright as that from the sun, the skin increases to temperatures of 39.1°C and radicals are produced (Darvin et al., 2011). Increased temperature has shown to increase DNA damage and tumourigenesis in mice and HaCaT keratinocytes (Boukamp et al., 1999, Freeman and Knox, 1964). It may be that the negative effects of infrared seen in vitro and in vivo are due to heating rather than chemical changes in chromophores affecting signalling pathways.

3.4.2 Medium conditions with light irradiation

3.4.2.1 pH changes over the course of an irradiation

pH is normally buffered by gaseous CO_2 at 5% when in a humidified, 37° incubator. In the experiments detailed here, irradiation with infrared and visible light involved a period of up

to four hours outside the incubator, in which CO_2 would leave the medium resulting in a more alkaline environment for the cells. To minimise this, plates and dishes were wrapped in parafilm around the lid join. This reduced the increase in pH following 4 hours outside the CO_2 incubator but did not eliminate it. This was more favourable than the alternative option using another buffer, as the most appropriate alternative, HEPES, is shown to be light sensitive and causes damage to cells when it is present during irradiation with visible light.

3.4.2.2 Presence of FCS when out of incubator

Cells kept out of the incubator for the 4-hour duration were shown to have reduced viability 24 hours after the end of the 4-hour period when compared to those kept at 37°C and 5% CO_2 during the same period. This indicates the change in temperature from 37°C to room temperature of approximately 20°C, and/or the exposure to normal atmospheric CO_2 concentrations of 0.04% causing CO_2 to leave the medium and the pH to rise, has an effect on cell proliferation. As the cells were not washed before the addition of MTS, the number of cells in each condition will be the same. The lowered MTS signal immediately after incubation indicates metabolism in these cells has been reduced, though it is possible that some may have started to undergo apoptosis due to stress. The signal was less reduced at 24 hours, which may indicate recovery from the cold/reduced CO_2. In experiments where cells are exposed to light, the controls are treated in the same way as the conditions, other than the foil wrapped around the dish/plate to block light, so for the most part the difference in metabolism will be controlled for. The presence or absence of FCS did not significantly affect viability over the 4-hour period when cells were inside or outside the incubator.

3.4.2.3 HEPES and riboflavin presence do not affect viability after infrared irradiation

In the high intensity light condition, it was found that doses of up to 10 hours equivalent of solar infrared (360 $mJ.cm^{-2}$) had no significant effect on cell viability immediately or 24 hours after irradiation in either MTS or crystal violet stain assays. This indicates there is also no effect on metabolism when compared to control, as the results from crystal violet biomass staining showed the same lack of effect as the MTS assay.

Like the high intensity IR condition, the low intensity IR condition showed no significant change in viability as measured by MTS assay immediately or 24 hours after irradiation, as

seen in Figure 3-10. Additionally, there was no significant difference between the viability of the incubator control, which had been kept in the incubator for the irradiation duration, and the irradiation control, which was alongside the irradiated plate but in foil, indicating no effect of removal from the incubator for the duration of irradiation. However, it was noted that the standard deviation of the irradiation control when compared to incubator control was larger than that of the irradiated sample versus the irradiation control. With only 3 biological repeats it is difficult to make conclusions from this, though it could be the case that the irradiated sample and irradiation control are more similar than the incubator control and irradiated control, and that there may be an impact on cells due to time out of the incubator that was missed.

In any case, from the data it can be concluded that there is no effect of infrared at high or solar intensity on viability, despite the presence of HEPES and riboflavin in the irradiation medium. While HEPES presence was found to have no effect on viability during infrared irradiations, it was decided for the sake of comparability with the visible light irradiation data that it would not be included in further infrared irradiations.

3.4.2.4 HEPES, riboflavin and FCS in visible light and UV irradiations

3.4.2.4.1 Viability

The presence of both HEPES and riboflavin during visible light irradiations appeared to reduce the viability in both blue and red light irradiated conditions. Given riboflavin's absorbance is primarily in the UV and blue light parts of the solar spectrum up to ~520 nm, it was surprising to see a reduction in viability from red light irradiation. Only one repeat was carried out, so conclusions cannot be drawn, but it could be possible that scattered blue light wavelengths were reducing the viability of the cells in the red light condition. In any case, it was decided that HEPES and riboflavin should not be present together during irradiation with visible light wavelengths.

When riboflavin was present in the cell culture medium without HEPES it was shown to significantly reduce viability/metabolism in the blue light condition both immediately and 24 hours after irradiation, while there was no difference between control irradiation cells (where the plate was covered in foil) and incubator control cells (treated to same medium

conditions but remained in the incubator for the duration of irradiation). This indicates that even in the absence of HEPES, riboflavin is photosensitising and therefore cannot be present in the cell medium during irradiation.

On removal of riboflavin from medium completely through the use of the riboflavin-free DMEM "MEMO", irradiation with visible light caused no significant change in viability in any of the visible light irradiated conditions. Though not significant, the difference in viability/metabolism as measured by MTS in the cells irradiated with complete visible light (41-810 nm) at 0 hours was a 28% reduction ($p = 0.0596$). This is somewhat unexpected since without the potent photosensitiser riboflavin present during irradiation you would expect little impact on viability. However, a number of factors should also be taken into account. Though there was no riboflavin or phenol red in the medium during the irradiation, both had been incubated with the cells immediately prior to irradiation. While the concentration outside the cells may have been negligible due to washing with DPBS before replacing with MEMO, there may have been high concentrations of these molecules within the cells. Riboflavin is of course normally found in cells, and its presence in vivo may contribute to the damage caused to the skin by light, though the concentration in cell culture medium may artificially increase this above that in vivo as it is designed to allow optimal proliferation of cells, which could result in greater responses of cells in vitro to visible light.

3.4.2.4.2 Gene expression changes in cells in MEMO when unirradiated

When cells were without riboflavin and FCS for 24 hours were then returned to DMEM medium with normal riboflavin and 10% FCS for a further 24 hours, it was found that the cells had changed gene expression of MMPs and procollagen (>1 log 2-fold change for each gene, $p < 0.05$). While MMP1 and 3 more than halved, MMP2 and procollagen 1α both more than doubled. This pattern is almost the opposite of that seen in response to UV light, where MMP 1 and 3 both increase, procollagen 1α decreases and MMP2 stays the same. That the differences are large and present 24 hours after return to serum-containing medium indicates the cells have been changed and not returned to their original state as a result of the medium change. It may be that a slower reduction in serum content to say 1%, a short

washout period before irradiation, then return to low-serum DMEM after irradiation would be more beneficial for cell health. It is important to recognise this as a limitation of cell culture studies whereby the culture medium will never perfectly match in vivo extracellular conditions, but changes in these can have important effects on results.

3.4.2.4.3 Effect of medium on response to UV light

Viability/metabolism in cells irradiated in DPBS with 2.16 SEDs of complete solar simulated light after irradiation was reduced immediately and 24 hours after irradiation in cells cultured in phenol-containing DMEM prior to irradiation. This was different to what was seen in cells irradiated in DPBS that had previously been cultured in phenol-free DMEM, in which there was a reduction of viability/metabolism immediately after irradiation, but this had recovered and returned to normal 24 hours after irradiation. Further to this, differences in gene expression between cells cultured in phenol-containing or phenol-free medium were found, both after normal culture (unirradiated) but also in response to UV irradiation.

Gene expression is known to change as a result of irradiation with UV light. AP-1 and NF-κB are transcription factors which are both quickly upregulated after UV irradiation and regulate MMP and collagen expression (Fisher et al., 1996, Fisher et al., 1997, Rittié and Fisher, 2002). The difference in gene expression response seen between cells irradiated with 2.16 SEDs of light after being cultured in phenol-free medium, phenol-containing medium and MEMO medium containing no phenol red or riboflavin was unexpected.

The expected dose-dependent response was found in MEMO, suggesting the cells are behaving in the predicted way in this medium, but the response of cells to 2.16 SEDs of light after culture in phenol-free DMEM was different to this. There were no significant changes in gene expression seen from cells cultured in phenol-free DMEM to 2.16 SEDs of complete solar light, while there was a significant change in gene expression found in both MEMO and phenol-containing DMEM conditions. Returning to the gene expression in the controls (Figure 3-20), it appears that the cells in the phenol-free DMEM condition already have the higher expression of MMP1 and 3, typical of cells irradiated with UV compared to cells in phenol-containing DMEM, though it should be noted that the differences were not

significant. It seems however that the cells in this condition may already be in a stressed state, even though they have experienced no irradiation.

The only difference between the phenol-free and phenol-containing conditions was the content of phenol red in the medium. Maguire et al found that in the absence of riboflavin, irradiation-induced cell death was increased by phenol red, but the presence of phenol red and riboflavin reduced cell death compared to riboflavin in the absence of phenol red (Maguire et al., 2011). This is presumably due to the ability of phenol red to quench riboflavin fluorescence, thereby disrupting the process by which riboflavin forms radicals. However, in this thesis, the medium itself was not irradiated with solar simulated light, as on the cells it was replaced with DPBS for the irradiation, so the cause may have been the normal laboratory and tissue culture hood fluorescent lighting that medium is exposed to during normal handling. This agrees with what was found by Wang (1976) that the mere exposure to normal lighting of medium containing riboflavin can result in the decreased viability of the cells it is then used to culture (Wang, 1976, Wang and Nixon, 1978).

Growing cells without the presence of riboflavin over a long would be detrimental to the health of the cells, but given how photosensitising riboflavin is, and the ability of phenol red to reduce its sensitising ability, having both in medium leading up to irradiation then removing only during irradiation may be optimal. However, how these interact with components of FCS is a further complication in determining how best to culture cells when exposing them to light.

This pattern of gene expression has been shown to reduce the ability of melanoma to invade, suggesting a potential biological reason for these changes (Budden et al., 2021).

3.4.2.5 Multiple day exposures

3.4.2.5.1 Proliferation in MEMO over 4 days

For cells seeded in DMEM + 10% FCS the doubling time was calculated to be 25 hours, but for the cells in MEMO with no FCS, proliferation was reduced and doubling time was calculated to be 69 hours. Irradiated cells had a further dampened proliferation, with a doubling time calculated to be 14 days. This is in line with what was expected, knowing that

FCS presence is important for proliferation and that light-induced stress causes cell cycle arrest to allow DNA repair (Pavey et al., 2001). Because the unirradiated MEMO cells were kept in the incubator for the duration of the irradiation, it is not possible to separate the effect on cell proliferation of the light from the effect of the cells being out of the incubator for the ~4 hours. However, it is clear that one or both of these factors is reducing proliferation, as the number of cells counted from the irradiated condition on day 4 less than that from the unirradiated condition. As expected, the proliferation in MEMO decreased between days 1-2 and 2-3, as FCS components that had been at higher concentrations within the cells initially had decreased, however this was not then saved by the return to DMEM + 10% FCS on day 3, as the fold change between days 3-4 again reduced.

3.4.2.5.2 Changing medium on day 3 affects MTS signal

Compared to cells maintained for four days in MEMO medium with no riboflavin or FCS, cells changed into fresh MEMO, DMEM or DMEM + 10% FCS on day three appeared to have different metabolism on day four. While there was no significant difference in the number of cells counted by hemocytometer, or the biomass of adherent cells by crystal violet stain, there was a more than doubling of signal from MTS from cells in DMEM with no FCS compared to those left in MEMO, and more than tripling of MTS signal from cells in DMEM + 10% FCS. This is clearly not due to a change in cell number given the cell count and crystal violet results, but rather to do with the metabolism of the MTS into formazan product.

The reduction of MTT to formazan has been shown to be inhibited by the flavin protein inhibitor diphenylene iodonium, suggesting that tetrazolium metabolism carried out by a flavin oxidase (Berridge and Tan, 1993, Liu et al., 1997),. Given that MTT metabolism is reliant on the enzymatic action of flavin-reliant oxidases the addition of riboflavin in these experiments may just be allowing a higher rate of metabolism of MTS. The further addition of FCS increasing signal is unexpected, given that FCS would be expected to reduce signal due to the albumin component binding the formazan product and thus impeding its light absorbance ability (Huang et al., 2004). While it is clear that the MTS results do not indicate differences in cell number, it is possible that they are indicating riboflavin deficiency which would be detrimental to cell health, but further experiments would be required to

determine this. However, it would be recommended to use tetrazolium reduction-based assays with caution when cells are in different mediums, knowing how sensitive the assay may be to these.

3.4.2.5.3 Gene expression in cells incubated in MEMO for 3 days

After 3 days in MEMO and subsequent return to phenol-free DMEM + 10% FCS, cells had the opposite pattern of expression to cells incubated for 1 day in MEMO before return to DMEM + 10% FCS, when each was compared to cells kept in phenol-free DMEM + 10% for the whole duration. This pattern of decreased procollagen and increased MMP3 seen in the cells in MEMO for 3 days is indicative of cell stress, as this is also what is seen as a result of UV irradiation. That the cells had such a significant change after the additional 2 days of incubation in MEMO suggests that perhaps the medium conditions of this protocol are too stressful for the repeated irradiation of cells.

It is difficult to say that the cells in MEMO are necessarily *less* stressed than those in phenol-free DMEM, given the potential effects that phenol-free DMEM has on cells through the radical forming potential of riboflavin without quenching phenol red presence during normal cell culture medium handling. However, since the differences are clearly reversed after three days, it seems possible to conclude that the 2 extra days of culturing in MEMO rather than DMEM + 10% FCS does cause some cell stress.

Whether this is caused by the lack of serum or riboflavin, or both, is not known. The suggested maximum incubation in MEMO by the manufacturer is three days, though it has been shown that depleted riboflavin for four days has a detrimental impact on cultured cells, with increased levels of carbonylated proteins, increased strand breaks in DNA and cell cycle arrest (Manthey et al., 2006). On the other hand, serum starvation has large impacts on cell behaviour. A week of culture at 2% serum was shown to significantly reduce MMP1, MMP3 and COL13A1 in stromal cells (Tratwal et al., 2015), so three days at 0% serum is very likely to also have large effects.

3.4.2.5.4 Gene expression in cells irradiated daily with solar simulated light for 3 days

Cells in MEMO for three days, irradiated daily were shown to have increased MMP3 and procollagen, and increased MMP1 in the UV only condition. The pattern of change was the same as that found after a single dose of UV (Figure 3-24), but the fold change seen was much greater with ~6-fold increase in MMP1 and 3 after 3 irradiations versus ~2-fold increase after 1 irradiation. This is as expected; that the damage response would be amplified by additional doses of UV. However, given that the unirradiated control cells were already showing signs of potential stress compared to DMEM, and though the increases by UV light are compared to those unirradiated controls, it cannot be determined that this effect is purely UV driven or if the potentially already heightened stress state of the cells was contributing to these greater expression changes.

3.4.2.6 Optimising method for riboflavin and FCS washout before visible irradiation

The absence of riboflavin for the 4 hours was found to have no significant effect on viability/metabolism in HDFn cells immediately or 24 hours after irradiation. However, it was thought that the presence of riboflavin in the cell culture medium immediately prior to irradiation may artificially increase riboflavin concentration inside the cells, and thus ROS and oxidative stress within the cells when irradiated with light. To wash out any remaining riboflavin and any other potential photosensitisers from the FCS, cells were exposed to a number of washout conditions and imaged.

From both the imaging and the viability assays it was clear that the positive control condition of irradiation in medium containing both riboflavin and 10% FCS resulted in cell death. The MTS and alamar blue assays both showed very similar results, with no obvious difference in reliability as variances were similar. Between the two test conditions there was no clear difference in viability in the unirradiated controls and the irradiated test conditions, so either washout protocol could be considered acceptable. It was decided that the condition where cells were put into MEMO with 1% FCS for 22 hours, then changed to MEMO with no FCS for the final 2 hours before irradiation, would be the best for maintaining normal cell behaviours and limiting serum starvation responses.

Surprisingly, the unirradiated cells, and to a lesser extent the incubator control cells, in the phenol-free DMEM + 10% FCS condition appeared to have reduced viability compared to the incubator control and the other conditions. These dishes/plates were wrapped in foil so this was not a response to light. It is possible again that this was a result of riboflavin phototoxicity as a result of exposure to normal indoor fluorescent lighting potentially exposing the cells to increased radicals in the medium. It was also thought that this may have been a result of the medium of the phenol-free DMEM + 10% FCS condition not being refreshed 24 hours after seeding, so any cells that had not adhered and instead died were left to remain in the medium, unlike in the other conditions where the medium was replaced with MEMO (with or without FCS). These unadhered cells may have been undergoing apoptosis or be necrotic, releasing ROS and other stressors into the medium which would have affected the adhered cells (Gregory and Pound, 2010). As such this was not as relevant a positive control as intended, though there is still a negative response to irradiation which was expected.

3.5 Summary

Cell culture conditions are critically important to consider when undertaking experiments with light. Everything from the temperature control of the irradiation to the components of the medium must be optimised. It was found in the experiments detailed in this chapter that medium components HEPES, riboflavin and FCS affect the responses of cells to visible and UV light, and culturing cells without riboflavin and FCS affects the proliferation and gene expression of HDFn cells. Irradiations in infrared light are comparatively simple, as none of the components of cell culture medium absorb infrared light and therefore it is not photosensitising. Irradiations with infrared light can be carried out in any medium regardless of HEPES, riboflavin, tryptophan, phenol red or FCS content.

With irradiations with visible light, the situation is more complex. Irradiations with blue light between 410 and 510 nm result in a reduction in cell viability in cells irradiated in medium containing HEPES and riboflavin or riboflavin alone. It is better in these conditions to remove the HEPES, which is there as a buffer, even though this may result in increased pH over the course of an irradiation of four hours duration. Using MEMO medium, which has the same

composition as DMEM but without the riboflavin, without added FCS mitigates this. However, this comes with its own issues of effects induced by serum starvation. While it appears that culture of HDFn cells for 24 hours without riboflavin and FCS is not overly damaging to cell health, if this is extended to three days there are potentially detrimental impacts as measured by increases in expression of MMP3 and decrease of procollagen. It would be difficult to separate any effects of repeated doses over multiple days from the effects of serum starvation.

To mitigate the effects of serum starvation it appears to be possible to incubate cells with MEMO with 1% FCS for 22 hours prior to irradiation, then have another washout period with MEMO with no FCS for a further 2 hours before a visible light irradiation of 4 hours without compromising viability. It would be optimal to use an artificial serum with any light sensitive components excluded to for normal culture of the cells to allow the irradiation of cells to include this and to have a washout period for the riboflavin alone. Determining the optimal washout period for riboflavin would also be suggested for doing multiple day irradiations, as it would be detrimental to cell health to culture long term without riboflavin.

Furthermore, given the potential of riboflavin to be even more phototoxic in phenol red-free medium as compared to phenol-red-containing medium, great care must be taken when using this in tissue culture. Medium in its bottle is exposed to light at several points during tissue culture, from the light in the fridge, to the light it is exposed to while being warmed in a water bath, and the light in the tissue culture hood. While on cells, the medium is exposed to light during transport, in the tissue culture hood and while looking at cells through a light microscope. It has been recommended that DMEM be made up or purchased without riboflavin and tryptophan and stored in the dark, and only immediately before use to add the necessary riboflavin and tryptophan to limit their photosensitising capabilities (Wang, 1976). Another way to limit phototoxicity would be to use yellow filters over room lighting and culture hood lighting to eliminate photosensitising blue wavelengths when using this medium. These practices would be of benefit when using medium containing phenol red, as even though its radical producing properties are less than that of riboflavin, they still have

the potential to impact cells, and the presence of phenol red merely reduces the damage caused by riboflavin but does not eliminate it (Maguire et al., 2011).

Chapter 4 Assay optimisation and development

4.1 Introduction

It is important to find an appropriate housekeeping gene that is unaffected by the treatment or test that cells are put under in order to determine how the expression of target genes changes from an appropriate baseline. UV light can induce oxidative stress, DNA damage, changes to the cell cycle and apoptosis, all of which are processes in which many genes are involved. Thus, it is important to investigate how stable any chosen housekeeping gene is under irradiation conditions.

The Promega ROS-Glo assay is designed to measure hydrogen peroxide (H_2O_2) production directly in cell culture. The H_2O_2 substrate is added directly to the well of a 96-well plate where it reacts with H_2O_2 present, and the product of this reaction then reacts with a luciferin precursor to produce luciferin, the light from which can be measured in a luminescence plate reader. The light signal is said to be proportional to the H_2O_2 present in the sample well. Menadione as a positive control puts the cell in a state of oxidative stress. UV, particularly UVA, is known to cause oxidative stress within skin cells, which leads to damage within cells.

Polystyrene is the most common material for cell culture flasks, plates and dishes, and it absorbs some UV light, which leads to its degradation when used outside in some circumstances (Yousif and Haddad, 2013). On absorption, UV causes photooxidative degradation, breaking polymer chains and producing free radicals. Free hydrogen radicals can diffuse through the aromatic structure of the polymer. The surface chemistry of tissue culture plastics is known to affect the behaviour of cells (Hosoya et al., 2018), and during the sterilisation process radiation is used to eliminate contamination of cell cultures (Barker and LaRocca, 1994). The effect of this on cells already adhered to the plastic during irradiation is not known to have been studied.

The DCFDA assay is another reactive oxygen species (ROS) probe, though it is not specific to one type of ROS and will also react readily with reactive nitrogen species (RNS). Because of this it cannot be used as a direct measurement of the concentration of any particular species

within a cell, but rather a more general overview of the oxidative state of the cell. When incubated with cells, it diffuses across the cell membrane, where it is deacetylated by esterases into a compound which is reactive with ROS and when oxidised forms the fluorescent molecule DCF, with excitation at 485 nm and emission at 535 nm.

The MitoSOX assay detects superoxide production specifically at the mitochondrion, where superoxide is produced as a by-product of electron transfer along the ETC. It has been suggested that infrared light is absorbed by cytochrome C, changing the redox properties (Schroeder et al., 2007). Additionally, UV-induced oxidative damage at the mitochondria would be expected to increase superoxide levels, as has been shown previously though at higher doses of UVA (Swalwell et al., 2012a).

ATP production has been shown to change as a result of red and infrared irradiation in cells, though generally at much lower irradiances and doses than what would be received by the sun (0.5 $mW.cm^{-2}$ versus 40 $mW.cm^{-2}$ peak solar infrared intensity), although also using LEDs which only put out a band of light about 20 nm wide, compared to the entire spectrum from the sun (Li et al., 2021, Houreld et al., 2012, Ferraresi et al., 2015). This, therefore, relates more to red light or infrared therapy, where the irradiance and dose would be controlled and delivered using a lamp or LED array rather than sunlight irradiation. It has been suggested that increased ATP concentrations are protective against damage from UV light (Cao et al., 2007), and it has been speculated that infrared from the sun could have a protective effect through ATP levels.

While others tested ATP levels immediately after irradiation, Karu et al. demonstrated that a peak of ATP production in HeLa cells after irradiation with red light occurred 20 minutes after irradiation, which returned to baseline after 40 minutes (Karu et al., 1995). Given this, it was decided that a time course of ATP production measured every 5 minutes for 40 minutes would be useful to see if this could be found in irradiations with the fibroblasts used in this thesis.

DNA damage is known to be caused by UV light, and mitochondrial DNA (mtDNA) is particularly sensitive to this, as outlined in Chapter 1. The 11-kilo base PCR assay published

by Hanna et al describes a qPCR method of quantifying strand break damage in an 11,095-base region of the 16 kb mtDNA loop (Hanna et al., 2019). This assay is sensitive to strand breaks in the mtDNA loop, as the enzyme will not extend beyond double strand breaks in the DNA. As a control, in a separate PCR run an 83 bp fragment of the mtDNA loop is amplified and used to calculate the fold change through the -ΔΔct method.

Visible and infrared light transmittance through sunscreens is not currently regulated. While there exists a regulated method for the testing of sunscreen formulations in vitro to determine SPF, there is no commonly used equivalent test for longer wavelengths. It is, however, of interest to be able to test these qualities, as consumers are increasingly interested in the potential of wavelengths beyond UV to affect skin. As such, a method of spectroradiometry with a lamp producing visible light was developed and used to measure transmittance in sunscreen formulations.

The method of in vitro SPF testing involves the spreading of sunscreen on a roughened PMMA plate of 50 x 50 mm and 1.2 $mg.cm^{-2}$. Transmission spectra are then taken by shining a UV light through the plate. This method only measures up to 400 nm of light.

The method of visible light transmission testing detailed in this thesis tests transmission from 290 to 1000 nm. Instead of using a PMMA plate, Transpore tape was used, and sunscreen was applied to 2 $mg.cm^{-2}$ as this was found to spread more evenly on the rougher surface of the tape. The data are analysed to determine the transmission of all wavelengths between 400 and 420 nm, though the method is flexible enough to allow a range of any bandwidth to be selected between 290 and 1000 nm.

4.2 Materials and methods

4.2.1 Housekeeping gene expression and light irradiation

RNA extraction and reverse transcription were carried out as specified in Chapter 2. β-actin was tested as a housekeeping gene by comparing the Ct from the irradiated cells to that of the control cells where the cDNA concentration had been normalised by NanoDrop of the original RNA. Fold change was calculated as $2^{-\Delta Ct}$.

4.2.2 ROS measurement in cell culture dishes

4.2.2.1 ROS-Glo

Cells were seeded and irradiated as per irradiation protocol in Chapter 2, however instead of 100 ul of DPBS per well, 80 ul per well was added. H_2O_2 substrate solution was mixed from ROS-Glo kit (Promega, USA) by diluting H_2O_2 substrate in H_2O_2 substrate dilution buffer immediately before adding to wells. Menadione was made up to 20 uM in H_2O_2 substrate solution as a positive control. During irradiation, unirradiated control wells were in the same plate, but that side of the plate was wrapped in foil to ensure wells were not exposed to light. After irradiation, 20 ul of H_2O_2 substrate solution or 20 ul of H_2O_2 substrate solution with menadione was added to wells to a final volume of 100 ul and 25 uM H_2O_2 substrate. This was incubated at room temperature in the dark for four hours. ROS-Glo detection solution was made by adding 10 ul/ml each of D-cysteine and signal enhancer to luciferin detection reagent in reconstitution buffer. 50 ul of this ROS-Glo detection solution was added to each well of the 96-well plate. After 20 minutes of incubation at room temperature in the dark, luminescence was read on a TECAN plate reader (Tecan, Switzerland).

In the experiment in results section 4.3.2.1.2, the experimental design was such that the unirradiated and 2.16 SED irradiated wells with and without cells were within the same 96-well plate. The wells without cells were treated the same as those with cells, except that culture medium was used in place of cells in culture medium during seeding.

Pre-treatment of plates was achieved by placing the empty cell culture plate under the solar simulator and exposing it to the desired dose of solar light in SEDs, then immediately seeding HDFn cells and allowing them to adhere overnight in the incubator as per original protocol.

4.2.2.2 DCFDA in plate assay

The protocol for DCFDA in plate assay was based on that in Chapter 2 but altered to test different parts of the experimental design. Pre-treatment of plates was achieved by placing the empty cell culture plate under the solar simulator and exposing it to the desired dose of solar light in SEDs, then immediately seeding HDFn cells and leaving them to adhere overnight in the incubator as per the original protocol.

To examine if the DCFDA interacts with irradiated or pre-treated tissue culture plastics, the experiment was carried out with and without cells. These conditions were treated the same way with the same washing steps except that unlike when cells were present, the acellular condition did not have the DCFDA washed off after the 30-minute incubation with the dye. The reason for this was that if there was any reaction in the acellular condition, it would be more sensitive to this than if it were washed off.

To determine if the method of washing the DCFDA off the cells post-irradiation affected signal, two different washing methods were employed. The “gentle” method used 200 ul of DPBS pipetted slowly into the wells via the side of the well rather than directly onto the bottom of the well. This was then removed by pipetting slowly out from the well. This wash step was completed once after which 100 ul of DPBS was placed onto the cells to read the plate. The second method was more thorough. It involved three repeated washes with 200 ul DPBS, pipetted at a medium speed into the well via the side of the well, then aspirating the DPBS off with a Pasteur pipette attached to a vacuum aspiration pump, which removed the DPBS at a higher speed than pipette removal.

To examine how incubating with DCFDA prior to irradiation affected results, the method of Chapter 2 was altered to be acellular, with DCFDA in cell culture medium in the wells during the irradiation. A serial dilution was performed to make up the concentrations of DCFDA in the medium used. The DCFDA was not washed off prior to fluorescence measurement as per Chapter 2.

A further test of whether incubating with DCFDA and then washing off the excess and replacing with PBS before reading was carried out. DCFDA was incubated for 30 minutes before washing off gently and replacing with PBS and reading as per Chapter 2.

4.2.3 Co-staining MitoSOX and TMRE in flow cytometry

A method to test whether TMRE and MitoSOX could be stained together with DAPI was adapted from the method outlined in Chapter 2. The adapted method involved the same concentrations of MitoSOX and TMRE, but the staining was carried out in a volume of 500 ul in FACS tubes. 480 ul of 5 uM MitoSOX was added to the FACS tube, mixed by pipetting and

incubated at 37°, 5% CO_2 in a humidified incubator for 20 minutes, at which point 20 ul of 0.1 uM TMRE was added to a final concentration of 4 nM. This was returned to the incubator for a further 10 minutes before washing and running on the BD Symphony as per the previous method.

Though the wavelengths of the lasers used to excite MitoSOX and TMRE were chosen to maximise excitation of the target fluorophore and minimise excitation of the other, there was still some spillover (Figure 4-1), To account for this, compensation matrices were calculated for the spillover between MitoSOX and TMRE dyes and were applied to all equivalent experiments. Gating was carried out as per Chapter 2.

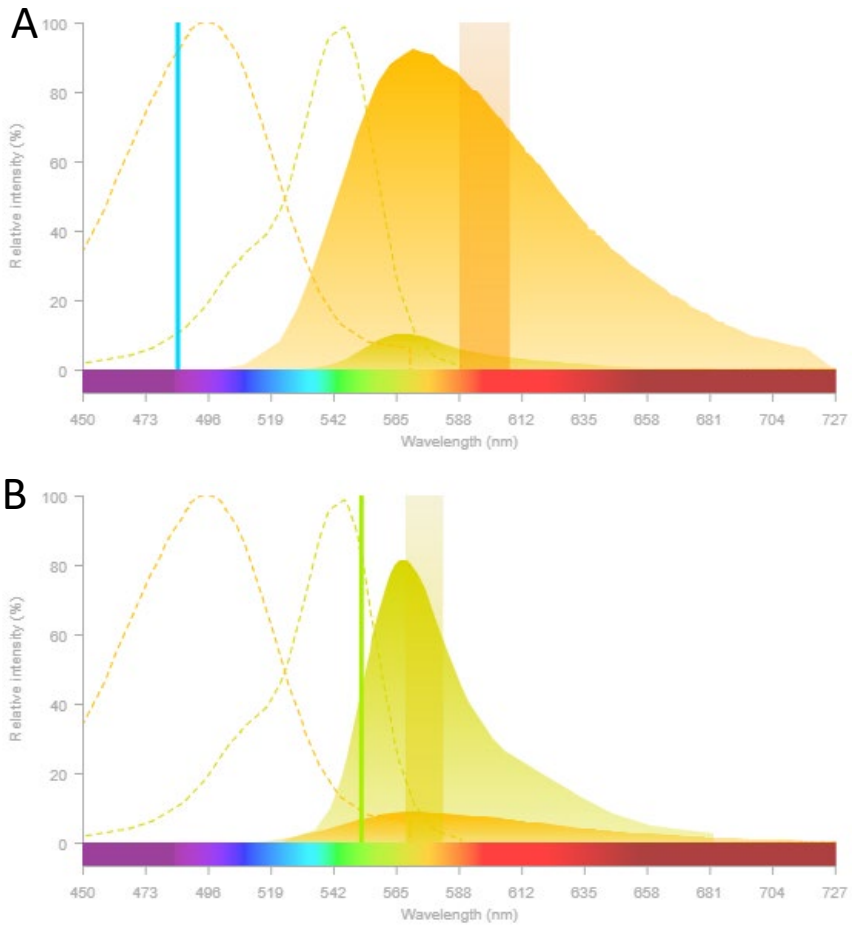

Figure 4-1 Emission spectra of MitoSOX (orange) and TMRE (yellow).
Panel A shows emission spectra when excited by 488 nm laser, and the highlighted bandpass represents the 610/30 nm emission filter. Panel B shows emission spectra when excited by 561 nm laser, and the highlighted bandpass represents the 586/15 nm emission filter. Spectra were generated using ThermoFisher Spectra Viewer tool.

4.2.4 MitoSOX concentration

To determine whether a lower concentration of MitoSOX would give the same information as the recommended 5 mM, a concentration of 1 mM was tested. The protocol was the same as in Chapter 2, but the MitoSOX was diluted 1 in 5 before adding the same volume to the medium.

4.2.5 11 kb mtDNA damage assay

4.2.5.1 83 bp qPCR

The 83 bp qPCR assay is run as a control to measure the amount of mtDNA present in a sample. A standard curve of DNA concentration was run; linear regression was performed to determine line of best fit, the R^2 was at least 0.98 and the slope was used to calculate efficiency which was between 90% and 100%. The primers, reagents and cycle conditions can be found in Table 4-1, Table 4-3 83 bp qPCR assay PCR cycle conditions and Table 4-3 respectively.

Table 4-1 83 bp qPCR assay primers

IS1 (*forward*)	GATTTGGGTACCACCCAAGTATTG
IS2 (*reverse*)	AATATTCATGGTGGCTGGCAGTA

Table 4-2 Composition of 83 bp qPCR reaction

Mastermix composition	**Volume (µl)**	**Final concentration**
PCR grade H_20	8.25	N/A
Forward primer (10 µM)	1	0.4 µM
Reverse primer (10 µM)	1	0.4 µM
SYBR® Green JumpStart™ Taq ReadyMix™ (2×)	12.5	1×
ROX reference dye (100×)	0.25	1×
Mastermix total	23	
DNA	2	
Reaction total	25	

Table 4-3 83 bp qPCR assay PCR cycle conditions

Stage	Temperature	Time (minutes)	Cycles
Initial denaturation	94	2	1
Denaturation	94	0.15	35 (*acquire at end of step*)
Annealing	60	0.45	
Extension	72	0.45	
Final extension	72	2	
StepOnePlus™ melt curve analysis			

4.2.5.2 DNA extraction

For all extractions, the QIAamp DNA Mini kit was used as per manufacturer protocol (Qiagen, Netherlands). In brief, cells were trypsinised and incubated with 200 ul Buffer AL at 70°C for 10 minutes. 200 ul of ethanol was added and mixed, and then the sample was added to the spin column and centrifuged at 6000 g for 1 minute. 500 ul of Buffer AW1 was added and the centrifugation was repeated. 500 ul of Buffer AW2 was added and the column was centrifuged at 16,000 g for 3 minutes. 200 ul of Buffer AE was added to the spin column and centrifuged at 6000 x g to elute the DNA. DNA was stored at -20°C.

4.2.5.3 Original Method

To attempt to quantify mtDNA strand breaks, an assay amplifying 11 kb of the 16 kb mtDNA loop using the Expand Long Template PCR Kit (Roche, Switzerland). The original method referred to here is that published (Hanna et al., 2019). Unless otherwise specified, the 20 ul qPCR reaction contained reagents as detained in Table 4-4. Primer sequences can be found in Table 4-6. The cycle method can be found in Table 4-5 Original PCR cycle conditions and Table 4-5. A no-template control was included in every plate, and the outside wells of the plate were not used to account for variances in their temperature compared to the inner wells in the heat block of the thermal cycler.

4.2.5.3.1 Reagents

Table 4-4 Reagents in original 11 kb PCR reaction

		StepOne		QuantStudio 3	
Reagent	Manufacturer	Final Concentration	Volume (ul)	Final Concentration	Volume (ul)
Expand Long Template PCR Kit Enzyme (5 U/ul)	Roche, Switzerland	0.075 U	0.3	0.075 U	0.3
Expand Long Template PCR Kit 10 x Buffer 2	Roche, Switzerland	1 x	2	1 x	2
SYBR Green (5 x in IDTE)	Lonza, Switzerland	0.1 x	0.4		
SYBR Green (100 x in IDTE)	Lonza, Switzerland			0.1 x	0.4
ROX (50 x)	ThermoFisher Scientific, USA	1 x	0.4	0.1 x	0.04
PCR nucleotide mix (10 mM dATP, dCTP, dGTP, and dTT)	Roche, Switzerland	500 uM	1	500 uM	1
RNase-free water	Integrated DNA Technologies, USA		12.7		13.06
Primer OLA (10 uM in IDTE)	Eurofins, Luxembourg	0.3 uM	0.6	0.3 uM	0.6
Primer D1B (10 uM in IDTE)	Eurofins, Luxembourg	0.3 uM	0.6	0.3 uM	0.6
DNA (6 ng/ul)		0.6 ng/ul	2	0.6 ng/ul	2

4.2.5.3.2 PCR cycle method

Figure 4-4-2 Cycle temperatures and times for original 11 kb PCR method.

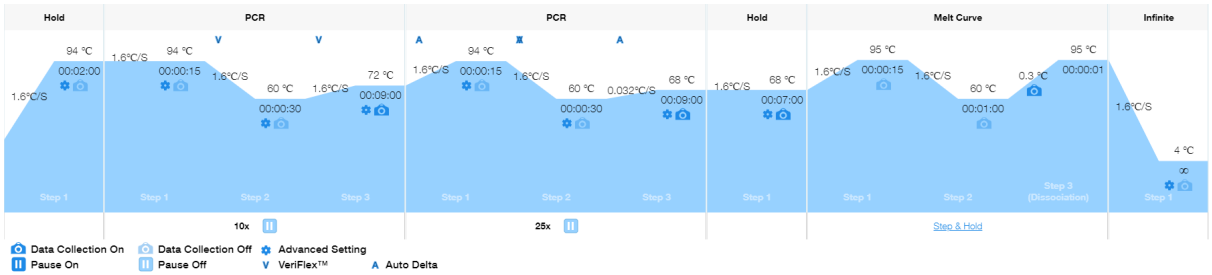

Table 4-5 Original PCR cycle conditions

Stage	Temperature	Time (minutes)	Cycles
Initial denaturation	94	2	1
Denaturation	94	0.15	10 (acquire at end of step)
Annealing	60	0.3	
Extension	72	9	
Denaturation	94	0.15	25 (acquire at end of step)
Annealing	60	0.3	
Extension	68	8.50 (+10 s per cycle)	
StepOnePlus™ melt curve analysis			

4.2.5.3.3 Primers

Table 4-6 from Primer BLAST

	Forward primer (DLB)	**Reverse primer (OLA)**
Sequence (5'->3')	ATGATGTCTGTGTGG AAAGTGGCTGTGC	GGGAGAAGCCCCG GCAGGTTTGAAGC
Length (base pairs)	28	26
Tm (Primer BLAST)	67.55	71.47
Tm (Thermo Fisher Tm calculator)	74.9	79.2
GC%	50	65.38
Self-complementarity	3	4
Self-3' complementarity	2	3
Template start	16274	5179
Template end	16247	5204

4.2.5.4 Optimising extension and annealing temperature

The optimal annealing temperature recommended by the manufacturer is 45 - 65°C. The original assay used an annealing temperature of 60°C. To determine the effects of annealing temperature on off-target binding, a plate with 6 annealing temperatures (60, 62, 64, 66, 68 and 70°C) and 4 different DNA concentrations (10, 4, 1,6 and 0.64 ng/reaction) for each temperature was run.

Extension temperature was tested by running two temperature conditions within the same plate. One where the extension temperature was 72°C for the first 10 cycles then 68° for the

subsequent 25, as per the original assay, and the other had a consistent temperature of 68°C throughout the 35 cycles, as per the manufacturer's recommendations.

4.2.5.5 mtDNA isolation

In an attempt to reduce off-target binding, mitochondria were isolated, and the DNA was extracted from the isolated mitochondria sample. Three buffers were prepared. Buffer A was made up of 10mM NaCl, 1.5mM $MgCl_2$, 10mM Tris-HCL (pH7.5), with PIC added just before using, with the buffer made to 1 x PIC from a 25 x stock. 2.5x Buffer B in $T_{10}E_{20}$ buffer (525 mM mannitol, 175mM sucrose, 12.5 mM Tris-HCl, 2.5mM EDTA, pH 7.6) and 1 x Buffer B (210mM mannitol, 70mM sucrose, 5mM Tris-HCL, 1mM EDTA, pH 7.5) were prepared. The protocol was carried out at 4°C, with all reagents and equipment also at 4°C.

10^7 HDFn cells were trypsinised and centrifuged at 1000 g for 5 minutes. Cells were resuspended in 2 ml of Buffer A and allowed to swell for 20 minutes. A Dounce homogeniser was used at ~1600 rpm for 30 strokes. 1.33 ml of 2.5 x Buffer B was added to give a final concentration of 1 x Buffer B. This was mixed and kept on ice for 30 minutes before centrifuging for 10 minutes at 1000 g. The supernatant was collected, and the centrifuge step was repeated twice with 1 x Buffer B. The supernatant was then collected, and the mitochondria pelleted for 10 minutes at 8000 g. After this, the pellet was resuspended in water and an RNA extraction was performed as per the protocol in section 0.

When the mtDNA was run on qPCR, an 83 bp PCR was run alongside the 11 kb PCR. The mtDNA concentration was unknown as the concentration was too low to measure with a NanoDrop, so the lines of best fit from the serial dilution of the mtDNA and total DNA isolations were used to calculate the predicted concentration of whole DNA the mtDNA would have come from. This was used to plot the ct values from the 11 kb versus the log2[DNA concentration] alongside the whole DNA extraction, where mtDNA was not isolated so genomic DNA was included and measurable on a NanoDrop. The calculation was performed so the lines of best fit, which had slightly differing slopes, crossed in the centre of the DNA points (see Figure 4-29).

4.2.5.6 Optimising buffer in PCR reaction

For this experiment, the buffer in the reaction mix was changed. The Long Template PCR Kit comes with three buffers, each with different components and designed to best fit different lengths of PCR product. Buffer 1 contains 17.5 mM $MgCl_2$ and is intended for use with 0.5 – 9 kb products, Buffer 2 contains 27.5 mM $MgCl_2$ and is intended for use with 9 – 12 kb products, and Buffer 3 contains 27.5 mM $MgCl_2$ and additional detergents, intended for use with PCR products longer than 12 kb. The original assay used buffer 2, as this would be suggested for the 11 kb product, but the troubleshooting guide suggests trying the different buffers to see if 1 or 3 amplifies more effectively.

The original protocol was used, with the only change being that buffer 2 from the newest kit was replaced with one of the other buffers. Buffer 2 was replaced with buffers 1 and 3, and an additional buffer 2 (labelled buffer 2B) which was Buffer 2 but from an older kit. All were run on the same plate with a range of DNA concentrations (25, 10, 4, 1.6 and 0.64 ng/reaction) to ensure comparability.

4.2.5.7 Gel electrophoresis of PCR products

4.2.5.7.1 4% gel

The 4% agarose gel was used for elucidating short products such as primer dimer. 50 ml of 10 x TBE buffer was diluted with 450 ml of Mili-Q water for 1 x working buffer. 4 g of agarose was washed into a bottle with 100 ml 1 x TBE buffer, swirled to mix and microwaved for approximately 1.5 minutes or until the agarose had dissolved. This was left to cool slightly before gently mixing in 5 ul of dye (Gel Red Nucleic Acid stain, Biotium, USA) and pouring into a gel rack with taped sides and an 11-well comb. The gel was left to set for 1 hour, then removed from the rack and placed in a gel tank with enough TBE buffer to just cover it. 1 ul of DNA loading gel (B7025S, New England Biolabs, USA) was mixed with 5 ul of DNA sample from the PCR reaction. This was mixed and the 6 ul total was added to a well in the gel. 2 ul of ladder (Ultra Low Range DNA Ladder, Invitrogen, UK) was mixed with 1 ul of dye and 4 ul of water and added to lane 1. The gel was run for an hour at 50 V. Imaging was performed on a Licor Odyssey Fc (Licor, UK).

4.2.5.7.2 0.8% gel

The 0.8% gel was used for elucidating the 11 kb product. The method of preparation for the 0.8% gel was the same as the 4% gel apart from the following differences:

1. 0.8 g of agarose was added to 100 ml Mili-Q water rather than 4 g
2. Working buffer was prepared using 10 ml of 50 x TAE buffer in 490 ml of Mili-Q water, rather than 50 ml of 10x TBE buffer in 450 ml of Mili-Q water
3. The DNA dye and proportions were as such: 1 ul of GelPilot Dye (Qiagen, Netherlands) was mixed with 2 ul of DNA sample from the PCR reaction and 2 ul Mili-Q water, and the 5 ul total added to the well in the gel
4. The ladder used was different: 5 ul of ladder (High Range Ladder, Qiagen, Netherlands) was added to lane 1
5. The gel was run for an hour at 100 V rather than 50 V

4.2.6 ATP measurement assay

The Promega CellTiter-Glo assay (Promega, USA) was used to measure ATP production as per the manufacturer's protocol. In brief, CellTiter-Glo Substrate was mixed with CellTiter-Glo Buffer, 100 ul of which was then added to the well of a 96-well plate. This was mixed on a rocking platform for 2 minutes then allowed to incubate at room temperature for 10 minutes before luminescence was read on a plate reader (Tecan, Switzerland).

4.2.7 Transmission testing of formulations

To test the ability of an ingredient or combination of ingredients, a control formulation with the same base ingredients but no additional filtering ingredients was used. The formulations were stored in the fridge for a minimum of 24 hours prior to use to limit the evaporation of formulation during weighing. A small amount of the formulation was put in a clean weight boat so the formulation container could remain closed during weighing. With a clean pipette tip, the formulation was transferred to a 50 mm x 50 mm square of translucent Transpore tape (3M, ID 7100004870) on a tared scale. The formulation was applied in small dots evenly across the tape until 50 mg of formulation was applied, to apply 2 $mg.cm^{-2}$ across the area. A loosely gloved finger was used to lightly spread the formulation over the tape in circles to distribute evenly. Next, a tightly gloved finger was used with medium pressure side to side

then up and down across the tape. The tape was then left to dry for 40 minutes to ensure the formulation had formed a film before testing.

Sunscreens tested were provided by CRODA, and information on formulations is confidential. Each formulation is represented with an identifying code in this thesis.

The spectroradiometer used was the FLAME and the light source used was the solar simulator, as detailed in Chapter 2 with no additional filters added. This was allowed to warm up by leaving it which switched on for 10 minutes before any measurements were taken. Measurements were taken by suspending the tape just above the sensor of the spectroradiometer from three different locations on the tape, used to generate an average transmittance. The experiment was repeated on three separate occasions to represent three biological repeats.

4.3 Results

4.3.1 Housekeeping gene expression and light irradiation

4.3.1.1 Beta-actin expression appears to change with solar irradiation

Effects of solar light on the housekeeping gene β-actin were assayed using the TaqMan gene expression PCR assay (Figure 4-3). When comparing the raw ct value of β-actin in HDFn cells which had been irradiated with 2.16 SEDs of complete solar light to control cells was reduced by 43% (a fold change of -0.85).

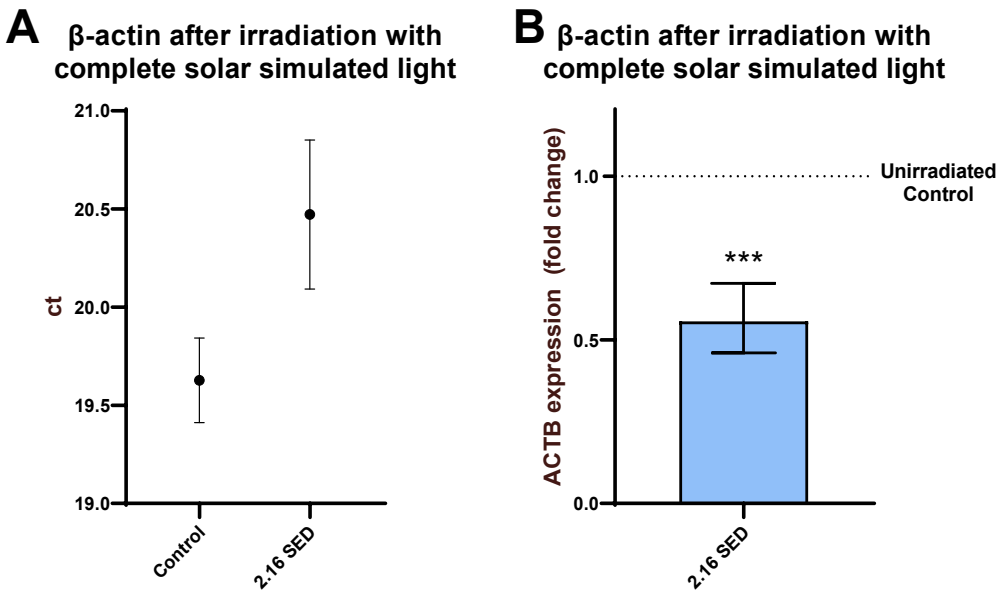

Figure 4-3 Effect of 2.16 SEDs of complete solar on β-actin expression in HDFn cells assayed using TaqMan assay in PCR

Cells were seeded in complete, phenol-free DMEM with 10% FCS. Irradiation was carried out in PBS, after which cells were returned to complete, phenol-free DMEM with 10% FCS. 2.16 SEDs of complete, solar simulated light delivered over ~2 minutes. RNA was extracted 24 hours after the end of irradiation. Unirradiated controls were under the lamp during irradiation but wrapped in foil to receive 0 SEDs of light. Temperature was controlled using a stand. Panel A shows raw ct values, B shows expression as fold change of unirradiated control. Data in panel B normalised to unirradiated control. (***): $p \leq 0.001$, one-sample t-test on log2 transformed data. Graphs show geometric means ±95 % CI, N = 6, n = 2

4.3.1.2 GAPDH does not change with 2.16 SED of solar-simulated UV

Effects of solar light on the housekeeping gene GAPDH were assayed using the TaqMan gene expression PCR assay (Figure 4-4). When comparing the raw ct value of GAPDH in cells which had been irradiated with 2.16 SEDs of complete solar light to control cells was not significantly affected, although the change induced by 4.32 SEDs was significantly reduced by 44%.

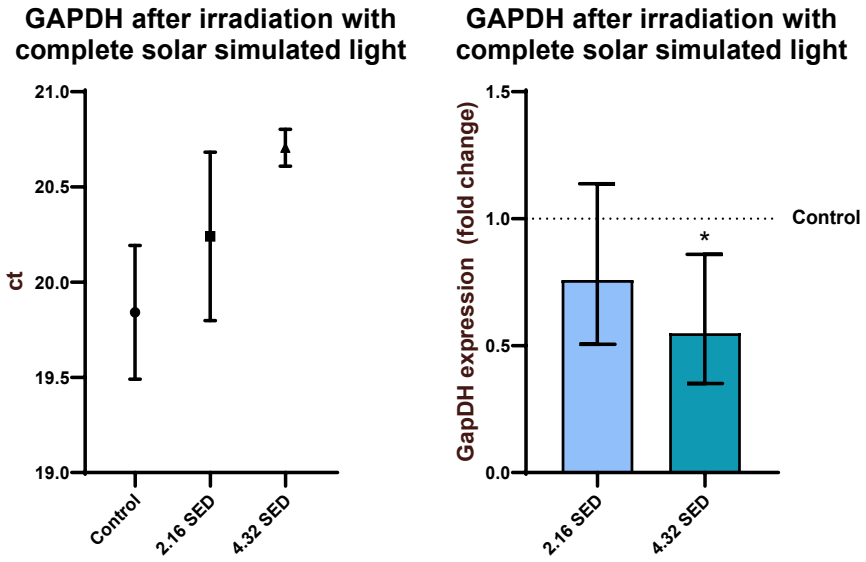

Figure 4-4 Effect of 2.16 SEDs of complete solar simulated light on GAPDH expression in HDFn fibroblasts assayed using TaqMan assay in PCR.

Cells were seeded in complete, phenol-free DMEM with 10% FCS. Irradiation was carried out in PBS, after which cells were returned to complete, phenol-free DMEM with 10% FCS. 2.16 SEDs of complete, solar simulated light or UV only light was delivered over ~2 or ~3 minutes respectively. RNA was extracted 24 hours after the end of irradiation. Unirradiated controls were under the lamp during irradiation but wrapped in foil to receive 0 SEDs of light. Temperature was controlled using a stand. Panel A shows raw ct values, B shows expression as fold change of unirradiated control. Data in panel B normalised to unirradiated control. (*): $p \leq 0.05$, one-sample t-test on log2 transformed data; data represent means (left) and geometric means (right) ± 95% CI, N = 3, n = 3

4.3.2 ROS measurement in cell culture plastics

4.3.2.1 ROS-Glo interactions with cell culture plastic

4.3.2.1.1 Irradiation affects ROS-Glo signal when no cells are present

When ROS-Glo assay is added to a 96-well plate containing no cells after irradiation with complete solar simulated light including UV, there is a false positive result, whereby irradiated wells have a 4.4-fold increased signal compared to unirradiated wells (Figure 4-5). There is also an increased signal in unirradiated control wells between plates where wells on the irradiated side were given different doses of light. The control cells in the 8.64 SED irradiated plate had a 3.9-fold greater signal than control wells from the 2.16 SED irradiated plate, even though all control wells had been under foil during the irradiation to eliminate light exposure.

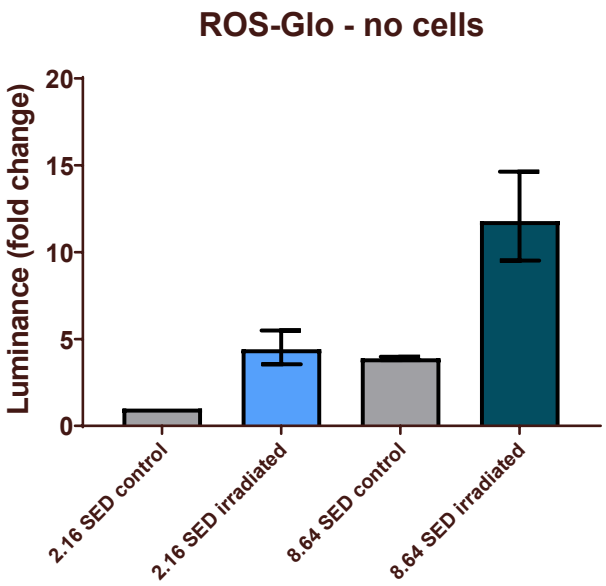

Figure 4-5 Effect of 2.16 and 8.64 SEDs of complete solar simulated light on ROS-Glo signal in 96-well plate without cells.
A white-walled, 96-well plate was covered in foil on one side to act as the unirradiated control, while the other side of the plate was exposed to the light from the solar simulator. 2.16 and 8.64 SEDs of complete, solar simulated light was delivered over ~2 minutes and ~8 minutes respectively. Temperature was controlled with a stand. Irradiation was carried out in PBS, to which the ROS-Glo reaction and later detection solutions were added directly. Data were normalised to 2.16 SED unirradiated control. Data represent geometric means ± geometric SD, N = 2, n = 3

4.3.2.1.2 Presence of HDFn cells reduces signal

In a 96-well plate seeded such that some wells contained cells and others only culture medium, half the plate was irradiated with 2.16 SED of complete solar simulated light while the other side was covered in foil to maintain darkness (Figure 4-6). There was a 50% reduction in signal in the irradiated wells with cells compared to the irradiated wells without cells. There was also a 43% reduction in signal from the unirradiated control wells containing cells compared to the control wells not containing cells.

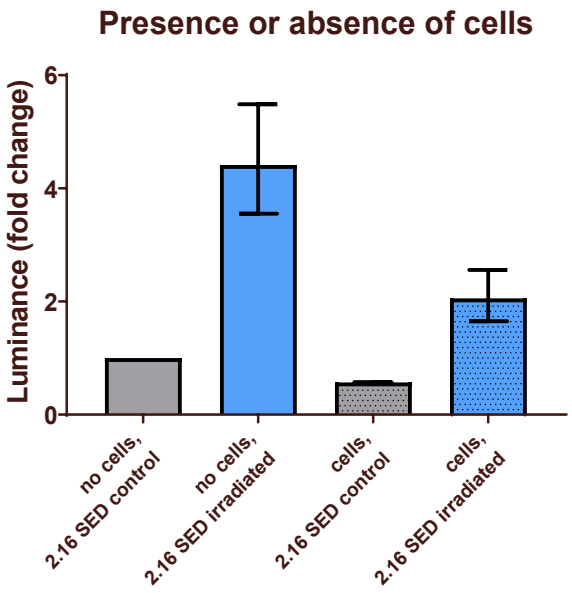

Figure 4-6 Effect of 2.16 SEDs of complete solar simulated light on ROS-Glo signal in 96-well plate wells with and without HDFn cells.
Cells were seeded in a white-walled, 96-well plate in complete, phenol-containing DMEM with 10% FCS. Wells without cells had only medium present. The plate was covered in foil on one side to act as the unirradiated control, while the other side of the plate was exposed to the light from the solar simulator. 2.16 and 8.64 SEDs of complete, solar simulated light was delivered over ~2 minutes and ~8 minutes respectively. Temperature was controlled with a stand. Irradiation was carried out in PBS, to which the ROS-glo reaction and later detection solutions were added directly after irradiation. Data were normalised to the "no cells" 2.16 SED unirradiated control. Plain bars show wells with no cells, spotted bars show wells with cells. Data represent geometric means ± geometric SD, N = 2, n = 3

4.3.2.1.3 Pre-treatment increases signal the next day

When seeded in plates that had been irradiated with 8.64 SED of complete solar simulated light prior to seeding, there was an increase in the signal compared to that from wells in plates that had not been pre-treated, but the effect was not large (Figure 4-7).

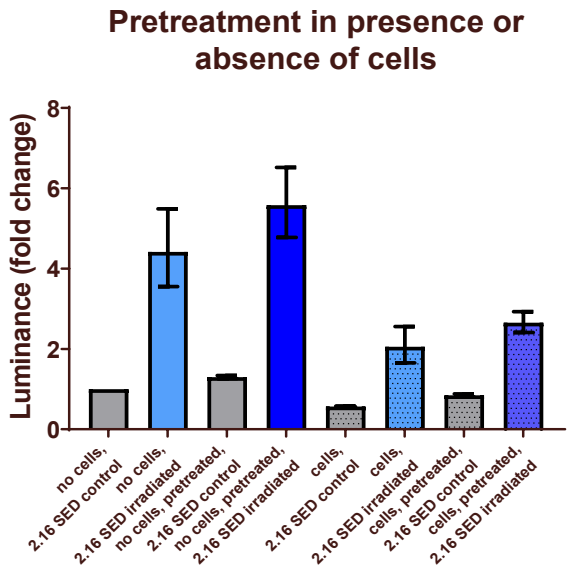

Figure 4-7 Effect of pre-treating plates with 8.64 SEDs of complete solar simulated light on ROS-Glo signal in wells with and without HDFn cells and their response to 2.16 SEDs.
Pre-treatment was carried out immediately before seeding and involved irradiation of the entire white-walled 96-well plate with 8.64 SEDs of complete, solar simulated light. Cells were seeded in complete, phenol-containing DMEM with 10% FCS. Wells without cells had only medium present. The plate was covered in foil on one side to act as the unirradiated control, while the other side of the plate was exposed to the light from the solar simulator. 2.16 and 8.64 SEDs of complete, solar simulated light was delivered over ~2 minutes and ~8 minutes respectively. Temperature was controlled with a stand. Irradiation was carried out in PBS, to which the ROS-Glo reaction and later detection solutions were added directly after irradiation. Data were normalised to the "no cells" 2.16 SED unirradiated control. Plain bars show wells with no cells, spotted bars show wells with cells. Data represent geometric means ± geometric SD, N = 2, n = 3

4.3.2.2 DCFDA does not interact with TC plastic

To ensure that DCFDA had no interaction with tissue culture plastic that had previously been irradiated, or that irradiation of an exposed part of the plate affects covered, control wells, an experiment comparing irradiations with and without cells was carried out (Figure 4-8). In wells without cells, DCFDA added after irradiation gave little signal, and this was the same between irradiated and control wells regardless of the dose of light. When cells were present, there was a greater DCFDA signal even in unirradiated wells, indicating that the DCFDA signal, when incubated after irradiation and washed off, represents a signal from the cells rather than an interaction with the tissue culture plastic.

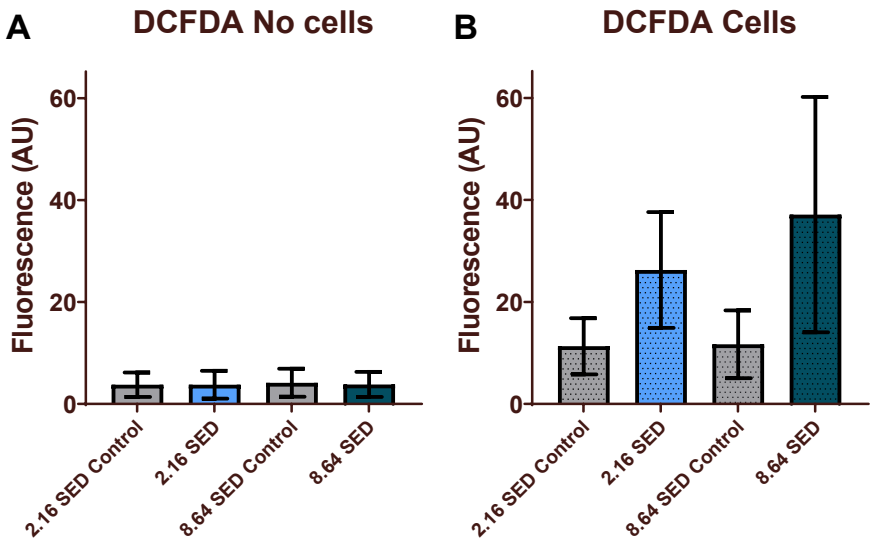

Figure 4-8 DCFDA signal when incubated after irradiation then washed off, with and without HDFn cells present.

Panel A shows DCFDA signal from well with no cells present, B shows signal from wells with cells. Cells were seeded in a white-walled, 96-well plate in complete, phenol-containing DMEM with 10% FCS. Wells without cells had only medium present. The plate was covered in foil on one side to act as the unirradiated control, while the other side of the plate was exposed to the light from the solar simulator. 2.16 and 8.64 SEDs of complete, solar simulated light was delivered over ~2 minutes and ~8 minutes respectively. Temperature was controlled with a stand. Irradiation was carried out in PBS, after which cells were incubated with DCFDA for 30 minutes and returned to fresh, complete, phenol-free DMEM with 10% FCS for plate reading. Plain bars show wells with no cells, spotted bars show wells with cells. Data represent means ± SD, N = 3, n = 3

4.3.2.3 Washing method affects DCFDA signal

On observing that there looked to be fewer and more detached cells when viewed under the microscope after washing the DCFDA from cells, a test was carried out to compare a gentle and a more thorough wash on DCFDA signal. With one gentle was of 200 ul of PBS, removed by pipette, the fluorescence signal was found to be greater than when washed three times with PBS and aspirated off with vacuum aspiration, which resulted in an 80% reduced signal. With gentle washing, the cells under the microscope appeared to be better adhered to the plastic.

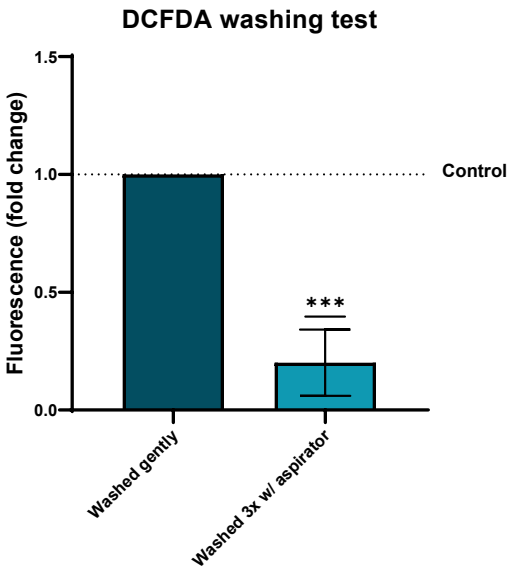

Figure 4-9 DCFDA after vigorous washing causes loosened HDFn cells to detach and a reduction in signal.

Cells were seeded in a white-walled, 96-well plate in complete, phenol-containing DMEM with 10% FCS. Cells were either washed 3x and an aspirator used to remove washes, or washed once, using a pipette to remove medium and wash. Cells were incubated with DCFDA for 30 minutes and returned to fresh, complete, phenol-free DMEM with 10% FCS for plate reading. Data were normalised to the "washed gently" condition. (***): $p \leq 0.001$, one-sample t-test on log2 transformed data; data represent means ± SD, N = 5, n = 3

4.3.2.4 Irradiating a cell culture plate before seedings HDFn cells affects DCFDA signal

4.3.2.4.1 Unirradiated controls show lower DCFDA signal in pre-treated plates

When the tissue culture plate was irradiated with 8.64 SEDs of solar simulated light immediately before seeding HDFn cells on, it was noticed that unirradiated control cells in pre-treated plates had a lower signal from DCFDA than those from normal, not-pre-treated tissue culture plates (Figure 4-10).

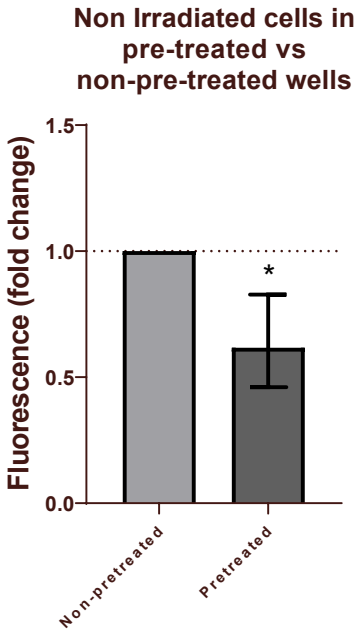

Figure 4-10 DCFDA signal from HDFn cells seeded in wells pre-treated with 8.64 SEDs of solar simulated light was lower than from cells seeded in non-pre-treated wells.
Pre-treatment was carried out immediately before seeding and involved irradiation of the entire white-walled 96-well plate with 8.64 SEDs of complete, solar simulated light. Cells were seeded in complete, phenol-containing DMEM with 10% FCS. Cells were incubated with DCFDA for 30 minutes and returned to fresh, complete, phenol-free DMEM with 10% FCS for plate reading. Data were normalised to the non-pretreated condition. (*): $p \leq 0.05$, one-sample t-test on log2 transformed data; data represent geometric means ± geometric SD, N = 3, n = 3.

4.3.2.4.2 The increase in ROS is statistically unaffected by plate pre-treatment

When HDFn cells seeded in a non-pre-treated plate, irradiation significantly increased DCFDA signal (180% increase compared to unirradiated controls) (Figure 4-11). The increase from irradiation in plates that were pre-treated was 255%, which was not significantly different.

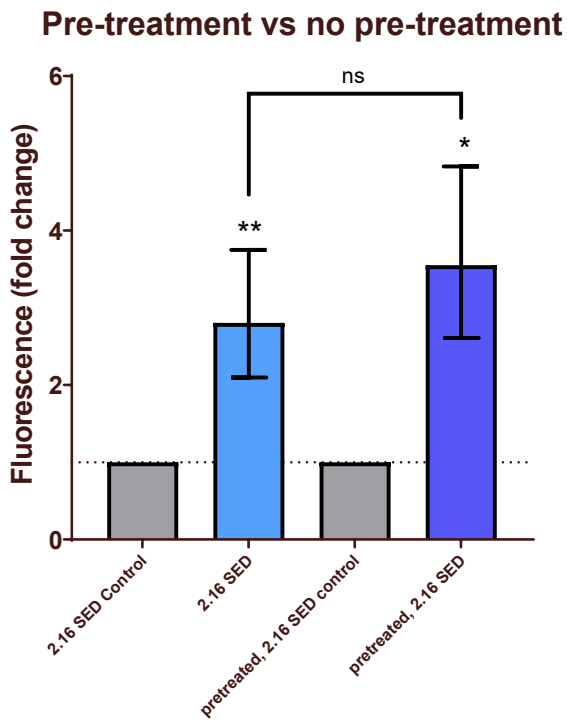

Figure 4-11 DCFDA signal from HDFn cells irradiated with 2.16 SEDs of solar simulated light compared to unirradiated cells in pre-treated and non-pre-treated plates.
Pre-treatment was carried out immediately before seeding and involved irradiation of the entire white-walled 96-well plate with 8.64 SEDs of complete, solar simulated light delivered over ~8 minutes. Cells were seeded in complete, phenol-containing DMEM with 10% FCS. The plate was covered in foil on one side to act as the unirradiated control, while the other side of the plate was exposed to the light from the solar simulator. 2.16 SEDs of complete, solar simulated light was delivered over ~2 minutes. Temperature was controlled with a stand. Irradiation was carried out in PBS, after which cells were incubated with DCFDA for 30 minutes and returned to fresh, complete, phenol-free DMEM with 10% FCS for plate reading. Data were normalised to the respective unirradiated control. Plain bars show wells with no cells, spotted bars show wells with cells. (*): $p \leq 0.05$; (**): $p \leq 0.01$, one-sample t-test on log2 transformed data; (ns): no significant difference, two-tailed unpaired student's t-test; data represent geometric means ± geometric SD, N = 3, n = 3.

4.3.2.4.3 Pre-treating plates does not affect cell viability in unirradiated HDFn cells

To determine whether the decrease in DCFDA signal from pre-treated plates was due to a decrease in the number of cells adhered, the viability in unirradiated cells in non-pre-treated, 2.16 SED and 8.64 SED pre-treated plates was compared (Figure 4-12). There was no significant difference in the viability of cells in these different conditions immediately or 24 hours after irradiation.

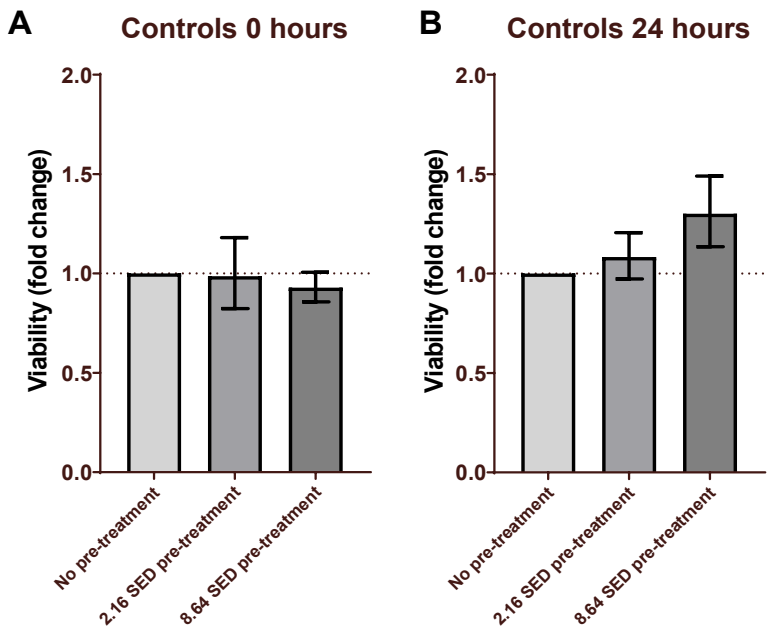

Figure 4-12 MTS viability in non-irradiated control HDFn cells in pre-treated and non-pre-treated plates.

Pre-treatment was carried out immediately before seeding and involved irradiation of the entire clear-walled 96-well plate with 2.16 or 8.64 SEDs of complete, solar simulated light delivered over ~2 or ~8 minutes respectively. Cells were seeded in complete, phenol-containing DMEM with 10% FCS. Cells were incubated with DCFDA for 30 minutes and returned to fresh, complete, phenol-free DMEM with 10% FCS for plate reading. Data were normalised to the non-pretreated control. Panel A: viability immediately after irradiation; B: viability 24 hours after irradiation. No significant differences with one-sample t-test of long2 transformed data; data represent geometric means ± geometric SD, N = 3, n = 3.

4.3.2.4.4 Pre-treatment of plates does not affect viability after irradiation

After irradiation with 2.16 or 8.64 SEDs of complete solar simulated light, there was found to be no difference in viability in any pre-treatment condition immediately after irradiation (Figure 4-13). 24 hours after irradiation, there was a significant decrease in viability for all irradiated conditions ($p < 0.05$, one-sample t-test), but there was no difference between pre-

treatment groups ($p > 0.05$, 2-way ANOVA).

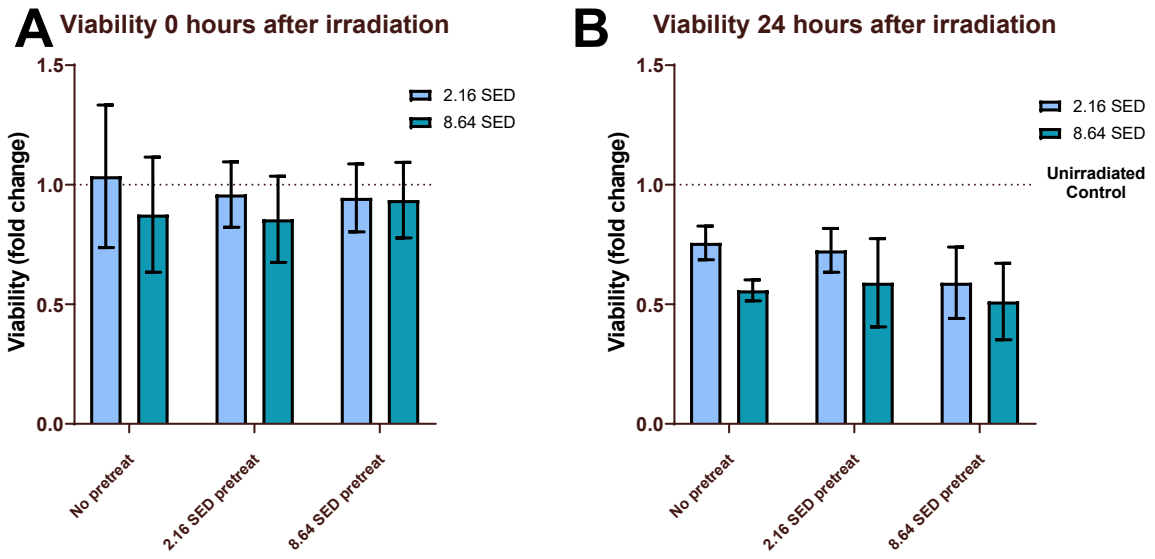

Figure 4-13 MTS viability in 2.16 and 8.64 SED irradiated HDFn cells in pre-treated and non-pre-treated plates.

Pre-treatment was carried out immediately before seeding and involved irradiation of the entire white-walled 96-well plate with 2.16 or 8.64 SEDs of complete, solar simulated light delivered over ~2 ~8 minutes respectively. Cells were seeded in complete, phenol-containing DMEM with 10% FCS. The plate was covered in foil on one side to act as the unirradiated control, while the other side of the plate was exposed to the light from the solar simulator. 2.16 and 8.64 SEDs of complete, solar simulated light were delivered over ~2 or ~8 minutes respectively. Temperature was controlled with a stand. Irradiation was carried out in PBS, after which cells were returned to fresh, complete, phenol-free DMEM with 10% FCS. Data were normalised to the respective unirradiated control. Panel A: viability immediately after irradiation; B: viability 24 hours after irradiation. Data represent means ± SD, N = 3, n = 3.

4.3.2.5 DCFDA presence during infrared irradiation generates signal in absence of HDFn cells

When present in wells during acellular irradiation with infrared light, DCFDA will give a concentration-dependent increase in response, dependent on temperature and irradiance (Figure 4-14). For the 26° 100 mW/cm^2 condition, even at 0.1 uM the DCFDA signal was increased by 140% without any cells present. Without knowing the concentration of DCFDA that would be in the cells, and whether the DCFDA in the cells would respond to light in the same way as it does in the medium surrounding the cells, it would be impossible to whether an increase in DCFDA signal was due to an increase in ROS production within the cell, or an artefact of the DCFDA reaction with the light and/or medium.

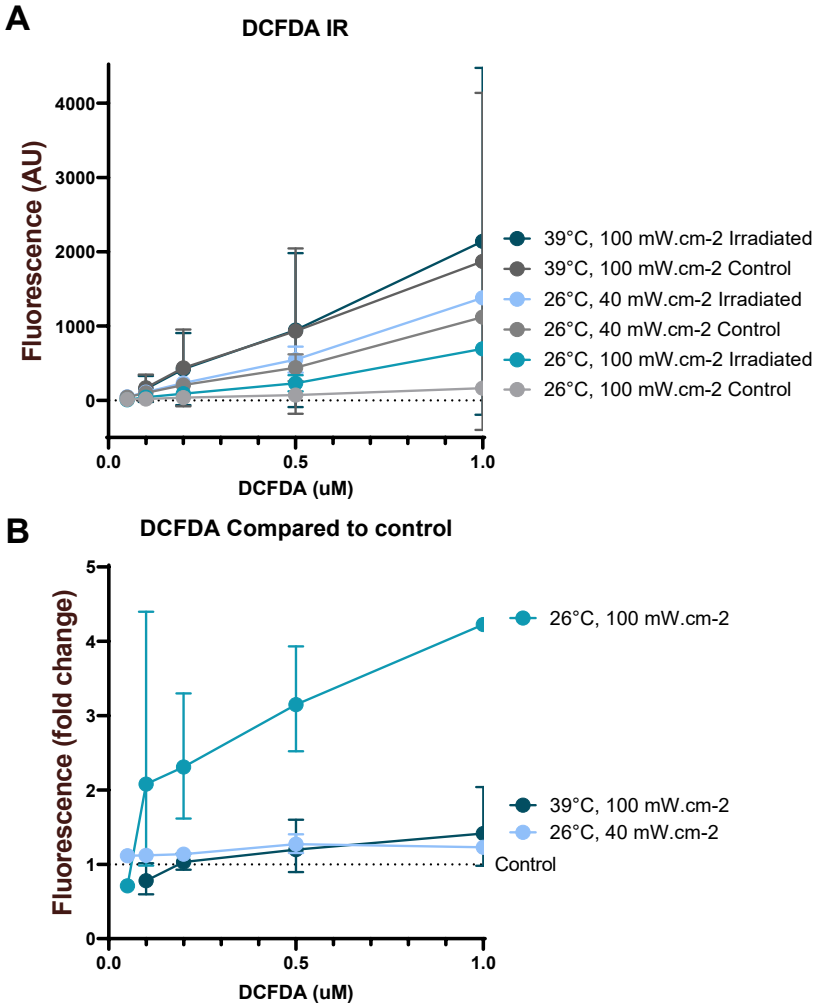

Figure 4-14 DCFDA at various concentrations in cell culture medium in an acellular experiment shows an increase in signal when exposed to infrared light.
DCFDA was added to a white-walled 96-well plate at increasing concentrations in complete, phenol-free DMEM with 10% FCS, which was read immediately after irradiation without washing. Temperature was controlled with a stirred water bath at 26°C or 39°C. Irradiation was carried out with the Hydrosun IR Lamp at 100 mW.cm^{-2} for 60 minutes for a dose of 360 J.cm^{-2} or 40 mW.cm^{-2} for 150 minutes for a dose of 360 J.cm^{-2}. Unirradiated controls were under the lamp during irradiation but wrapped in foil to receive 0 J.cm^{-2} of light. Data in panel B normalised to unirradiated control. Panel A: fluorescence as measured in arbitrary units, data represent means ± SD. B: fluorescence as a fold change from unirradiated control. Data represent geometric means ± geometric SD. N = 2, n = 3

4.3.2.6 DCFDA addition before and after infrared irradiation in presence of HDFn cells

4.3.2.6.1 DCFDA added to HDFn cells after infrared irradiation shows no change in signal

When DCFDA is incubated with the well with the cells during the irradiation, not washed off beforehand, there is an increase in signal from DCFDA (Figure 4-15). However, when DCFDA

was incubated with the cells after irradiation, there was no change in the fluorescence signal.

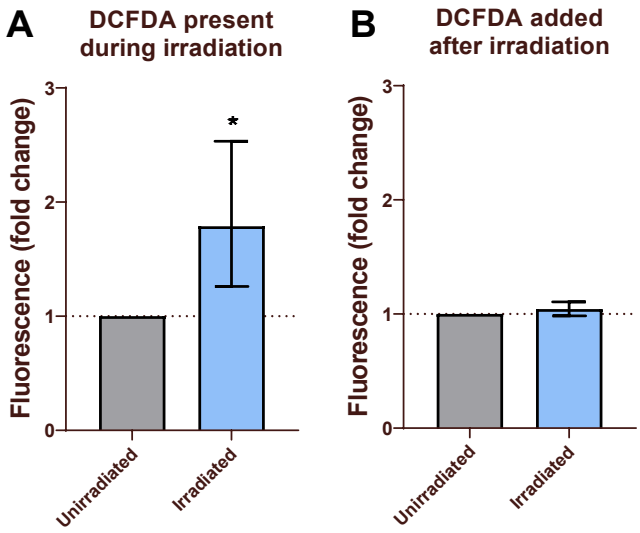

Figure 4-15 DCFDA presence in wells alongside HDFn cells during infrared irradiation
Cells were irradiated with the Hydrosun IR Lamp at 100 mW.cm^{-2} for 60 minutes, 360 J.cm^{-2} dose, equivalent to 2.5 hours of solar IR. Cells in Panel A were incubated with DCFDA in complete, phenol-free DMEM with 10% FCS during the irradiation itself, which was washed off and replaced with fresh medium after irradiation. Cells in Panel B show signal after DCFDA was incubated with cells only after irradiation before washing off and replacing with fresh, complete, phenol-free DMEM with 10% FCS. Unirradiated controls were under the lamp during irradiation but wrapped in foil to receive 0 J.cm^{-2} of light. Temperature was controlled with a stirred water bath. (*): $p \leq 0.05$, one-sample t-test on log2 transformed data; data represent geometric means ± geometric SD, N = 5, n = 3.

4.3.2.6.2 DCFDA incubated then washed off beforehand also gives false positives

When DCFDA probe is incubated with HDFn cells then washed off before infrared irradiation, there is an increase seen in fluorescence in some irradiation conditions (Figure 4-16).

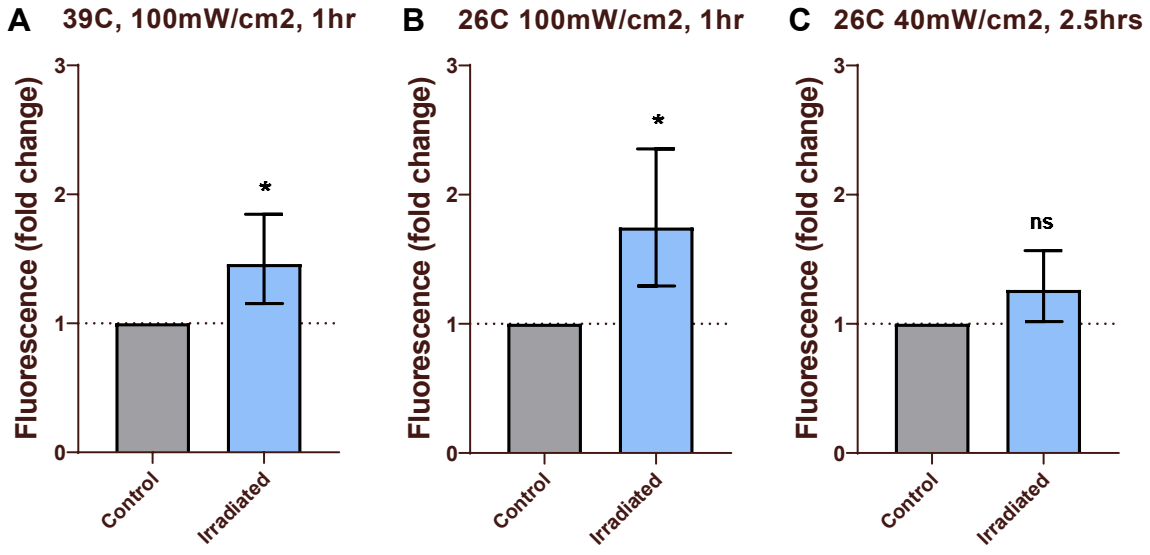

Figure 4-16 Incubation of DCFDA probe and washing off before irradiation.
Cells were incubated with DCFDA for 30 minutes before medium was replaced with complete, phenol-free DMEM with 10% FCS for the irradiation itself, after which luminance was immediately read. Cells were irradiated with the Hydrosun IR Lamp at 100 mW.cm^{-2} for 60 minutes at 39°C (Panel A) or 26° (Panel B), or 40 mW.cm^{-2} for 150 minutes (Panel C). Each received a total dose of 360 J.cm^{-2}, equivalent to 2.5 hours of solar IR. Unirradiated controls were under the lamp during irradiation but wrapped in foil to receive 0 J.cm^{-2} of light. Temperature was controlled with a stirred water bath. (*): p ≤ 0.05, one-sample t-test on log2 transformed data; data represent geometric means ± geometric SD, N = 5, n = 3.

4.3.3 Co-staining MitoSOX and TMRE in flow cytometry

TMRE is an indicator of mitochondrial membrane integrity, while MitoSOX indicates superoxide presence in the mitochondria. Both stains have a degree of spillover into the emissions channels of the other stain. When uncompensated, single-stained TMRE cells had 6% of the fluorescence as single-stained MitoSOX cells with the blue 488 nm laser, however when co-stained the fluorescence was 35% greater than MitoSOX alone (Figure 4-17, panel A). This was not accounted for through compensation (Figure 4-17, panel B). When excited with the 561 nm laser which primarily excites the TMRE fluorophore, the fluorescence from the MitoSOX single-stained cells was 12% of that from the TMRE single-stained cells (Figure 4-17, panel C). However, the cells stained with both MitoSOX and TMRE had a significantly lower fluorescence than those stained with TMRE alone. Again, this was not accounted for through compensation (Figure 4-17, panel D).

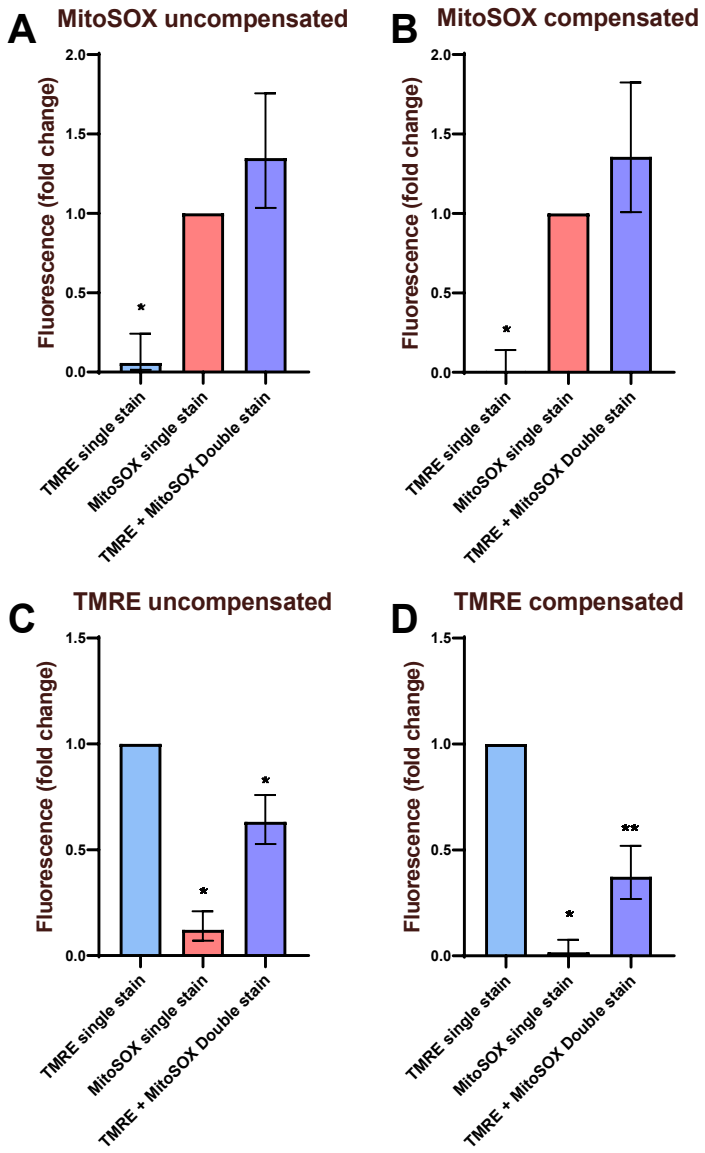

Figure 4-17 Co-staining of MitoSOX and TMRE has unexpected effects on fluorescence.
Untreated cells were stained with TMRE, MitoSOX or both co-stained together. Panel A: 488 nm excitation laser and 610/20 emission filter (MitoSOX emission filter) with MitoSOX and TMRE stained HDFn cells. Double staining increases fluorescence above the sum of single-stained cell fluorescence when uncompensated. Panel B: As panel A but with compensation applied. Panel C: 561 nm laser with 586/15 nm emission filter (TMRE emission filter) with MitoSOX and TMRE stained cells. Panel D: As panel C but with compensation applied. (*): $p \leq 0.05$; (**): $p \leq 0.01$, one-sample t-test on log2 transformed data; data represent geometric means ± geometric SD, N = 3

4.3.4 MitoSOX concentration

To determine whether the same response would be seen with a lower concentration of MitoSOX as the recommended 5 mM concentration, 1 mM MitoSOX was tested (Figure

4-18). The fluorescence in the stained cells was much lower in the 1 mM condition, but more importantly, the positive control cells treated with antimycin A showed a lower degree of increase in the 1 mM concentration than the 5 mM concentration (35% increase versus 79% increase respectively).

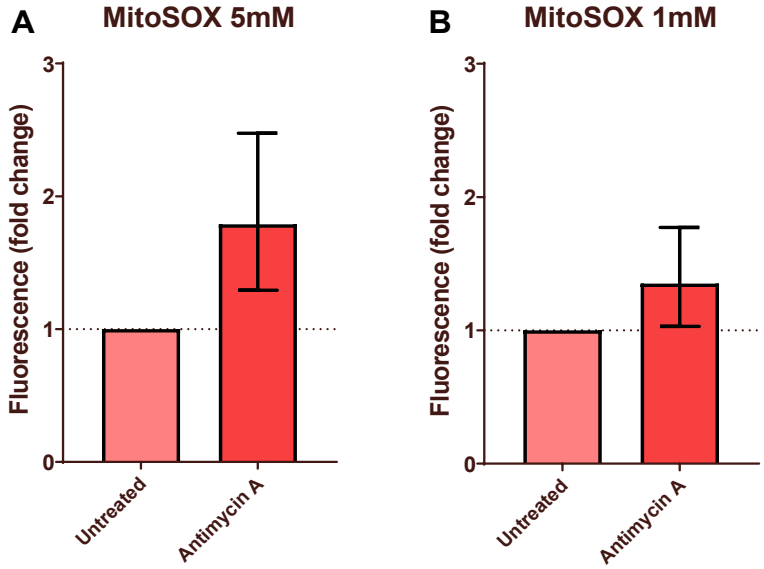

Figure 4-18 Fluorescence of MitoSOX at 5 mM and 1mM in HDFn cells after treatment with antimycin A.
Cells were untreated or treated with antimycin A and stained with 5 mM MitoSOX (Panel A) or 1 mM MitoSOX (Panel B). Data were normalised to untreated control cells. Data represent geometric means ± geometric SD, N = 2

4.3.5 11 kb mtDNA damage assay

4.3.5.1 Original assay

The linear range of the original assay was published in the paper (Hanna et al., 2019) and can be seen in Figure 4-19. The range of concentrations shown to be part of the linear range is highlighted by the dashed box.

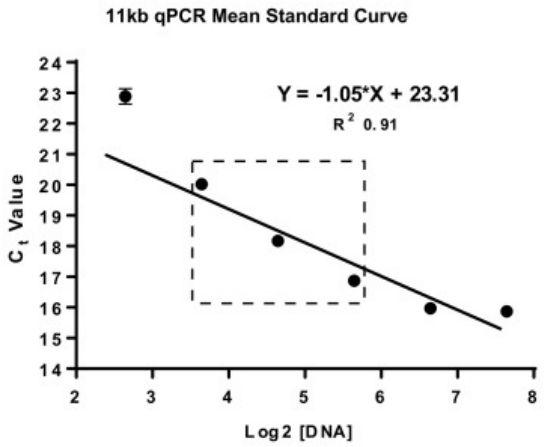

DNA (ng)	Log2 [DNA]
200	7.64
100	6.64
50	5.64
25	4.64
12.5	3.64
6.25	2.64

Download : Download high-res image (191KB) Download : Download full-size image

Fig. 2. Mean standard curve for 11 kb qPCR determined the linear range to lie between 10 and 50 ng, whereby a doubling of DNA concentration corresponded to a 1 C_t difference. Mean + SEM data of primary keratinocyte, primary fibroblast and HDFn cell line DNA (n=9, per data point).

Figure 4-19 Linear range of 11 kb assay as previously published.
Linear range is calculated between 12.5 ng/reaction and 100 ng/reaction.

Below 12.5 ng/reaction the slope is greater than -1, indicating that the reaction is being limited at lower concentrations by the formation of off-target products or primer dimers. Above 100 ng/reaction the slope is less than -1, indicating that the reaction is being inhibited.

4.3.5.2 Optimisation

4.3.5.2.1 Extension temp changing after 10 cycles

The original method of having the first 10 cycles extend at 72°C and the next 25 extend at 68°C was compared to a new method of having the PCR extend at 68°C throughout. The original method was also to set the threshold consistently at 1.25. This was above the point at which the increase in fluorescence and therefore DNA product was exponential, rather when it had become linear. If the StepOne software were to calculate the threshold itself, it would place it in the exponential expansion phase. However, with the change in extension phase temperature at cycle 10, a threshold in the exponential phase of the PCR reaction would be placed where some of the lines would cross in between cycles 10 and 11, leading to a result where the temperature of measurement for some samples was different to that

of others and the fluorescence was therefore different, meaning that comparisons were invalid (Figure 4-20 and Figure 4-21).

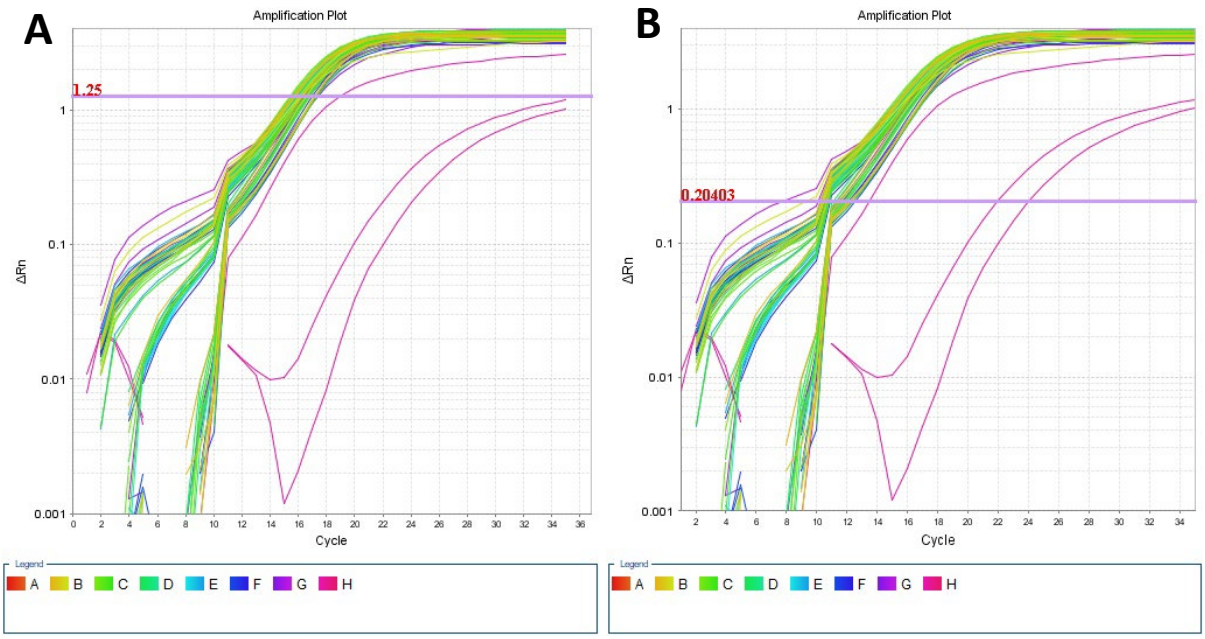

Figure 4-20 A PCR run from the original method.
The automatic assignment of a threshold puts it in the part of the curve which is affected by the change in extension temperature after cycle 10 (B). This was why the threshold was previously changed. However, it was always put at 1.25 (A), where the software would calculate it to be lower, which would sometimes be between cycles 10 and 11 when the temperature at the time the reading was taken increased.

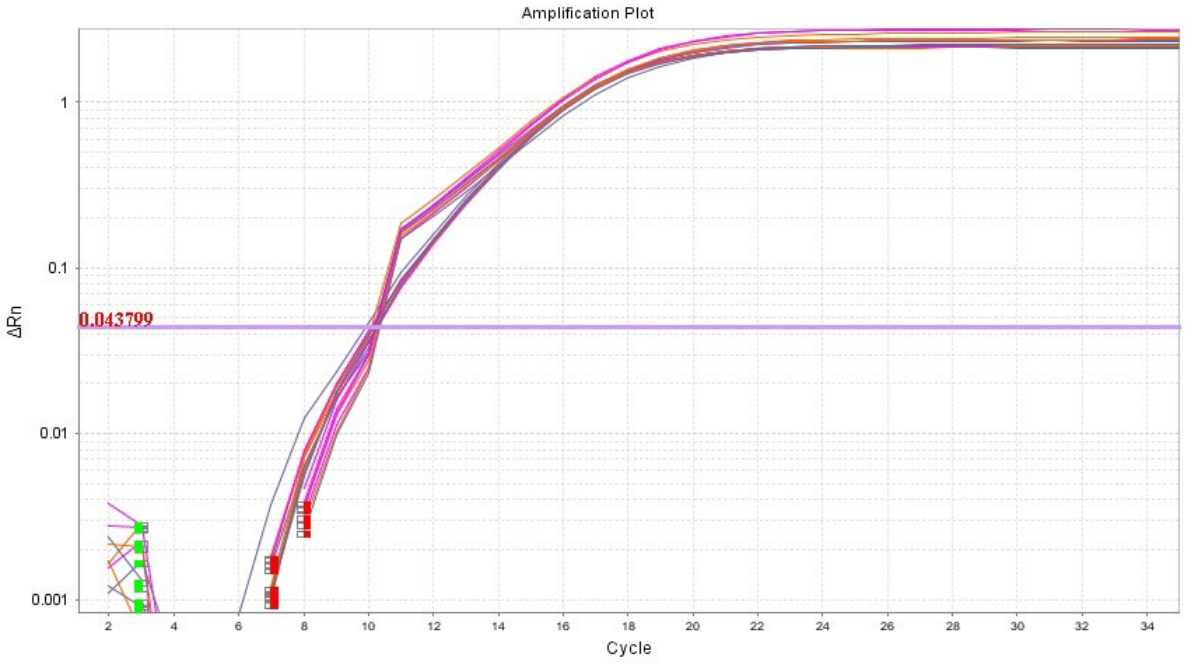

Figure 4-21 Amplification plot of DNA with different amplification temperature settings
Amplified at 68°C for all cycles (smooth line) or 72°C for the first 10 cycles then 68°C for the last 25 cycles (jagged line). Horizontal line shows threshold as calculated by StepOne software.

4.3.5.2.2 Efficiency and non-linear standard curves

4.3.5.2.2.1 Primer dimer in samples run with original protocol in 2018

To check for the presence of primer dimer and other off-target products in previous 11 kb qPCR runs using the original method, DNA from a plate that had been run by Gewei Zhu using the original protocol in 2018 and subsequently stored at -20°C was run on a 0.8% and a 4% gel (Figure 4-22). Products were seen in the 4% gel at the 60 bp mark which are likely to be due to primer dimer, along with other products. These primer dimers were seen in all of the PCR reactions tested, including those which did not amplify any 11 kb product seen on the 0.8% gel.

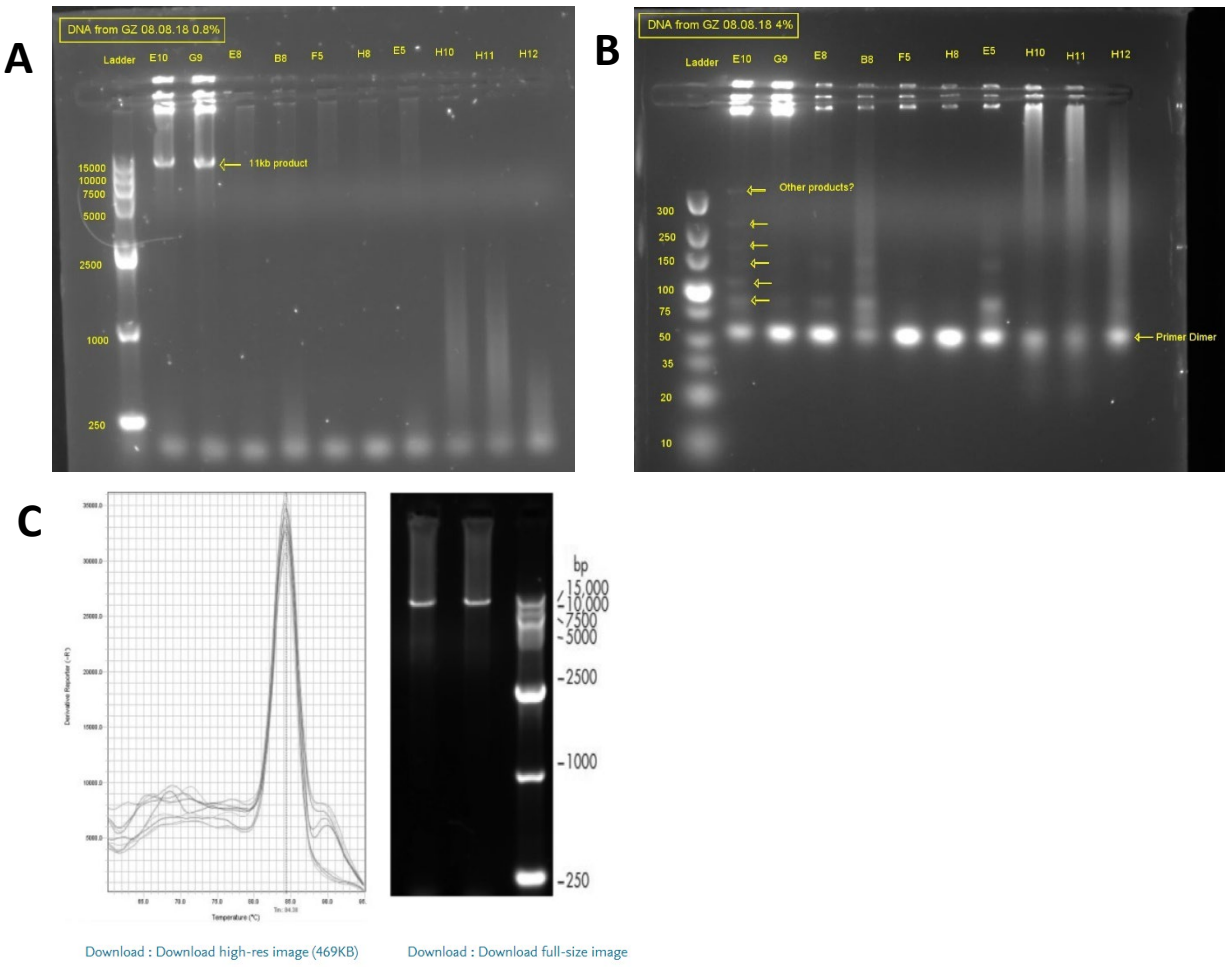

Fig. 3. Melt curve analysis and agarose gel show positive 11 kb amplicons, with no evidence of non-specific binding or primer-dimer.

Figure 4-22 11kb products run on 0.8% and 4% agarose gels

0.8% gel (Panel A) shows 11 kb product presence, 4% gel (Panel B) shows primer dimer presence, Panel C shows melt curve from the original paper.

4.3.5.2.2.2 Optimising annealing temperature

To determine whether altering the annealing temperature of the PCR reaction would reduce primer dimer and/or off-target binding, 60, 62, 64, 66, 68 and 70°C annealing temperatures were tested with DNA concentrations of 10 (Figure 4-23), 4 (Figure 4-24), 1.6 (Figure 4-25), 0.64 (Figure 4-26) and 0 (Figure 4-27) ng per reaction. The original method used a 60°C annealing temperature, though the manufacturer recommends between 45 and 65°C. The lower the annealing temperature, the greater the likelihood of off-target binding and amplification, and the production of primer dimers. The effects of increased annealing temperature can be seen in the melt curve and is particularly evident when the concentration of DNA is reduced. In the no-template control, there is amplification at the

lower temperatures but not the higher annealing temperatures, suggesting that there is primer dimer formation that is favoured by lower temperatures.

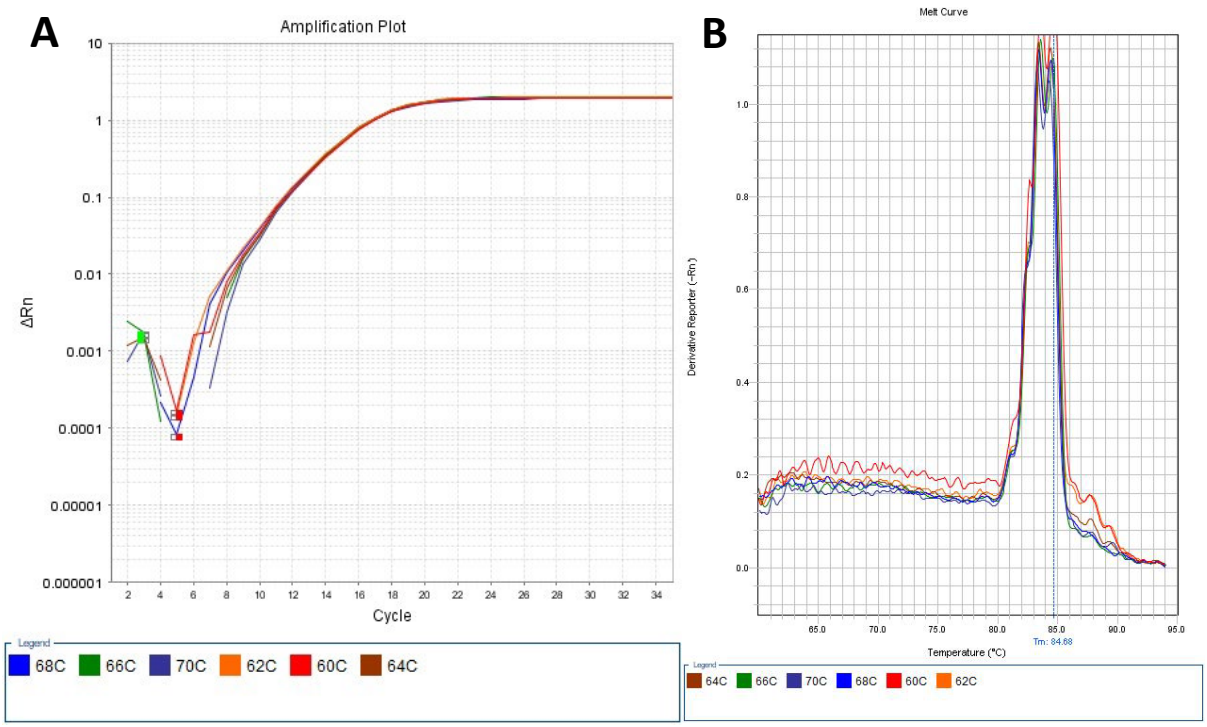

Figure 4-23 Amplification of 10 ng of DNA/reaction at various annealing temperatures.
This shows little evidence of primer dimer in the melt curve (panel B) and a normal shape to the amplification curve (panel A).

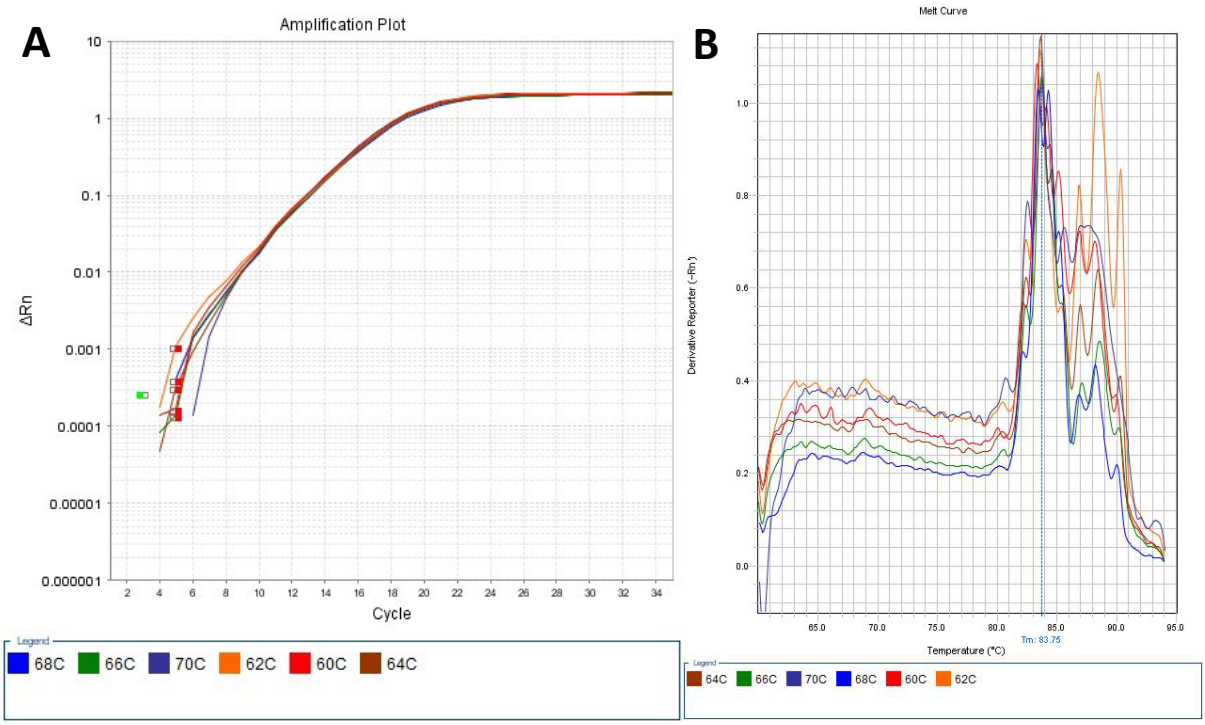

Figure 4-24 Amplification of 4 ng of DNA/reaction at various annealing temperatures.
This shows evidence of primer dimer in the melt curve (panel B) but a normal shape to the amplification curve (panel A). The higher the annealing temperature, the lower the peak of primer dimer (at around 88.5°C) in the melt curve.

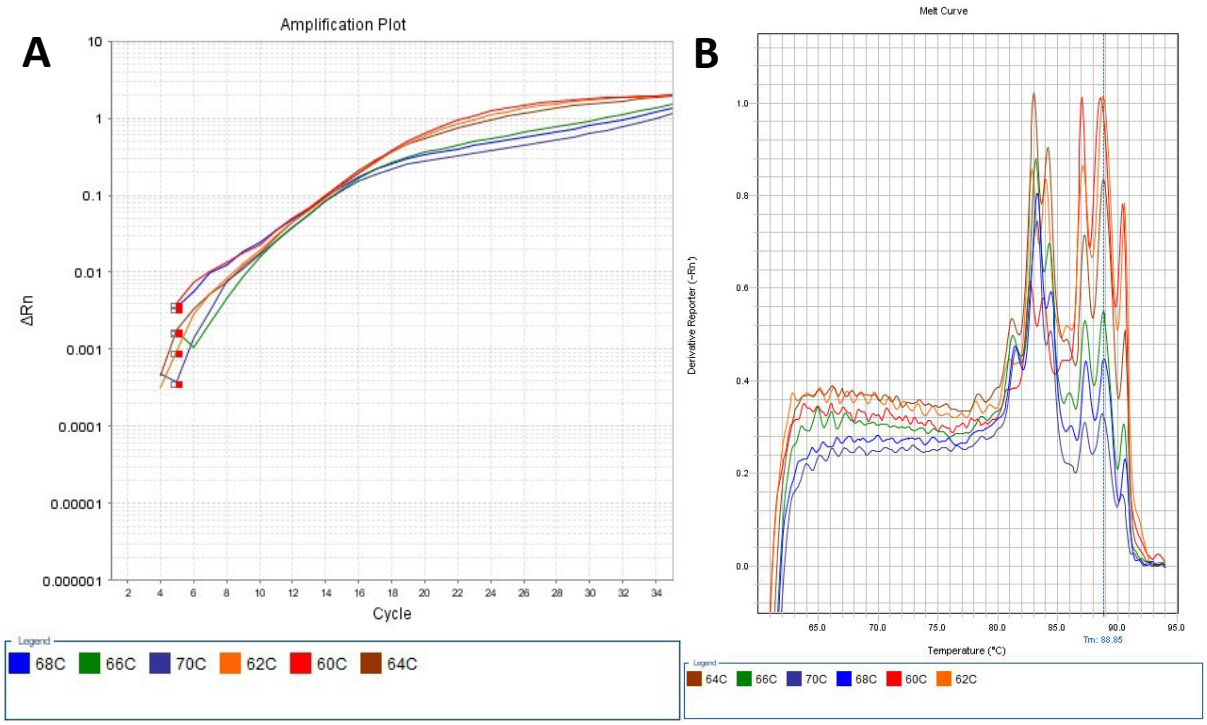

Figure 4-25 Amplification of 1.6 ng of DNA/reaction at various annealing temperatures.
This shows evidence of primer dimer in the melt curve (panel B) and an abnormal shape to the amplification curve (panel A). The higher the annealing temperature, the lower the peak of primer dimer (at around 88.5°C) in the melt curve, but also the more abnormal shape to the amplification curve.

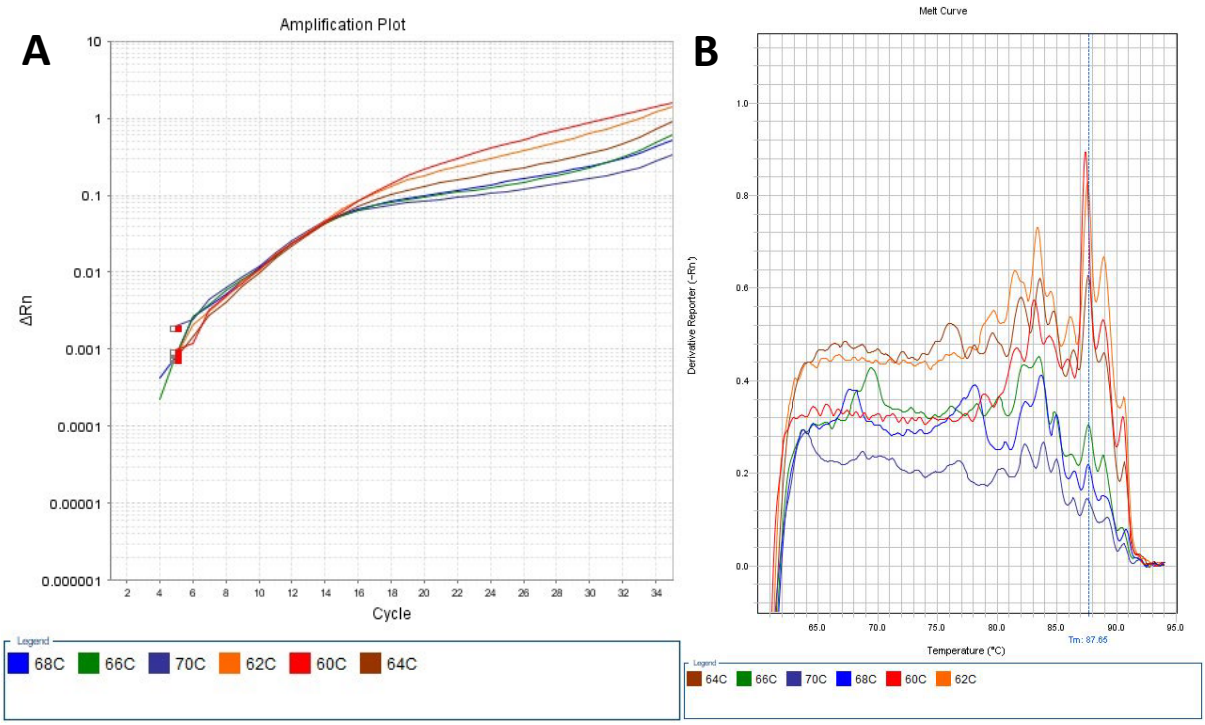

Figure 4-26 Amplification of 0.64 ng of DNA/reaction at various annealing temperatures.
This shows little evidence of 11 kb product and evidence of primer dimer in the melt curve (panel B). There is an abnormal shape to the amplification curve (panel A) at all annealing temperatures. The higher the annealing temperature, the lower the peak of primer dimer (at around 88.5°C) in the melt curve, but also the more abnormal shape to the amplification curve.

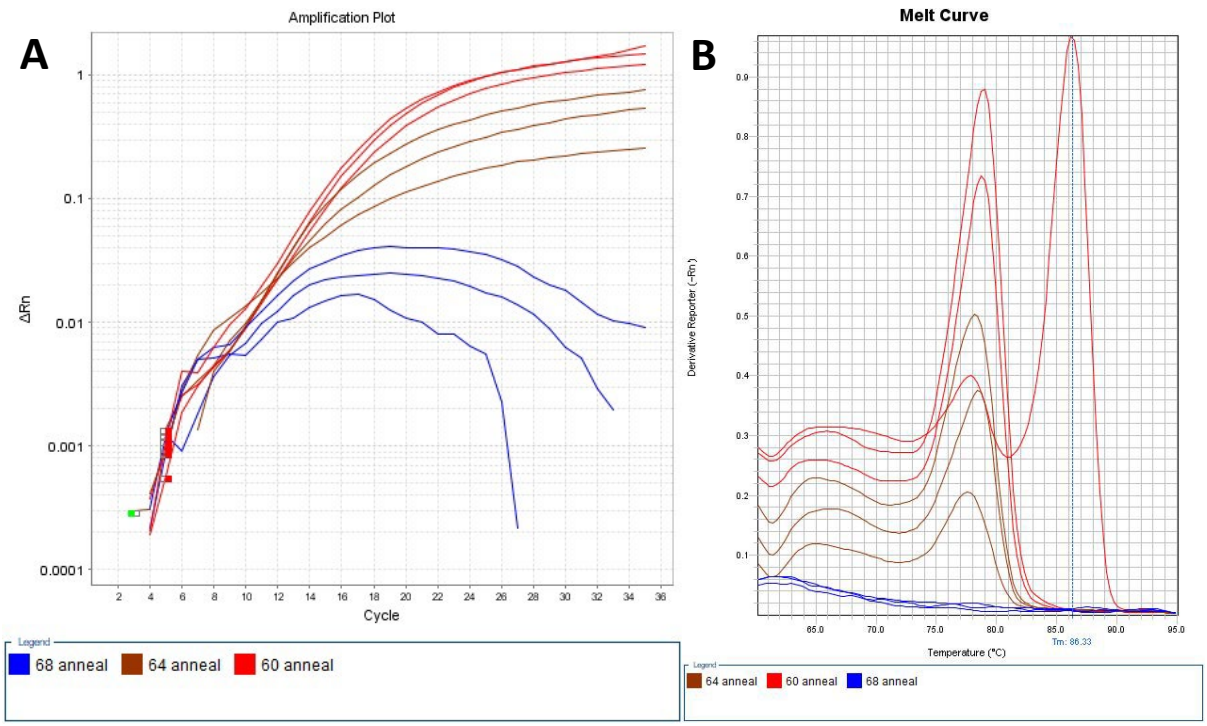

Figure 4-27 Higher anneal reduces amplification in NTC
Panel A shows amplification curve, panel B shows melt curve.

To determine the presence of 11 kb produce and off-target products such as primer dimer, the PCR products were run on 4% and 0.8% gels. 10 ng of DNA was added to the PCR reactions using the original protocol edited by using an extension temperature of 68°C for cycles 1-10 (instead of the original 72°C) and using annealing temperatures indicated in **Error! Reference source not found.**.

Evidence of off-target binding was seen in all conditions containing DNA, with a band appearing at approximately 60 base pairs that is suspected to represent primer dimer. Regardless of extension and annealing temperatures, there are a number of additional bands seen in the channels of each DNA sample. This suggests that the change in extension temperature, as expected, does not affect the products. This also suggests that the increase in annealing temperature does not remove the products of off-target binding.

Table 4-7 PCR products run in lanes of gels in Figure 4-28.

Lane	1	2	3	4	5	6	7	8	9	10	11
Date of PCR		17.12.20	17.12.20	17.12.20	17.12.20	17.12.20	17.12.20	17.12.20	17.12.20	17.12.20	17.12.20
Well	Ultra low range DNA ladder	D2	D3	D10	D11	F1	F4	F9	F12	E2	E3
DNA amount (ng/well)		10	10	10	10	1	1	1	1	NTC	NTC
Annealing temp		60	60	68	68	60	60	68	68	60	60
Extension temp cycles 1-10		72	68	72	68	72	68	72	68	72	68

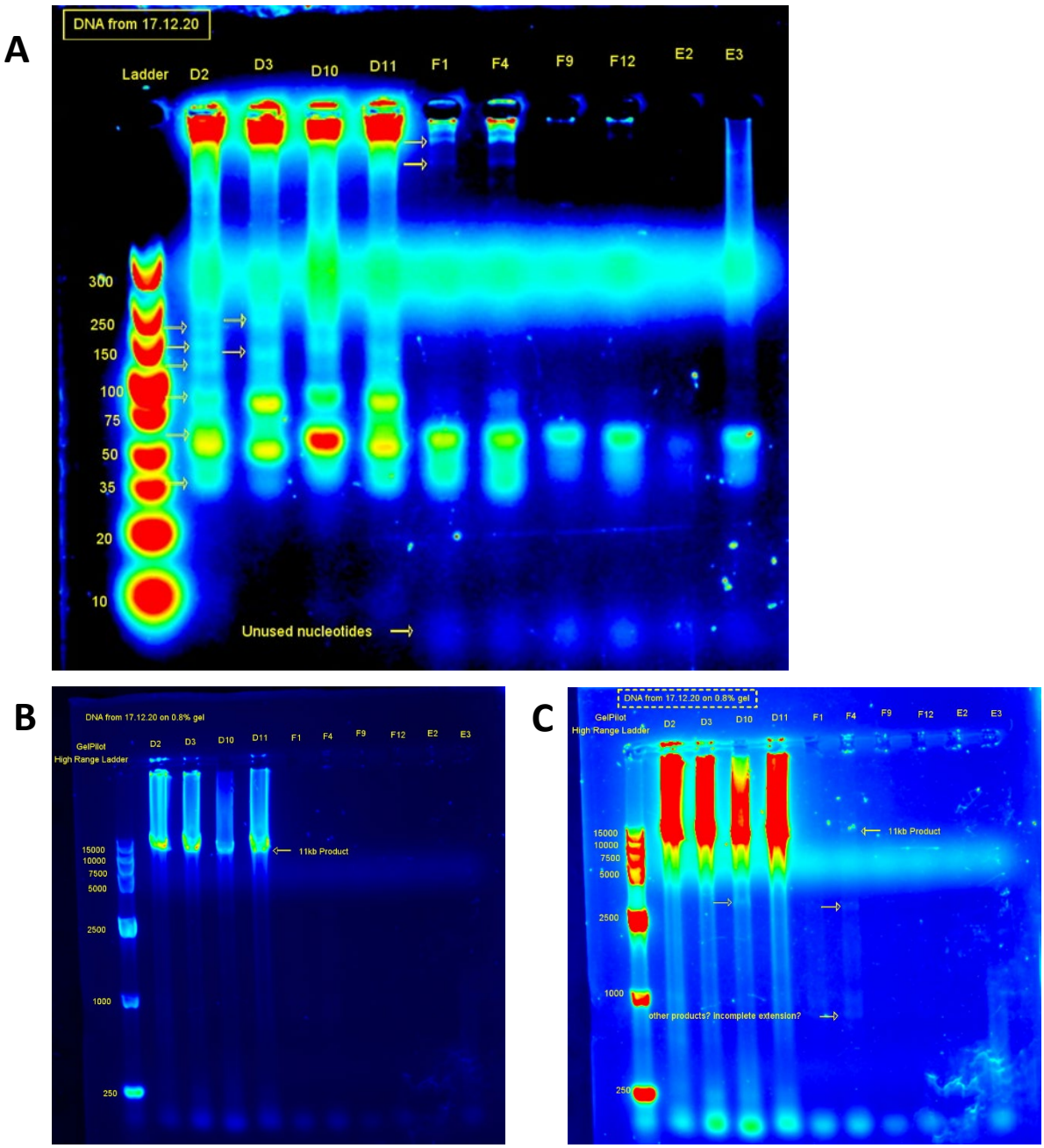

Figure 4-28 4% and 0.8% agarose gel with ladder showing products from 10 ng and no template control

Panel A: 4% agarose gel with ladder showing products from 10 ng or no template control, Panel B and C: 0.8% agarose gel with ladder showing products from 10 ng or no template control. Panel B shows normal exposure, Panel C shows overexposed gel to highlight potential other products.

4.3.5.2.2.3 Isolating mtDNA

In order to determine whether off-target binding could be limited by removing genomic DNA from the samples run on qPCR, mitochondria were isolated before the DNA extraction. Due to the much lower concentration of DNA in the isolated mtDNA sample vs the whole-cell

DNA sample, the concentration had to be calculated using a standard curve of the 83 bp qPCR run. Isolated mtDNA was run on PCR with a 1 in 2 dilution alongside whole DNA extraction.

Using the lines of best fit from the 83 bp run in Figure 4-29 panel A, the concentration of whole-cell DNA that would have been present if extracted alongside the mtDNA was calculated. Panel B shows the cts from the 83 bp run using these calculated concentrations along the x-axis. These concentrations were then used to plot the 11 kb qPCR data which can be seen in Panel C.

It is clear from Panel C that the isolated mtDNA did not demonstrate a linear standard curve of expression, indicating that there is still off-target binding, perhaps primer dimer. The melt curve demonstrating products with different melt temperatures can be seen in Figure 4-30, panel B. It was suspected that the variability in the 11 kb PCR reaction from the mtDNA extraction was due to the low concentrations of DNA extracted, as mitochondria are lost in the process of separation from other organelles. Given that this experiment required a large number of cells to test, it was not deemed important to continue pursuing this as a route of optimisation.

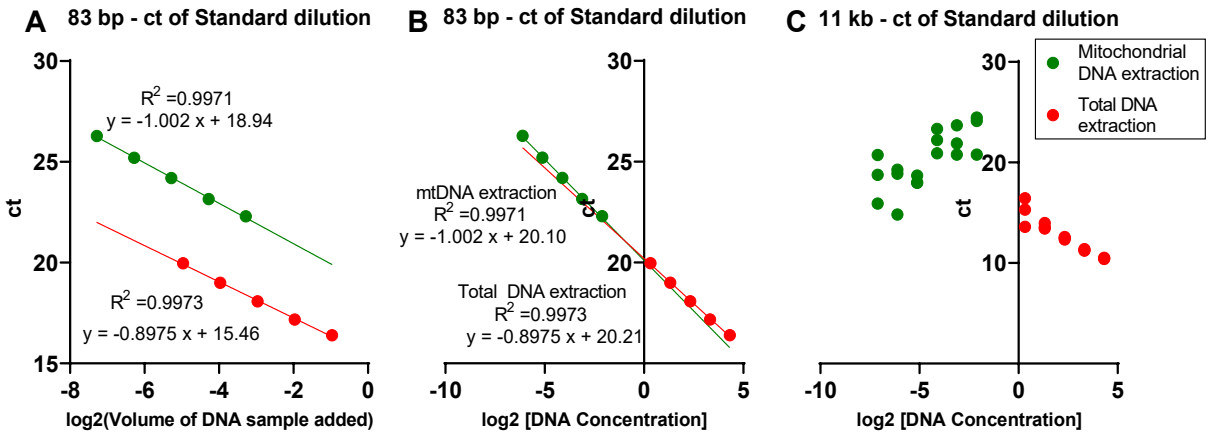

Figure 4-29 83 bp qPCR and 11 kb of same samples
A: 83 qPCR on graph of ct versus log2(volume of sample added), used to calculate concentration by aligning lines of best fit; B: the same 83 bp data as left but with calculated log2[DNA concentration] on x-axis; C: 11 kb of same samples using calculated mtDNA extraction DNA concentration.

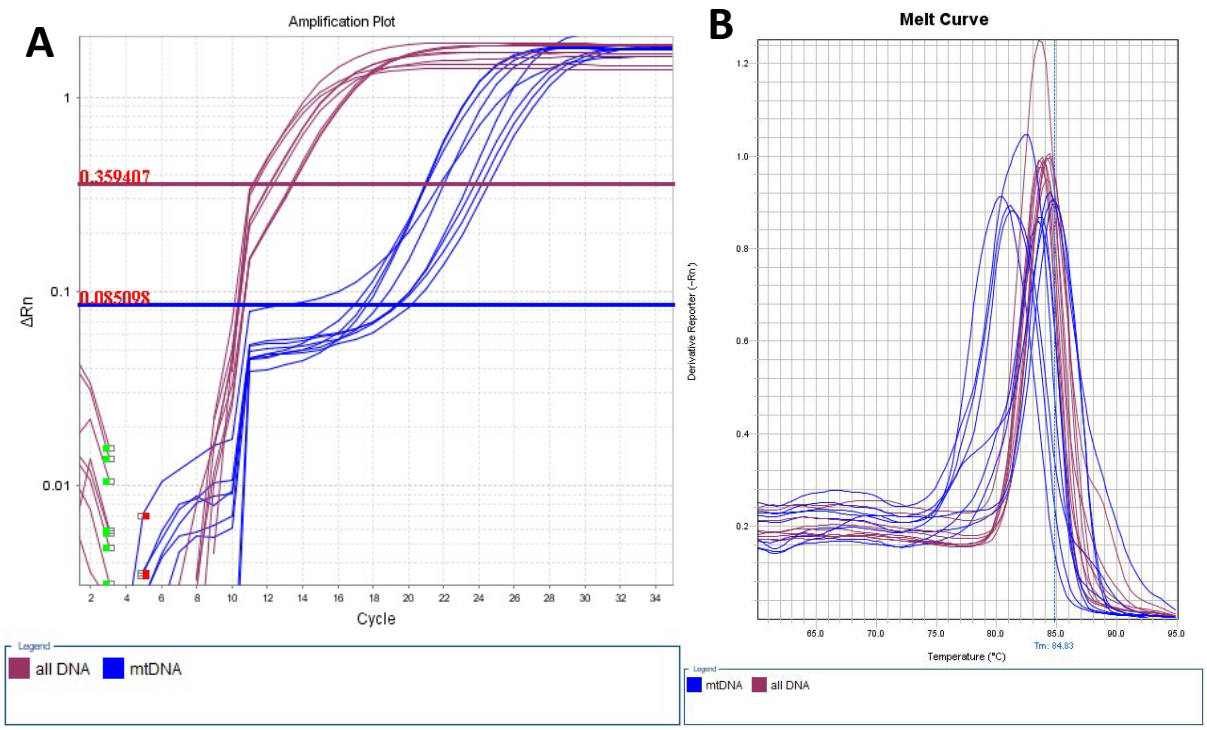

Figure 4-30 Amplification plot and melt curve of 11 bp PCR
A shows amplification plot and B shows melt curve of same 11 bp PCR run as in Figure 4-29.

4.3.5.2.2.4 Optimising buffer in PCR reaction

It was found that using buffers 1 or 3 resulted in only off-target products being formed. This can be seen from the melt curve in Figure 4-31, where only buffers 2 and 2B had a product at 84°C. At other DNA concentrations tested there was also no 84°C product (data not shown).

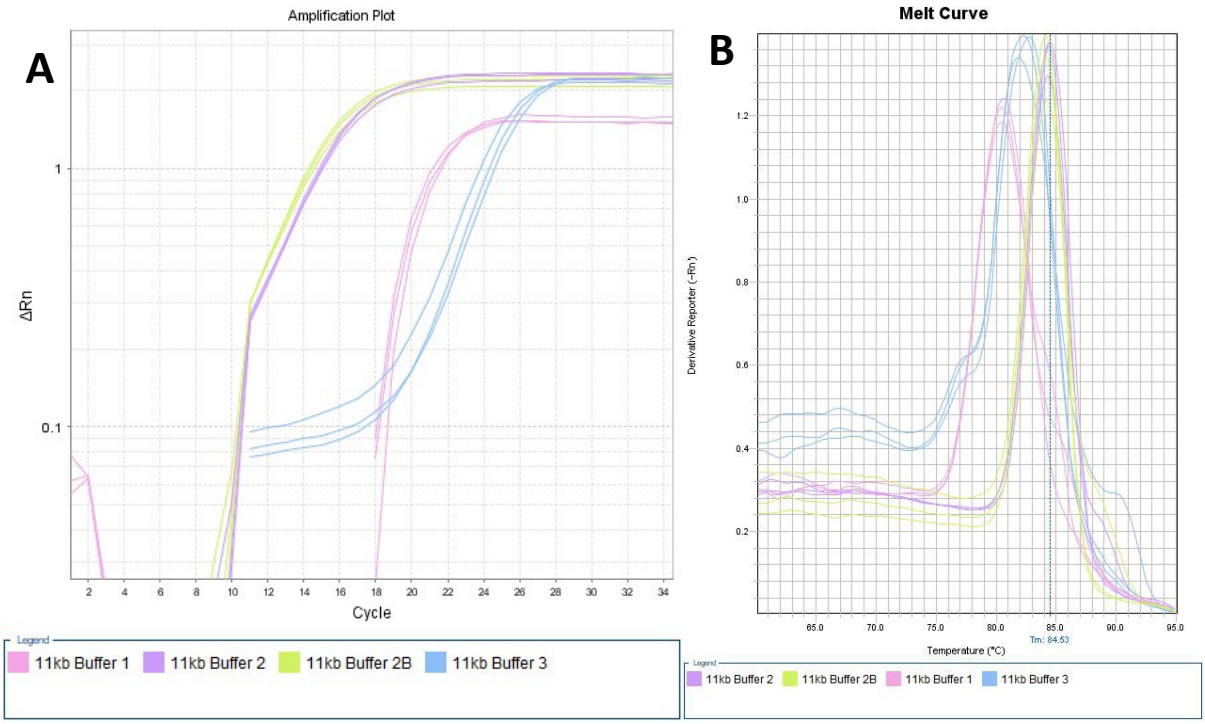

Figure 4-31 Testing different buffers in the 11 kb reaction with 25 ng/reaction of DNA
Buffers 2 and 2B give the best amplification with the 11 kb reaction with lowest ct and standard deviation between replicates.

4.3.5.2.2.5 Linear range of optimised PCR reaction

A final standard curve was carried out to compare the new annealing temperatures and reagents with the linear range from the original assay. A line was plotted between the points at 10 and 50 ng/reaction, from which a slope and efficiency were calculated and compared to those calculated from the original assay with a line in red (Figure 4-32).

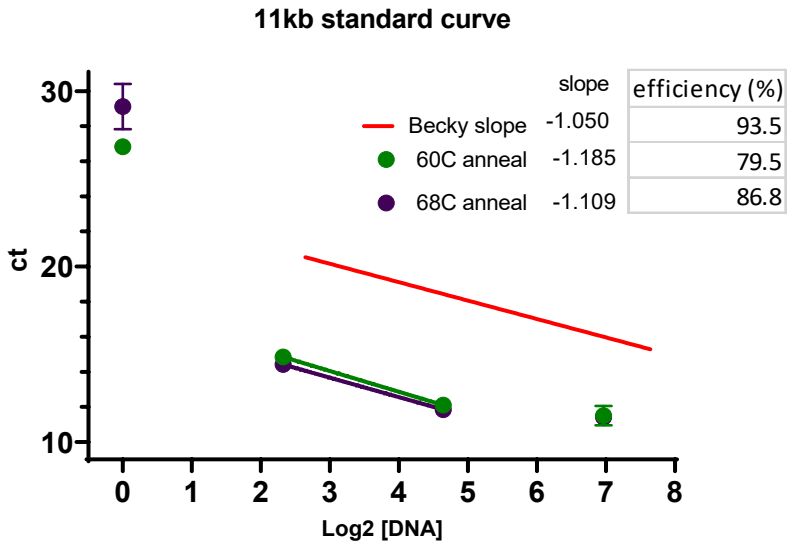

Figure 4-32 Standard curve of original and altered assay.
Slope from original assay paper (red) and altered assay with 68°C extension throughout, at 2 different annealing temperatures. Changing the annealing temperature did not improve the assay.

4.3.6 ATP measurement assay

4.3.6.1 Neither solar simulated complete light nor infrared influence ATP levels

When HDFn cells were irradiated with high intensity (360 mW.cm^{-2}) infrared light and incubated with CellTiter-Glo either immediately or 24 hours after irradiation, there was no change in ATP measured for any of the doses of light delivered (Figure 4-33, one-sample 2 tailed student's t-test).

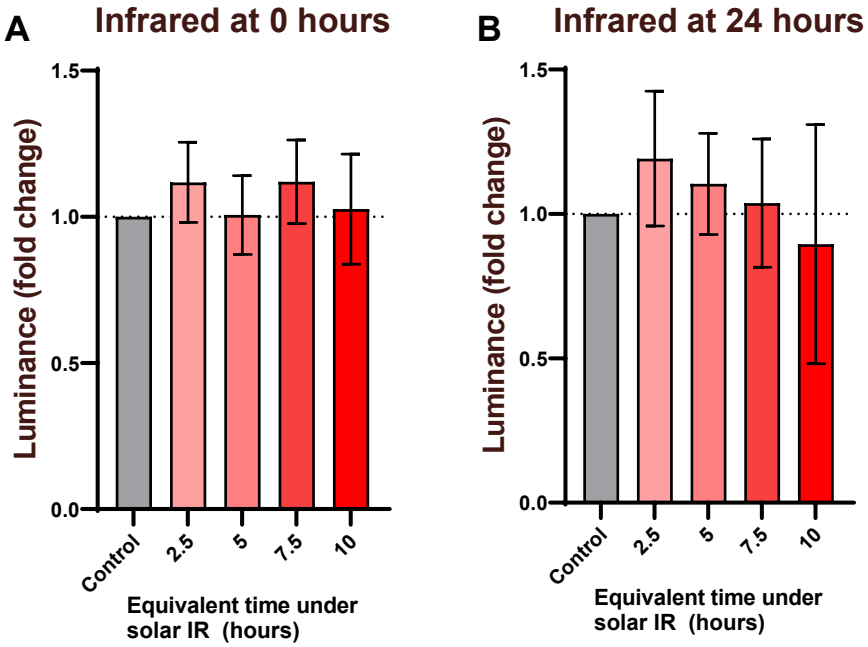

Figure 4-33 Change in ATP production by HDFn cells 0 or 24 hours after irradiation with high intensity infrared

Cells were seeded in complete, phenol-containing DMEM with 10% FCS, and irradiated in phenol-free DMEM with 10% FCS, in which it remained after irradiation. Cells were irradiated with 360 mW.cm^{-2} for 16.7, 33.3. 50 ot 66.7 minutes for doses of 360, 720, 1080 and 1440 J.cm^{-2} equivalent to 2.5, 5, 7.5 or 10 hours of solar infrared respectively. Unirradiated controls were under the lamp during irradiation but wrapped in foil to receive 0 J.cm^{-2} of light. Temperature was controlled with a stirred water bath. CTG signal 0 (A) or 24 (B) hours after irradiation with high intensity IR. Data represent means ± SD, N = 3, n = 3

When HDFn cells were irradiated with 2.16 SEDs of complete solar simulated light and incubated with CellTiter-Glo either immediately or 24 hours after irradiation, there was again no change in ATP measured (Figure 4-34, one-sample 2 tailed student's t-test).

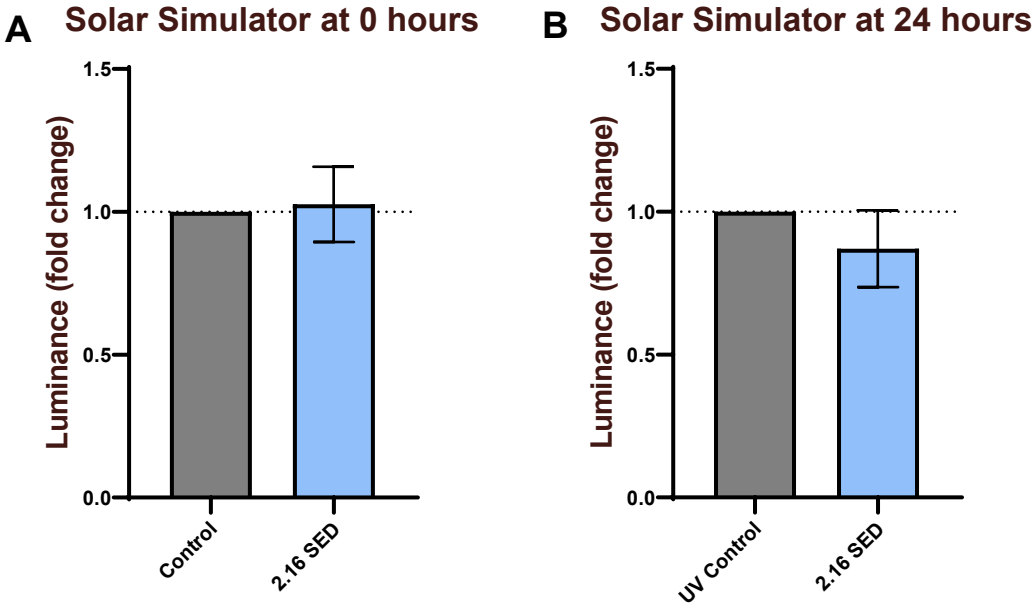

Figure 4-34 Change in ATP production 0 or 24 hours after irradiation with complete solar simulated light

Cells were seeded in complete, phenol-free DMEM with 10% FCS, which was replaced with PBS for irradiation with 2.16 SEDs of complete, solar simulated light delivered over ~2 minutes. Cells in Panel A were incubated with CellTiter Glo immediately after irradiation. Cells in Panel B show signal after a further 24 hours in complete, phenol-free DMEM with 10% FCS. Unirradiated controls were under the lamp during irradiation but wrapped in foil to receive SEDs of light. Temperature was controlled with a stand. Data represent means ± SD, N = 3, n = 3

4.3.6.2 No clear change at any timepoint up to 40 minutes after irradiation

A time course was carried out of time from the end of the irradiation to the moment the CellTiter-Glo was added to the well every 5 minutes up to 40 minutes from the end of the irradiation for both 2.16 SEDs of complete solar simulated light and 10 hours (360 $mJ.cm^{-2}$) of high intensity infrared light (Figure 4-35). For infrared light the earliest time point that could be reasonably managed was 15 minutes. At no point was the luminescence from the irradiated cells significantly different from that if unirradiated control cells (one-sample 2 tailed student's t-test).

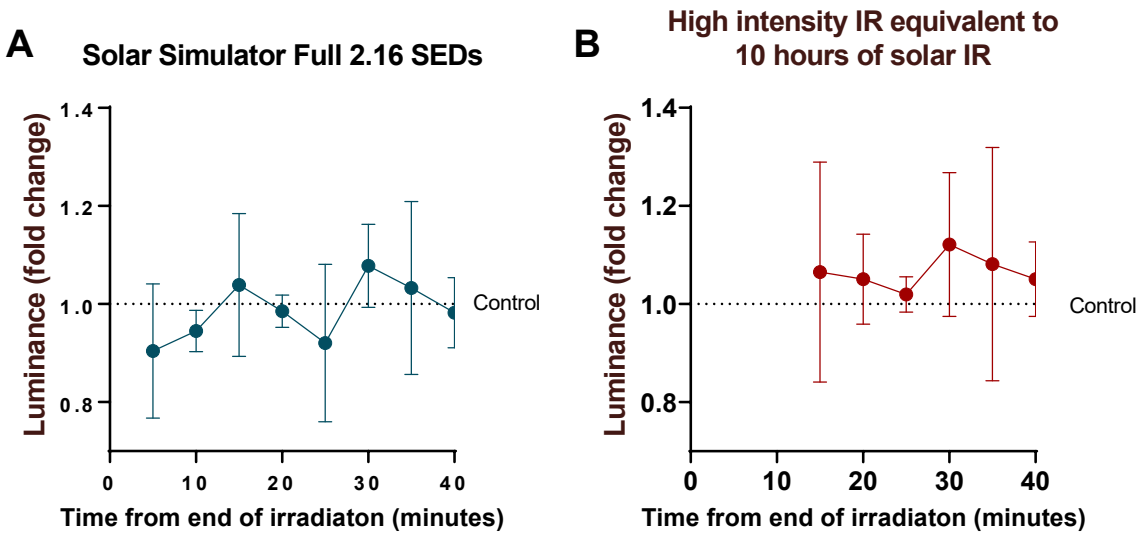

Figure 4-35 Luminescence in HDFn cells time course after the end of irradiation
Cells in panel A were seeded in complete, phenol-free DMEM with 10% FCS, which was replaced with PBS for irradiation with 2.16 SEDs of complete, solar simulated light delivered over ~2 minutes. Cells were returned to fresh medium after irradiation. Temperature was controlled with a stand. Cells in panel B were seeded in complete, phenol-free DMEM with 10% FCS and remained in this for irradiation with 1440 J.cm^{-2} infrared delivered with the Hydrosun lamp over 66.7 minutes at an irradiance of 360 mW.cm^{-2}. Termperature was controlled with a stirred water bath. Unirradiated controls were under the lamp during irradiation but wrapped in foil to receive 0 SEDs/0 J.cm^{-2} of light. Luminescence as fold change of unirradiated control when CellTitre-Glo was added up to 40 minutes after the end of irradiation. Data represent means ± SD, N = 3, n = 3

4.3.7 Transmission testing of formulations

Formulations were spread on Transpore tape and tested under the solar simulator using the FLAME spectroradiometer. Irradiance at the UVB end of the spectrum was too low to accurately calculate transmission, but for all visible wavelengths, transmission could be calculated. In this experiment, ingredients were being tested in their ability to protect from blue light particularly. To examine this, a mean of the % transmittance of all light between 400 and 420 nm was taken, and it was demonstrated that up to 50% of blue light between these wavelengths could be blocked by these formulations.

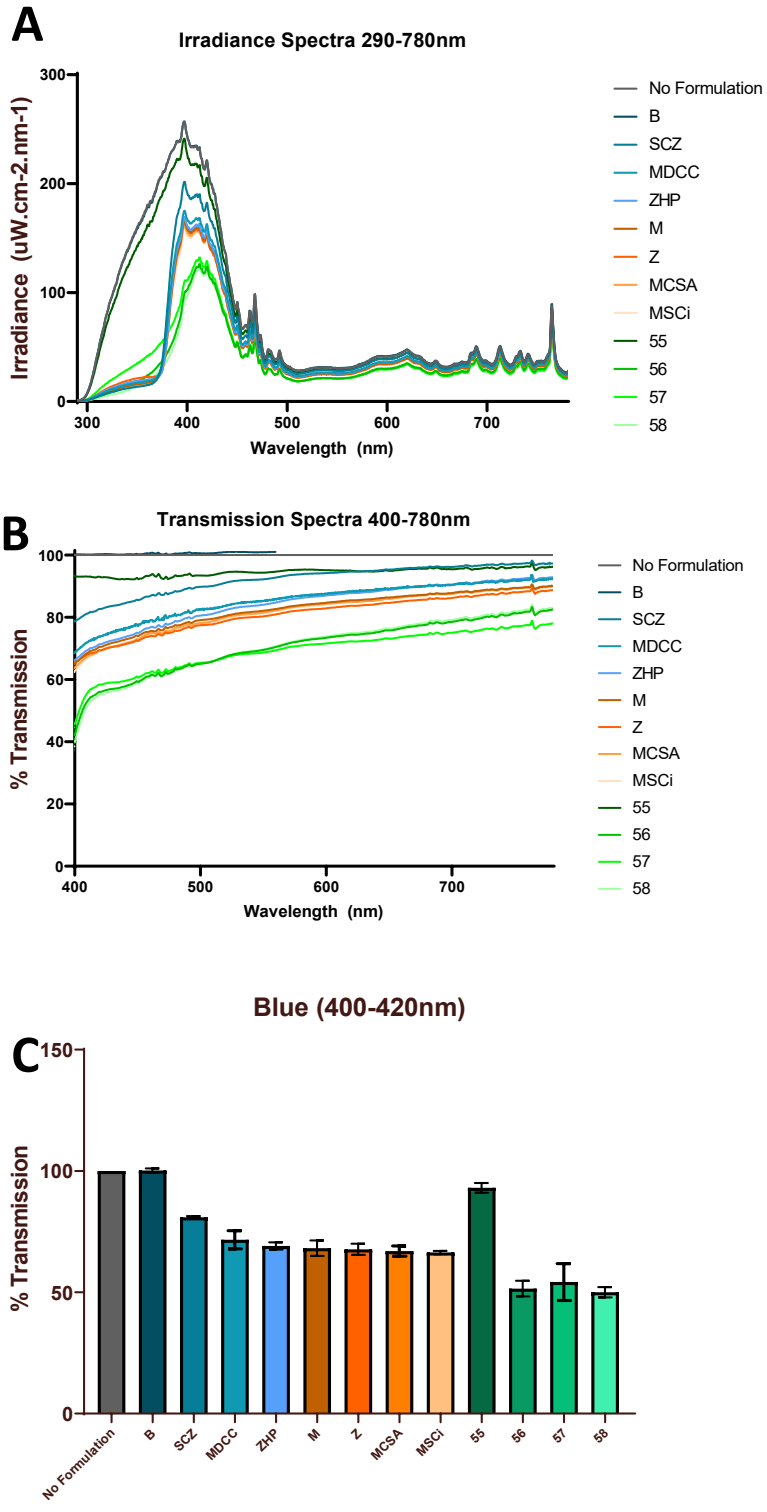

Figure 4-36 Transmission spectrum of UV and visible light through different formulations
Transmission was tested with the FLAME spectroradiometer and Newport solar simulator. Panel A shows irradiance spectrum of UV and visible light through different formulations, B shows % transmission of visible light wavelengths through the same formulations, C shows the % transmittance of wavelengths between 400 and 420 nm through each of the formulations.

4.4 Discussion

4.4.1 Housekeeping gene expression and light irradiation

When looking for the effects of solar simulated light on gene expression in HDFn cells, it was found the β-actin gene was changed 24 hours after irradiation with 2.16 SEDs of solar simulated light. This was found by comparing the ct of the irradiated and control cells, after putting the same amount of cDNA in having measured the RNA using a NanoDrop and calculating fold change by $2^{-\Delta ct}$. This indicates that β-actin is not an appropriate housekeeping gene to use with irradiation of solar simulated light.

GAPDH was tested as an alternative, and it was found to be unchanged by 2.16 SEDs of complete solar simulated light, although changed by 4.32 SEDs. 4.32 SEDs is above the doses used to test for damage, as this causes greater cell death, but it was included to determine if 2.16 SEDs would be the upper limit for UV dosing experiments looking at gene expression with qPCR. It was decided that GAPDH would be used as a housekeeping gene for all experiments as they would not exceed 2.16 SEDs, and not to use greater doses as these would affect the GAPDH housekeeping gene, possibly due to the induction of cell death.

4.4.2 ROS measurement in cell culture plastics

4.4.2.1 ROS-Glo assay

The Promega ROS-Glo assay is a luminescent assay designed to measure the level of hydrogen peroxide (H_2O_2) in cell culture. A substrate is added to the well of a 96-well plate containing cells which reacts with H_2O_2 to produce a luciferin precursor, after which the addition of a detection solution produces a light signal which is proportional to the H_2O_2 level in the well. It was found however that when used in a standard, polystyrene, 96-well plate that had been irradiated with complete solar simulated light, there was an increase in signal in exposed wells compared to foil-covered control wells within the same plate, in the absence of cells. There was a 3.4-fold increase in ROS-Glo signal from the irradiated wells compared to the unirradiated control wells. Furthermore, when comparing the foil-covered, unirradiated control wells of a plate where the irradiated side received 8.64 SEDs to the control wells of a plate where the irradiated side received 2.16 SEDs, there was an increase in signal of 2.9-fold. These results indicate that not only is ROS-Glo reacting with the plate as

a result of it having been irradiated, but also that there is an effect that can be measured on the side of the plate that has received no irradiation. Given that polystyrene absorbs UV light (see Chapter 2, Irradiation through a plate lid), it is possible that due to the poly-aromatic structure of polystyrene, that light is promoting electrons in the plastic that are then reactive with the ROS-Glo assay substrate.

The presence of cells was found to decrease the signal from ROS-Glo in both irradiated and unirradiated wells by 43% and 54% respectively. This indicates that the signal from the presence of cells cannot even be separated from that of the plastic, as there is an interaction there that the addition of the two signals cannot explain. It may be that the ROS-Glo was interacting with the plastic surface, and when the exposed surface area was covered by adherent cells the signal was reduced.

Furthermore, pre-treatment of cell culture plates with 8.64 SEDs of complete solar simulated light immediately before seeding with cells (or leaving without cells in the acellular condition) was found to increase the signal from ROS-Glo. This means that exposure to light even the day prior to ROS-Glo assay use affects the results of the assay.

The effect of irradiating a plate before adding ROS-Glo on the resulting signal in acellular experiments should not be understated. That adding cells to a plate actually reduces the signal from ROS-Glo after irradiation highlights that most of the signal from these experiments is not coming from H_2O_2 produced by the cells as a result of irradiation, but rather from the effect the light has had on the tissue culture plastics. While this effect was seen with ultraviolet light, it is not known whether visible or infrared lights would have any similar effect, though it would be likely to be to a much lower degree given the higher energy and higher absorbance of UVB wavelengths by polystyrene. It would be useful to know whether standard laboratory lighting or cell culture hood lights would have any effect on the tissue culture plastic that would then react with ROS-Glo, as this would further limit its usefulness. It may be that there is a different effect of irradiation on plastics such as polypropylene or materials such as glass which are also used in cell culture, or whether the radical reaction properties materials exhibit are affected by coatings used for improved cell

adherence. The use of the ROS-Glo assay should be approached with caution, especially in experiments involving UV light.

4.4.2.2 DCFDA in cell culture plastics

A concern was that DCFDA may react to acellular irradiation experiments in a similar way to ROS-Glo. To test this, acellular experiments where DCFDA was added to irradiated and unirradiated wells of 96-well tissue culture plates after exposure to complete solar light from 290-3000 nm, incubated with DCFDA for 30 minutes as per the usual protocol, then not washed off before reading to ensure sensitivity to any reactions. There was no change in signal in wells that had been irradiated compared to controls that had been kept in the dark. There was also no difference in wells that had been pre-treated the day before and those irradiated with a higher dose of 8.64 SEDs before the addition of DCFDA. This enables the conclusion that there are no DCFDA interactions with previously irradiated tissue culture plastics, and it can be used to test for cellular ROS when added after irradiation without concern for acellular reactions.

To ensure that DCFDA was sensitive to the production of ROS, known to be produced by cells as a result of UV irradiation, DCFDA was incubated with cells after irradiation with 2.16 or 8.64 SEDs of complete solar simulated light (including UV) and washed off before reading, as per the protocol in Chapter 2. There was a 190% increase in fluorescence with irradiation of 2.16 SEDs, indicating that the assay was sensitive to the presence of light-induced ROS production. An increase of 300% was found in cells irradiated with 8.64 SEDs, showing that, as expected, the size of the increase in ROS is dose-dependent.

4.4.2.3 Washing of cells incubated with DCFDA

After incubating with DCFDA for 30 minutes in a humidified incubator at 30 °C and 5% CO_2 and subsequent thorough washing, it was observed under the microscope that cells appeared to be less well adhered and fewer in number. An experiment comparing a gentle wash to a thorough wash showed that thorough washing reduced the signal from DCFDA by 80%. Given the reduced number of cells viewed under the microscope, it was thought this was due to the washing off during aspiration. To minimise this, gentle washing was used going forward.

4.4.2.4 Prior irradiation of cell culture plastic affects DCFDA signal from unirradiated cells

To determine whether the pre-treatment of cell culture plates with UV affected the cells when they were subsequently seeded onto them, plates treated with 8.64 SEDs of complete solar simulated light were seeded with cells alongside plates without this treatment. After adhering overnight, half of each plate was irradiated with 2.16 SEDs of complete solar light, and the other half was left unirradiated by covering with foil. The DCFDA signal from unirradiated cells that were seeded in a plate that had been irradiated was 38% lower than the DCFDA signal from those in a non-pre-treated plate. When cells in pre-treated and non-pre-treated plates were exposed to 2.16 SEDs of complete solar simulated light, both had increased DCFDA signal compared to the relevant control. The absolute signal from irradiated cells in pre-treated plates was less than that from the non-pre-treated plates, but when each irradiated condition was compared to its respective control, the calculated increase was not significantly different between the two conditions.

To determine if this was due to a proliferation effect, resulting in fewer cells adhering and being present when the DCFDA assay was performed, an MTS assay was carried out on cells seeded in plates pre-treated with 0 SEDs (no pre-treatment), 2.16 SEDs or 8.64 SEDs. The viability was assayed at the time the irradiation and subsequent DCFDA assay would have taken place and also 24 hours after this. At both time points, there was no significant difference in viability in either of the pre-treated conditions compared to the no-pre-treatment condition, suggesting that cell number was not the reason for a difference in DCFDA signal between pre-treated and non-pre-treated plates. Furthermore, cells that were irradiated with either 2.16 or 8.64 SEDs of complete solar simulated light in 2.16 or 8.64 SED pre-treated plates had the same viability immediately and 24 hours post-irradiation compared to cells irradiated in non-pre-treated plates, so the reduction in viability of cells exposed to UV light was not affected by pre-treatment of the plate. This indicates that the effect of pre-treatment of plates before seeding on cells (as demonstrated with DCFDA) is not to do with initial adherence or proliferation.

We know that irradiation affects the plastic of tissue culture plates when no cells are in them from the results with ROS-Glo that show an increased signal in plates that have been

exposed to light without cells present. It could be that previous irradiation of tissue culture plastic affects the behaviour of cells in some way other than proliferation or adherence. The rest of the work in this thesis does not involve the pre-treatment of tissue culture plastics, but it is important to note that the irradiation of the plastics when the cells are adhered may have an unexpected effect on the cells, that would be difficult to separate from the effect of the light on the cells directly. This is an additional limitation of experiments with monolayer cells, and another reason that the data cannot be expected to fully represent what would happen to cells in vivo.

4.4.2.5 Presence of DCFDA during irradiation

Though it is known that DCFDA is sensitive to activation by UV light and will give a false positive signal after irradiation with such without any reaction with ROS (Boulton et al., 2011), it was not known whether the same would be true for irradiation with infrared light from the Hydrosun lamp. Irradiations with this lamp take up to 2.5 hours in this set of experiments, compared to the roughly 2 minutes to irradiate with the 2.16 SEDs of complete solar simulated light. Thus, it was thought that if the DCFDA was present for the duration of the irradiation it would be more sensitive to the ROS produced, as during the 2.5-hour irradiation, transient ROS would be eliminated by cellular antioxidant mechanisms.

Once DCFDA is incubated with the cells it is washed off. Given that the concentration of DCFDA in the cells was unknown, and how much of the DCFDA that had entered the cells would be released into the irradiation medium, a range of concentrations of DCFDA from 0.05 to 1 uM was tested in medium in acellular conditions under the Hydrosun lamp. 3 irradiation conditions were tested which delivered the same total dose of 360 $mJ.cm^{-2}$ of infrared light. These were: 40 $mW.cm^{-2}$ for 2.5 hours at 26°C, 100 $mW.cm^{-2}$ for 1 hour at 26°C and 100 $mW.cm^{-2}$ for 1 hours at 39°C. For each condition, a control was included which was covered in foil during the irradiation. It was found that it was possible for the irradiated condition to reach a 300% higher fluorescent signal compared to the control (100 mW/cm^{-2}, 26°C for 1 hour, 1 uM DCFDA). From this it was determined that if the DCFDA was present in the medium or cells during irradiation, the results may not be due to irradiation but rather activation of the DCFDA by the infrared light. Additionally, it was found that incubation at a

higher temperature (39°C rather than 26°) increased the DCFDA signal in control wells and that a longer duration of incubation of the controls at 26°C (2.5 hours rather than 1 hour) increased the DCFDA signal in the unirradiated controls. These differences demonstrate that it would be difficult to compare between conditions even if the DCFDA was not activated by light, further rendering its presence during irradiation an unsuitable method for ROS measurement.

4.4.2.6 DCFDA added after irradiation shows no signal

When the DCFDA probe was incubated with the cells after infrared irradiation as per the protocol in Chapter 2, there was no increase in signal. This could be due to no ROS being produced, or it could be that the cell had an increased ROS over the duration of the irradiation, but this did not overwhelm the cells' antioxidant capabilities, or that the increase in ROS was transient and only present during the irradiation itself.

As predicted by the acellular results, when the DCFDA probe was incubated with the cells prior to irradiation, there was an increase in signal. It is not possible however to determine whether this was because of ROS or because of the activation of the probe by the light.

4.4.3 Co-staining TMRE and MitoSOX

MitoSOX Red is a dye which is targeted to mitochondria. It is rapidly oxidised by superoxide but not other forms of reactive oxygen species or reactive nitrogen species, and when oxidised it becomes fluorescent. Given that superoxide is produced by mitochondria under normal circumstances but can increase under oxidative stress, it was tested as an indicator of stress as a result of irradiation. TMRE is a stain which accumulates in mitochondria to indicate mitochondrial membrane potential. The greater the negative membrane potential, the greater the accumulation of cationic TMRE. Depolarisation of mitochondria can happen as a result of damage and mitophagy and results in a large release of superoxide, which could confound MitoSOX results if included with the data from normal healthy cells with healthy mitochondria. Cells in which the mitochondrial membrane has become depolarised can thus be gated out where the TMRE signal has been lost.

However, it was found that the addition of TMRE appeared to increase the MitoSOX signal above the signal when TMRE was absent. The increase in signal was greater than any expected spill-over, given the low fluorescence of TMRE in the 610/20 nm emission channel with the 488 nm laser. It could be the case that the presence of TMRE was increasing the superoxide release from the mitochondria or that the dyes were otherwise interacting. Additionally, when the double-stained cells were run through the 561 nm laser with 586/15 nm emission filters, the TMRE signal was reduced by the presence of MitoSOX. This was unexpected, as with both dyes present the fluorescence would be expected to be greater than the sum of its parts, rather than significantly less. This could have been due to the MitoSOX dye itself changing the mitochondrial membrane potential, or an interaction between the dyes. In either case, it was decided to use the dyes separately. Although this did allow for gating out of any TMRE negative cells, it was found that after gating by cells size and DAPI signal, for all conditions there were no TMRE negative cells.

4.4.4 MitoSOX concentration

Given that MitoSOX could potentially change the mitochondrial membrane potential and therefore the behaviour of the mitochondria, a lower concentration of MitoSOX was tested to see if the same results could be gathered while having a lesser impact on the mitochondria. Antimycin A was used as a positive control, which when added to cells would act as an electron transport chain inhibitor by binding complex III and inhibiting electron transfer between cytochrome b and c. This results in increased superoxide production through electron leak. However, at the lower concentration of 1 mM, the MitoSOX dye was less sensitive to changes in superoxide, detecting only a 35% increase in superoxide on incubation with antimycin A compared to the 79% detected with 5 mM MitoSOX. This indicates that the suggested concentration of 5 mM would be the most sensitive to changes in superoxide at the mitochondrion, and this concentration was used for all experiments.

4.4.5 11 kb mtDNA damage assay

4.4.5.1 Original assay

The 11 kb PCR assay method was designed as a measure of mitochondrial DNA (mtDNA) damage (Hanna et al., 2019). The primers amplify a region of mtDNA ~11,000 bases long, but

if there are any strand breaks in the mtDNA in that region of amplification, the enzyme will not proceed and that mtDNA molecule will not amplify. Thus, the lower the ct value, the greater the amount of intact mtDNA present in the sample. The higher the ct value, the more mtDNA in the sample has strand breaks and thus did not amplify.

Initial tests with this assay were found to have erratic results with a high standard deviation between technical replicates. Thus, an investigation into the problem was started, which revealed several issues with the assay, including lack of linear range, inappropriate threshold setting and primer dimer.

When the linear range of the original assay was examined, it appeared to be a curve through which a straight line had been plotted, rather than a straight line. While a linear range should ideally cover 5 logs of DNA concentration (e.g. 1 pg to 100 ng), the linear range of this assay was reported to be between 10 and 50 ng of DNA, which equates to 0.7 logs (Figure 4-19). This linear range implies that a ct value of below 17.3 or above 19.6 should be discarded. The published protocol suggests the use of 12.5 ng of DNA. The linear range was designed using undamaged control DNA from cells that were not exposed to any UV or other light, so 12.5 ng of DNA on this linear range would be expected to have a ct of 19.3. Damaged DNA would have a ct greater than this, as the premise of the assay is that the greater the damage to DNA, the less is able to be amplified and thus the higher ct. With an initial concentration of 12.5 ng the remaining linear range is just 0.3 ct, between 19.3 and 19.6.

The threshold setting was also an issue with the way the assay was designed. The fluorescence measurement of the SYBR was taken at the end of the extension stage of the PCR cycle, the temperature of which changes from 72°C in cycles 1-10 to 68°C from cycles 11-35. The fluorescence of the SYBR is affected by the temperature at which it is measured, which in this reaction results in a sudden jump up in fluorescence between cycles 10 and 11. The automatic threshold set by the software was then calculated to be between these cycles, but for different concentrations of DNA added, the cycle threshold could be before this jump, distorting the results. The original protocol avoided this by putting the threshold much higher in the amplification graph, when the reaction may have left the exponential

growth phase necessary for measuring ct, into the non-exponential plateau phase (Figure 4-20).

To test the assay, new HPLC-purified primers, enzyme, SYBR, ROX and DNase-free water were bought in to ensure that the assay was unaffected by expired or incorrectly stored consumables.

4.4.5.2 Optimising extension temperature

In order to avoid the potential problems caused by the change in elongation stage temperature from 72°C to 68°C after cycle 10, the temperature was changed to 68°C throughout the PCR. This is the temperature recommended for the reaction by the manufacturer and was not found to negatively impact the amplification of the product (Figure 4-21).

4.4.5.3 Linear range and efficiency

The linear range of the assay was the next issue addressed. The linear range should cover a large range of DNA concentrations, and the slope of the line on a semi-log graph of ct versus log2[DNA concentration] should be equal to 1. The slope of the line represents the efficiency of the reaction, where 1 means the reaction is 100%. Efficiency should be between 90-110%. Efficiency outside this range can be caused by issues such as enzyme inhibition and primer dimer.

Primer dimer is an issue that was found to have been present in experiments using the original protocol, even when it had low standard deviations between technical repeats (Figure 4-22). When a 4% gel was run to elucidate any short products, a strong band was found in all 11 kb reactions with 10 ng of DNA along with multiple other bands up to 300 bp. It is likely that the band at ~60 bp represents primer dimer, and it is possible that the others represent primer trimer and other multiples of primers, or off-target binding of the primers to other parts of DNA.

4.4.5.4 Optimising annealing temperature

When the original method was altered to have a consistent extension temperature of 68°C and run on a PCR with annealing temperatures ranging from 60 to 70°C (Figure 4-23 to

Figure 4-27), evidence of primer dimer/off-target binding was seen in the melt curves of all DNA concentrations from no template, 0.64, 16, 4 and 10 ng per reaction. This can be seen in the additional peaks with a melting temperature of 88°C, where the 11 kb product melting temperature is at 84 °C. From the melt graphs, it appears that the higher the concentration of DNA, the less primer dimer/off-target binding is seen, and also the higher the annealing temperature then the less primer dimer is seen, particularly in the no template control. However, at lower concentrations, the lower annealing temperature seemed to cause the amplification curve to have an unusual shape.

When DNA from a PCR with different combinations of original and new extension temperatures and different annealing temperatures (Figure 4-28) was run on a gel, it was found that in all conditions that primer dimers/off-target binding products were present. There were more at higher DNA concentrations (10 ng compared to 1 ng), showing that a single melt curve peak does not necessarily mean for a single product. When the same samples were run on a 0.8% gel, there was no presence of 11 kb product in the 1 ng DNA reactions, only the 10 ng DNA reactions. It was concluded that changing the annealing temperatures did not eliminate primer dimer/off-target binding.

4.4.5.5 mtDNA isolation

The concentration of mtDNA was unknown, so a 1 in 2 dilution series was run alongside a 1 in 2 dilution series of whole DNA extraction from 20 ng to 1.25 ng with both 11 kb and 83 bp qPCR protocols. The lines of best fit from the 83 bp from the isolated mitochondrial DNA extraction and the whole DNA extraction were used to predict the concentration of whole DNA extraction that would be expected from the ct at the dilution of the isolated mtDNA extraction. When plotted on a graph of ct versus log2 fold change, there was no relationship between concentration and ct, and the standard deviation between replicates was very high (Figure 4-29). In addition, the melt curves were not reliably at 84°C, where the 11 kb product should be, and there was often more than one peak (Figure 4-30). The conclusion from this experiment is that there is too low a yield of mtDNA from an isolation and subsequent DNA extraction to use for qPCR.

4.4.5.6 Optimising buffer in PCR reaction

The Roche Expand Long Template Kit comes with three buffers, intended to best amplify different lengths of product. Buffer 1 contains 17.5 mM $MgCl_2$ at 10 x concentration and is designed for products between 0.5 and 9 kb in length; buffer 2 contains 27.5 mM $MgCl_2$ at 10 x concentration and is designed for products between 9 and 12 kb in length; buffer 3 contains 27.5 mM $MgCl_2$ plus detergents at 10 x concentration and is designed for products between 12 and 20 kb in length. Buffer 2 has originally been used for the 11 kb product as is recommended by Roche, but it is also recommended to try the others as a troubleshooting step. Both buffers 1 and 3 amplified far later than buffer 2 (Figure 4-31), while the buffer 2 from an older kit (labelled as buffer 2B) appeared to work equally well as the buffer 2 from the current kit. The melt curves of buffers 1 and 3 were lower than 84°C, but both also had a great number of additional peaks than buffer 2, old and new. This indicates the buffer 2 is the most appropriate buffer for the 11 kb experiment.

4.4.5.7 11 kb summary

After failing to improve the linear range or the off-target/primer dimer products of the 11 kb assay (Figure 4-32), it was decided that a great deal of further work on this assay would be necessary before it could be validated as a quantitative assay. It may be possible to improve these by using different primers, however, moving on to other projects was prioritised.

4.4.6 ATP measurement assay

In an attempt to determine if irradiation was affecting the mitochondria of the cell and thus the energy balance and ATP production, CellTiter-Glo was used. There was no significant change in ATP levels measured with the assay at any time point after irradiation, so the assay was not pursued further.

4.4.7 Transmission testing of formulations

The transmission of visible light through formulations is a useful tool for testing the ability of ingredients to block visible light. Using a spectroradiometer means the method is particularly flexible in that the transmittance through any specific waveband can be calculated as required. In this instance, the focus was on the highest energy blue light defined by the band of 400 – 420 nm, but blue light could have been more broadly measured by 400 – 450 nm, or

another definition of interest. Until there is an action spectrum of the biological effects of visible light, it is difficult to weight wavelengths in the way they have been weighted in the UV region by the erythemal action spectrum used to calculate SEDs.

4.4.8 Summary

This section details the optimisation of assays used in this thesis. While it appeared that the ROS-Glo H_2O_2 assay was sensitive to radical changes in the polystyrene tissue culture plastic as a result of irradiation, it was demonstrated that DCFDA shows no such reaction with the tissue culture plastics. DCFDA does have the ability to make cells less well adhered to the tissue culture plate, meaning that cells can be washed off if extreme care is not taken during wash steps. Because of this, flow cytometry may be a more accurate way of measuring DCFDA fluorescence as a result of irradiation.

The 11 kb mtDNA damage assay, either in the original protocol or with amended cycle temperature settings, does not function as a quantitative assay. The reported linear range of 2.3-fold change in intact 11 kb mtDNA fragments is not large enough to constitute a reliable linear range for qPCR, especially when reported differences of up to 36-fold in mtDNA damage as a result of irradiation cannot fit within the reported linear range. The assay may be improved by changing the primers or enzyme, but the current protocol should not be used.

A method for quantifying the ability of ingredients in formulations to block visible light from the skin has been demonstrated to show useful results. This method can be employed to examine individual wavelengths or larger wavebands depending on need.

Chapter 5 Effects of UV, visible and infrared light on cells

5.1 Introduction

5.1.1 ROS production

During mitochondrial respiration, ROS are produced at a low concentration as a by-product. Under normal conditions, these ROS are controlled by cellular antioxidants, which limit any damage they may cause. Much of the accumulated skin photodamage that comes from solar light exposure is due to oxidative stress within cells. This is particularly pertinent in dermal fibroblasts, as it is UVA, visible and infrared light that predominantly penetrates the stratum corneum and epidermis to reach the dermis, while much, though not all, of the UVB has already been absorbed. Wavelengths longer than those found in the UVB waveband are more weakly absorbed by DNA, though it is clear that they still cause cellular damage including indirectly to DNA. It is known that both UVA and UVB produce ROS, and visible light and infrared light have now also been demonstrated to be able to produce ROS in skin. The redox imbalance caused by solar light results in changes in cell behaviour and gene expression.

In order to determine if irradiances and doses of infrared light similar to that of the sun would be able to induce ROS formation in HDFn cells in temperature-controlled conditions, a range of doses was tested. Complete solar simulated light delivering 2.16 SEDs of UV was used as a positive control.

The DCFDA assay measures both ROS and RNS species, being non-specific in its reactions with these. It is not targeted and as such measures ROS throughout the cytoplasm. Conversely, MitoSOX dye reacts selectively with superoxide but no other ROS or RNS and is targeted to the mitochondria, allowing changes in ROS originating from the ETC or other mitochondrial components to be measured. ROS was measured both immediately and 24 hours after irradiation in response to UV light, to determine how the exposure to oxidative stress would affect the redox state in cells.

410-810 nm light from the solar simulator was divided into 100 nm wavebands: blue (410 - 510 nm), green (515-610 nm), red (610-710 nm) and far red (715-810 nm) using longpass

and shortpass filters. Here they are referred to as visible light conditions, even though the far red condition contains wavelengths above the 780 nm cut-off that defines visible light. These were to separate the effects of the different wavebands, as different wavelengths have been shown to have different biological effects.

5.1.2 Gene expression

UV irradiation has been shown to lead to changes in gene expression in skin cells. In particular relevance to photoaging, genes which code for proteins that are related to components of the extracellular matrix (ECM) are affected. The ECM in the dermis contains collagens, elastin, and hyaluronic acid, all of which are important for maintaining the structure of skin. While it is important for the skin to be able to remodel after injuries such as wounds to allow healing and regeneration of tissue, if this process is aberrantly upregulated it can result in the degradation of otherwise healthy ECM. Matrix metalloproteinases are upregulated as a result of irradiation with UV light, and this family of enzymes is responsible for the breakdown of skin collagen and elastin. After being broken down, they are often not replaced in the same way, leaving broken collagen fragments where long chains were before. This leaves the dermis less plump and elastic, leading to deep wrinkles and a photoaged phenotype.

It has been suggested that it is through increased ROS by infrared light, these genes are upregulated, contributing to photoaging (Calles et al., 2010, Schroeder et al., 2010). In this thesis, the effect of exposure to infrared light over 1 day or 3 days on the expression of extracellular matrix genes was examined under the hypothesis that any change in the expression of these genes would be amplified by repeated exposures.

The transcriptome provides great insight into the behaviour of cells. RNA Sequencing (RNA-Seq) gives precise measurements of gene expression and can be used to find differences between cells exposed to different experimental conditions.

There has been one previous study of the transcriptome of skin cells in vitro in response to infrared irradiation, carried out with microarray (Calles et al., 2010). In this study, high-intensity infrared irradiances were used – 360 $mW.cm^{-2}$, 9 times higher than the maximal

irradiance from the sun at 40 $mW.cm^{-2}$. It was reported that temperature was controlled to be maintained at below 37°C with a plate connected to a thermostated bath, though not whether temperature in plates was measured directly. As far as the author is aware there has been no transcriptomic study into the effects of visible light on skin.

5.2 Materials and methods

5.2.1 Reactive oxygen species production

5.2.1.1 DCFDA plate assay

5.2.1.1.1 Change in signal by filters

HDFn cells were seeded as per protocol in Chapter 2. Cells were irradiated as per protocol in Chapter 2 under complete solar light from the solar simulator for the duration of irradiation required to deliver 2.16 SEDs of erythemally effective UV (~2 minutes), before being incubated with DCFDA for 30 minutes at 37°C, 5% CO_2 as per protocol in Chapter 2. Control wells were covered in foil to eliminate any light, "no filter" cells had no filter over them, and other wells were covered in various filters as detailed in Table 2-3 which were rested on top of the plate during irradiation. DCFDA staining was carried out as per protocol in Chapter 2.

5.2.1.1.2 Change in DCFDA signal 0 and 24 hours after irradiation containing UV

HDFn cells were seeded as per protocol in Chapter 2. The following day, cells were irradiated with 2.16 SEDs of erythemally effective UV as per protocol in Chapter 2, before the DCFDA assay was used as per protocol in Chapter 2. Following incubation, cells were gently washed with 200 ul DPBS and left in DPBS to read fluorescence on a TECAN plate reader. Cells to be assayed at 24 hours were not placed in DCFDA immediately after irradiation but rather returned to the incubator in complete, phenol-free DMEM + 10% FCS for 24 hours before washing with DPBS and staining with DCFDA as above.

5.2.1.1.3 DCFDA signal in response to infrared light

Cells were seeded as above in section 5.2.1.1.2. The only difference in protocol was that before irradiation with infrared light, phenol-containing medium was replaced with complete, phenol-free DMEM with 10% FCS rather than PBS, which after irradiation was

washed off with 3 x 200 ul DPBS before incubation with DCFDA in DPBS. Infrared irradiations were carried out as per protocol in Chapter 2.

5.2.1.2 Flow cytometry of DCFDA and MitoSOX

5.2.1.2.1 UV, visible and infrared

Cells were prepared for flow cytometry as per protocol in Chapter 2. Briefly, irradiated cells were collected in wells of a round-bottomed 96-well plate. Cells were stained with MitoSOX + DAPI, DCFDA + PI or TMRE + PI in DPBS and kept on ice in 1% FCS until reading with the BD Symphony cytometer. Debris and cell clumps were gated out with forward and side scatter measures, dead cells were gated out with either PI or DAPI. From the remaining cells, median fluorescence was recorded and compared to controls. Data from at least 4 replicate experiments were pooled and presented as fold change relative to control. Data were log transformed for analysis with two-tailed, one-sample t-tests and two-tailed students t-test.

Cells irradiated with complete solar simulated light or UV were irradiated in DPBS. Cells irradiated with infrared were irradiated in complete, phenol-free DMEM with 10% FCS. Cells irradiated with visible light were irradiated in MEMO. All conditions were seeded in complete, phenol-containing DMEM with 10% FCS except the visible light condition which was seeded in MEMO with no FCS. Irradiations were carried out as per protocol in Chapter 2.

5.2.1.2.2 Infrared then UV irradiation

Two different irradiation protocols were used to test the effects of irradiating cells with infrared light prior to complete solar simulated light.

The first protocol used cells that had been seeded as per protocol in Chapter 2 in complete, phenol-containing DMEM with 10% FCS. The following day they were washed and changed to complete, phenol-free DMEM + 10% FCS before irradiation with high intensity infrared (360 $mW.cm^2$, 288 $J.cm^{-2}$) for 13.3 minutes. The medium was washed off and replaced with DPBS before irradiation with 2.16 SEDs of complete solar simulated light. After this, cells were stained and ran on flow cytometry as normal.

The second protocol used cells seeded in MEMO medium with no FCS. These cells were not washed before irradiation with either infrared or complete solar simulated light, they were

left in MEMO the entire time. They were irradiated with medium intensity infrared light (100 $mW.cm^{-2}$) for 2 hours, to give a dose equivalent to 5 hours of solar infrared (720 $J.cm^{-2}$). After irradiation with infrared light, they were immediately irradiated with 2.16 SEDs of complete solar simulated light in the same MEMO medium. The cells were then stained and run on flow cytometry as normal.

5.2.2 qPCR gene expression of infrared irradiated cells

HDFn cells were seeded as per protocol in Chapter 2 but in complete, phenol-free DMEM with 10% FCS. The following day, the cells were irradiated in the same medium, and after irradiation, the medium was refreshed with fresh complete, phenol-free DMEM + 10% FCS. 24 hours after irradiation, RNA was extracted as per protocol in Chapter 2.

5.2.3 Multiple-day exposures

5.2.3.1.1 High intensity infrared in DMEM over three days

HDFn cells were seeded as per protocol in Chapter 2 except only 5 x 10^4 cells/dish in 35 mm dishes and in complete, 10% FCS, phenol-free DMEM. The following day, the cells were irradiated in the same medium, but after each irradiation, the medium was refreshed with new complete, phenol-free DMEM + 10% FCS. This irradiation and medium replacement process was repeated over 2 more days, with the irradiation starting at the same time each day. 24 hours after the final irradiation, RNA was extracted as per protocol in Chapter 2.

5.2.4 RNA Sequencing

HDFn cells were seeded as per protocol in Chapter 2 except in complete, 10% FCS, phenol-free DMEM. The following day, the medium was changed to MEMO + 1% FCS for the first washout period of 22 hours. 22 hours later, the medium was replaced with MEMO with 0% FCS for a 2-hour washout period. Following this, the medium was refreshed with MEMO with 0% FCS and cells were irradiated as per Chapter 2 though all light conditions were irradiated in MEMO. After irradiation in MEMO, cells were returned to complete, 10% FCS, phenol-free DMEM in the humidified, 37°C, 5% CO_2 incubator. 24 hours after the end of irradiation, RNA was extracted using the RNeasy Kit as per protocol in Chapter 2. Following extraction, RNA was stored at -80°C.

RNA samples were assessed for quality on an Agilent TapeStation (Agilent, USA). mRNA Sequencing was carried out by Jon Coxhead of the Newcastle University Genomics Facility at a read depth of 15M 100 base pair single reads per sample on an Illumina NovaSeq SP flow cell (Illumina, USA).

RNA Sequencing analysis was carried out by John Casement of the Newcastle University Bioinformatics Facility. The quality of FASTQ files was assessed with FastQC (version 11.8). Reads were quantified against transcripts using Salmon (version 0.12.0). Salmon quantifies reads against transcripts. To obtain gene-level counts, the R package 'tximport' (version 1.18.0) was used. Differential gene expression analysis was carried out with the R package DESeq2 (version 1.30.1). Adjusted p values were calculated using the Benjamini-Hochberg method. Comparisons carried out were as follows: high intensity infrared 2- and 10-hour equivalent doses to the high intensity infrared control. Low intensity infrared 2-hour dose to low intensity infrared control. Blue, green, red, far red, and complete visible conditions were compared to the visible control. Complete solar simulated light and UV-only were compared to the solar light control.

Pathway analyses was carried out using the Qiagen Ingenuity Pathway Analysis software (IPA, http://www.ingenuity.com). A base mean cut-off of 10 was used, a log 2 fold change of ± 0.5 (representing a 41% increase or 29% decrease in expression) and an adjusted p value of 0.05 (-log 2 adjusted p of 4.32) were used to refine differentially expressed gene (DEGs) lists. Only the complete solar simulated light and UV only conditions had sufficient DEGs to carry out pathway analyses. Significantly affected pathways were those with a p value of < 0.05.

5.3 Results

5.3.1 Reactive oxygen species production

5.3.1.1 DCFDA plate assay

5.3.1.1.1 Filters reduce DCFDA signal from same duration exposures

A 2.16 SED dose of complete solar simulated light was delivered to cells with or without filters, and the resulting change in ROS production was measured with DCFDA (Figure 5-1). As expected, since all filters block some UV light, all filters reduced the ROS as measured

with DCFDA to some extent. The IR, plastic, 780 longpass and UV filters all reduced the signal to a point where it was not significantly different to that from unirradiated cells. The window glass, neutral density and IR/VIS filter reduced it but not completely, which was expected as all of these let through decent amounts of UV.

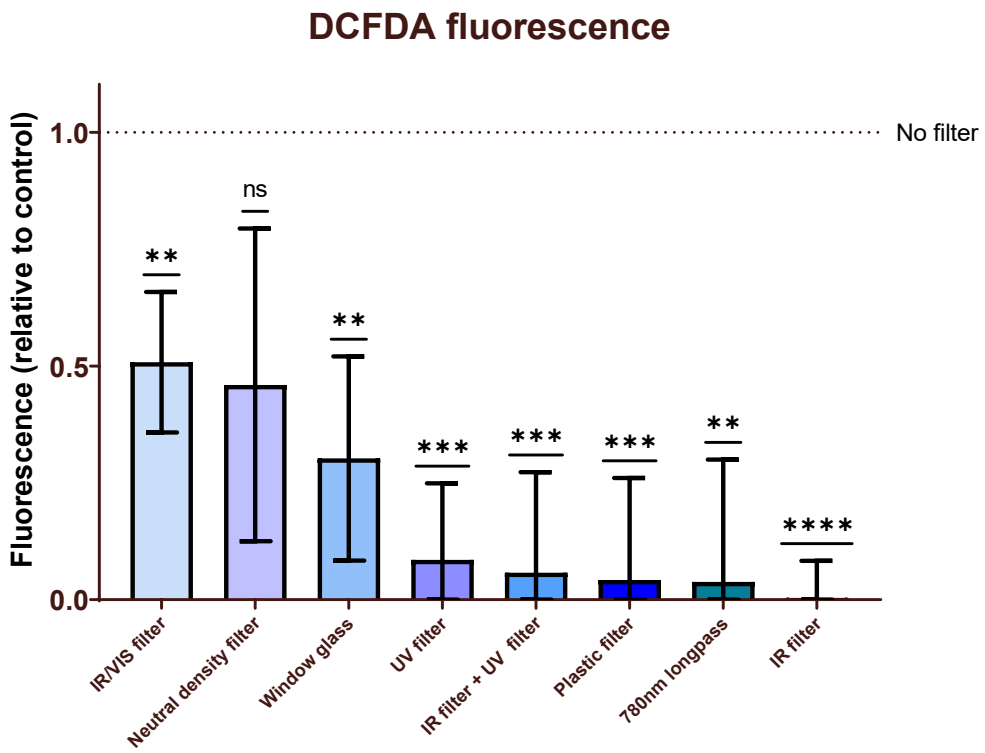

Figure 5-1 The reduction of fluorescence signal from DCFDA in cells exposed to light through a filter compared to light with no filter.
Cells were seeded in complete, phenol-containing DMEM with 10% FCS. Prior to irradiation, medium was replaced with PBS. Irradiation time was the same for all conditions at approximately ~2 minutes duration, which delivered 2.16 SEDs when no filter was present. A stand was used for temperature control. Unirradiated controls were under the lamp during irradiation but wrapped in foil to receive 0 J.cm^{-2} of light. Data from cells exposed to light through a filter was normalised to that from cells exposed with no filter to the 2.16 SED dose of light and the unirradiated control. (**): $p < 0.01$, (***): $p < 0.001$, (****): $p < 0.0001$, one-sample t-test; data represent means ± SD, N = 5, n = 3

5.3.1.1.2 Complete solar simulated light increases signal from DCFDA at 0 hours, but appears to decrease it after 24 hours

HDFn cells irradiated with 2.16 SEDs of complete solar simulated light had a significant increase of 2.9-fold as compared to unirradiated controls immediately after irradiation ($p = 0.048$, one-sample t-test) (Figure 5-2). 24 hours after irradiation, there was a significant

decrease in fluorescence from irradiated cells compared to unirradiated controls of 49% ($p = 0.03$, one-sample t-test).

DCFDA signal appeared to decrease in unirradiated controls compared to the incubator control at 24 hours, though this was not significant (42% decrease, $p = 0.17$).

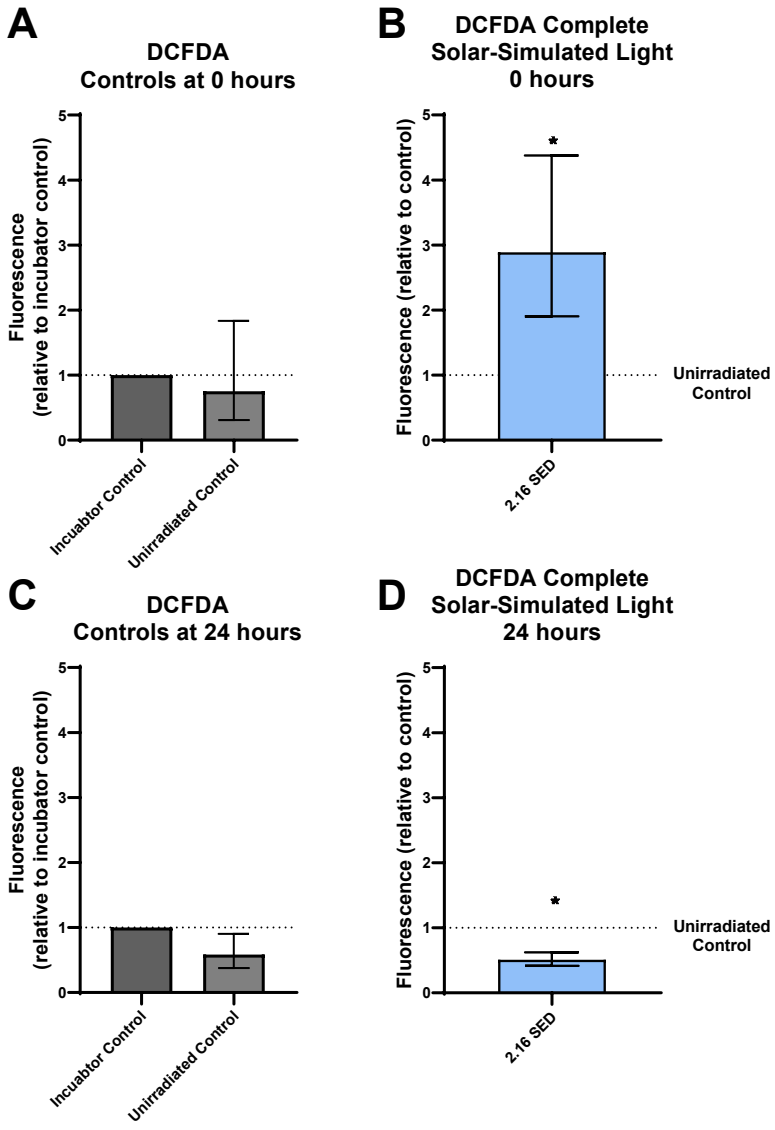

Figure 5-2 DCFDA signal from HDFn cells irradiated with 2.16 SEDs of complete solar simulated light
Cells were seeded in complete, phenol-free DMEM with 10% FCS, which was replaced with PBS the following day for irradiation, after which the cells were returned to fresh, complete, phenol-free DMEM with 10% FCS. DCFDA was incubated with cells after irradiation and washed off before data collection. 2.16 SEDs of complete, solar simulated light or UV only light was delivered over ~2 or ~3 minutes respectively. Incubator controls experienced the same wash steps but remained in the incubator during irradiation. Unirradiated controls were under the lamp during irradiation but wrapped in foil to receive 0 J.cm^{-2} of light. Temperature was controlled using a stand. Data from irradiated cells were normalised to unirradiated controls. Unirradiated control data were normalised to incubator controls for comparison. Panel A: unirradiated controls compared to incubator controls immediately after irradiation. Panel B: Irradiated cells compared to unirradiated controls immediately after irradiation. Panel C: unirradiated controls compared to incubator controls 24 hours after irradiation. Panel D: irradiated cells compared to unirradiated controls 24 hours after irradiation. (*): $p < 0.05$, one-sample t-test on log transformed data; data represent geometric means ± geometric SD, N = 3, n = 3

5.3.1.1.3 Low intensity infrared does not change signal from DCFDA immediately after irradiation

A 2-hour dose of infrared light at an irradiance equal to that at noon, midsummers day in the Mediterranean (288 J.cm^{-2}, 40 mW.cm^{-2}) was delivered to HDFn cells (Figure 5-3). Immediately after irradiation, there was no difference in DCFDA signal compared to the irradiation control. When the irradiation control was compared to the incubator control there was no significant difference in fluorescence.

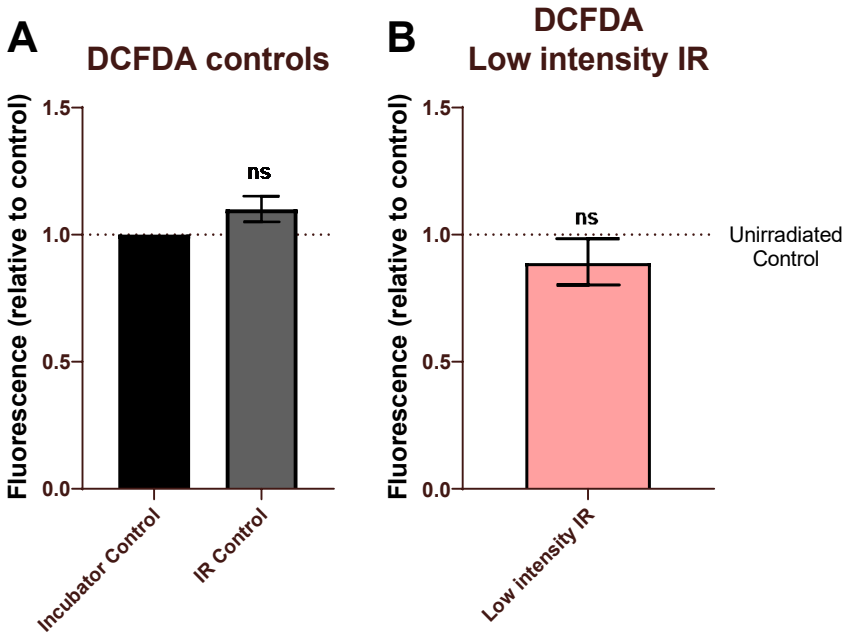

Figure 5-3 A 2-hour dose of infrared light was delivered to HDFn cells in temperature-controlled plates and assayed with DCFDA

Cells were seeded in complete, phenol-free DMEM with 10% FCS, in which they were irradiated the following day. DCFDA was incubated with cells after irradiation and washed off before data collection. 360 J.cm^{-2} of infrared light was delivered over 2 hours at 40 mW.cm^{-2}. Incubator controls experienced the same wash steps but remained in the incubator during irradiation. Unirradiated controls were under the lamp during irradiation but wrapped in foil to receive 0 J.cm^{-2} of light. Temperature was controlled with a stirred water bath. Data from irradiated cells were normalised to unirradiated controls. Unirradiated control data were normalised to incubator controls for comparison. Panel A: unirradiated controls compared to incubator controls. Panel B: Irradiated cells compared to unirradiated controls. (ns): $p \geq 0.05$, one-sample t-test on log transformed data; data represent geometric means ± geometric SD, N = 3, n = 3

5.3.1.1.4 High intensity infrared does not change signal from controls immediately or at 24 hours after irradiation

As with low intensity infrared, high intensity infrared caused no significant changes in DCFDA signal after irradiation (Figure 5-4). This was also true 24 hours after irradiation. There appeared to be a decrease in DCFDA signal between irradiation and incubator controls at both 0 and 24 hours post-irradiation, but this was not significant.

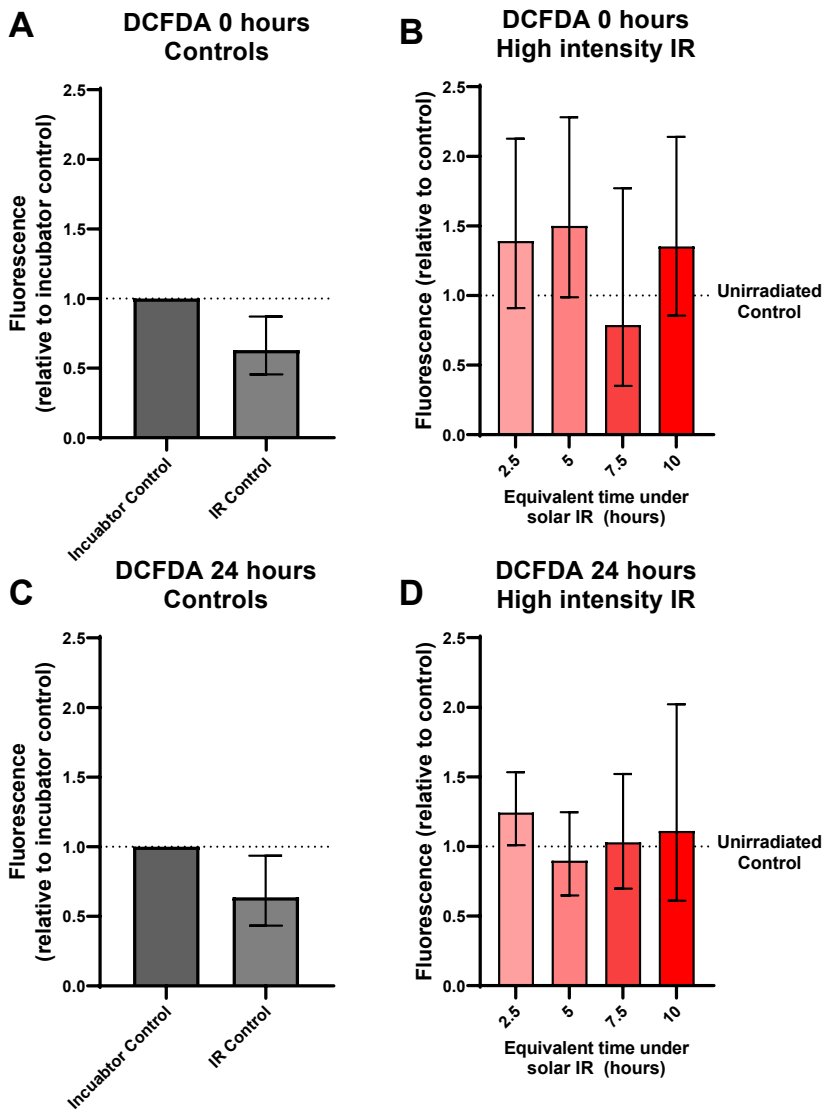

Figure 5-4 DCFDA fluorescence from HDFn cells exposed to a 2 or 10-hour dose of infrared light was temperature-controlled plates.

Cells were seeded in complete, phenol-free DMEM with 10% FCS, in which the cells were irradiated the following day. DCFDA was incubated with cells after irradiation and washed off before data collection. Infrared was delivered from the Hydrosun infrared lamp at 360 mW.cm^{-2} for 16.7, 33.3, 50 or 66.7 minutes, delivering a dose of 360, 720, 1080 or 1440 mJ.cm^{-2} equivalent to 2.5, 5, 7.5 or 10 hours of solar infrared respectively. Incubator controls experienced the same wash steps but remained in the incubator during irradiation. Unirradiated controls were under the lamp during irradiation but wrapped in foil to receive 0 J.cm^{-2} of light. Temperature was controlled using a stirred water bath. Data from irradiated cells were normalised to unirradiated controls. Unirradiated control data were normalised to incubator controls for comparison. Panel A: unirradiated controls compared to incubator controls immediately after irradiation. Panel B: Irradiated cells compared to unirradiated controls immediately after irradiation. Panel C: unirradiated controls compared to incubator controls 24 hours after irradiation. Panel D: irradiated cells compared to unirradiated controls 24 hours after irradiation. Data represent geometric means ± geometric SD, N = 3, n = 3

5.3.1.2 Flow cytometry of DCFDA and MitoSOX

5.3.1.2.1 TMRE

When mitochondrial membrane potential was measured using TMRE stain, there was no difference in fluorescence compared to unirradiated controls in HDFn cells irradiated with 2.16 SEDs of complete solar simulated light (delivered over approximately 2 minutes), or with a 2- or 10-hour equivalent solar dose of high intensity infrared light (360 mW.cm^{-2}, 288 or 1440 J.cm^{-2} respectively) (Figure 5-5). Neither solar simulator unirradiated control cells nor infrared unirradiated control cells had any significant differences in fluorescence compared to the incubator control. Low intensity IR was not examined with TMRE, it was presumed to have no effect since complete solar light and high intensity IR had no effect.

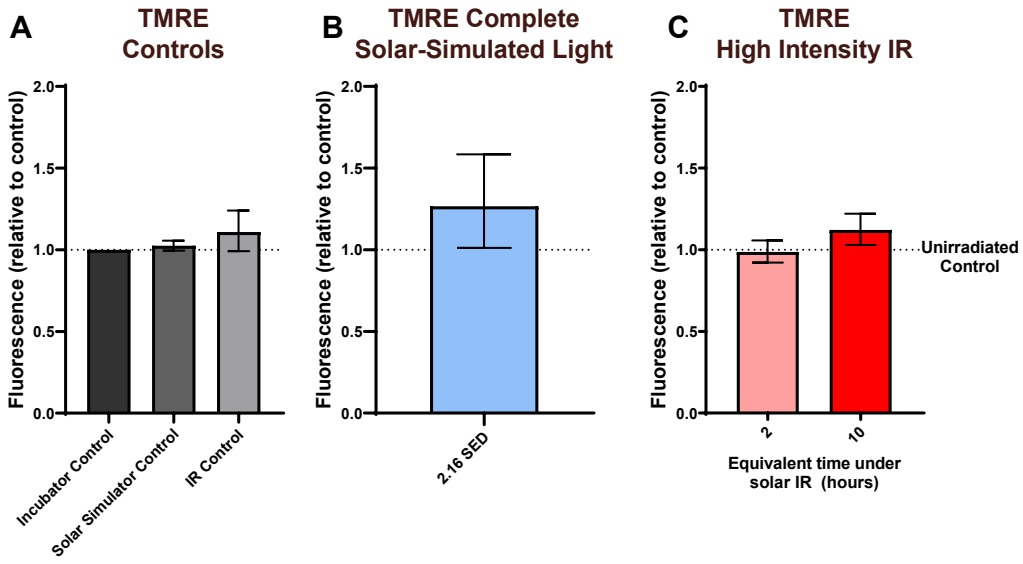

Figure 5-5 TMRE mitochondrial membrane potential stain in HDFn cells irradiated with UV and infrared light

After irradiation, cells were stained with TMRE. All cells were seeded in complete DMEM with 10% FCS. Cells irradiated with 2.16 SEDs of complete solar simulated light over ~2 minutes were irradiated in PBS. Cells irradiated with infrared with 360 mW.cm^{-2} for 13.3 or 66.7 minutes to deliver 288 or 1440 J.cm^{-2} equivalent to 2 or 10 hours of infrared from the sun respectively were irradiated in the same DMEM they were seeded in. Incubator controls experienced the same wash steps but remained in the incubator during irradiation time. Unirradiated controls were under the lamp during irradiation but wrapped in foil to receive 0 J.cm^{-2} of light. Temperature control for complete solar simulated light delivery was a stand, and for infrared was a stirred water bath. Panel A shows unirradiated controls compared to the incubator control. Panel B shows 2.16 SED irradiated cells compared to their unirradiated controls, and Panel C shows the IR irradiated cells compared to their unirradiated

control. No significant differences with a one-sample t-test on log transformed data; data represent geometric means ± geometric SD, N = 3

5.3.1.2.2 DCFDA and MitoSOX

5.3.1.2.2.1 Signal from unirradiated wells in different media

When HDFn cells were kept in MEMO medium for 1 day before staining with DCFDA, they were found to have a 77% lower DCFDA signal compared to cells which were kept in complete, phenol-free DMEM + 10% FCS (p = 0.024) (Figure 5-6). There was no change in MitoSOX signal between the medium conditions.

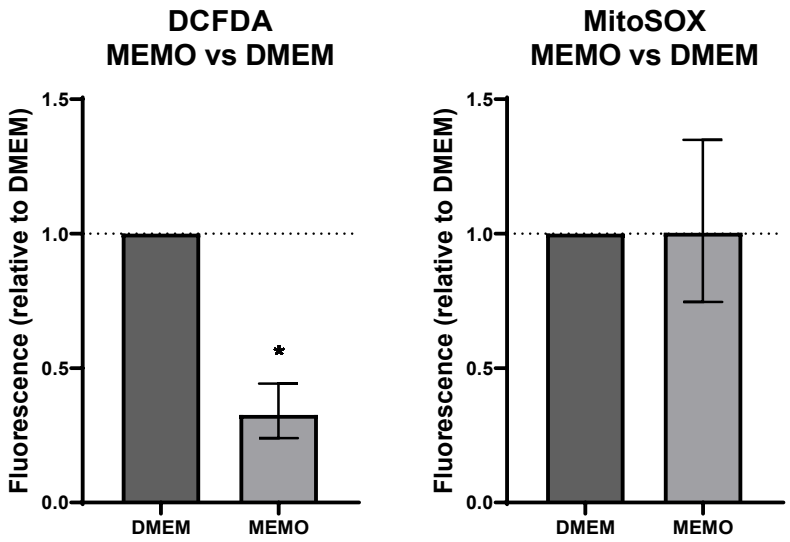

Figure 5-6 DCFDA and MitoSOX signal from unirradiated HDFn cells in MEMO compared to complete, phenol-free DMEM
Cells were seeded in complete, phenol-free DMEM with 10% FCS or in MEMO. 24 hours later they were stained with DCFDA (Panel A) or MitoSOX (Panel B) with fluorescence measured by flow cytometry. (*): p < 0.05, one-sample t-test on log transformed data; data represent geometric means ± geometric SD, N = 3

5.3.1.2.2.2 Signal from irradiated HDFn cells

Compared to the relevant incubator control condition (complete, phenol-free DMEM with 10% FCS for solar simulator and infrared, MEMO for visible irradiation, each irradiation control compared to an incubator control in the appropriate medium) there was no significant change in the irradiation control that was under the lamp but in foil in either DCFDA (Figure 5-7 A). In MitoSOX stained cells, signal was significantly increased by 12% in infrared controls compared to incubator DMEM controls (Figure 5-7 F, p = 0.044).

There was a significant increase in DCFDA signal in cells irradiated with 2.16 SEDs of complete solar simulated light or 2.16 SEDs of UV only (Figure 5-7 B, 2.40 and 2.2-fold increases, $p = 0.0004$ and $p = 0.0007$ respectively). There was no significant difference in the responses between the complete solar simulated light and UV only irradiated cells (two-tailed students t-test). There was no difference in signal from cells stained with MitoSOX in either condition.

There was a 37% increase in MitoSOX in cells irradiated with complete visible light compared to irradiation controls, but the difference was not statistically significant (Figure 5-7 H, $p = 0.099$). There were no significant differences in DCFDA or MitoSOX signal in any of the visible light irradiated conditions (Figure 5-7 C and H).

While there was a significant increase in DCFDA fluorescence with a 2-hour dose of solar (low) intensity infrared, this was only 17% (Figure 5-7 E, $p = 0.0195$). There were no other significant differences in DCFDA or MitoSOX signal compared to irradiation controls in cells irradiated with high or solar intensity infrared (Figure 5-7 D, E, I and J).

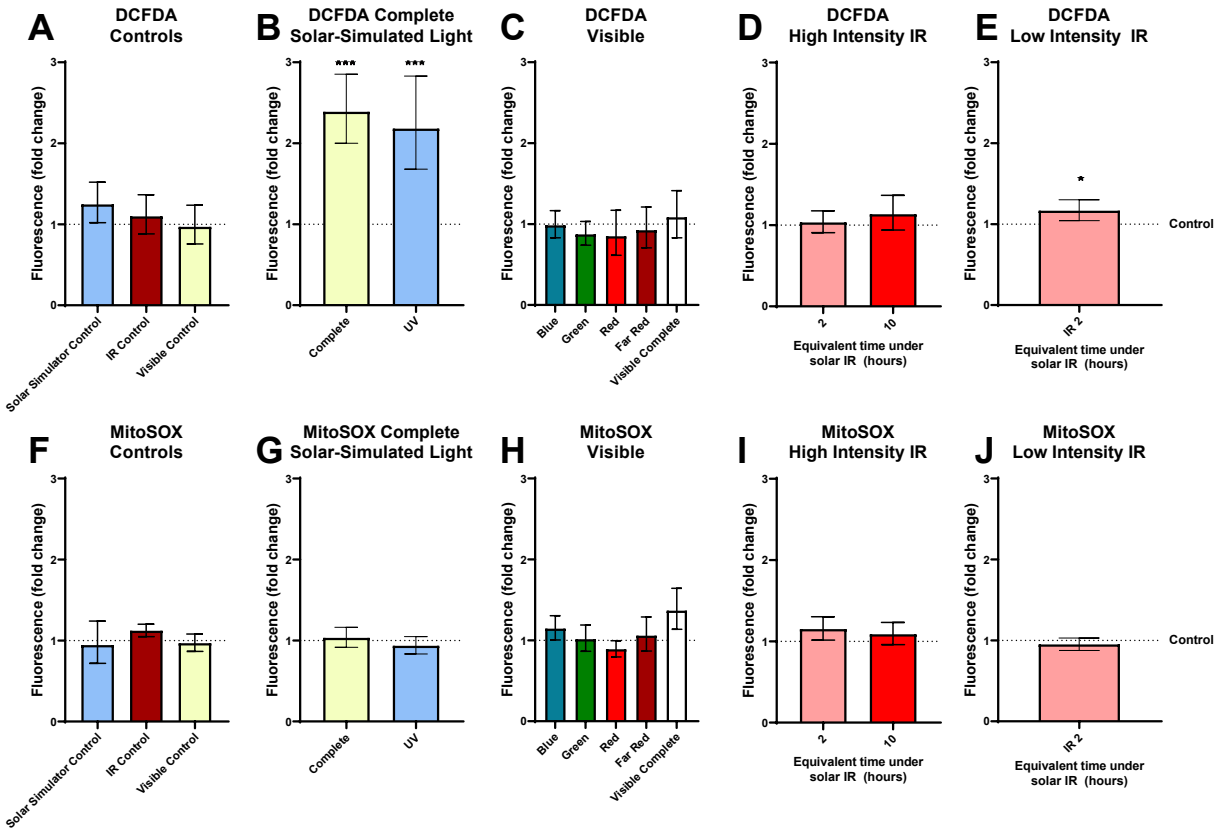

Figure 5-7 ROS production as measured by DCFDA and MitoSOX on HDFn cells irradiated with solar simulated light, visible light or infrared light

Effects on ROS production as measured by DCFDA and MitoSOX on cells irradiated with solar simulated light; 2.16 SEDs of either complete solar simulated light or UV only delivered over ~2 or ~3 minutes respectively on DCFDA (B) or MitoSOX (G) signal; 1-hour equivalent solar dose of visible light from blue (410 – 510 nm), green (515 – 610 nm), red (610 – 710 nm), far red (715 – 810 nm) or complete visible (410 – 810 nm) wavebands on DCFDA (C) or MitoSOX (H) signal; 2 or 10-hour equivalent solar doses (288 or 1440 J.cm^{-2} at 360 mW.cm^{-2}) of high intensity infrared on DCFDA (D) or MitoSOX (I) signal; 2-hour solar intensity infrared dose (2 hours at 40 mW.cm^{-2}) on DCFDA (E) or MitoSOX (J) signal. Temperature control was a stand for the visible and solar simulated light, and a stirred water bath for infrared light. Unirradiated controls were under the lamp during irradiation but wrapped in foil to receive 0 J.cm^{-2} of light. Data from irradiated cells were normalised to their respective unirradiated controls. (*): p < 0.05, (***): p < 0.001, one-sample t-test on log transformed data; data represent geometric means ± geometric SD, N = at least 4.

5.3.1.2.3 Infrared and complete solar light in subsequent irradiations

5.3.1.2.3.1 DMEM, 360 mW.cm^{-2}, 2-hour equivalent

HDFn cells were exposed to a 2-hour equivalent dose of high intensity infrared light in phenol-free complete 10% FCS DMEM, and subsequently irradiated with 2.16 SEDs of complete solar simulated light in DPBS (IR/SS condition in Figure 5-8). Additionally, there was

a condition irradiated with infrared but remained covered in foil during the 2.16 SED irradiation (IR/C in Figure 5-8) and a condition that was not irradiated with infrared through being wrapped in foil but was exposed to the 2.16 SEDs of light (C/SS in Figure 5-8). Finally, there was a condition that remained in foil, unirradiated during both infrared and 2.16 SED irradiations (C/C in Figure 5-8).

There was found to be no difference in TMRE signal between the incubator control and the irradiation control cells that were in foil for the IR irradiation and the subsequent irradiation with complete solar simulated UV light (C/C). Furthermore, there was no significant effect of infrared, complete solar simulated light or both together on TMRE signal.

In control cells (C/C) the DCFDA was higher than in incubator controls, but this difference was not significant (2.2 fold increase, $p = 0.09$).

DCFDA signal was shown to significantly increase in cells exposed to 2.16 SEDs of solar simulated light irrespective of infrared irradiation (66% increase, $p = 0.018$, for cells irradiated with solar simulator only, or 90% increase, $p = 0.029$ for cells irradiated with both solar simulated light and infrared). There was no significant difference between these responses when infrared was or was not irradiated beforehand ($p = 0.5$, unpaired 2 tailed t-test).

MitoSOX signal was increased in irradiation controls compared to incubator controls by 81% ($p = 0.025$). However, there was no increase between any of the irradiated conditions and the irradiation control, which reflects the results seen with single complete solar simulated light and infrared light irradiations.

When cells were irradiated in DPBS with 2.16 SEDs of complete solar simulated light after being in the water bath for the duration of infrared irradiation (66.7 minutes) but not irradiated with infrared light, the DCFDA response was lower than when the cells were not in the water bath for that duration (66% increase versus 139% increase, $p = 0.001$, Figure 5-8 D "C/SS" versus Figure 5-7 B "Complete"). There was no significant difference between responses in MitoSOX.

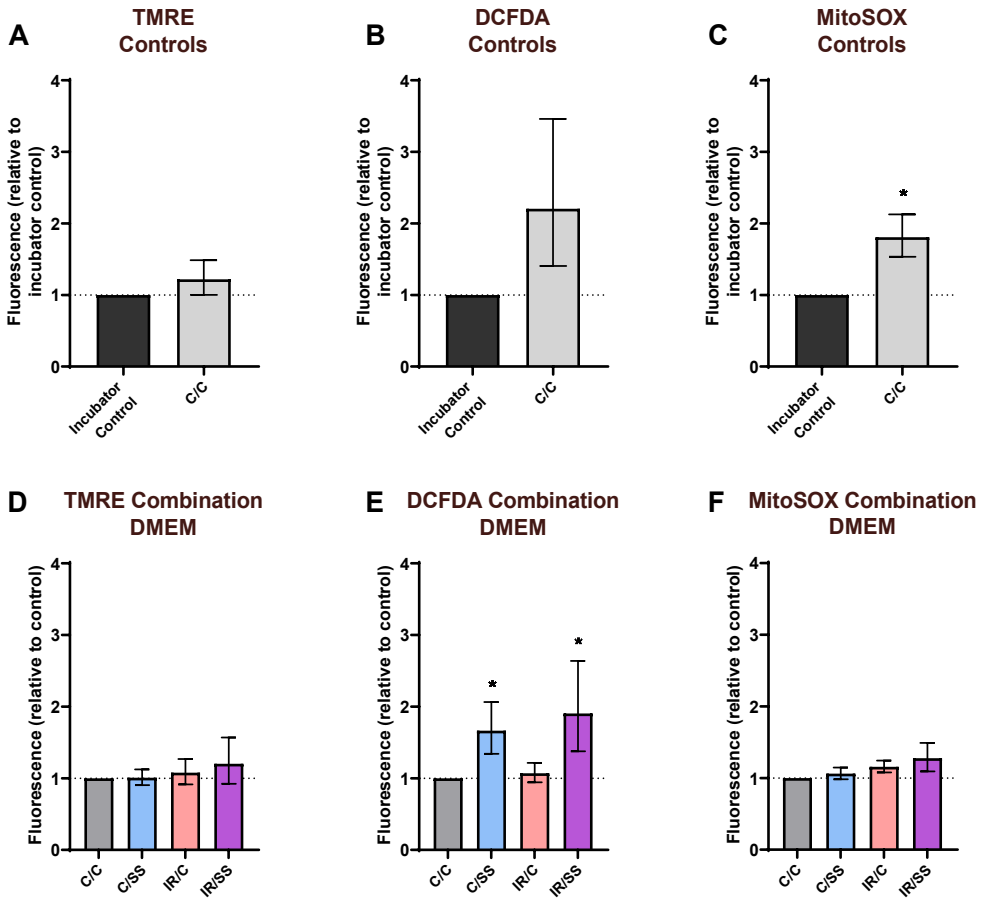

Figure 5-8 Effects on ROS production as measured by DCFDA and MitoSOX on HDFn cells irradiated with infrared then UV light in complete, phenol-free DMEM

Cells irradiated with 1440 J.cm^{-2} infrared at 360 mW.cm^{-2} for 66.7 minutes only (IR/C), 2.16 SEDs of solar simulated light over ~2 minutes only (C/SS), or both (IR/SS) compared to unirradiated control cells (C/C). TMRE signal in irradiated controls versus incubator controls (A) or irradiated cells versus unirradiated controls (D); DCFDA signal in irradiated controls versus incubator controls (B) or irradiated cells versus unirradiated controls (E); MitoSOX signal in irradiated controls versus incubator controls (C) or irradiated cells versus unirradiated controls (F). Incubator controls experienced the same wash steps but remained in the incubator during irradiation time. Unirradiated controls were under the lamp during irradiation but wrapped in foil to receive 0 J.cm^{-2} of light. Temperature control was a stand for the visible and solar simulated light, and a stirred water bath for infrared light. Data from irradiated cells were normalised to unirradiated controls. Unirradiated control data were normalised to incubator controls for comparison. (*): $p < 0.05$, one-sample t-test on log transformed data; data represent geometric means ± geometric SD, N = 3

5.3.1.2.3.2 MEMO, 100 mW.cm^{-2}, 5-hour equivalent

The experiment above was repeated, except the HDFn cells were cultured in MEMO for 24 hours before the irradiation and during the irradiation and were irradiated with 720 J.cm^{-2} of

100 mW.cm^{-2}, rather irradiation in DMEM/DPBS with 288 J.cm^{-2} of 360 mW.cm^{-2} (Figure 5-9). The 2.16 SED dose of complete solar simulated light remained the same.

There were no significant differences between incubator control and irradiation control (C/C) cells, though there was a non-significant 43% increase in MitoSOX signal ($p = 0.12$).

The increase in ROS by 2.16 SEDs of complete solar simulated light significantly increased DCFDA signal (one-sample t-test compared to unirradiated control, 48% increase, $p = 0.04$ and 48% increase, $p = 0.004$ for without and with IR irradiation respectively) though there was no significant difference caused by the presence of infrared irradiation ($p = 0.96$, two-tailed unpaired t-test).

In cells stained with MitoSOX there was also a significant increase in signal in response to irradiation with 2.16 SEDs of complete solar simulated light (one-sample t-test compared to unirradiated control, 31% increase, $p = 0.02$ and 21% increase, $p = 0.04$ for without and with IR irradiation respectively) though there was no significant difference caused by the presence of infrared irradiation ($p = 0.4$, two-tailed unpaired t-test).

Compared to cells irradiated in DPBS, cells irradiated in MEMO after being in a water bath for 2 hours (unirradiated with infrared) had a significantly lower DCFDA response to 2.16 SEDs of complete solar simulated light (31% increase versus 139% increase, $p = 0.001$, Figure 5-9 top right “C/SS” versus Figure 5-7 B “Complete”). However, there was a significantly increased response in MitoSOX (48% increase versus 3% increase, $p = 0.014$, Figure 5-9 bottom right “C/SS” versus Figure 5-7 B “Complete”).

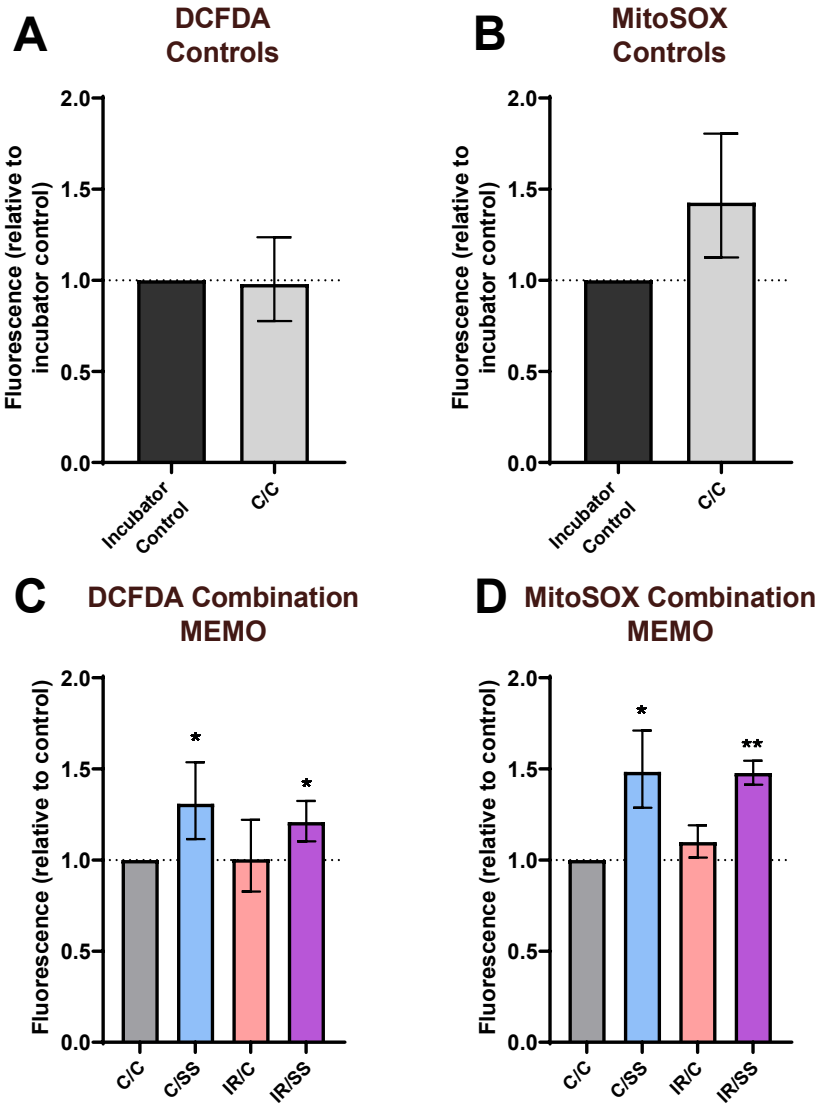

Figure 5-9 Effects on ROS production as measured by DCFDA and MitoSOX on HDFn cells irradiated with infrared then UV light in MEMO

Cells irradiated with 720 J.cm^{-2} infrared only at 100 mW.cm^{-2} for 2 hours (IR/C), 2.16 SEDs of solar simulated light over ~2 minutes only (C/SS), or both (IR/SS) compared to unirradiated control cells (C/C). Incubator controls experienced the same wash steps but remained in the incubator during irradiation time. Unirradiated controls were under the lamp during irradiation but wrapped in foil to receive 0 J.cm-2 of light. Temperature control was a stand for the visible and solar simulated light, and a stirred water bath for infrared light. DCFDA signal in irradiated controls versus incubator controls (A) or irradiated cells versus unirradiated controls (C); MitoSOX signal in irradiated controls versus incubator controls (B) or irradiated cells versus unirradiated controls (D). Data from irradiated cells were normalised to unirradiated controls. Unirradiated control data were normalised to incubator controls for comparison. (*): $p < 0.05$, (**): $p < 0.01$, one-sample t-test on log transformed data; data represent geometric means ± geometric SD, N = 3

5.3.2 qPCR gene expression

5.3.2.1 Single dose, low intensity IR does not affect MMP or COL1A1 gene expression

When irradiated with a single 288 J.cm^{-2} dose of 40 mW.cm^{-2} infrared light when temperature was controlled, there was no change in the expression of MMP1, 2, 3 or COL1A1 compared to unirradiated controls (Figure 5-10). Irradiation took place in seeding medium of complete, phenol-free DMEM with 10% FCS. When unirradiated controls were compared to incubator controls there was significantly lower expression of MMP3 (43% decrease, p = 0.026).

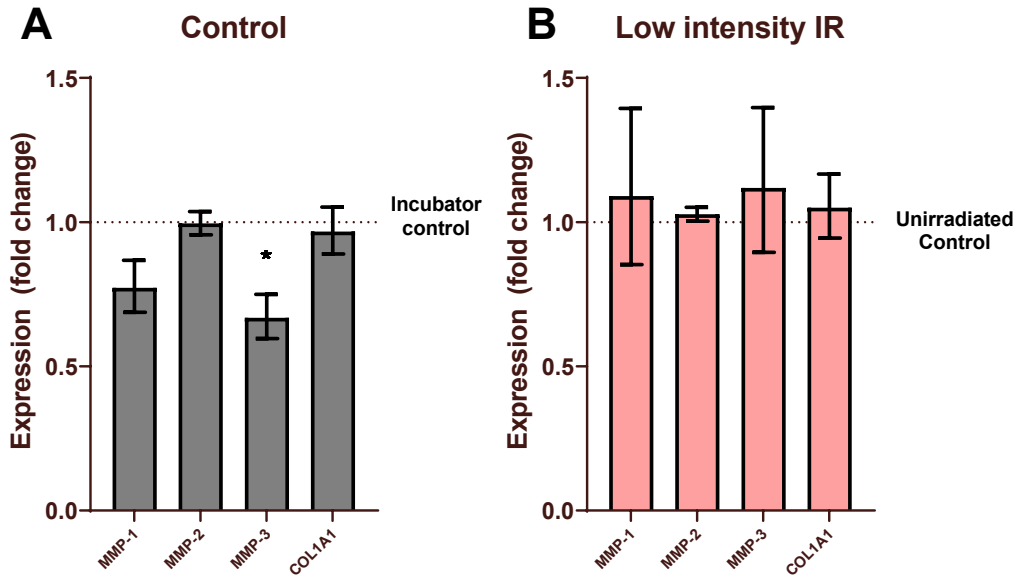

Figure 5-10 Gene expression in HDFn cells in complete 10% FCS phenol-free DMEM irradiated with low intensity infrared.
Cells seeded and irradiated in complete, phenol-free DMEM with 10% FCS were irradiated with 2 hours of low intensity infrared at 40 mW.cm^{-2} for a dose of 288 J.cm^{-2} (Panel B). Unirradiated controls compared to incubator controls (Panel A). RNA was extracted 24 hours after the end of irradiation. Temperature was controlled with a stirred water bath. Incubator controls experienced the same wash steps but remained in the incubator during irradiation time. Unirradiated controls were under the lamp during irradiation but wrapped in foil to receive 0 J.cm-2 of light. Data from irradiated cells were normalised to unirradiated controls. Unirradiated control data were normalised to incubator controls for comparison. (*): $p < 0.05$, one-sample t-test on log transformed data; data represent geometric means ± geometric SD, N = 3, n = 3

5.3.2.2 Repeated dosing of high intensity IR does not affect MMP or COL1A1 gene expression

When HDFn cells in complete, phenol-free DMEM with 10% FCS were irradiated with high intensity infrared every day for three days with a 2- or 10-hour equivalent dose of solar

infrared, there was no difference in gene expression in either condition compared to unirradiated control cells (Figure 5-11). There was no difference between unirradiated controls and incubator controls.

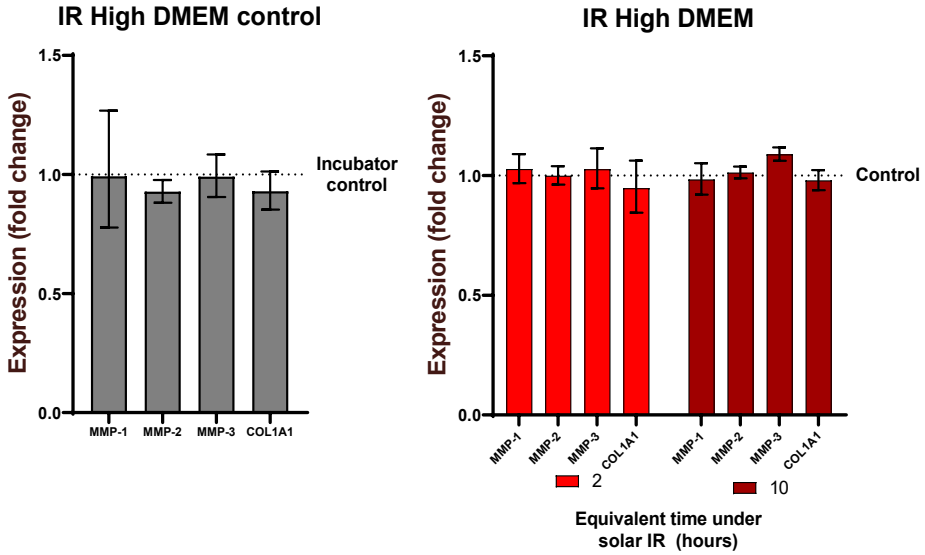

Figure 5-11 Gene expression in HDFn cells in complete 10% FCS phenol-free DMEM irradiated with 2 or 10 hours of low intensity infrared every day for 3 days
Cells seeded and irradiated in complete, phenol-free DMEM with 10% FCS were irradiated with 2 hours of low intensity infrared at 40 mW.cm^{-2} for a dose of 288 J.cm^{-2} (Panel B). Unirradiated controls compared to incubator controls (Panel A). Temperature was controlled with a stirred water bath. Incubator controls experienced the same wash steps but remained in the incubator during irradiation time. Unirradiated controls were under the lamp during irradiation but wrapped in foil to receive 0 J.cm-2 of light. RNA extracted 24 hours after final irradiation. Expression assayed with TaqMan qPCR. Data from irradiated cells were normalised to unirradiated controls. Unirradiated control data were normalised to incubator controls for comparison. Data represent geometric means ± geometric SD, N = 2, n = 3

5.3.3 RNA Sequencing

5.3.3.1 Differentially expressed genes

The infrared and visible light conditions had too few DEGs to carry out pathway analyses. There were differences in the number of DEGs between the cells irradiated with complete solar simulated light versus UV only, with 639 genes significantly differentially expressed compared to control in both, 291 only by complete solar simulated light and 225 only by UV only. In both UV irradiated conditions there were greater numbers of downregulated genes than upregulated genes, which is consistent with the literature (Alafiatayo et al., 2020).

Interestingly, the complete visible condition, while having only 41 DEGs, reflected this pattern. Of all the longer wavelength conditions, it was the one with the largest number of DEGs.

Table 5-1 Genes from each condition with >10 base mean, log2 fold change of ± 0.5 and adjusted p value of 0.05.

Condition	Number of DEGs	Upregulated	Downregulated
Blue	2	0	2
Green	4	0	4
Red	5	1	4
Far red	1	1	0
Complete visible	41	10	31
Low intensity infrared 2-hour dose	3	3	0
High intensity infrared 2-hour equivalent dose	4	2	2
High intensity infrared 10-hour equivalent dose	7	3	4
Complete solar simulated light	930	383	547
Solar simulated UV only	864	360	504

From the volcano plots of Figure 5-12, it is clear that the conditions containing UV wavelengths had many more significantly changed genes than those without. It is also clear that the complete visible condition was more changed than the 100 nm waveband conditions (blue, green, red and far red).

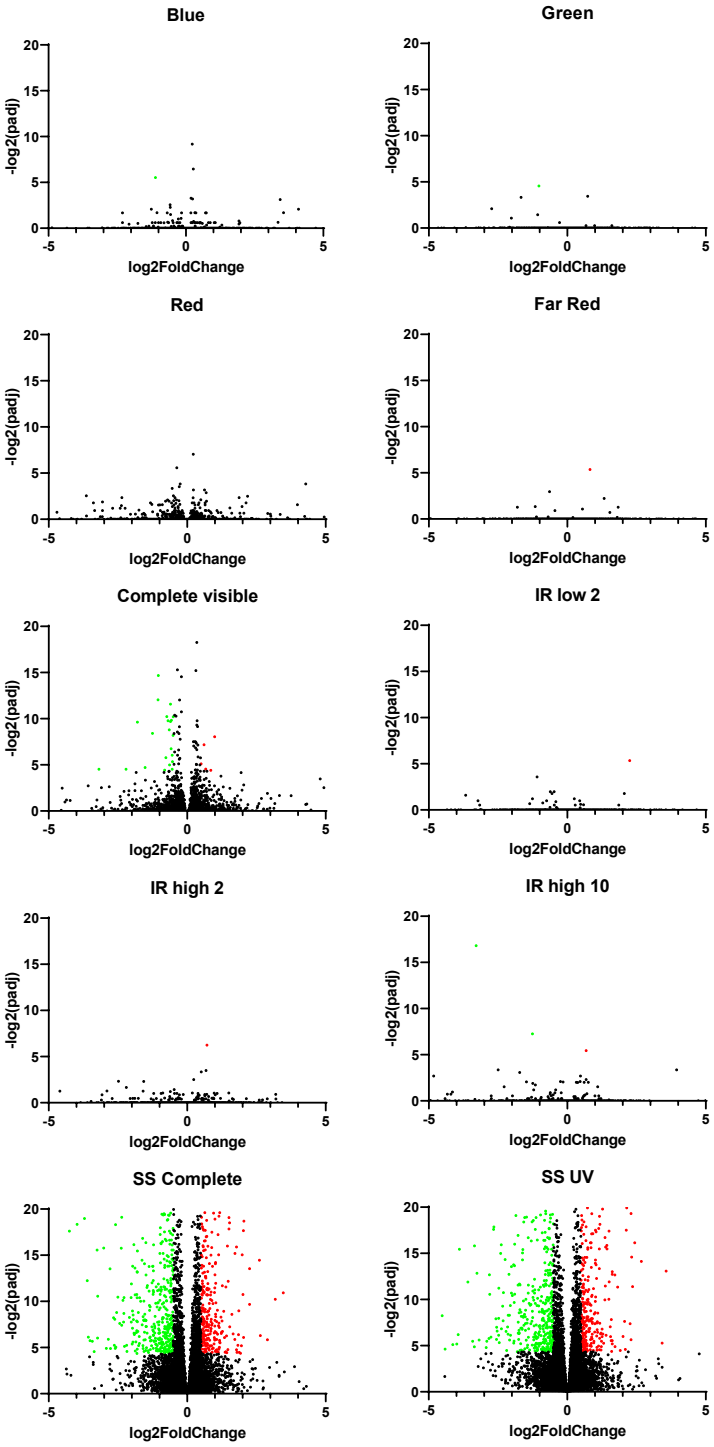

Figure 5-12 Volcano plots of adjusted p value versus log2 fold change.
Green represents significantly downregulated genes; red represents significantly upregulated genes.

5.3.3.2 Pathway analysis

When the gene lists of the complete solar simulated light and UV only conditions were put into the IPA pathway analysis software, a list of significantly affected pathways was produced. The lists for the two conditions were then compiled for further analyses (see Appendix for complete list). A shortened list of pathways with a z score of ≥ 1.5 or ≤ -1.5 was used to see which pathways had been significantly upregulated or downregulated (**Error! Reference source not found.**). This list contained 22 pathways, though not all were relevant to skin. Those that were not (mainly related to neurons, cardiac or adipose tissue) were not included for further analysis, leaving 6 pathways.

The p53 pathway was found to be significantly upregulated in both complete solar simulated light and UV only conditions. The WNT/β-catenin pathway and BRCA1 in DNA damage response pathways were significantly upregulated in the complete solar light condition but not the UV only condition. Cell cycle control of chromosomal replication and IL-15 production pathway were downregulated in both UV-containing conditions, and estrogen-mediated S-phase entry was downregulated in the complete solar light condition only.

Table 5-2 Pathways significantly changed by either complete solar simulated light or UV only with z-score ≥ 1.5 or ≤ -1.5.

Pathways in bold indicate pathways thought to be relevant to skin fibroblasts and are represented in heat maps in Figure 5-13.

	Complete solar simulated light		UV only	
	p-value	z-score	p-value	z-score
Cardiac Hypertrophy Signaling (Enhanced)	4.7E-07	-1.8	5.4E-06	-2.1
p53 Signaling	1.0E-05	2.1	4.2E-06	2.1
Dilated Cardiomyopathy Signaling Pathway	2.4E-05	-1.7	1.2E-04	-0.9
CDK5 Signaling	2.3E-04	-1.9	4.0E-04	-1.4
Estrogen-mediated S-phase Entry	2.6E-04	-1.6	0.001	-1.3
Synaptogenesis Signaling Pathway	0.001	-3.4	0.106	-3.1
Cell Cycle Control of Chromosomal Replication	0.001	-2.8	0.000	-2.8
Glioma Signaling	0.002	-1.6	0.003	-0.4
Neurovascular Coupling Signaling Pathway	0.007	-3.0	0.071	-2.9
WNT/β-catenin Signaling	0.010	1.5	0.000	0.5
GP6 Signaling Pathway	0.016	-2.5	0.244	-1.6
Endocannabinoid Neuronal Synapse Pathway	0.019	1.7	0.011	0.3
Role of BRCA1 in DNA Damage Response	0.025	1.6	0.126	1.0
White Adipose Tissue Browning Pathway	0.027	-1.9	0.087	-2.1
Gustation Pathway	0.032	-2.1	0.358	-0.8
IL-15 Production	0.033	-1.7	0.223	-1.6
Dopamine-DARPP32 Feedback in cAMP Signaling	0.033	-1.7	0.019	-1.3
Oxytocin In Spinal Neurons Signaling Pathway	0.035	-2.0	0.028	-2.0
Endothelin-1 Signaling	0.045	1.7	0.026	1.2
Apelin Adipocyte Signaling Pathway	0.046	2.0	0.031	1.0
Oxytocin Signaling Pathway	0.048	-1.5	0.048	-1.3
Synaptic Long Term Depression	0.049	-1.2	0.060	-1.5

As the complete solar simulated light condition had the greatest number of DEGs overall, the DEGs from this condition in the 6 pathways identified above were ranked from greatest upregulation to greatest downregulation and the expression of those genes in all the conditions tested are shown on the heat maps in Figure 5-13. Though the other conditions did not have enough DEGs to test with IPA, the genes in the pathways changed by UV light could be compared.

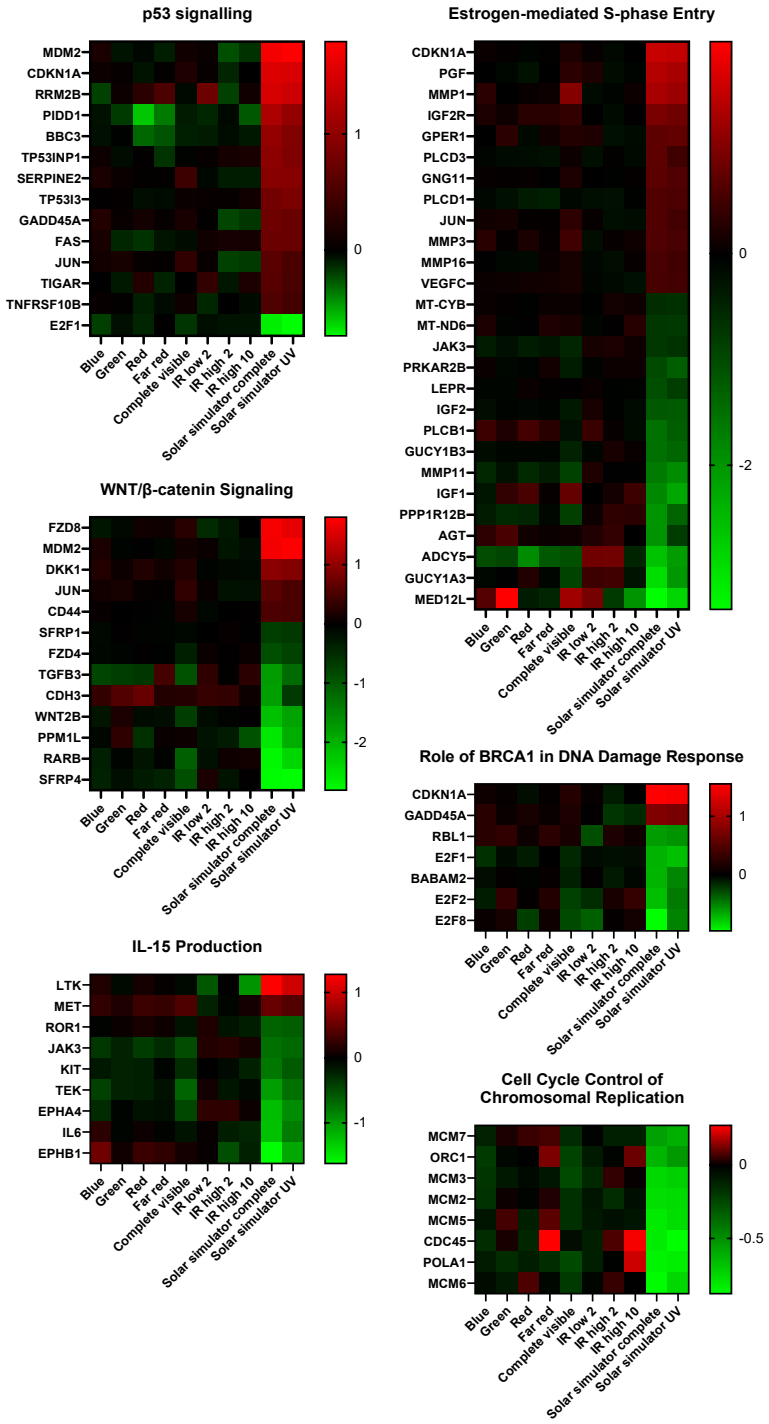

Figure 5-13 Heat maps of pathways thought to be relevant to skin fibroblasts that were significantly changed by complete solar simulated light or UV only.

5.3.3.3 *Individual genes of note*

Some genes had a similar pattern of expression in the complete visible and the UV irradiated conditions, such as MMP1 and MMP3, though not all ECM proteins were affected in the same way, with COL1A1 being affected only by UV and not the visible light. Ferritin light and heavy chains had significantly increased expression in the complete visible condition but not the UV conditions. Ferritin heavy chain was also significantly upregulated in the blue light irradiated condition, but the light chain was not.

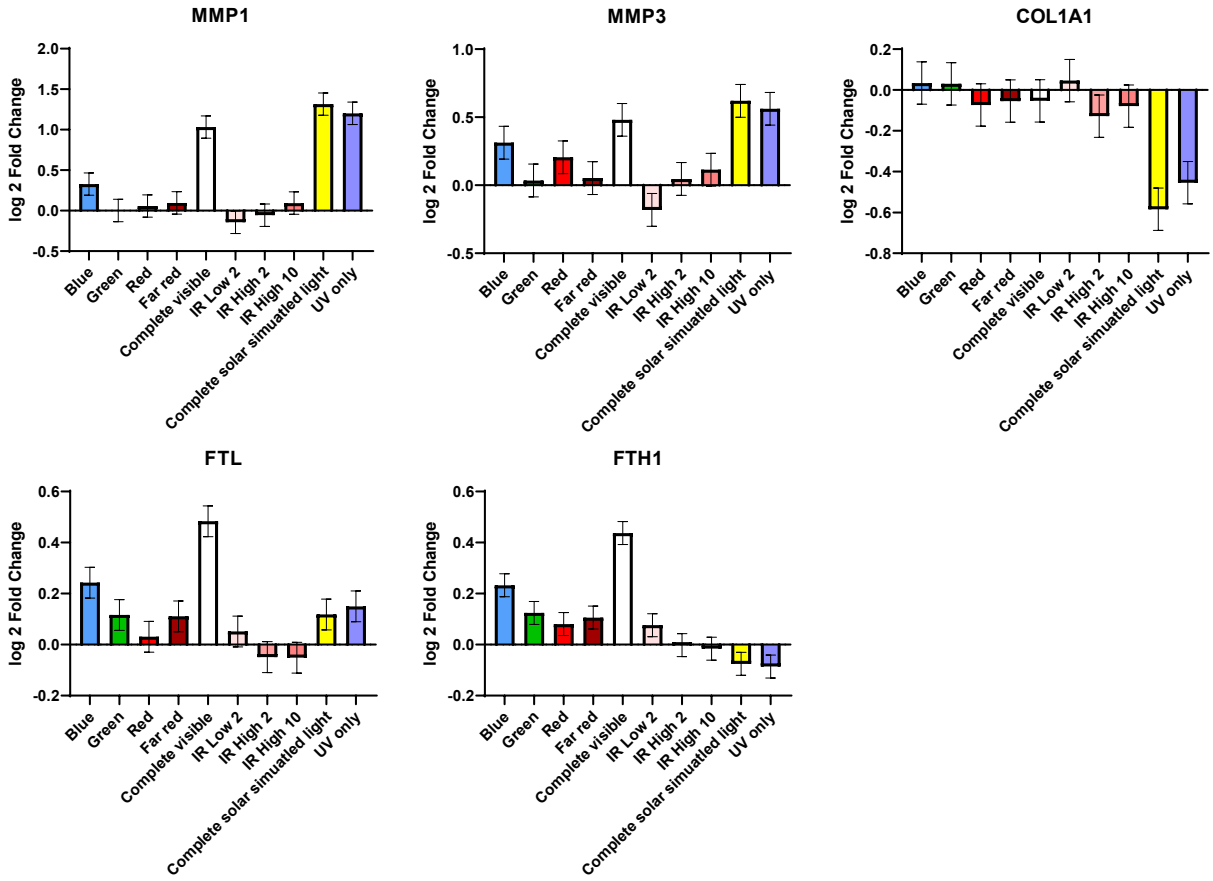

Figure 5-14 Expression of genes across each condition, each as compared to condition control. *Error bars represent mean ± SEM, N=3.*

5.4 Discussion

5.4.1 Reactive oxygen species production

5.4.1.1 DCFDA plate assay

The effect of filters on the DCFDA signal from irradiation with 2.16 SEDs of complete solar simulated light demonstrates that the DCFDA assay performs as expected, reflecting the increase in ROS seen by different wavelengths of incident light.

DCFDA signal was increased nearly 3-fold in cells irradiated with 2.16 SEDs of complete solar simulated light. This shows that the cells are experiencing oxidative stress as a result of irradiation, which is expected given what has been shown previously many times in the literature. 24 hours after irradiation, however, ROS was seen to be 42% lower in irradiated wells compared to unirradiated wells. This could represent several biological phenomena. Firstly, it may be that some cells have undergone apoptosis as a result of irradiation, detached from the culture plastic and were subsequently washed off during the DCFDA assay, resulting in fewer cells being present in the well when the plate was read. Secondly, it could represent that since the cells have experienced DNA damage as a result of the irradiation and have arrested the cell cycle in order to repair the damage, proliferation would be reduced in these cells and the cell number would be less in the irradiated wells compared to the unirradiated wells. Thirdly, it could be that as a response to the oxidative stress experienced 24 hours earlier, the cells have increased the production of antioxidants and reduced basal ROS levels in the cell. This has been demonstrated to happen in response to UVA irradiation in melanoma cells (Hansda and Ghosh, 2021).

With both low and high intensity infrared irradiation, there was no change in DCFDA signal after irradiation. There was also no change in DCFDA signal from cells 24 hours after high-intensity irradiation. There were no differences between irradiation and incubator controls. These results indicate that there is no ROS production or oxidative stress as a result of infrared irradiation.

5.4.1.2 Flow cytometry of DCFDA and MitoSOX

5.4.1.2.1 TMRE

TMRE staining with flow cytometry was used to examine the mitochondrial membrane potential in cells treated with light. UV has been shown to change the mitochondrial membrane potential in a cell density and time-dependent manner in HaCaT cells (Zanchetta et al., 2010) though not in fibroblasts (Kelly and Murphy, 2016).

The other reason for including a measure of mitochondrial membrane potential was that any cells with depolarised mitochondrial membranes would need to be excluded from MitoSOX readings since this would release the MitoSOX into the cytoplasm and give high MitoSOX fluorescence which could skew results. In these experiments however there was no such population of low TMRE staining after gating out dead cells and debris, so it could be assumed that in the separately stained MitoSOX condition, such cells would also not be present.

5.4.1.2.2 ROS detection in unirradiated cells

There was a 77% reduction in the DCFDA signal from cells that had been incubated in MEMO for 24 hours prior to staining compared to cells that had been maintained in phenol-free medium for 24 hours prior to staining. The difference in DCFDA signal could be due to several factors. Because the cells were serum-starved for the 24 hours leading up to the irradiation, it is likely that the cells were stalled in their cycle at G_0, reducing proliferation and perhaps metabolism. Additionally, reduced riboflavin may have affected the redox systems within the cells, though it would be expected that a reduction in flavocoenzymes would increase ROS through leak from an ETC with reduced efficiency.

DCFDA signal was shown to increase 9-fold and MitoSOX 7-fold in serum-starved cells for 24 hours as detected by flow cytometry in hybridoma cells (Liu et al., 2012). DCFDA signal was increased 3-fold in serum-limited dermal fibroblasts for 48 hours (De Rasmo et al., 2011) and DH2 signal was increased similarly in serum-starved dermal fibroblasts (Boraldi et al., 2008).

In mouse macrophages, 6 hours of riboflavin deficiency resulted in a reduction in superoxide required for an effective phagocyte immune response (Schramm et al., 2014). However, in

intestinal cells, riboflavin depletion for 24 hours increased DCFDA signal (Lee et al., 2013). In liver cells, 4 days of riboflavin deficiency led to cell cycle arrest, a reduction in glutathione reductase activity and an increase in carbonylated proteins and DNA strand breaks suggestive of oxidative stress (Manthey et al., 2006). In the experiments in this thesis, riboflavin starvation for one day in HDFns led to a reduction in stress signal as measured by MMP1 reduction, but after 3 days saw an apparent reversal of gene expression pattern, which could indicate an initial drop in oxidative stress then an increase with duration of riboflavin deficiency.

5.4.1.2.3 UV induction of ROS

When the response of cells to irradiation with complete solar simulated light and UV only light was tested with DCFDA through flow cytometry, there was an increase in signal compared to unirradiated controls of over 2-fold. This was expected and was in a similar range to when the cells were tested with DCFDA in a plate assay, indicating that despite its limitations, DCFDA in a plate assay is still effective at reflecting cellular ROS. Given that the two conditions received the same dose of UV light in SEDs with similar UVA and UVB composition, it seems logical that they would both have the same degree of increase in ROS signal. The additional wavelengths of visible light in the "complete" condition delivered in the approximately 2 minutes the 2.16 SEDs took to deliver would have been equivalent to about 45 seconds of solar visible light, so it would not be expected that this component would cause any significant change in ROS during this length of irradiation.

There was no change in signal from MitoSOX however, which was somewhat surprising. MitoSOX signal has been shown to increase as a result of UVA irradiation in unpigmented melanoma cells (Swalwell et al., 2012a), though these were irradiated in the presence of riboflavin which may explain the difference to the results in this thesis where riboflavin was washed out, along with the difference in cell type. Other papers have shown no effects of UVA or UVB on MitoSOX signal from fibroblasts, but Schroeder et al. reported an increase in MitoSOX from infrared irradiation with only a 30 $J.cm^{-2}$ dose, though there is no mention of temperature control so this may have been caused by heating (Schroeder et al., 2007). The high DCFDA signal and unchanged MitoSOX signal from UV-irradiated cells suggest that the

ROS produced by the UV light was not specifically superoxide in mitochondria, but rather ROS produced elsewhere in the cell, as DCFDA reacts with more ROS species and within the cytoplasm. Chromophores for UV exist throughout the cell, and UV-induced DNA mutations would not yet have had an effect on the ETC component transcription. UVA has been shown to decrease the ATP content of cells and the oxygen consumption rate of mitochondria, which could indicate less activity in the ETC (Djavaheri-Mergny et al., 2001). This would be expected to cause a reduction in superoxide production, though here neither an increase nor reduction was seen.

5.4.1.2.4 Visible light induction of ROS

There were no significant changes in ROS measurement by either DCFDA or MitoSOX by visible light irradiation. It was expected that visible light, in particular blue light, would have increased the ROS in cells. Liebel et al showed that visible light from a source similar to the one used in the complete visible condition in this thesis (i.e., with a broad range of irradiation wavelengths) increased DCFDA signal (Liebel et al., 2012). However, their method of incubating cells with DCFDA prior to irradiation has been shown to increase DCFDA in this thesis with infrared light (see Chapter 3) (Swalwell et al., 2012b), and they irradiated in medium containing riboflavin which has been shown to generate ROS with visible light (Silva et al., 1994, Wang and Nixon, 1978, Maguire et al., 2011).

However, the lack of ROS measured may be due to the low intensity of the light from the solar simulator compared to that of the sun. The blue light condition was about 63% as bright as solar noon sunlight from the midsummer Mediterranean sun, though the intensity would be about the same as that found in Newcastle-upon-Tyne, UK at solar noon in mid-September. This meant that the irradiation took approximately 1 hour and 35 minutes to deliver the one-hour dose of blue light, and the complete visible condition was comparatively less at 37% the average irradiance across all wavelengths compared to solar intensity across the same wavelengths, resulting in an irradiation time of approximately 2 hours 41 minutes. With these long irradiation times, any ROS generated may have already reacted with either antioxidants or cellular components, and thus not be detectable by DCFDA or MitoSOX probes. Alternatively, it could be that if ROS are being produced due to

visible irradiation, they are not produced at such a high rate or total amount that they overwhelm the cells' antioxidant capacity, and most of the radicals have reacted with endogenous antioxidants like glutathione or catalase.

5.4.1.2.5 UV and infrared in subsequent irradiations

When cells were irradiated with infrared and then complete solar simulated light in either DMEM/DPBS or MEMO, the infrared light made no impact on the DCFDA or MitoSOX signal. However, there were some unexpected results in the effects of the 2.16 SED dose of complete solar simulated light on the cells that had been in the water bath but were not exposed to the infrared light. These cells had reduced DCFDA response to the 2.16 SEDs, even though the irradiation conditions were identical other than the prior incubation in the water bath rather than remaining in the incubator. The exposure of these cells for 66.7 minutes to a lower CO_2 (with atmospheric CO_2 approximately 0.04% and incubator CO_2 5%) and temperature (water bath temperature 26 – 31°C versus incubator 37°C) may be the reason for this, as there were no other differences in the handling of the cells. The unirradiated control cells that were in the water bath were found to have higher DCFDA than those that were in the incubator at that time, so potentially the cells were exposed to stress before this, making the increase in stress by UV lower.

The unirradiated control cells in MEMO, however, had no higher DCFDA signal than the incubator controls in MEMO, so there was no apparent increase in stress due to the irradiation conditions. There was however still a reduced DCFDA response to 2.16 SEDs, which could potentially be due to the difference in riboflavin in the cells. The washout period may have reduced the riboflavin and therefore its photosensitising effects on the cells, but additionally, the riboflavin starvation was previously shown to reduce the basal DCFDA signal from the cells, indicating potential impacts on the redox state of the cells.

Furthermore, cells in MEMO had significantly increased MitoSOX signal when exposed to UV light, whereas cells previously incubated in DMEM repeatedly showed no increase in MitoSOX signal. This is a surprising difference, which could be due to a number of factors. The incubation in the water bath may have made a difference to the cells, as it did with DMEM, or the riboflavin and serum starvation conditions.

5.4.2 qPCR gene expression

When HDFn cells were irradiated with a single dose low intensity infrared light there was no difference in gene expression between cells irradiated with a 2- or 10-hour dose of infrared light in DMEM + 10% FCS every day for three days compared to unirradiated controls. In cells irradiated over three days with a high intensity and dose of infrared light, there was again no difference in gene expression. It would be expected that any effect of a single infrared irradiation would be amplified by repeated irradiation over there days, but the lack of any change to gene expression implies that where others have published changes in MMP expression after infrared irradiation, it may have been due to inadequate temperature control rather than to effects of the wavelengths themselves.

5.4.3 RNA Sequencing

5.4.3.1 RNA Sequencing overview

As expected, the UV light had the greatest effect, with over 800 genes with base mean expression greater than 10, adjusted p value greater than 0.05 and log 2 fold change greater than ± 0.5 in both conditions (complete solar simulated light and UV only). The number of DEGs was very low in all the other conditions, with infrared producing a maximum of 7 DEGs from the > 15 000 genes tested. Complete visible light showed the largest change of all these longer wavelength conditions, which is expected given that the dose of light was larger in this condition than the others combined in these experiments (as there were some gaps between wavebands, e.g. blue was 410 - 510 nm and green was 515 – 610 nm). This result would also be expected where it is believed that blue light from the sun has the greatest effect of all the visible light components on skin, as this condition had a higher dose of blue light than the blue light condition by 70% (84.3 $J.cm^{-2}$ versus 49.7 $J.cm^{-2}$). The effects of the ~100 nm wavebands did not add up to the sum of its parts – the complete visible conditions – in terms of DEGs. This may have been due to the statistical cut-offs used if the same genes were changed but were only changed enough to be significant by the complete visible condition. The effect could potentially be synergistic, but more experiments would need to be performed to support this conclusion.

5.4.3.2 Pathway analysis

From the heat maps, it appears as though the pattern of gene expression from the complete visible condition is similar to that of UV but altered to a lesser extent in most of the 8 pathways except p53 signalling. It could be that visible light can have effects on these pathways, though this would need to be investigated further before conclusions could be drawn. There was no obvious similarity between the infrared conditions and the UV irradiated conditions, which may have been expected if it was it was believed that infrared causes oxidative stress as UV does, though this is not thought to be likely from the results in this thesis.

p53 signalling was significantly downregulated in both UV-containing conditions. p53 is a tumour suppressing mechanism which is activated in response to DNA damage and is known to be activated in response to UV irradiation in skin by affecting the transcription of genes leading to arrest of cell-cycle progression or induction of apoptosis (Sakaguchi et al., 1998). While this pathway was upregulated in the UV irradiated conditions, there was no similar pattern of regulation from the DEGs from any of the other conditions. There was potentially an opposite activation pattern in the high intensity infrared light conditions, though the changes in expression were small. As expected, the pathway "Cell cycle control of chromosomal regulation" was downregulated significantly in both UV irradiated conditions, given the expected DNA damage by UV and upregulation of the p53 pathway (Enoch and Norbury, 1995).

The "Estrogen-mediated S-phase entry" pathway was also significantly downregulated in both conditions. While the fibroblast cells were not exposed to different levels of estrogen with irradiation conditions, this pathway being downregulated is related to the p53 and cell cycle control of replication pathways and provides further evidence of the influence of UV on the cell cycle. Of all the conditions that did not include UV wavelengths, the complete solar simulated light condition was most similar in its pattern of gene expression in this pathway, though there were some differences in this pattern. Further work to determine the cell cycle and proliferation effects of physiological levels of visible light would be useful to determine how likely this is to be relevant to skin in sunlight in vivo.

The BRCA1 DNA damage response pathway was significantly upregulated in cells irradiated with complete solar simulated light, but not UV-only. BRCA1 is another tumour suppressor gene and is important in DNA repair and DNA-damage-induced apoptosis. It is involved in the repair of double strand breaks but also inter-strand crosslinking and ROS damage (Pathania et al., 2011).

The WNT/β-catenin signalling pathway was significantly upregulated in both the UV irradiated conditions, though the z-score was higher for the complete solar simulated light condition rather than the UV only condition. Wnt proteins are growth factors involved in development, and influence cell differentiation and proliferation. Wnt signalling in skin has been shown to occur during wound healing as a response to UV irradiation (Houschyar et al., 2015, Rognoni et al., 2021). The visible light conditions, particularly the complete visible condition, appeared to have a similar but less pronounced pattern of activation in the DEGs of the complete solar simulated light WNT/β-catenin signalling pathway, which may indicate activation of this pathway but to a lesser degree.

The IL-15 production pathway was significantly downregulated by complete solar simulated light, but not by UV only. IL-15 is an immunomodulating cytokine produced in fibroblasts and keratinocytes in the skin. IL-15 mRNA expression has been seen to be induced 1 and 6 hours after UVB irradiation of dermal cells but then reduce at 24 hours (Mohamadzadeh et al., 1995). It may be that the reduction in IL-15 production found after 24 hours in this study comes after an enhancement of the pathway sooner after irradiation.

Differences between complete solar simulated light and UV only are potentially due to the differences in visible and infrared light components, but it is more likely to be due to the differences in UVA and UVB composition. In the UV only condition, only 7% of the erythemally-weighted UV is UVA, whereas the complete solar simulated light condition is 14% erythemally-weighted UVA.

5.4.3.3 Individual genes

There were few similarities between the results in these data and those in the paper by Calles on infrared effects on transcription (Calles et al., 2010). Of the 13 genes they took for

further analysis, 10 had high enough expression to be found in the dataset in this thesis, and none had a significantly different expression compared to control with adjusted p value. With unadjusted p value, only one had a significantly changed expression, ITPR2, which was only decreased in the high intensity infrared 2-hour dose condition.

Of all the conditions irradiated with only longer wavelengths, only the complete visible condition showed results of note. ECM degrading proteins MMP1 and MMP3 were upregulated by the complete visible condition to a similar degree to the UV conditions, though COL1A1 expression was not changed unlike in the UV conditions. It is possible that these effects could be through the effects of blue light, as although this condition showed less of a response than the complete visible condition it was the most similar of the visible wavebands and would be expected to be less if only the blue is having an effect as the dose of blue light was higher in the complete visible condition than the blue condition.

Ferritin light and heavy chains were upregulated in the complete visible condition, but not in the UV irradiated conditions. Blue seemed to have a similar but less pronounced response. UVA irradiation has been shown to induce labile iron release through damage to lysosomes and ferritin by ROS, resulting in downstream induction of NF-κB (Reelfs et al., 2004, Pourzand et al., 1999). The free iron can then catalyse the Fenton reaction, creating hydroxide ions and hydroxyl radicals from hydrogen peroxide, exacerbating oxidative damage. UVA has been shown to induce ferritin expression in epidermal and dermal cells (Applegate et al., 1998), and visible white and blue light has been shown to cause damage through iron in eye cells (Ohishi et al., 2006, Rodriguez and Fliesler, 2009). Visible light here may be causing oxidative stress through the same process, with the increase in ferritin expression a result of oxidative stress catalysed by iron.

One of the major differences between the visible irradiation and the UV irradiations was the duration of exposure; the complete visible condition was delivered over ~2.5 hours and the UV conditions over ~2-3 minutes. If both are causing responses due to ROS or oxidative stress, the lower level, longer duration may be affecting the cells in a different manner.

5.4.3.4 Limitations

Due to the low dose of visible and infrared lights, few DEGs were indicated by the thresholds of adjusted $p < 0.05$ and log 2-fold change $> \pm 0.5$. This limited the analysis that could be performed to the comparison of expression in pathways upregulated by UV rather than direct pathway analysis. Further insight from this data could be gleaned through altering the thresholds for significance, though this runs the risk of indicating genes and pathways that are not truly affected.

5.4.4 Summary

In all experiments, it was found that when temperature was controlled for, there was no change in ROS production or gene expression when cells were irradiated with infrared light. There was no significant effect of infrared on the expression of MMP1, 2, 3 or collagen with single or repeated infrared dosing, indicating that these acute infrared doses do not affect the extracellular matrix regulation by fibroblasts when the temperature does not exceed 37°C.

Visible light was also found to have no effect on reactive oxygen species production after washout of riboflavin and 24 hours of serum starvation. It may be possible that if there was no riboflavin washout that riboflavin in the cells would have been photosensitising, but it is difficult to compare in vitro conditions such as cellular riboflavin to those found in vivo, making it difficult to best mimic the actual effects that the presence of riboflavin at "normal" skin concentrations has when it is exposed to sunlight. The other difference between the visible light irradiation and the UV irradiations which makes it more difficult to compare is that the visible light was delivered over up to four hours, whereas the UV dose was delivered in a maximum of ~3 minutes. If the visible light was inducing ROS, it would have been over a longer time period, over which the cells may have been better able to cope with slower ROS production. In the UV condition, the ROS would have been generated over a shorter time period and more quickly overwhelmed the cells' antioxidant capacity, allowing measurable ROS to be present during DCFDA staining.

From the RNA sequencing results, it is clear that the infrared had little effect on cells, and the visible had much less of an effect than the UV-containing conditions. It is possible from

examining individual genes from the complete solar light condition that there may have been some changes in cell behaviour, though to a lesser degree. ECM-modulating enzymes MMP1 and MMP3 were induced by the complete visible light condition, and ferritin was induced, indicating a potential ROS-mediated effect on cell photoaging from visible light.

Chapter 6 Discussion

6.1 Overview

The study of visible and infrared light in vitro is complex and affected by many variables. The literature is full of conflicting data about the effects of these wavelengths in the skin from sunlight and from lamps for clinical use, with data showing harm through oxidative stress or heating but also data showing benefits for wound healing clinically (Barolet et al., 2016, Grether-Beck et al., 2014).

In vitro, culture conditions can have a great impact on irradiation effects seen in cells, as light has the ability to radicalise tissue culture plastics, produce radicals in the presence of components of cell culture medium, and cause damaging temperature increases. This thesis has demonstrated the effects of some of these issues and methods for resolving them.

6.2 Irradiation conditions for in vitro visible and infrared light

Infrared light is responsible for the "warmth" transmitted by solar light. Skin surface temperature during sun exposure has been shown to be increased above the temperature of unirradiated skin, and of skin when the body is in shade, though it does not appear to exceed 37°C (Kurazumi et al., 2014, Petersen et al., 2014, Cho et al., 2008). At high temperatures, artificial infrared irradiation both in vitro and in vivo has the ability to generate heat shock responses which can appear similar to UV damage responses, with increased MMP-1 and MMP-3 (Park et al., 2004). It is then difficult to determine what effect is occurring from the heating effect of infrared light rather than a chromophore-mediated effect, given that they can appear the same.

In the literature, different methods are used for the control of temperature during irradiations, and sometimes temperature control is not mentioned at all. In this thesis, a method using tissue culture plates and dishes suspended in a stirred water bath with the bottom of the plate/dish in contact with the water was demonstrated through thermal imaging to control temperature to below 37°C. The temperature of the cells did increase over the course of infrared irradiation from room temperature at the start to ~32°C at the

end, though it was measured to be the same in exposed and foil-covered, unirradiated wells or dishes.

While many UV irradiations, including those used as positive controls in this thesis, are carried out over a period of minutes, this does not represent the condition of skin exposed to sunlight. Exposing cell in vitro to irradiances of visible and infrared light which are comparable to that from the sun requires long-duration exposures. These come with issues, such as medium composition and, when out of the incubator, temperature and pH. Medium which is normally buffered by 5% CO_2 in a humidified incubator will become more alkaline over time when exposed to atmospheric CO_2 concentrations of 0.04%. While any change in pH will be the same in irradiated and unirradiated plates/dishes, an increased pH may affect the cells' responses to light, potentially by compounding the stress experienced (Schneider et al., 2007, Gethin, 2007, Petronini et al., 1995). The tissue culture buffer HEPES, which is widely used to maintain physiological pH in variable CO_2 conditions, is reactive in the presence of visible light, resulting in the production of H_2O_2, cell toxicity and death. This has been demonstrated in this thesis, where blue light had the greatest loss of cell viability after irradiation in medium containing HEPES. The method detailed in this thesis involves wrapping parafilm around the plate or dish to minimise gas exchange over the course of the irradiation. It did not stop the pH of the medium from increasing, but the increase was reduced compared to dishes where the film was not in place. This method could be improved by irradiation being carried out inside an incubator, though this limits the light sources which could be used.

Further medium limitations come from the presence of riboflavin in cell medium. Riboflavin absorbs UV and visible light up to 540 nm, and after absorption of light reacts with tryptophan to produce ROS. Flavins in cells are components of flavocoenzymes which are essential to the function of many flavoproteins which maintain electron transport chain function and redox homeostasis. In the cell, these can also be photosensitising, but without them, the cell does not function normally. There is therefore a balance to be struck between minimising the photosensitising presence of riboflavin and negatively affecting cell behaviour by riboflavin starvation.

Many studies irradiate cells with visible light in DMEM, MEM or opti-MEM, which contain riboflavin, and some leave the cells in the irradiation medium after irradiation. Generation of ROS and damage from oxidative stress would be expected from cells incubated in medium that had been irradiated prior to putting it on the cells, and it has been shown that medium exposed to visible light reduces the proliferation of cells due to the photoproducts of riboflavin (Wang, 1976). In order to avoid this, MEMO medium, which has the same formulation as DMEM except for the lack of riboflavin, was used. A protocol for the washout of riboflavin and photosensitising FBS components over 24 hours was employed for visible light exposures to ensure that the effects seen are not from prior riboflavin loading in cells.

6.3 Assays for irradiation

Solar light has been shown to induce the formation of ROS in skin, leading to damage to DNA, lipids, proteins and other cellular components. Assaying ROS in adherent cells in vitro requires the cells to become adhered to a plate or dish, commonly made from polystyrene which can be treated to enhance adherence. Polystyrene is an aromatic polymer which absorbs light, particularly in the UVB region of the solar spectrum, which can produce free radicals and affect cell adherence (Welle and Gottwald, 2002). Experiments in this thesis show that the Promega ROS-Glo assay, which is designed to react with H_2O_2 in cells to give a concentration-dependent luminescent signal, reacts with UV-irradiated polystyrene, generating false positives. This was shown to be dose-dependent in a non-linear fashion, and also to increase signal from unirradiated plastic on the covered side of the polystyrene 96-well plate though to a lesser extent than the irradiated side. This demonstrates that this assay should not be used for irradiation experiments involving UV and potentially other wavelengths.

DCFDA was shown not to respond in this manner to irradiated tissue culture plastics, though it was demonstrated that DCFDA was sensitive to light itself, even when irradiated with infrared light. This means that for any experiment involving light irradiation it would be unwise to incubate cells with DCFDA until light exposure has ceased.

During flow cytometry experiments, the co-staining of MitoSOX for mitochondrial superoxide measurement and TMRE for mitochondrial membrane potential measurement

demonstrated an interaction of the stains with each other. This could have been either through each stain affecting the other dye itself, or the superoxide/membrane potential being stained. This does not mean that the stains themselves are not useful, though it does imply that these stains should be used with caution, and the biological effects and interactions of the stains themselves considered when interpreting results.

The 11 kb mtDNA strand break assay in its current form cannot be used as a quantitative assay, as the results cannot be plotted on a graph with a linear range (Hanna et al., 2019). It may be possible to use this as a qualitative assay, but it would require further development to enable it to be used as a quantitative measure of DNA strand breaks.

6.4 Effects of solar intensity visible and infrared lights

When appropriate temperature controls are put in place, infrared light at low and high intensities does not induce the formation of ROS measurable with DCFDA, which does not support the theory that infrared in sunlight induces ROS. Furthermore, it does not affect the formation of ROS as a result of UV irradiation, which does not support the theory that infrared has a protective effect on skin against subsequent UV irradiation. Similarly, the expression of ECM genes (MMPs and collagen) was unaffected by infrared light under both high intensity and low, physiological intensity conditions. Of course, in this thesis, the temperature of irradiated and unirradiated cells was kept the same, so while this opposes the effect of any chromophore-induced effects it may still be possible that infrared can affect skin in vivo by changing its temperature.

Visible light at an intensity lower than that from the noon, midsummer Mediterranean sun was found to have no effect on ROS production when irradiated in medium without riboflavin. There is the possibility that other studies may have been unintentionally creating ROS through riboflavin-mediated photosensitivity, resulting in greater responses in vitro than should be expected in vivo.

6.5 RNA sequencing

As expected, cells irradiated with UV had a greater number of differentially expressed genes (DEGs) than cells irradiated with the longer wavelength components of solar light. While

there were differences between the complete solar simulated light condition and the UV only condition, this is likely due to differing compositions of UVA and UVB light rather than additional longer wavelengths at lower intensity.

Infrared irradiation of HDFn cells had very little effect on gene expression. In each of the 3 infrared irradiated conditions, there were a maximum of 7 DEGs, of which several were not protein-coding genes. While this opposes the studies that suggest that infrared causes oxidative stress, ECM remodelling or retrograde mitochondrial signalling, it is possible that these are seen in those studies as a response to the heating induced by infrared light rather than the wavelengths themselves (Piazena and Kelleher Debra, 2010, Jung et al., 2010). To model the effects of infrared-induced heating in vivo in monolayer cells in vitro, it would be necessary to tightly control the temperature to accurately reflect the in vivo temperature, though it is difficult to know the exact temperature of the different depths of skin during sun exposure as this is dependent on many factors. The data in this thesis show that there are no acute infrared irradiation effects when temperature is controlled that would necessitate protection in sunscreen, though this cannot take into account any chronic effects, especially when heating is involved, and it may be useful in sun protection to protect against these heating effects.

Visible light was found to have a greater effect than infrared, with complete visible light having the most DEGs of the visible conditions. This would be expected with its greatest irradiance overall, and greater blue dose than the blue condition alone, though it makes it more difficult to compare these two conditions. ECM remodelling genes MMP1 and MMP3 were significantly upregulated in the complete visible light condition as they were in the UV irradiated conditions, while ferritin light and heavy chains were induced in the complete visible light condition and not at all in the UV conditions. It may be that there are effects on skin from the irradiation of sunlight-intensity visible light when delivered over relevant timescales, such as the ~2.5-hour irradiation used in this thesis. This could be a factor to consider when irradiating in conjunction with UV, but also through sunscreens. These allow through small amounts of UV but all the visible light, potentially contributing to damage and photoaging even in the presence of sun protection.

6.6 Future work

Going forward, it should be a priority for in vitro studies involving light irradiation to carefully consider the conditions that cells are irradiated in. To understand the effects of infrared light, they must be separated into photochemical (mediated by chromophores), and heating (through the ability of infrared to be absorbed by water and increase temperatures in skin). Irradiance and dosing must also be taken into account: though many studies use high intensity infrared light as a method of mimicking the exposure of skin to much lower intensity infrared light from the sun, this is clearly not a perfect comparison, and the results can be due to changes in temperature above what normal irradiance may cause, confounding the comparison to sunlight.

In terms of infrared protection, it is not yet clear whether this is something that must be taken into account when formulating sunscreens. In vivo studies separating the effects of UV, visible and infrared in volunteers exposed to real sunlight, measuring temperature of the skin surface and also the underlying tissues would be very informative. Should temperature increase to a damaging degree, infrared could exacerbate damage by UV light. In this case, it may be useful to include infrared-reflecting ingredients in sunscreens to limit or slow the increase in temperature caused by infrared. However, it may be that a change in temperature has no effect or even a protective effect as some believe.

The role of iron and ferritin in the effects of visible light on skin is an area which has yet to have much research. As visible light may induce oxidative stress, how similar this is to the processes involved in UV-induced oxidative stress is not well elucidated. Further investigation into the role of iron in oxidative stress caused by visible light will be necessary to determine the importance of these processes in sun damage and photoaging.

One of the limitations of the work on visible light in this thesis is that although every care has been taken to eliminate UV “contamination” of visible light irradiations, meaning any UV getting through was undetectable, even trace UV could have effects on cells given the power of each photon. Validation of this work with light sources from which UV is not produced at all, thus removing any doubt of the source of biological effects seen would be valuable. Furthermore, for in vitro irradiation with visible light, experiments to determine different

riboflavin concentrations present in medium prior to irradiation affects the response of cells to light would be useful, as the effects of riboflavin presence or starvation will both impact the results seen.

Appendices

Appendix A: IPA Pathways significantly affected

Table A-1 Significantly affected pathways of complete solar simulated light and UV only conditions. *Where there is no z-score, there was not enough information to determine direction of change of the pathway.*

	Complete solar simulated light		UV only	
	p-value	z-score	p-value	z-score
Hepatic Fibrosis / Hepatic Stellate Cell Activation	7.9E-09		7.4E-06	
Axonal Guidance Signaling	1.0E-08		1.1E-06	
Sertoli Cell-Sertoli Cell Junction Signaling	1.1E-07		9.5E-08	
Protein Kinase A Signaling	2.9E-07	-1.061	1.8E-05	-0.816
Cardiac Hypertrophy Signaling (Enhanced)	4.7E-07	-1.808	5.4E-06	-2.058
Cellular Effects of Sildenafil (Viagra)	1.7E-06		4.4E-04	
p53 Signaling	1.0E-05	2.111	4.2E-06	2.111
RHOGDI Signaling	1.1E-05	1.069	3.3E-05	0.535
cAMP-mediated signaling	1.4E-05	-1.213	3.9E-05	-1
Aryl Hydrocarbon Receptor Signaling	1.7E-05	-0.258	1.4E-06	-1
Pulmonary Fibrosis Idiopathic Signaling Pathway	2.0E-05	-1.177	4.6E-06	-0.784
Dilated Cardiomyopathy Signaling Pathway	2.4E-05	-1.732	1.2E-04	-0.905
Tumor Microenvironment Pathway	2.5E-05	-0.688	3.0E-05	-0.943
Molecular Mechanisms of Cancer	3.5E-05		6.6E-06	
Hepatic Fibrosis Signaling Pathway	6.0E-05	-1.177	7.6E-05	-1.177
Inhibition of Matrix Metalloproteases	6.2E-05	-0.707	3.4E-05	0
Semaphorin Neuronal Repulsive Signaling Pathway	1.1E-04	0.535	0.002	0.577
Colorectal Cancer Metastasis Signaling	1.3E-04	0	3.9E-07	-0.626
Cell Cycle: G1/S Checkpoint Regulation	1.5E-04	0.333	0.002	0
Glioblastoma Multiforme Signaling	1.5E-04	-0.577	5.6E-05	-1.069
Pancreatic Adenocarcinoma Signaling	1.8E-04	0.378	0.001	0
HIF1α Signaling	1.9E-04	-0.229	6.6E-05	0.229
Leukocyte Extravasation Signaling	2.2E-04	0.775	4.8E-07	-0.243
CDK5 Signaling	2.3E-04	-1.89	4.0E-04	-1.414
Estrogen-mediated S-phase Entry	2.6E-04	-1.633	0.001	-1.342
Regulation of Actin-based Motility by Rho	2.8E-04	0.378	0.002	0.378
GPCR-Mediated Integration of Enteroendocrine Signaling Exemplified by an L Cell	3.4E-04	-1.134	0.001	-0.816
Caveolar-mediated Endocytosis Signaling	3.4E-04		0.003	

	Complete solar simulated light		UV only	
	p-value	z-score	p-value	z-score
Leptin Signaling in Obesity	3.8E-04		0.004	
Cardiac Hypertrophy Signaling	4.9E-04	-0.471	0.003	-0.258
Synaptogenesis Signaling Pathway	5.1E-04	-3.411	0.106	-3.051
Signaling by Rho Family GTPases	7.2E-04	-1.069	0.002	-1.069
Agranulocyte Adhesion and Diapedesis	7.6E-04		3.2E-05	
Cell Cycle Control of Chromosomal Replication	8.3E-04	-2.828	4.8E-04	-2.828
TR/RXR Activation	8.5E-04		0.021	
PI3K/AKT Signaling	8.7E-04	-0.378	3.5E-04	-1
Osteoarthritis Pathway	9.1E-04	-0.277	0.002	-0.535
HGF Signaling	9.5E-04	0	0.012	-1.134
Sperm Motility	9.5E-04	-0.905	0.045	-1.414
Ephrin Receptor Signaling	0.001	-0.447	0.038	-0.447
Role of NFAT in Cardiac Hypertrophy	0.001	-0.5	0.003	0
Superpathway of Serine and Glycine Biosynthesis I	0.001		0.020	
Glioma Signaling	0.002	-1.633	0.003	-0.378
Paxillin Signaling	0.002	0	0.003	-0.378
Estrogen Receptor Signaling	0.002	-0.408	0.002	0
Actin Nucleation by ARP-WASP Complex	0.002	1	0.012	1
Cell Cycle Regulation by BTG Family Proteins	0.002	-1.342	0.033	
Cardiac β-adrenergic Signaling	0.002	-1	0.002	-1.414
Wound Healing Signaling Pathway	0.002	-0.229	0.005	0.728
Bladder Cancer Signaling	0.003		0.002	
Agrin Interactions at Neuromuscular Junction	0.004	0	4.8E-04	-0.378
Role of Macrophages, Fibroblasts and Endothelial Cells in Rheumatoid Arthritis	0.004		4.0E-05	
Clathrin-mediated Endocytosis Signaling	0.004		0.028	
Prostanoid Biosynthesis	0.005		0.004	
D-myo-inositol-5-phosphate Metabolism	0.005	0	0.006	-0.333
G-Protein Coupled Receptor Signaling	0.005	-1.121	0.007	-0.667
GADD45 Signaling	0.005	1.134	0.014	0.816
Retinoic acid Mediated Apoptosis Signaling	0.005	0.378	0.137	0
ILK Signaling	0.006	0.577	0.003	0.277
HOTAIR Regulatory Pathway	0.006	-0.277	3.5E-04	-1.291
RAR Activation	0.007		0.001	
Role of Osteoblasts, Osteoclasts and Chondrocytes in Rheumatoid Arthritis	0.007		1.8E-04	
Neurovascular Coupling Signaling Pathway	0.007	-3	0.071	-2.887
Death Receptor Signaling	0.008	0.333	0.001	0.632

	Complete solar simulated light		UV only	
	p-value	z-score	p-value	z-score
BEX2 Signaling Pathway	0.009	1.414	3.3E-04	0.632
P2Y Purigenic Receptor Signaling Pathway	0.009	0	0.033	0.816
MYC Mediated Apoptosis Signaling	0.009	0	2.2E-04	0.707
Germ Cell-Sertoli Cell Junction Signaling	0.009		0.027	
WNT/Ca+ pathway	0.009	0.378	0.001	0
Factors Promoting Cardiogenesis in Vertebrates	0.009	-1.155	0.013	-0.905
Neuregulin Signaling	0.010		0.041	
WNT/β-catenin Signaling	0.010	1.508	2.1E-04	0.535
Tumoricidal Function of Hepatic Natural Killer Cells	0.010		0.044	
Complement System	0.010	-0.447	0.033	0
Cyclins and Cell Cycle Regulation	0.010	-1.134	0.060	-1.342
Superpathway of Inositol Phosphate Compounds	0.011	0.302	0.005	-0.302
Sphingosine-1-phosphate Signaling	0.011	0.816	0.018	0.447
Glucocorticoid Receptor Signaling	0.011		0.019	
Ovarian Cancer Signaling	0.012	1	0.002	1
Serine Biosynthesis	0.012		0.010	
Gap Junction Signaling	0.012		0.006	
Apelin Endothelial Signaling Pathway	0.013	-1.414	0.095	-1.342
Apelin Liver Signaling Pathway	0.013	-1	0.054	
Growth Hormone Signaling	0.013	-1.342	0.085	
Regulation of Cellular Mechanics by Calpain Protease	0.014		0.074	
Breast Cancer Regulation by Stathmin1	0.015	0	0.005	-0.354
Acute Phase Response Signaling	0.016	-0.707	0.020	0.707
GP6 Signaling Pathway	0.016	-2.53	0.244	-1.633
Oncostatin M Signaling	0.018	0.447	0.052	0
Adenosine Nucleotides Degradation II	0.018		0.014	
Chondroitin Sulfate Degradation (Metazoa)	0.018		0.014	
Endocannabinoid Neuronal Synapse Pathway	0.019	1.667	0.011	0.333
PTEN Signaling	0.019	0.816	0.011	0
Atherosclerosis Signaling	0.020		0.001	
3-phosphoinositide Degradation	0.021	0	0.026	-0.378
GNRH Signaling	0.021	0.333	0.106	0
Integrin Signaling	0.022	-0.577	0.025	-0.302
Dopamine Receptor Signaling	0.023		0.047	
STAT3 Pathway	0.024	0.447	0.001	0

	Complete solar simulated light		UV only	
	p-value	z-score	p-value	z-score
PPARα/RXRα Activation	0.024	0.378	0.013	0.378
Ceramide Biosynthesis	0.024		0.210	
Role of BRCA1 in DNA Damage Response	0.025	1.633	0.126	1
UVA-Induced MAPK Signaling	0.025	0	0.016	
ERK/MAPK Signaling	0.025	-1	0.028	-1.265
Relaxin Signaling	0.025	-1.134	0.034	-0.378
SNARE Signaling Pathway	0.025	-1.265	0.295	0
iNOS Signaling	0.026	1	0.004	0
GPCR-Mediated Nutrient Sensing in Enteroendocrine Cells	0.026	0.378	0.043	0
White Adipose Tissue Browning Pathway	0.027	-1.897	0.087	-2.121
Nitric Oxide Signaling in the Cardiovascular System	0.028	-1	0.044	0
Tight Junction Signaling	0.028		0.035	
PFKFB4 Signaling Pathway	0.028	0.447	0.074	1
D-myo-inositol (1,4,5,6)-Tetrakisphosphate Biosynthesis	0.028	-0.378	0.036	-0.816
D-myo-inositol (3,4,5,6)-tetrakisphosphate Biosynthesis	0.028	-0.378	0.036	-0.816
ID1 Signaling Pathway	0.029	-1.387	0.007	-0.535
Purine Nucleotides Degradation II (Aerobic)	0.029		0.023	
Actin Cytoskeleton Signaling	0.032	-0.707	0.034	-0.707
Coronavirus Pathogenesis Pathway	0.032	1.387	0.018	0.277
Gustation Pathway	0.032	-2.111	0.358	-0.816
Inhibition of Angiogenesis by TSP1	0.032		0.005	
Thrombin Signaling	0.033	0.333	0.008	0.632
CD40 Signaling	0.033	-0.447	3.5E-04	0
IL-15 Production	0.033	-1.667	0.223	-1.633
Dopamine-DARPP32 Feedback in cAMP Signaling	0.033	-1.732	0.019	-1.265
Circadian Rhythm Signaling	0.033		0.063	
Oxytocin In Spinal Neurons Signaling Pathway	0.035	-2	0.028	-2
Gαs Signaling	0.036	0.378	0.023	0.378
Asparagine Biosynthesis I	0.036		0.033	
BMP signaling pathway	0.037	-0.816	0.161	-0.447
Chronic Myeloid Leukemia Signaling	0.039		0.144	
Folate Transformations I	0.039		0.261	
α-Adrenergic Signaling	0.041		0.287	
Endothelin-1 Signaling	0.045	1.732	0.026	1.155

	Complete solar simulated light		UV only	
	p-value	z-score	p-value	z-score
Regulation Of The Epithelial Mesenchymal Transition By Growth Factors Pathway	0.045	0	0.055	-0.905
Apelin Adipocyte Signaling Pathway	0.046	2	0.031	1
Glioma Invasiveness Signaling	0.047	0.447	0.093	0
IL-17A Signaling in Fibroblasts	0.047		0.001	
CREB Signaling in Neurons	0.048	-0.962	0.074	0
Oxytocin Signaling Pathway	0.048	-1.5	0.048	-1.291
Glycine Betaine Degradation	0.048		0.286	
Pyrimidine Deoxyribonucleotides De Novo Biosynthesis I	0.048		0.006	0
Synaptic Long Term Depression	0.049	-1.155	0.060	-1.508
Adrenomedullin signaling pathway	0.056	-1.155	0.034	-0.577
Retinoate Biosynthesis I	0.063		0.012	0
Chemokine Signaling	0.068	0	0.017	1.134

References

ALAFIATAYO, A. A., LAI, K.-S., AHMAD, S., MAHMOOD, M. & SHAHARUDDIN, N. A. 2020. RNA-Seq analysis revealed genes associated with UV-induced cell necrosis through MAPK/TNF-α pathways in human dermal fibroblast cells as an inducer of premature photoaging. *Genomics,* 112**,** 484-493.

ALBRECHT-BUEHLER, G. 1991. Surface extensions of 3T3 cells towards distant infrared light sources. *The Journal of cell biology,* 114**,** 493-502.

ALBRECHT, S., JUNG, S., MÜLLER, R., LADEMANN, J., ZUBERBIER, T., ZASTROW, L., REBLE, C., BECKERS, I. & MEINKE, M. C. 2019. Skin type differences in solar-simulated radiation-induced oxidative stress. *British Journal of Dermatology,* 180**,** 597-603.

APPLEGATE, L., SCALETTA, C., PANIZZON, R., FRENK, E., HOHLFELD, P. & SCHWARZKOPF, S. 2000. Induction of the putative protective protein ferritin by infrared radiation: implications in skin repair. *International Journal of Molecular Medicine,* 5**,** 247-298.

APPLEGATE, L. A., SCALETTA, C., PANIZZON, R. & FRENK, E. 1998. Evidence that ferritin is UV inducible in human skin: Part of a putative defense mechanism. *Journal of Investigative Dermatology,* 111**,** 159-163.

ASHOORI, M. & SAEDISOMEOLIA, A. 2014. Riboflavin (vitamin B2) and oxidative stress: a review. *British Journal of Nutrition,* 111**,** 1985-1991.

BAIN, J., RUSCH, H. & KLINE, B. 1943. The effect of temperature upon ultraviolet carcinogenesis with wave lengths 2,800–3,400 Å. *Cancer Research,* 3**,** 610-612.

BALASUBRAMANIAM, S. & YAPLITO-LEE, J. 2020. Riboflavin metabolism: role in mitochondrial function. *Journal of Translational Genetics and Genomics,* 4**,** 285-306.

BARKER, S. L. & LAROCCA, P. J. 1994. Method of production and control of a commercial tissue culture surface. *Journal of tissue culture methods,* 16**,** 151-153.

BAROLET, D., CHRISTIAENS, F. & HAMBLIN, M. R. 2016. Infrared and skin: Friend or foe. *Journal of Photochemistry and Photobiology B: Biology,* 155**,** 78-85.

BERNEBURG, M., PLETTENBERG, H. & KRUTMANN, J. 2000. Photoaging of human skin. *Photodermatology, Photoimmunology & Photomedicine: Review article,* 16**,** 239-244.

BERRIDGE, M. V. & TAN, A. S. 1993. Characterization of the Cellular Reduction of 3-(4,5-dimethylthiazol-2-yl)-2,5-diphenyltetrazolium bromide (MTT): Subcellular Localization, Substrate Dependence, and Involvement of Mitochondrial Electron Transport in MTT Reduction. *Archives of Biochemistry and Biophysics,* 303**,** 474-482.

BESS, A. S., CROCKER, T. L., RYDE, I. T. & MEYER, J. N. 2012. Mitochondrial dynamics and autophagy aid in removal of persistent mitochondrial DNA damage in Caenorhabditis elegans. *Nucleic Acids Research,* 40**,** 7916-7931.

BIRCH-MACHIN, M. A., TINDALL, M., TURNER, R., HALDANE, F. & REES, J. L. 1998. Mitochondrial DNA Deletions in Human Skin Reflect Photo- Rather Than Chronologic Aging. *Journal of Investigative Dermatology,* 110**,** 149-152.

BIRCH - MACHIN, M. A. & BOWMAN, A. 2016. Oxidative stress and ageing. *British Journal of Dermatology,* 175**,** 26-29.

BIRKET, M. J. & BIRCH-MACHIN, M. A. 2007. Ultraviolet radiation exposure accelerates the accumulation of the aging-dependent T414G mitochondrial DNA mutation in human skin. *Aging Cell,* 6**,** 557-564.

BIRKET, M. J., PASSOS, J. F., VON ZGLINICKI, T. & BIRCH-MACHIN, M. A. 2009. The Relationship between the Aging- and Photo-Dependent T414G Mitochondrial DNA Mutation with Cellular Senescence and Reactive Oxygen Species Production in Cultured Skin Fibroblasts. *Journal of Investigative Dermatology,* 129**,** 1361-1366.

BLUME-PEYTAVI, U., KOTTNER, J., STERRY, W., HODIN, M. W., GRIFFITHS, T. W., WATSON, R. E., HAY, R. J. & GRIFFITHS, C. E. 2016a. Age-associated skin conditions and diseases: current perspectives and future options. *The Gerontologist,* 56**,** S230-S242.

BLUME-PEYTAVI, U., KOTTNER, J., STERRY, W., HODIN, M. W., GRIFFITHS, T. W., WATSON, R. E. B., HAY, R. J. & GRIFFITHS, C. E. M. 2016b. Age-Associated Skin Conditions and Diseases: Current Perspectives and Future Options. *The Gerontologist,* 56**,** S230-S242.

BÖHM, F., DRYGALLA, F., CHARLESWORTH, P., BÖHM, K., TRUSCOTT, T. G. & JOKIEL, K. 1995. BILIRUBIN PHOTOTOXICITY TO HUMAN CELLS BY GREEN LIGHT PHOTOTHERAPY in vitro. *Photochemistry and Photobiology,* 62**,** 980-983.

BORALDI, F., ANNOVI, G., PAOLINELLI-DEVINCENZI, C., TIOZZO, R. & QUAGLINO, D. 2008. The effect of serum withdrawal on the protein profile of quiescent human dermal fibroblasts in primary cell culture. *Proteomics,* 8**,** 66-82.

BOUKAMP, P., POPP, S., BLEUEL, K., TOMAKIDI, E., BÜRKLE, A. & FUSENIG, N. E. 1999. Tumorigenic conversion of immortal human skin keratinocytes (HaCaT) by elevated temperature. *Oncogene,* 18**,** 5638-5645.

BOULTON, S., ANDERSON, A., SWALWELL, H., HENDERSON, J. R., MANNING, P. & BIRCH-MACHIN, M. A. 2011. Implications of using the fluorescent probes, dihydrorhodamine 123 and 2′,7′-dichlorodihydrofluorescein diacetate, for the detection of UVA-induced reactive oxygen species. *Free Radical Research,* 45**,** 115-122.

BRAND, M. D. 2000. Uncoupling to survive? The role of mitochondrial inefficiency in ageing. *Experimental Gerontology,* 35**,** 811-820.

BROWN, W. M., GEORGE, M. & WILSON, A. C. 1979. Rapid evolution of animal mitochondrial DNA. *Proceedings of the National Academy of Sciences,* 76**,** 1967-1971.

BRUZELL ROLL, E. & CHRISTENSEN, T. 2005. Formation of photoproducts and cytotoxicity of bilirubin irradiated with turquoise and blue phototherapy light. *Acta Paediatrica,* 94**,** 1448-1454.

BUDDEN, T., GAUDY-MARQUESTE, C., PORTER, A., KAY, E., GURUNG, S., EARNSHAW, C. H., ROECK, K., CRAIG, S., TRAVES, V., KRUTMANN, J., MULLER, P., MOTTA, L., ZANIVAN, S., MALLIRI, A., FURNEY, S. J., NAGORE, E. & VIRÓS, A. 2021. Ultraviolet light-induced collagen degradation inhibits melanoma invasion. *Nature Communications,* 12**,** 2742.

BUECHNER, N., SCHROEDER, P., JAKOB, S., KUNZE, K., MARESCH, T., CALLES, C., KRUTMANN, J. & HAENDELER, J. 2008. Changes of MMP-1 and collagen type I alpha 1 by UVA, UVB and IRA are differentially regulated by Trx-1. *Experimental Gerontology,* 43**,** 633-637.

CALLES, C., SCHNEIDER, M., MACALUSO, F., BENESOVA, T., KRUTMANN, J. & SCHROEDER, P. 2010. Infrared A Radiation Influences the Skin Fibroblast Transcriptome: Mechanisms and Consequences. *Journal of Investigative Dermatology,* 130**,** 1524-1536.

CAO, C., HEALEY, S., AMARAL, A., LEE-COUTURE, A., WAN, S., KOUTTAB, N., CHU, W. M. & WAN, Y. S. 2007. ATP-sensitive potassium channel: A novel target for protection against UV-induced human skin cell damage. *Journal of Cellular Physiology,* 212**,** 252-263.

CASTELLANO-PELLICENA, I., UZUNBAJAKAVA, N. E., MIGNON, C., RAAFS, B., BOTCHKAREV, V. A. & THORNTON, M. J. 2019. Does blue light restore human epidermal barrier function via activation of Opsin during cutaneous wound healing? *Lasers in Surgery and Medicine,* 51**,** 370-382.

CHANCE, B., SIES, H. & BOVERIS, A. 1979. Hydroperoxide metabolism in mammalian organs. *Physiological Reviews,* 59**,** 527-605.

CHEN, Q., FISCHER, A., REAGAN, J. D., YAN, L. J. & AMES, B. N. 1995. OXIDATIVE DNA-DAMAGE AND SENESCENCE OF HUMAN-DIPLOID FIBROBLAST CELLS. *Proceedings of the National Academy of Sciences of the United States of America,* 92**,** 4337-4341.

CHEN, Z., SEO, J. Y., KIM, Y. K., LEE, S. R., KIM, K. H., CHO, K. H., EUN, H. C. & CHUNG, J. H. 2005. Heat Modulation of Tropoelastin, Fibrillin-1, and Matrix Metalloproteinase-12 in Human Skin In Vivo. *Journal of Investigative Dermatology,* 124**,** 70-78.

CHINNERY, P. F., TAYLOR, G. A., HOWELL, N., BROWN, D. T., PARSONS, T. J. & TURNBULL, D. M. 2001. Point Mutations of the mtDNA Control Region in Normal and Neurodegenerative Human Brains. *The American Journal of Human Genetics,* 68**,** 529-532.

CHIRIKHINA, E., CHIRIKHIN, A., XIAO, P., DEWSBURY-ENNIS, S. & BIANCONI, F. 2020. In vivo assessment of water content, trans-epidermial water loss and thickness in human facial skin. *Applied Sciences,* 10**,** 6139.

CHO, S., LEE, M. J., KIM, M. S., LEE, S., KIM, Y. K., LEE, D. H., LEE, C. W., CHO, K. H. & CHUNG, J. H. 2008. Infrared plus visible light and heat from natural sunlight participate in the expression of MMPs and type I procollagen as well as infiltration of inflammatory cell in human skin in vivo. *Journal of Dermatological Science,* 50**,** 123-133.

CHUA, S. H., ANG, P. O. R., KHOO LAWRENCE S, W. & GOH, C. L. 2007. Nonablative Infrared Skin Tightening in Type IV to V Asian Skin: A Prospective Clinical Study. *Dermatologic Surgery,* 33**,** 146-151.

COELHO, S. G., CHOI, W., BRENNER, M., MIYAMURA, Y., YAMAGUCHI, Y., WOLBER, R., SMUDA, C., BATZER, J., KOLBE, L., ITO, S., WAKAMATSU, K., ZMUDZKA, B. Z., BEER, J. Z., MILLER, S. A. & HEARING, V. J. 2009. Short- and long-term effects of UV radiation on the pigmentation of human skin. *The journal of investigative dermatology. Symposium proceedings,* 14**,** 32-35.

CROSS, F. 1967. On a turf (peat) fire cancer: malignant change superimposed on erythema ab igne. *Proceedings of the Royal Society of Medicine,* 60**,** 1307-1308.

DARVIN, M. E., HAAG, S. F., MEINKE, M. C., STERRY, W. & LADEMANN, J. 2011. Determination of the influence of IR radiation on the antioxidative network of the human skin. *Journal of Biophotonics,* 4**,** 21-29.

DE RASMO, D., GATTONI, G., PAPA, F., SANTERAMO, A., PACELLI, C., COCCO, T., MICELLI, L., SARDARO, N., LARIZZA, M., SCIVETTI, M., MILANO, S. & SIGNORILE, A. 2011. The β-adrenoceptor agonist isoproterenol promotes the activity of respiratory chain complex I and lowers cellular reactive oxygen species in fibroblasts and heart myoblasts. *European Journal of Pharmacology,* 652**,** 15-22.

DIFFEY, B. 2015. Solar Spectral Irradiance and Summary Outputs Using Excel. *Photochemistry and Photobiology,* 91**,** 553-557.

DIFFEY, B. & CADARS, B. 2016. An appraisal of the need for infrared radiation protection in sunscreens. *Photochemical & Photobiological Sciences,* 15**,** 361-364.

DJAVAHERI-MERGNY, M., MARSAC, C., MAZIERE, C., SANTUS, R., MICHEL, L., DUBERTRET, L. & MAZIERE, J. C. 2001. UV-A irradiation induces a decrease in the mitochondrial respiratory activity of human NCTC 2544 keratinocytes. *Free Radical Research,* 34**,** 583-594.

DOBSON, A. W., XU, Y., KELLEY, M. R., LEDOUX, S. P. & WILSON, G. L. 2000. Enhanced mitochondrial DNA repair and cellular survival after oxidative stress by targeting the human 8-oxoguanine glycosylase repair enzyme to mitochondria. *Journal of Biological Chemistry,* 275**,** 37518-37523.

DONG KELLY, K., DAMAGHI, N., PICART STEPHANIE, D., MARKOVA NELLI, G., OBAYASHI, K., OKANO, Y., MASAKI, H., GRETHER‐BECK, S., KRUTMANN, J., SMILES KENNETH, A. & YAROSH DANIEL, B. 2008. UV‐induced DNA damage initiates release of MMP‐1 in human skin. *Experimental Dermatology,* 17**,** 1037-1044.

DROBETSKY, E. A., TURCOTTE, J. & CHATEAUNEUF, A. 1995. A role for ultraviolet A in solar mutagenesis. *Proceedings of the National Academy of Sciences,* 92**,** 2350-2354.

DUTEIL, L., QUEILLE-ROUSSEL, C., LACOUR, J.-P., MONTAUDIÉ, H. & PASSERON, T. 2020. Short-term exposure to blue light emitted by electronic devices does not worsen melasma. *Journal of the American Academy of Dermatology,* 83**,** 913-914.

ENOCH, T. & NORBURY, C. 1995. Cellular responses to DNA damage: cell-cycle checkpoints, apoptosis and the roles of p53 and ATM. *Trends in Biochemical Sciences,* 20**,** 426-430.

ESHAGHIAN, A., VLEUGELS, R. A., CANTER, J. A., MCDONALD, M. A., STASKO, T. & SLIGH, J. E. 2006. Mitochondrial DNA Deletions Serve as Biomarkers of Aging in the Skin, but Are Typically Absent in Nonmelanoma Skin Cancers. *Journal of Investigative Dermatology,* 126**,** 336-344.

FANG, E. F., SCHEIBYE-KNUDSEN, M., CHUA, K. F., MATTSON, M. P., CROTEAU, D. L. & BOHR, V. A. 2016. Nuclear DNA damage signalling to mitochondria in ageing. *Nature Reviews Molecular Cell Biology,* 17**,** 308-321.

FERRARESI, C., KAIPPERT, B., AVCI, P., HUANG, Y.-Y., DE SOUSA, M. V. P., BAGNATO, V. S., PARIZOTTO, N. A. & HAMBLIN, M. R. 2015. Low-level Laser (Light) Therapy Increases Mitochondrial Membrane Potential and ATP Synthesis in C2C12 Myotubes with a Peak Response at 3–6 h. *Photochemistry and Photobiology,* 91**,** 411-416.

FINKEL, T. 2011. Signal transduction by reactive oxygen species. *Journal of Cell Biology,* 194**,** 7-15.

FINLAYSON, L., BARNARD, I. R., MCMILLAN, L., IBBOTSON, S. H., BROWN, C. T. A., EADIE, E. & WOOD, K. 2021. Depth penetration of light into skin as a function of wavelength from 200 to 1000 nm. *Photochemistry and Photobiology*.

FISHER, G. J., DATTA, S. C., TALWAR, H. S., WANG, Z. Q., VARANI, J., KANG, S. & VOORHEES, J. J. 1996. Molecular basis of sun-induced premature skin ageing and retinoid antagonism. *NATURE,* 379**,** 335-339.

FISHER, G. J., WANG, Z., DATTA, S. C., VARANI, J., KANG, S. & VOORHEES, J. J. 1997. Pathophysiology of premature skin aging induced by ultraviolet light. *New England Journal of Medicine,* 337**,** 1419-1429.

FORMENTINI, L., SANTACATTERINA, F., NÚÑEZ DE ARENAS, C., STAMATAKIS, K., LÓPEZ-MARTÍNEZ, D., LOGAN, A., FRESNO, M., SMITS, R., MURPHY, M. P. & CUEZVA, J. M.

2017. Mitochondrial ROS Production Protects the Intestine from Inflammation through Functional M2 Macrophage Polarization. *Cell Reports,* 19**,** 1202-1213.
FRAGA, C. G., SHIGENAGA, M. K., PARK, J. W., DEGAN, P. & AMES, B. N. 1990. Oxidative damage to DNA during aging: 8-hydroxy-2'-deoxyguanosine in rat organ DNA and urine. *Proceedings of the National Academy of Sciences,* 87**,** 4533-4537.
FRANK, S., MENEZES, S., LEBRETON-DE COSTER, C., OSTER, M., DUBERTRET, L. & COULOMB, B. 2006. Infrared radiation induces the p53 signaling pathway: role in infrared prevention of ultraviolet B toxicity. *Experimental Dermatology,* 15**,** 130-137.
FREEMAN, R. G. & KNOX, J. M. 1964. Influence of temperature on ultraviolet injury. *Archives of Dermatology,* 89**,** 858-864.
FREITAS, R. A. 1999. *Nanomedicine, volume I: basic capabilities*, Landes Bioscience Georgetown, TX.
FUSHIMI, T., INUI, S., NAKAJIMA, T., OGASAWARA, M., HOSOKAWA, K. & ITAMI, S. 2012. Green light emitting diodes accelerate wound healing: characterization of the effect and its molecular basis in vitro and in vivo. *Wound Repair and Regeneration,* 20**,** 226-235.
GARRIDO, N., GRIPARIC, L., JOKITALO, E., WARTIOVAARA, J., BLIEK, A. M. V. D. & SPELBRINK, J. N. 2003. Composition and Dynamics of Human Mitochondrial Nucleoids. *Molecular Biology of the Cell,* 14**,** 1583-1596.
GEBHARD, D., MATT, K., BURGER, K. & BERGEMANN, J. 2014. Shortwave UV-Induced Damage as Part of the Solar Damage Spectrum Is Not a Major Contributor to Mitochondrial Dysfunction. *Journal of Biochemical and Molecular Toxicology,* 28**,** 256-262.
GENDRON, S. P., BASTIEN, N., MALLET, J. D. & ROCHETTE, P. J. 2013. The 3895-bp mitochondrial DNA deletion in the human eye: a potential involvement in corneal ageing and macular degeneration. *Mutagenesis,* 28**,** 197-204.
GETHIN, G. 2007. The significance of surface pH in chronic wounds. *Wounds uk,* 3**,** 52.
GNIADECKA, M., LOCKANDERSEN, J., OLIVARIUS, F. D. F. & WULF, H. C. 1996. Skin temperature and phototest evaluation. *Photodermatology Photoimmunology & Photomedicine,* 12**,** 189-193.
GODLEY, B. F., SHAMSI, F. A., LIANG, F.-Q., JARRETT, S. G., DAVIES, S. & BOULTON, M. 2005. Blue Light Induces Mitochondrial DNA Damage and Free Radical Production in Epithelial Cells*. *Journal of Biological Chemistry,* 280**,** 21061-21066.
GREGORY, C. D. & POUND, J. D. 2010. Microenvironmental influences of apoptosis in vivo and in vitro. *Apoptosis,* 15**,** 1029-1049.
GRETHER-BECK, S., MARINI, A., JAENICKE, T. & KRUTMANN, J. 2014. Photoprotection of human skin beyond ultraviolet radiation. *Photodermatology Photoimmunology & Photomedicine,* 30**,** 167-174.
GRETHER‐BECK, S., MARINI, A., JAENICKE, T. & KRUTMANN, J. 2015. Effective photoprotection of human skin against infrared A radiation by topically applied antioxidants: results from a vehicle controlled, double‐blind, randomized study. *Photochemistry and photobiology,* 91**,** 248-250.
GRZELAK, A., RYCHLIK, B. & BARTOSZ, G. 2001. Light-dependent generation of reactive oxygen species in cell culture media. *Free Radical Biology and Medicine,* 30**,** 1418-1425.

HAGANDER, L. G., MIDANI, H. A., KUSKOWSKI, M. A. & PARRY, G. J. G. 2000. Quantitative sensory testing: effect of site and skin temperature on thermal thresholds. *Clinical Neurophysiology,* 111**,** 17-22.

HAMANAKA, R. B., GLASAUER, A., HOOVER, P., YANG, S., BLATT, H., MULLEN, A. R., GETSIOS, S., GOTTARDI, C. J., DEBERARDINIS, R. J., LAVKER, R. M. & CHANDEL, N. S. 2013. Mitochondrial Reactive Oxygen Species Promote Epidermal Differentiation and Hair Follicle Development. *Science Signaling,* 6**,** ra8-ra8.

HAN, D., WILLIAMS, E. & CADENAS, E. 2001. Mitochondrial respiratory chain-dependent generation of superoxide anion and its release into the intermembrane space. *Biochemical Journal,* 353**,** 411-416.

HANNA, R., CROWTHER, J. M., BULSARA, P. A., WANG, X., MOORE, D. J. & BIRCH-MACHIN, M. A. 2019. Optimised detection of mitochondrial DNA strand breaks. *Mitochondrion,* 46**,** 172-178.

HANSDA, S. & GHOSH, R. 2021. Bystander effect of ultraviolet A radiation protects A375 melanoma cells by induction of antioxidant defense. *Journal of Environmental Science and Health, Part C***,** 1-22.

HANSON, K. M. & SIMON, J. D. 1998. Epidermal trans-urocanic acid and the UV-A-induced photoaging of the skin. *Proceedings of the National Academy of Sciences,* 95**,** 10576-10578.

HARBOTTLE, A. & BIRCH-MACHIN, M. 2006. Real-time PCR analysis of a 3895 bp mitochondrial DNA deletion in nonmelanoma skin cancer and its use as a quantitative marker for sunlight exposure in human skin. *British journal of cancer,* 94**,** 1887-1893.

HARBOTTLE, A., MAKI, J., REGULY, B., WITTOCK, R., ROBINSON, K., PARR, R. & BIRCH‐MACHIN, M. 2010. Real‐time polymerase chain reaction analysis of a 3895‐bp mitochondrial DNA deletion in epithelial swabs and its use as a quantitative marker for sunlight exposure in human skin. *British Journal of Dermatology,* 163**,** 1291-1295.

HARMAN, D. 1956. Aging: A Theory Based on Free Radical and Radiation Chemistry. *Journal of Gerontology,* 11**,** 298-300.

HARMAN, D. 1992. Free radical theory of aging. *Mutation Research/DNAging,* 275**,** 257-266.

HAYDONT, V., BERNARD, B. A. & FORTUNEL, N. O. 2019. Age-related evolutions of the dermis: Clinical signs, fibroblast and extracellular matrix dynamics. *Mechanisms of Ageing and Development,* 177**,** 150-156.

HELD, P. 2012. An introduction to reactive oxygen species. *Tech Resources-App Guides,* 802**,** 5-9.

HENG, J. K., AW, D. C. W. & TAN, K. B. 2014. Solar Elastosis in Its Papular Form: Uncommon, Mistakable. *Case Reports in Dermatology,* 6**,** 124-128.

HOFFMANN, G. 2007. Principles and working mechanisms of water-filtered infrared-A (wIRA) in relation to wound healing. *GMS Krankenhaushygiene Interdisziplinar,* 2**,** Doc54.

HOFFMANN, G. 2009. Water-filtered infrared-A (wIRA) in acute and chronic wounds. *GMS Krankenhaushygiene Interdisziplinar,* 4**,** Doc12.

HOPKINS, S. L., SIEWERT, B., ASKES, S., VELDHUIZEN, P., ZWIER, R., HEGER, M. & BONNET, S. 2016. An in vitro cell irradiation protocol for testing photopharmaceuticals and the effect of blue, green, and red light on human cancer cell lines. *Photochemical & Photobiological Sciences,* 15**,** 644-653.

HOSOYA, K., TAKAHASHI, K., OYA, K. & IWAMORI, S. 2018. Effect of distance between ultraviolet lamp and polystyrene cell culture substrate on surface modification by active oxygen species. *Transactions of the JSME (in Japanese),* 84**,** 17-00561-17-00561.

HOURELD, N. N., MASHA, R. T. & ABRAHAMSE, H. 2012. Low-intensity laser irradiation at 660nm stimulates cytochrome c oxidase in stressed fibroblast cells. *Lasers in Surgery and Medicine,* 44**,** 429-434.

HOUSCHYAR, K. S., MOMENI, A., PYLES, M. N., MAAN, Z. N., WHITTAM, A. J. & SIEMERS, F. 2015. Wnt signaling induces epithelial differentiation during cutaneous wound healing. *Organogenesis,* 11**,** 95-104.

HUANG, K. T., CHEN, Y. H. & WALKER, A. M. 2004. Inaccuracies in MTS assays: major distorting effects of medium, serum albumin, and fatty acids. *BioTechniques,* 37**,** 406-412.

HUDSON, L., BOWMAN, A., RASHDAN, E. & BIRCH-MACHIN, M. A. 2016. Mitochondrial damage and ageing using skin as a model organ. *Maturitas,* 93**,** 34-40.

HUNTER, S. E., JUNG, D., DI GIULIO, R. T. & MEYER, J. N. 2010. The QPCR assay for analysis of mitochondrial DNA damage, repair, and relative copy number. *Methods (San Diego, Calif.),* 51**,** 444-451.

IMHOFF, B. R. & HANSEN, J. M. 2009. Extracellular redox status regulates Nrf2 activation through mitochondrial reactive oxygen species. *Biochemical Journal,* 424**,** 491-500.

IMPROTA, R. & DOUKI, T. 2021. *DNA Photodamage*, Royal Society of Chemistry.

INDO, H. P., DAVIDSON, M., YEN, H.-C., SUENAGA, S., TOMITA, K., NISHII, T., HIGUCHI, M., KOGA, Y., OZAWA, T. & MAJIMA, H. J. 2007. Evidence of ROS generation by mitochondria in cells with impaired electron transport chain and mitochondrial DNA damage. *Mitochondrion,* 7**,** 106-118.

J. S. ZIGLER, JR., LEPE-ZUNIGA, J. L., VISTICA, B. & GERY, I. 1985. Analysis of the Cytotoxic Effects of Light-Exposed Hepes-Containing Culture Medium. *In Vitro Cellular & Developmental Biology,* 21**,** 282-287.

JANTSCHITSCH, C., WEICHENTHAL, M., MAEDA, A., PROKSCH, E., SCHWARZ, T. & SCHWARZ, A. 2011. Infrared radiation does not enhance the frequency of ultraviolet radiation - induced skin tumors, but their growth behaviour in mice. *Experimental Dermatology,* 20**,** 346-350.

JUHLIN, L. 1997. Hyaluronan in skin. *Journal of internal medicine,* 242**,** 61-66.

JUNG, T., HÖHN, A., PIAZENA, H. & GRUNE, T. 2010. Effects of water-filtered infrared A irradiation on human fibroblasts. *Free Radical Biology and Medicine,* 48**,** 153-160.

KAMMEYER, A. & LUITEN, R. M. 2015. Oxidation events and skin aging. *Ageing Research Reviews,* 21**,** 16-29.

KANE, K. S. & MAYTIN, E. V. 1995. Ultraviolet B-induced apoptosis of keratinocytes in murine skin is reduced by mild local hyperthermia. *Journal of investigative dermatology,* 104**,** 62-67.

KARU, T. 1999. Primary and secondary mechanisms of action of visible to near-IR radiation on cells. *Journal of Photochemistry and Photobiology B: Biology,* 49**,** 1-17.

KARU, T., PYATIBRAT, L. & KALENDO, G. 1995. Irradiation with He Ne laser increases ATP level in cells cultivated in vitro. *Journal of Photochemistry and Photobiology B: Biology,* 27**,** 219-223.

KARU, T. I. & KOLYAKOV, S. 2005. Exact action spectra for cellular responses relevant to phototherapy. *Photomedicine and Laser Therapy,* 23**,** 355-361.
KARU, T. I., PYATIBRAT, L. V., KOLYAKOV, S. F. & AFANASYEVA, N. I. 2005. Absorption measurements of a cell monolayer relevant to phototherapy: Reduction of cytochrome c oxidase under near IR radiation. *Journal of Photochemistry and Photobiology B: Biology,* 81**,** 98-106.
KARU TIINA, I. 2008. Mitochondrial Signaling in Mammalian Cells Activated by Red and Near - IR Radiation. *Photochemistry and Photobiology,* 84**,** 1091-1099.
KARU TIINA, I. 2010. Multiple roles of cytochrome c oxidase in mammalian cells under action of red and IR - A radiation. *IUBMB Life,* 62**,** 607-610.
KELLY, J. & MURPHY, J. E. J. 2016. Mitochondrial tolerance to single and repeat exposure to simulated sunlight in human epidermal and dermal skin cells. *Journal of Photochemistry and Photobiology B-Biology,* 165**,** 298-304.
KHRAPKO, K., COLLER, H. A., ANDRÉ, P. C., LI, X. C., HANEKAMP, J. S. & THILLY, W. G. 1997. Mitochondrial mutational spectra in human cells and tissues. *Proceedings of the National Academy of Sciences of the United States of America,* 94**,** 13798-13803.
KIELBASSA, C., ROZA, L. & EPE, B. 1997. Wavelength dependence of oxidative DNA damage induced by UV and visible light. *Carcinogenesis,* 18**,** 811-816.
KIM, M.-S., KIM, Y. K., CHO, K. H. & CHUNG, J. H. 2006a. Regulation of type I procollagen and MMP-1 expression after single or repeated exposure to infrared radiation in human skin. *Mechanisms of Ageing and Development,* 127**,** 875-882.
KIM, M., KIM, J., JEONG, S. W., JO, H. & PARK, H. J. 2018. Long-pulsed 1064-nm Nd: YAG laser ameliorates LL-37-induced rosacea-like skin lesions through promoting collagen remodeling in BALB/c mice. *Lasers in Medical Science,* 33**,** 393-397.
KIM, M. S., KIM, Y., CHO, K. & CHUNG, J. 2006b. Infrared exposure induces an angiogenic switch in human skin that is partially mediated by heat. *British Journal of Dermatology,* 155**,** 1131-1138.
KING, A., GOTTLIEB, E., BROOKS, D. G., MURPHY, M. P. & DUNAIEF, J. L. 2004. Mitochondria - derived reactive oxygen species mediate blue light - induced death of retinal pigment epithelial cells¶. *Photochemistry and photobiology,* 79**,** 470-475.
KLEINPENNING, M. M., SMITS, T., FRUNT, M. H. A., VAN ERP, P. E. J., VAN DE KERKHOF, P. C. M. & GERRITSEN, R. M. J. P. 2010. Clinical and histological effects of blue light on normal skin. *Photodermatology, Photoimmunology & Photomedicine,* 26**,** 16-21.
KLIGMAN, A. M. 1969. Early Destructive Effect of Sunlight on Human Skin. *JAMA,* 210**,** 2377-2380.
KLIGMAN, L. H. 1982. Intensification of ultraviolet-induced dermal damage by infrared radiation. *Archives of Dermatological Research,* 272**,** 229-238.
KNELS, L., VALTINK, M., DE LA VEGA MARIN, J., STEINER, G., ROEHLECKE, C., KRUEGER, A. & FUNK, R. H. W. 2012. Effects of Temperature and Water-Filtered Infrared-A Alone or in Combination on Healthy and Glyoxal-Stressed Fibroblast Cultures. *Oxidative Medicine and Cellular Longevity,* 2012**,** 274953.
KOHLI, I., BRAUNBERGER, T. L., NAHHAS, A. F., MIRZA, F. N., MOKHTARI, M., LYONS, A. B., KOLLIAS, N., RUVOLO, E., LIM, H. W. & HAMZAVI, I. H. 2020. Long-wavelength

Ultraviolet A1 and Visible Light Photoprotection: A Multimodality Assessment of Dose and Response. *Photochemistry and Photobiology,* 96**,** 208-214.

KRISHNAN, K. J. & BIRCH-MACHIN, M. A. 2006. The Incidence of Both Tandem Duplications and the Common Deletion in mtDNA from Three Distinct Categories of Sun-Exposed Human Skin and in Prolonged Culture of Fibroblasts. *Journal of Investigative Dermatology,* 126**,** 408-415.

KRISHNAN, K. J., HARBOTTLE, A. & BIRCH-MACHIN, M. A. 2004. The use of a 3895 bp mitochondrial DNA deletion as a marker for sunlight exposure in human skin. *Journal of investigative dermatology,* 123**,** 1020-1024.

KRISHNAN, K. J., REEVE, A. K., SAMUELS, D. C., CHINNERY, P. F., BLACKWOOD, J. K., TAYLOR, R. W., WANROOIJ, S., SPELBRINK, J. N., LIGHTOWLERS, R. N. & TURNBULL, D. M. 2008. What causes mitochondrial DNA deletions in human cells? *Nature Genetics,* 40**,** 275-279.

KUNZLI, B. M., LIEBL, F., NUHN, P., SCHUSTER, T., FRIESS, H. & HARTEL, M. 2013. Impact of Preoperative Local Water-Filtered Infrared A Irradiation on Postoperative Wound Healing A Randomized Patient- and Observer-Blinded Controlled Clinical Trial. *Annals of Surgery,* 258**,** 887-894.

KURAZUMI, Y., ISHII, J., KONDO, E., FUKAGAWA, K., BOLASHIKOV, Z. D., SAKOI, T., TSUCHIKAWA, T., MATSUBARA, N. & HORIKOSHI, T. 2014. The influence of outdoor thermal environment on young Japanese females. *International Journal of Biometeorology,* 58**,** 963-974.

LAKSHMI, R., LAKSHMI, A. & BAMJI, M. 1990. Mechanism of impaired skin collagen maturity in riboflavin or pyridoxine deficiency. *Journal of Biosciences,* 15**,** 289-295.

LAKSHMI, R., LAKSHMI, A. & BAMJI, M. S. 1989. Skin wound healing in riboflavin deficiency. *Biochemical medicine and metabolic biology,* 42**,** 185-191.

LANGTON, A. K., HALAI, P., GRIFFITHS, C. E., SHERRATT, M. J. & WATSON, R. E. 2016. The impact of intrinsic ageing on the protein composition of the dermal-epidermal junction. *Mechanisms of Ageing and Development,* 156**,** 14-16.

LASK, G., FOURNIER, N., TRELLES, M., ELMAN, M., SCHEFLAN, M., SLATKINE, M., NAIMARK, J. & HARTH, Y. 2005. The utilization of nonthermal blue (405–425 nm) and near infrared (850–890 nm) light in aesthetic dermatology and surgery—a multicenter study. *Journal of Cosmetic and Laser Therapy,* 7**,** 163-170.

LEE, E.-S., CORFE, B. M. & POWERS, H. J. 2013. Riboflavin depletion of intestinal cells in vitro leads to impaired energy generation and enhanced oxidative stress. *European Journal of Nutrition,* 52**,** 1513-1521.

LEE HYOUN, S., LEE DONG, H., CHO, S. & CHUNG JIN, H. 2006. Minimal heating dose: a novel biological unit to measure infrared irradiation. *Photodermatology, Photoimmunology & Photomedicine,* 22**,** 148-152.

LEE YOUNG, M., LI WEN, H., KIM YEON, K., KIM KYU, H. & CHUNG JIN, H. 2008. Heat‐induced MMP‐1 expression is mediated by TRPV1 through PKCα signaling in HaCaT cells. *Experimental Dermatology,* 17**,** 864-870.

LI, W.-H., SEO, I., KIM, B., FASSIH, A., SOUTHALL, M. D. & PARSA, R. 2021. Low-level red plus near infrared lights combination induces expressions of collagen and elastin in human skin in vitro. *International Journal of Cosmetic Science,* 43**,** 311-320.

LI, W. H., LEE, Y. M., KIM, J. Y., KANG, S., KIM, S., KIM, K. H., PARK, C.-H. & CHUNG, J. H. 2007. Transient Receptor Potential Vanilloid-1 Mediates Heat-Shock-Induced Matrix Metalloproteinase-1 Expression in Human Epidermal Keratinocytes. *Journal of Investigative Dermatology,* 127**,** 2328-2335.

LIEBEL, F., KAUR, S., RUVOLO, E., KOLLIAS, N. & SOUTHALL, M. D. 2012. Irradiation of Skin with Visible Light Induces Reactive Oxygen Species and Matrix-Degrading Enzymes. *Journal of Investigative Dermatology,* 132**,** 1901-1907.

LIEBMANN, J., BORN, M. & KOLB-BACHOFEN, V. 2010. Blue-light irradiation regulates proliferation and differentiation in human skin cells. *Journal of Investigative Dermatology,* 130**,** 259-269.

LIU, S.-Y., CHEN, C.-L., YANG, T.-T., HUANG, W.-C., HSIEH, C.-Y., SHEN, W.-J., TSAI, T.-T., SHIEH, C.-C. & LIN, C.-F. 2012. Albumin prevents reactive oxygen species-induced mitochondrial damage, autophagy, and apoptosis during serum starvation. *Apoptosis,* 17**,** 1156-1169.

LIU, Y., PETERSON, D. A., KIMURA, H. & SCHUBERT, D. 1997. Mechanism of Cellular 3-(4,5-Dimethylthiazol-2-yl)-2,5-Diphenyltetrazolium Bromide (MTT) Reduction. *Journal of Neurochemistry,* 69**,** 581-593.

LOCKANDERSEN, J., THERKILDSEN, P., OLIVARIUS, F. D., GNIADECKA, M., DAHLSTROM, K., POULSEN, T. & WULF, H. C. 1997. Epidermal thickness, skin pigmentation and constitutive photosensitivity. *Photodermatology Photoimmunology & Photomedicine,* 13**,** 153-158.

MAGUIRE, A., MORRISSEY, B., WALSH, J. E. & LYNG, F. M. 2011. Medium-mediated effects increase cell killing in a human keratinocyte cell line exposed to solar-simulated radiation. *International Journal of Radiation Biology,* 87**,** 98-111.

MAHMOUD, B. H., HEXSEL, C. L., HAMZAVI, T. H. & LIM, H. W. 2008. Effects of visible light on the skin. *Photochemistry and Photobiology,* 84**,** 450-462.

MAHNS, A., MELCHHEIER, I., SUSCHEK, C. V., SIES, H. & KLOTZ, L.-O. 2003. Irradiation of cells with ultraviolet-A (320-400 nm) in the presence of cell culture medium elicits biological effects due to extracellular generation of hydrogen peroxide. *Free radical research,* 37**,** 391-397.

MAILLOUX, R. J. & HARPER, M. E. 2011. Uncoupling proteins and the control of mitochondrial reactive oxygen species production. *Free Radical Biology and Medicine,* 51**,** 1106-1115.

MANN, T., EGGERS, K., RIPPKE, F., TESCH, M., BUERGER, A., DARVIN, M. E., SCHANZER, S., MEINKE, M. C., LADEMANN, J. & KOLBE, L. 2020. High-energy visible light at ambient doses and intensities induces oxidative stress of skin—Protective effects of the antioxidant and Nrf2 inducer Licochalcone A in vitro and in vivo. *Photodermatology, Photoimmunology & Photomedicine,* 36**,** 135-144.

MANTHEY, K. C., RODRIGUEZ-MELENDEZ, R., HOI, J. T. & ZEMPLENI, J. 2006. Riboflavin deficiency causes protein and DNA damage in HepG2 cells, triggering arrest in G1 phase of the cell cycle. *The Journal of nutritional biochemistry,* 17**,** 250-256.

MATSUMURA, Y. & ANANTHASWAMY, H. N. 2004. Toxic effects of ultraviolet radiation on the skin. *Toxicology and Applied Pharmacology,* 195**,** 298-308.

MCGREGOR, J. 1999. Acute effects of ultraviolet radiation on the skin. *Dermatology in general medicine*.

MCKINLAY, A. 1987. A reference action spectrum for ultraviolet erythema in human skin. *CIE journal,* 6**,** 17-22.
MENEZES, S., COULOMB, B., LEBRETON, C. & DUBERTRET, L. 1998. Non-Coherent Near Infrared Radiation Protects Normal Human Dermal Fibroblasts from Solar Ultraviolet Toxicity. *Journal of Investigative Dermatology,* 111**,** 629-633.
MICHIKAWA, Y., MAZZUCCHELLI, F., BRESOLIN, N., SCARLATO, G. & ATTARDI, G. 1999. Aging-Dependent Large Accumulation of Point Mutations in the Human mtDNA Control Region for Replication. *Science,* 286**,** 774-779.
MIWA, S., ST-PIERRE, J., PARTRIDGE, L. & BRAND, M. D. 2003. Superoxide and hydrogen peroxide production by Drosophila mitochondria. *Free Radical Biology and Medicine,* 35**,** 938-948.
MOHAMADZADEH, M., TAKASHIMA, A., DOUGHERTY, I., KNOP, J., BERGSTRESSER, P. R. & CRUZ, P. D. 1995. ULTRAVIOLET-B RADIATION UP-REGULATES THE EXPRESSION OF IL-15 IN HUMAN SKIN. *Journal of Immunology,* 155**,** 4492-4496.
MONTAUDIÉ, H., LACOUR, J.-P., ROSTAIN, G., DUTEIL, L. & PASSERON, T. 2014. Solar urticaria to visible light triggered by light-emitting diode therapy. *Journal of the American Academy of Dermatology,* 71**,** e74-e75.
MULLER, F. L., LIU, Y. & VAN REMMEN, H. 2004. Complex III releases superoxide to both sides of the inner mitochondrial membrane. *Journal of Biological Chemistry,* 279**,** 49064-49073.
MURPHY, M. P. 2009. How mitochondria produce reactive oxygen species. *Biochemical journal,* 417**,** 1-13.
NAKASHIMA, Y., OHTA, S. & WOLF, A. M. 2017. Blue light-induced oxidative stress in live skin. *Free Radical Biology and Medicine,* 108**,** 300-310.
NISSANKA, N., MINCZUK, M. & MORAES, C. T. 2019. Mechanisms of Mitochondrial DNA Deletion Formation. *Trends in Genetics,* 35**,** 235-244.
OHISHI, K., ZHANG, X. M., MORIWAKI, S., HIRAMITSU, T. & MATSUGO, S. 2006. In the presence of ferritin, visible light induces lipid peroxidation of the porcine photoreceptor outer segment. *Free Radical Research,* 40**,** 799-807.
OIKARINEN, A. 1994. Aging of the skin connective tissue: how to measure the biochemical and mechanical properties of aging dermis. *Photodermatology, photoimmunology & photomedicine,* 10**,** 47-52.
OKA, S., OHNO, M., TSUCHIMOTO, D., SAKUMI, K., FURUICHI, M. & NAKABEPPU, Y. 2008. Two distinct pathways of cell death triggered by oxidative damage to nuclear and mitochondrial DNAs. *The EMBO Journal,* 27**,** 421-432.
OPLÄNDER, C., CORTESE, M. M., KORTH, H.-G., KIRSCH, M., MAHOTKA, C., WETZEL, W., PALLUA, N. & SUSCHEK, C. V. 2007. The impact of nitrite and antioxidants on ultraviolet-A-induced cell death of human skin fibroblasts. *Free Radical Biology and Medicine,* 43**,** 818-829.
OPLÄNDER, C., HIDDING, S., WERNERS, F. B., BORN, M., PALLUA, N. & SUSCHEK, C. V. 2011. Effects of blue light irradiation on human dermal fibroblasts. *Journal of Photochemistry and Photobiology B: Biology,* 103**,** 118-125.
PARK, C.-H., LEE, M. J., AHN, J., KIM, S., KIM, H. H., KIM, K. H., EUN, H. C. & CHUNG, J. H. 2004. Heat Shock-Induced Matrix Metalloproteinase (MMP)-1 and MMP-3 Are Mediated

through ERK and JNK Activation and via an Autocrine Interleukin-6 Loop. *Journal of Investigative Dermatology,* 123**,** 1012-1019.
PATHANIA, S., NGUYEN, J., HILL, S. J., SCULLY, R., ADELMANT, G. O., MARTO, J. A., FEUNTEUN, J. & LIVINGSTON, D. M. 2011. BRCA1 Is Required for Postreplication Repair after UV-Induced DNA Damage. *Molecular Cell,* 44**,** 235-251.
PAVEY, S., RUSSELL, T. & GABRIELLI, B. 2001. G2 phase cell cycle arrest in human skin following UV irradiation. *ONCOGENE,* 20**,** 6103-6110.
PETERSEN, B., PHILIPSEN, P. A. & WULF, H. C. 2014. Skin temperature during sunbathing - relevance for skin cancer. *Photochemical & Photobiological Sciences,* 13**,** 1123-1125.
PETRONINI, P. G., ALFIERI, R., CAMPANINI, C. & BORGHETTI, A. F. 1995. Effect of an alkaline shift on induction of the heat shock response in human fibroblasts. *Journal of Cellular Physiology,* 162**,** 322-329.
PIAZENA, H. & KELLEHER, D. 2008. Comments on "Cellular response to infrared radiation involves retrograde mitochondrial signaling". *Free Radical Biology and Medicine,* 44**,** 1869.
PIAZENA, H. & KELLEHER DEBRA, K. 2010. Effects of Infrared‐A Irradiation on Skin: Discrepancies in Published Data Highlight the Need for an Exact Consideration of Physical and Photobiological Laws and Appropriate Experimental Settings. *Photochemistry and Photobiology,* 86**,** 687-705.
PIAZENA, H., MEFFERT, H. & UEBELHACK, R. 2017. Spectral Remittance and Transmittance of Visible and Infrared‐A Radiation in Human Skin—Comparison Between in vivo Measurements and Model Calculations. *Photochemistry and Photobiology,* 93**,** 1449-1461.
PIAZENA, H., PITTERMANN, W., MÜLLER, W., JUNG, K., KELLEHER, D. K., HERRLING, T., MEFFERT, P., UEBELHACK, R. & KIETZMANN, M. 2014. Effects of water-filtered infrared-A and of heat on cell death, inflammation, antioxidative potential and of free radical formation in viable skin – First results. *Journal of Photochemistry and Photobiology B: Biology,* 138**,** 347-354.
PIRKMAJER, S. & CHIBALIN, A. V. 2011. Serum starvation: caveat emptor. *American Journal of Physiology-Cell Physiology,* 301**,** C272-C279.
POURANG, A., TISACK, A., EZEKWE, N., TORRES, A. E., KOHLI, I., HAMZAVI, I. H. & LIM, H. W. 2021. Effects of visible light on mechanisms of skin photoaging. *Photodermatology, Photoimmunology & Photomedicine,* n/a.
POURZAND, C., WATKIN, R. D., BROWN, J. E. & TYRRELL, R. M. 1999. Ultraviolet A radiation induces immediate release of iron in human primary skin fibroblasts: the role of ferritin. *Proceedings of the National Academy of Sciences,* 96**,** 6751-6756.
POWERS, J. M., MURPHY, G., RALPH, N., O'GORMAN, S. M. & MURPHY, J. E. J. 2016. Mitochondrial DNA deletion percentage in sun exposed and non sun exposed skin. *Journal of Photochemistry and Photobiology B: Biology,* 165**,** 277-282.
QUINLAN, C. L., TREBERG, J. R., PEREVOSHCHIKOVA, I. V., ORR, A. L. & BRAND, M. D. 2012. Native rates of superoxide production from multiple sites in isolated mitochondria measured using endogenous reporters. *Free Radical Biology and Medicine,* 53**,** 1807-1817.

RAY, P. D., HUANG, B. W. & TSUJI, Y. 2012. Reactive oxygen species (ROS) homeostasis and redox regulation in cellular signaling. *Cellular Signalling,* 24**,** 981-990.

REELFS, O., TYRRELL, R. M. & POURZAND, C. 2004. Ultraviolet A Radiation-Induced Immediate Iron Release Is a Key Modulator of the Activation of NF-κB in Human Skin Fibroblasts. *Journal of Investigative Dermatology,* 122**,** 1440-1447.

REITER, R. J., MELCHIORRI, D., SEWERYNEK, E., POEGGELER, B., BARLOW-WALDEN, L., CHUANG, J., ORTIZ, G. G. & ACUÑACASTROVIEJO, D. 1995. A review of the evidence supporting melatonin's role as an antioxidant. *Journal of Pineal Research,* 18**,** 1-11.

RISTOW, M. & SCHMEISSER, K. 2014. MITOHORMESIS: PROMOTING HEALTH AND LIFESPAN BY INCREASED LEVELS OF REACTIVE OXYGEN SPECIES (ROS). *Dose-Response,* 12**,** 288-341.

RITTIÉ, L. & FISHER, G. J. 2002. UV-light-induced signal cascades and skin aging. *Ageing Research Reviews,* 1**,** 705-720.

RODRIGUEZ, I. R. & FLIESLER, S. J. 2009. Photodamage Generates 7-keto- and 7-hydroxycholesterol in the Rat Retina via a Free Radical-mediated Mechanism. *Photochemistry and Photobiology,* 85**,** 1116-1125.

ROGNONI, E., GOSS, G., HIRATSUKA, T., SIPILA, K. H., KIRK, T., KOBER, K. I., LUI, P. P., TSANG, V. S., HAWKSHAW, N. J., PILKINGTON, S. M., CHO, I., ALI, N., RHODES, L. E. & WATT, F. M. 2021. Role of distinct fibroblast lineages and immune cells in dermal repair following UV radiation-induced tissue damage. *Elife,* 10.

SAKAGUCHI, K., HERRERA, J. E., SAITO, S. I., MIKI, T., BUSTIN, M., VASSILEV, A., ANDERSON, C. W. & APPELLA, E. 1998. DNA damage activates p53 through a phosphorylation–acetylation cascade. *Genes & development,* 12**,** 2831-2841.

SANDBY-MOLLER, J., POULSEN, T. & WULF, H. C. 2003. Epidermal thickness at different body sites: relationship to age, gender, pigmentation, blood content, skin type and smoking habits. *Acta Dermato Venereologica,* 83**,** 410-413.

SANDER, C. S., CHANG, H., SALZMANN, S., MÜLLER, C. S. L., EKANAYAKE-MUDIYANSELAGE, S., ELSNER, P. & THIELE, J. J. 2002. Photoaging is Associated with Protein Oxidation in Human Skin In Vivo. *Journal of Investigative Dermatology,* 118**,** 618-625.

SCHIEKE, S. M., STEGE, H., KÜRTEN, V., GRETHER-BECK, S., SIES, H. & KRUTMANN, J. 2002. Infrared-A Radiation-Induced Matrix Metalloproteinase 1 Expression is Mediated Through Extracellular Signal-regulated Kinase 1/2 Activation in Human Dermal Fibroblasts. *Journal of Investigative Dermatology,* 119**,** 1323-1329.

SCHNEIDER, L. A., KORBER, A., GRABBE, S. & DISSEMOND, J. 2007. Influence of pH on wound-healing: a new perspective for wound-therapy? *Archives of Dermatological Research,* 298**,** 413-420.

SCHRAMM, M., WIEGMANN, K., SCHRAMM, S., GLUSCHKO, A., HERB, M., UTERMÖHLEN, O. & KRÖNKE, M. 2014. Riboflavin (vitamin B2) deficiency impairs NADPH oxidase 2 (Nox2) priming and defense against Listeria monocytogenes. *European Journal of Immunology,* 44**,** 728-741.

SCHROEDER, P., CALLES, C., BENESOVA, T., MACALUSO, F. & KRUTMANN, J. 2010. Photoprotection beyond Ultraviolet Radiation - Effective Sun Protection Has to Include Protection against Infrared A Radiation-Induced Skin Damage. *Skin Pharmacology and Physiology,* 23**,** 15-17.

SCHROEDER, P. & KRUTMANN, J. 2008. In vivo relevance of infrared a radiation-induced skin damage: Reply to Piazena and Kelleher, Letter to the Editor, Free Radical Biology and Medicine, 2008. *Free Radical Biology and Medicine,* 44**,** 1870-1871.

SCHROEDER, P., LADEMANN, J., DARVIN, M. E., STEGE, H., MARKS, C., BRUHNKE, S. & KRUTMANN, J. 2008. Infrared Radiation-Induced Matrix Metalloproteinase in Human Skin: Implications for Protection. *Journal of Investigative Dermatology,* 128**,** 2491-2497.

SCHROEDER, P., POHL, C., CALLES, C., MARKS, C., WILD, S. & KRUTMANN, J. 2007. Cellular response to infrared radiation involves retrograde mitochondrial signaling. *Free Radical Biology and Medicine,* 43**,** 128-135.

SCOTT, T. L., CHRISTIAN, P. A., KESLER, M. V., DONOHUE, K. M., SHELTON, B., WAKAMATSU, K., ITO, S. & D'ORAZIO, J. 2012. Pigment‐independent cAMP‐mediated epidermal thickening protects against cutaneous UV injury by keratinocyte proliferation. *Experimental dermatology,* 21**,** 771-777.

SETLOW, R. B., GRIST, E., THOMPSON, K. & WOODHEAD, A. D. 1993. WAVELENGTHS EFFECTIVE IN INDUCTION OF MALIGNANT-MELANOMA. *Proceedings of the National Academy of Sciences of the United States of America,* 90**,** 6666-6670.

SHADEL, G. S. & CLAYTON, D. A. 1997. MITOCHONDRIAL DNA MAINTENANCE IN VERTEBRATES. *Annual Review of Biochemistry,* 66**,** 409-435.

SHAHRAD, P. & MARKS, R. 1977. The wages of warmth: changes in erythema ab igne. *British Journal of Dermatology,* 97**,** 179-186.

SHIN, M. H., MOON, Y. J., SEO, J.-E., LEE, Y., KIM, K. H. & CHUNG, J. H. 2008. Reactive oxygen species produced by NADPH oxidase, xanthine oxidase, and mitochondrial electron transport system mediate heat shock-induced MMP-1 and MMP-9 expression. *Free Radical Biology and Medicine,* 44**,** 635-645.

SHIN, M. H., SEO, J.-E., KIM, Y. K., KIM, K. H. & CHUNG, J. H. 2012. Chronic heat treatment causes skin wrinkle formation and oxidative damage in hairless mice. *Mechanisms of Ageing and Development,* 133**,** 92-98.

SILVA, E., UGARTE, R., ANDRADE, A. & EDWARDS, A. M. 1994. Riboflavin-sensitized photoprocesses of tryptophan. *Journal of Photochemistry and Photobiology B: Biology,* 23**,** 43-48.

SONG, S., ZHANG, Y., FONG, C.-C., TSANG, C.-H., YANG, Z. & YANG, M. 2003. cDNA Microarray Analysis of Gene Expression Profiles in Human Fibroblast Cells Irradiated with Red Light. *Journal of Investigative Dermatology,* 120**,** 849-857.

SORRELL, J. M., BABER, M. & CAPLAN, A. 2004. Site‐matched papillary and reticular human dermal fibroblasts differ in their release of specific growth factors/cytokines and in their interaction with keratinocytes. *Journal of cellular physiology,* 200**,** 134-145.

SORRELL, J. M., BABER, M. A. & CAPLAN, A. I. 1996. Construction of a bilayered dermal equivalent containing human papillary and reticular dermal fibroblasts: use of fluorescent vital dyes. *Tissue engineering,* 2**,** 39-49.

SORRELL, J. M. & CAPLAN, A. I. 2004. Fibroblast heterogeneity: more than skin deep. *Journal of Cell Science,* 117**,** 667-675.

SRIRAM, G., BIGLIARDI, P. L. & BIGLIARDI-QI, M. 2015. Fibroblast heterogeneity and its implications for engineering organotypic skin models in vitro. *European Journal of Cell Biology,* 94**,** 483-512.

SVOBODOVÁ, A. R., GALANDÁKOVÁ, A., ŠIANSKÁ, J., DOLEŽAL, D., LICHNOVSKÁ, R., ULRICHOVÁ, J. & VOSTÁLOVÁ, J. 2012. DNA damage after acute exposure of mice skin to physiological doses of UVB and UVA light. *Archives of Dermatological Research,* 304**,** 407-412.

SWALWELL, H., LATIMER, J., HAYWOOD, R. M. & BIRCH-MACHIN, M. A. 2012a. Investigating the role of melanin in UVA/UVB- and hydrogen peroxide-induced cellular and mitochondrial ROS production and mitochondrial DNA damage in human melanoma cells. *Free Radical Biology and Medicine,* 52**,** 626-634.

SWALWELL, H., LATIMER, J., HAYWOOD, R. M. & BIRCH-MACHIN, M. A. 2012b. Investigating the role of melanin in UVA/UVB-and hydrogen peroxide-induced cellular and mitochondrial ROS production and mitochondrial DNA damage in human melanoma cells. *Free Radical Biology and Medicine,* 52**,** 626-634.

TERRA, V. A., SOUZA-NETO, F. P., PEREIRA, R. C., SILVA, T. N. X., COSTA, A. C. C., LUIZ, R. C., CECCHINI, R. & CECCHINI, A. L. 2012. Time-dependent reactive species formation and oxidative stress damage in the skin after UVB irradiation. *Journal of Photochemistry and Photobiology B: Biology,* 109**,** 34-41.

TRATWAL, J., MATHIASEN, A. B., JUHL, M., BRORSEN, S. K., KASTRUP, J. & EKBLOND, A. 2015. Influence of vascular endothelial growth factor stimulation and serum deprivation on gene activation patterns of human adipose tissue-derived stromal cells. *Stem Cell Research & Therapy,* 6**,** 62.

UETSU, N., MIYAUCHI-HASHIMOTO, H., OKAMOTO, H. & HORIO, T. 2000. The clinical and photobiological characteristics of solar urticaria in 40 patients. *British Journal of Dermatology,* 142**,** 32-38.

VELTRI, K., ESPIRITU, M. & SINGH, G. 1990. Distinct genomic copy number in mitochondria of different mammalian organs. *Journal of cellular physiology,* 143**,** 160-4.

VERZIJL, N., DEGROOT, J., THORPE, S. R., BANK, R. A., SHAW, J. N., LYONS, T. J., BIJLSMA, J. W., LAFEBER, F. P., BAYNES, J. W. & TEKOPPELE, J. M. 2000. Effect of collagen turnover on the accumulation of advanced glycation end products. *Journal of Biological Chemistry,* 275**,** 39027-39031.

WALLER, J. M. & MAIBACH, H. I. 2006. Age and skin structure and function, a quantitative approach (II): protein, glycosaminoglycan, water, and lipid content and structure. *Skin Research and Technology,* 12**,** 145-154.

WANG, R. J. 1976. Effect of room fluorescent light on the deterioration of tissue culture medium. *In Vitro,* 12**,** 19-22.

WANG, R. J. & NIXON, B. T. 1978. Identification of hydrogen peroxide as a photoproduct toxic to human cells in tissue-culture medium irradiated with “daylight” fluorescent light. *In Vitro,* 14**,** 715-722.

WEBB, A. R., SLAPER, H., KOEPKE, P. & SCHMALWIESER, A. W. 2011. Know Your Standard: Clarifying the CIE Erythema Action Spectrum. *Photochemistry and Photobiology,* 87**,** 483-486.

WEI, Y.-H., PANG, C.-Y., YOU, B.-J. & LEE, H.-C. 1996. Tandem duplications and large-scale deletions of mitochondrial DNA are early molecular events of human aging process. *Annals of the New York Academy of Sciences-Paper Edition,* 786**,** 82-101.

WELLE, A. & GOTTWALD, E. 2002. UV-Based Patterning of Polymeric Substrates for Cell Culture Applications. *Biomedical Microdevices,* 4**,** 33-41.

WISCHERMANN, K., POPP, S., MOSHIR, S., SCHARFETTER-KOCHANEK, K., WLASCHEK, M., DE GRUIJL, F., HARTSCHUH, W., GREINERT, R., VOLKMER, B., FAUST, A., RAPP, A., SCHMEZER, P. & BOUKAMP, P. 2008. UVA radiation causes DNA strand breaks, chromosomal aberrations and tumorigenic transformation in HaCaT skin keratinocytes. *Oncogene,* 27**,** 4269-4280.

XIONG, W., JIAO, Y., HUANG, W. W., MA, M. X., YU, M., CUI, Q. H. & TAN, D. Y. 2012. Regulation of the cell cycle via mitochondrial gene expression and energy metabolism in HeLa cells. *Acta Biochimica Et Biophysica Sinica,* 44**,** 347-358.

YANES, O., CLARK, J., WONG, D. M., PATTI, G. J., SANCHEZ-RUIZ, A., BENTON, H. P., TRAUGER, S. A., DESPONTS, C., DING, S. & SIUZDAK, G. 2010. Metabolic oxidation regulates embryonic stem cell differentiation. *Nature Chemical Biology,* 6**,** 411-417.

YOUNG, A. R. 1997. Chromophores in human skin. *Physics in Medicine & Biology,* 42**,** 789.

YOUSIF, E. & HADDAD, R. 2013. Photodegradation and photostabilization of polymers, especially polystyrene: review. *SpringerPlus,* 2**,** 398-398.

YUN, J. & FINKEL, T. 2014. Mitohormesis. *Cell metabolism,* 19**,** 757-766.

ZANCHETTA, L. M., KIRK, D., LYNG, F., WALSH, J. & MURPHY, J. E. J. 2010. Cell-density-dependent changes in mitochondrial membrane potential and reactive oxygen species production in human skin cells post sunlight exposure. *Photodermatology, Photoimmunology & Photomedicine,* 26**,** 311-317.

ZASTROW, L., GROTH, N., KLEIN, F., KOCKOTT, D., LADEMANN, J., RENNEBERG, R. & FERRERO, L. 2009. The missing link–light-induced (280–1,600 nm) free radical formation in human skin. *Skin pharmacology and physiology,* 22**,** 31-44.

ZHU, Y. J. & LU, T. J. 2010. A multi-scale view of skin thermal pain: from nociception to pain sensation. *Philosophical Transactions of the Royal Society A: Mathematical, Physical and Engineering Sciences,* 368**,** 521-559.